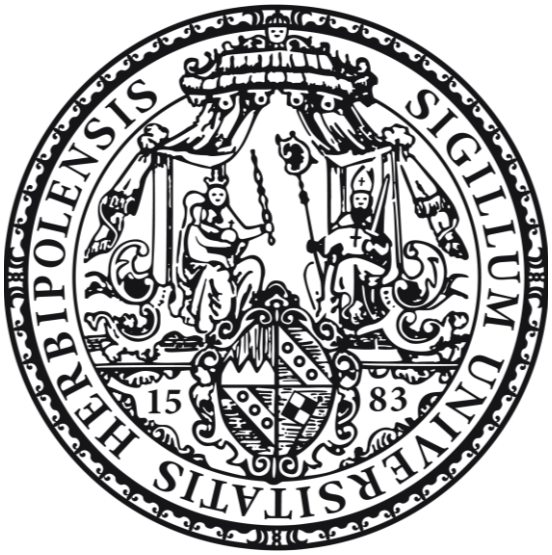

Establishment of an intestinal tissue model for pre-clinical screenings

Etablierung eines Darmgewebemodells für Präklinische Screenings

Doctoral thesis for a doctoral degree
at the Graduate School of Life Sciences (GSLS),
Julius-Maximilians-Universität Würzburg
Section Biomedicine

submitted by

Christina Fey

born in Aschaffenburg

Würzburg 2020

Submitted on: ……..……..

Members of the committee:

Chairperson: Prof. Dr. Thomas Dandekar

Primary Supervisor: PD Dr. Marco Metzger

Supervisor (Second): Prof. Dr. Heike Walles

Supervisor (Third): Prof. Dr. Nicolas Schlegel

Supervisor (Fourth): Prof. Dr. Andreas Friebe

Date of Public Defence: ……..……

Date of Receipt of Certificates: …….

Dedicated to my family

„Das schönste Glück des denkenden Menschen ist,

das Erforschliche erforscht zu haben und das

Unerforschliche zu verehren.“

-Johann Wolfgang von Goethe-

Table of contents

Abstract

The small intestine represents a strong barrier separating the lumen from blood circulation thereby playing a major role in the absorption and the transport of pharmacological agents prior to their arrival on the respective target site. In order to gain more knowledge about specialized uptake mechanisms and risk assessment for the patient after oral admission of drugs, intestinal *in vitro* models demonstrating a close similarity to the *in vivo* situation are needed.

In the past, cell line-based *in vitro* models composed of Caco-2 cells cultured on synthetic cell carriers represented the “gold standard” in the field of intestinal tissue engineering. Expressive advantages of these models are a reproducible, cost-efficient and standardized model set up, but cell function can be negatively influenced by the low porosity or unwanted molecular adhesion effects of the artificial scaffold material. Natural extracellular matrices (ECM) such as the porcine decellularized small intestinal submucosa (SIS) are used as alternative to overcome some common drawbacks; however, the fabrication of these scaffolds is time- and cost-intensive, less well standardized and the 3Rs (replacement, reduction, refinement) principle is not entirely fulfilled. Nowadays, biopolymer-based scaffolds such as the bacterial nanocellulose (BNC) suggest an interesting option of novel intestinal tissue engineered models, as the BNC shows comparable features to the native ECM regarding fiber arrangement and hydrophilic properties. Furthermore, the BNC is of non-animal origin and the manufacturing process is faster as well as well standardized at low costs.

In this context, the first part of this thesis analyzed the BNC as alternative scaffold to derive standardized and functional organ models *in vitro*. Therefore, Caco-2 cells were cultured on two versions of BNC with respect to their surface topography, the unmodified BNC as rather smooth surface and the surface-structured BNC presenting an aligned fiber arrangement. As controls, Caco-2 *in vitro* models were set up on PET and SIS matrices. In this study, the BNC-based models demonstrated organ-specific properties comprising typical cellular morphologies, a characteristic tight junction protein expression profile, representative ultrastructural features and the formation of a tight epithelial barrier together with a corresponding transport activity. In summary, these results validated the high quality of the BNC-based Caco-2 models under cost-efficient conditions and their suitability for pre-clinical research purposes. However, the full functional diversity of the human intestine cannot be presented by Caco-2 cells due to their tumorigenic background and their exclusive representation of mature enterocytes.

Next to the scaffold used for the setup of *in vitro* models, the cellular unit mainly drives functional performance, which demonstrates the crucial importance of mimicking the cellular diversity of the small intestine *in vitro*. In this context, intestinal primary organoids are of high interest, as they show a close similarity to the native epithelium regarding their cellular diversity comprising enterocytes, goblet cells, enteroendocrine cells, paneth cells, transit amplifying cells and stem cells. In general, such primary organoids grow in a 3D Matrigel®-based environment and a medium formulation supplemented with a variety of growth factors to maintain stemness, to inhibit differentiation and to stimulate cell migration supporting long-term *in vitro* culture.

Intestinal primary spheroid/organoid cultures were set up as Transwell®-like models on both BNC variants, which resulted in a fragmentary cell layer and thereby unfavorable properties of these scaffold materials under the applied circumstances. As the BNC manufacturing process is highly flexible, surface properties could be adapted in future studies to enable a good cell adherence and barrier formation for primary intestinal cells, too. However, the application of these organoid cultures in pre-clinical research represents an enormous challenge, as the *in vitro* culture is complex and additionally time- and cost-intensive.

With regard to the high potential of primary intestinal spheroids/organoids and the necessity of a simplified but predictive model in pre-clinical research purposes, the second part of this thesis addressed the establishment of a primary-derived immortalized intestinal cell line, which enables a standardized and cost-efficient culture (including in 2D), while maintaining the cellular diversity of the organoid *in vitro* cultures. In this study, immortalization of murine and human intestinal primary organoids was induced by ectopic expression of a 10- (murine) or 12-component (human) pool of genes regulating stemness and the cell cycle, which was performed in cooperation with the InSCREENeX GmbH in a 2D- and 3D-based transduction strategy. In first line, the established cell lines (cell clones) were investigated for their cell culture prerequisites to grow under simplified and cost-efficient conditions. While murine cell clones grew on uncoated plastic in a medium formulation supplemented with EGF, Noggin, Y-27632 and 10% FCS, the human cell clones demonstrated the necessity of a Col I pre-coating together with the need for a medium composition commonly used for primary human spheroid/organoid cultures. Furthermore, the preceding analyses resulted in only one human cell clone and three murine cell clones for ongoing characterization. Studies regarding the proliferative properties and the specific gene as well as protein expression profile of the remaining cell clones have shown, that it is likely that transient amplifying cells (TACs) were immortalized instead of the differentiated cell types localized in primary organoids, as 2D, 3D or Transwell®-based cultures resulted in slightly different gene expression profiles and in a dramatically reduced mRNA transcript level for the analyzed

marker genes representative for the differentiated cell types of the native epithelium. Further, 3D-cultures demonstrated the formation of spheroid-like structures; however without forming organoid-like structures due to prolonged culture, indicating that these cell populations have lost their ability to differentiate into specific intestinal cell types. The Transwell®-based models set up of each clone exhibit organ-specific properties comprising an epithelial-like morphology, a characteristic protein expression profile with an apical mucus-layer covering the villin-1 positive cell layer, thereby representing goblet cells and enterocytes, together with representative tight junction complexes indicating an integer epithelial barrier. The proof of a functional as well as tight epithelial barrier in TEER measurements and *in vivo*-like transport activities qualified the established cell clones as alternative cell sources for tissue engineered models representing the small intestine to some extent. Additionally, the easy handling and cell expansion under more cost-efficient conditions compared to primary organoid cultures favors the use of these newly generated cell clones in bioavailability studies.

Altogether, this work demonstrated new components, structural and cellular, for the establishment of alternative *in vitro* models of the small intestinal epithelium, which could be used in pre-clinical screenings for reproducible drug delivery studies.

Zusammenfassung

Der Dünndarm bildet eine starke Barriere aus, welche das Lumen vom Blutkreislauf trennt, und dadurch maßgeblich an der Absorption und dem Transport von pharmakologischen Wirkstoffen beteiligt ist, bevor diese ihren Wirkort erreichen. Um ein detaillierteres Wissen über die speziellen Aufnahmemechanismen zu erlangen und zur Risikoabschätzung für den Patienten nach oraler Aufnahme dieser Medikamente, sind intestinale *in vitro* Modelle erforderlich, die eine große Ähnlichkeit mit der Situation *in vivo* aufweisen.

In der Vergangenheit stellten Caco-2 Zelllinien-basierte *in vitro* Modelle, die auf synthetischen Trägerstrukturen aufgebaut sind, den „Goldstandard“ auf dem Gebiet der intestinalen Geweberekonstruktion dar. Bedeutende Vorteile dieser Modelle sind der reproduzierbare, kosteneffiziente und standardisierte Modellaufbau, jedoch können die zellulären Funktionen durch die geringe Porosität oder die unerwünschten molekularen Adhäsionseffekte des künstlichen Trägermaterials negativ beeinflusst werden. Um einige häufige Nachteile zu überwinden werden natürliche extrazelluläre Matrizen (ECM) wie die porzine dezellularisierte Dünndarm-submukosa (SIS) verwendet, jedoch ist die Herstellung dieser Trägerstrukturen zeit- und kostenintensiv, weniger gut standardisiert und entspricht nicht ganzheitlich dem 3R-Prinzip (Replace = Vermeiden, Reduce = Verringern, Refine = Verbessern). Heutzutage ermöglichen biopolymer-basierte Trägerstrukturen wie die bakterielle Nanozellulose (BNC) die Entwicklung von neuartigen intestinalen Gewebemodellen, da die BNC eine große Ähnlichkeit hinsichtlich der Faseranordnung und der hydrophilen Eigenschaften mit der nativen ECM aufweist. Darüber hinaus ist die BNC nicht tierischen Ursprungs und der Herstellungsprozess schneller, gut standardisiert als auch kostengünstig.

In diesem Zusammenhang wurde im ersten Teil dieser Arbeit nachgewiesen, dass die BNC als alternative Trägerstruktur für standardisierte und funktionelle Organmodelle *in vitro* geeignet ist. Dafür wurden Caco-2 Zellen auf zwei Varianten der BNC kultiviert, die sich in ihrer Oberflächentopographie unterscheiden, wobei die nicht-modifizierte BNC eine glatte Oberfläche und die oberflächen-strukturierte BNC eine ausgerichtete Faseranordnung aufweist. Als Kontrollen dienten Caco-2 zellbasierte *in vitro* Modelle, die auf PET- oder SIS-Matrizes aufgebaut wurden. In dieser Studie wiesen die BNC-basierten Modelle die wichtigsten organ-spezifischen Eigenschaften auf, darunter eine typische zelluläre Morphologie, ein charakteristisches Expressionsprofil der Tight Junction Proteine, repräsentative ultrastrukturelle Merkmale und die Bildung einer dichten epithelialen Barriere verbunden mit einer entsprechenden Transportaktivität. Zusammenfassend bestätigten diese Ergebnisse die hohe Qualität der BNC-basierten Caco-2 Modelle unter kosteneffizienten

Herstellbedingungen und ihre Eignung für präklinische Forschungszwecke. Allerdings kann die volle Funktionsvielfalt des menschlichen Darms durch Caco-2 Zellen aufgrund ihres kanzerogenen Ursprungs und der exklusiven Repräsentanz von Enterozyten nicht abgebildet werden.

Neben der Trägerstruktur die für den Aufbau der *in vitro* Modelle verwendet wird, trägt auch die zelluläre Einheit zur Etablierung von funktionalen Modellen bei, weshalb es von großer Bedeutung ist, die zelluläre Vielfalt des Dünndarms in diesen Modellen *in vitro* nachzuahmen. In diesem Zusammenhang sind die primären intestinalen Organoide, die sich hauptsächlich aus Enterozyten, Becherzellen, enteroendokrinen Zellen, Paneth Zellen, Vorläuferzellen und Stammzellen zusammensetzen, von großem Interesse, da die zelluläre Komponente eine große Ähnlichkeit zum nativen Epithel aufweist. Derartige primäre Organoide werden üblicherweise in einer 3D-Matrigel® Umgebung und einer speziellen Formulierung des Mediums, die mit einer Vielzahl an Wachstumsfaktoren ergänzt wird, um das Stammzellpotenzial zu erhalten, die Differenzierung zu hemmen, die Zellmigration zu stimulieren und somit eine langfristige *in vitro*-Kultivierung zu unterstützt.

Intestinale primäre Sphäroid-/Organoidkulturen wurden auf beiden BNC Varianten als Transwell®-ähnliche Modelle aufgebaut. Dabei zeigte sich eine fragmentierte Zellschicht was darauf schließen lässt, dass die Matrix unter diesen Bedingungen für den Modellaufbau ungeeignet ist. Da der BNC-Herstellungsprozess sehr flexibel ist, könnten die Oberflächen-eigenschaften in zukünftigen Studien angepasst werden, um so eine gute Zelladhäsion auch für primäre Darmzellen zu ermöglichen. Die Anwendung dieser Organoid-basierten Kulturen stellt jedoch für die präklinische Forschung eine enorme Herausforderung dar, da die Kultivierung komplex und zudem sehr zeit- und kosten-intensiv ist.

Im Hinblick auf das hohe Potenzial der primären intestinalen Sphäroide/Organoide und der Notwendigkeit eines vereinfachten aber prädiktiven Modells für präklinische Forschungs-zwecke, befasste sich der zweite Teil der Arbeit mit der Etablierung einer primären immortalisierten intestinalen Zelllinie, die eine standardisierte und kosteneffiziente Kultur ermöglicht, wobei die zelluläre Vielfalt der *in vitro* Organoid-Kulturen erhalten bleibt. In dieser Studie wurden primäre Organoide aus dem murinen und dem menschlichen Dünndarm durch die ektopische Expression eines 10- (murin) bzw. 12-Komponenten (human) Pools von Genen, welche im Hinblick auf die Regulation der Stammzellen und dem Zellzyklus bekannt sind, in Zusammenarbeit mit der InSCREENeX GmbH in einer 2D- und 3D-basierten Transduktionsstrategie immortalisiert. In erster Linie wurden die etablierten Zelllinien (Zellklone) auf ihren Bedarf an Wachstumsfaktoren für die Kultivierung unter vereinfachten und kosteneffizienten Bedingungen hin untersucht. Während die murinen Zellklone auf unbeschichteten Kunststoff in einer Mediumformulierung mit hEGF, mNoggin, Y-27632 und

10% FCS wuchsen, zeigten die humanen Zellklone eine Notwendigkeit für eine Col I-Vorbeschichtung zusammen mit einer Zusammensetzung des Mediums, wie sie üblicherweise für primäre humane Sphäroide/Organoide verwendet wird. Darüber hinaus führten diese vorangegangenen Analysen dazu, dass nur ein humaner Zellklon und drei murine Zellklone umfänglich charakterisiert wurden. Studien zu proliferativen Eigenschaften und spezifischen Gen- sowie Proteinexpressionsprofilen dieser Klone haben gezeigt, dass vermutlich Vorläuferzellen (TACs) anstelle der differenzierten Zelltypen der primären Organoide immortalisiert wurden, da die Kultivierung in 2D, 3D oder in Transwell®-basierten Modellen zu einem geringfügig veränderten Genexpressionsprofil im Vergleich untereinander und zudem zu einem stark reduzierten mRNA-Transkriptionswert für die analysierten Markergene, welche die differenzierten Zelltypen des nativen Epithels repräsentieren, die Folge war. Weiterhin zeigte die 3D-Kultivierung die Bildung von Sphäroid-ähnlichen Strukturen, jedoch keine Organoid-ähnlichen Strukturen unter verlängerten Kultur-bedingungen, was darauf hinweist, dass diese Zellpopulationen ihre Eigenschaft zur Differenzierung hin zu spezifischen intestinalen Zelltypen eingebüßt haben. Die Transwell®-basierten Modelle, welche für jeden Klon etabliert wurden, weisen zudem Organ-spezifische Eigenschaften auf, wie eine epitheliale Morphologie, ein charakteristisches Protein-expressionsprofil mit einer apikalen Schleimschicht, welche den Villin-1 positiven Zelllayer bedeckt und somit den Nachweis erbringt, dass die entstandenen immortalisierten Zellpopulationen zu einem gewissen Anteil aus Becherzellen und Enterozyten bestehen. Zudem konnten repräsentative Tight-Junction Komplexe, die auf eine dichte epitheliale Barriere hinweisen, in entsprechenden Proteinexpressionsprofilanalysen nachgewiesen werden. Der Nachweis einer sowohl dichten als auch funktionellen epithelialen Barriere konnte weitergehend durch TEER-Messungen und *in vivo*-ähnliche Transportmechanismen für die etablierten Zellklone qualifiziert werden, wodurch diese Zellen als alternative Zellquelle für *in vitro* Modelle des Dünndarms verwendet werden können. Darüber hinaus begünstigt die einfache Handhabung und Zellexpansion unter kostengünstigeren Bedingungen im Vergleich zu primären Organoidkulturen den Einsatz dieser neu-generierten Zellklone für Bioverfügbarkeits-Studien.

Zusammenfassend zeigte diese Arbeit neue Komponenten, strukturelle und zelluläre, für die Etablierung alternativer *in vitro*-Modelle des Dünndarmepithels, die in präklinischen Screenings für reproduzierbare Studien hinsichtlich der Medikamententestung verwendet werden können.

List of Figures & Tables

Abbreviations

°C	degree celsius
%	percent
®	registered
Ω	ohm
2D	two-dimensional
3D	three-dimensional
3Rs	replacement, reduction and refinement
5-HT	serotonin
µ	micro
µM/M	micromolar/molar
ab	apical/basolateral
ABC	ATP-binding cassette
ADP	adenosine diphosphate
AF	Alexa Fluor
AJ	adherens junction
ALT	alternative lengthening of telomeres
Anti-Anti	antibiotic-antimycotic
ATP	adenosine triphosphate
ba	basolateral/apical
BCRP	breast cancer resistance protein
Bmi1	B lymphoma Mo-MLV insertion region 1 homolog
BMP	bone morphogenetic protein
BMPRI/II	BMP receptor I/II
BNC	bacterial nanocellulose
bp	base pair(s)

BSA	bovine serum albumin
Cas9	CRISPR-associated protein 9
CBC	crypt base columnar cell
cDNA	complementary DNA
Chga	Chromogranin A
CLDN5	Claudin-5
cm^2/m^2	square centimeters/square meters
c-Myc	avian myelocytomatosis virus oncogene cellular homolog
CO_2	carbon dioxide
Col I	collagen-I
CRISPR	clustered regularly interspaced short palindromic repeats
d	day
DAPI	4',6'-diamidio-2-phylindole
DAPT	*N*-[*N*-(3,5-Difluorophenacetyl)-$_L$-alanyl]-*S*-phenylglycine *t*-butyl ester
Dll	delta-like ligand
DMEM	Dulbecco's Modified Eagle's Medium
DMSO	dimethyl sulfoxide
DNA	deoxyribonucleic acid
DNase	deoxyribonuclease
ECAD	E-cadherine
ECM	extracellular matrix
EDTA	ethylenediamine tetraacetic acid
EdU	5-ethynyl-2'-deoxyuridine
EEC	enteroendocrine cell
EF1-α	elongation factor-1 alpha
EFNB1	Ephrin-B1

e.g.	for example
EGTA	ethylene glycol-bis(β-aminoethyl ether)-*N,N,N',N'*-tetraacetic acid
EGF	epidermal growth factor
eGFP	enhanced green fluorescent protein
ERK	extracellular-signal-regulated kinase
EtOH	ethanol
et al.	et alii
f	female
FCS	fetal calf serum
FDA	Food and Drug Administration
FITC	fluorescein isothiocyanate
FN/Col I	fibronectin/collagen-I
g	unit of gravitational force or gram
GAB	guided assembly-based biolithography
GAG	glycosaminoglycan
GDP	guanosine diphosphate
GFP	green fluorescent protein
GI	gastrointestinal tract
GIP	glucose-dependent insulino-tropic peptide
Glc	glucose
GLP-1/-2	glucagon-like peptide-1/-2
GLUT	glucose transporter
Grb2	growth factor receptor-bound protein 2
h	hour or human
HBSS	Hanks' Balanced Salt Solution
H&E	hematoxylin & eosin

HEPES	4-(2-hydroxyethyl)-1-piperazineethanesulfonic acid
HES1	hairy and enhancer of split-1
HH	hedgehog
hOrg	human organoid
HPRT	hypoxanthine phosphoribosyltransferase
HTS	high throughput screening
Id	inhibitor of DNA binding 1
IF	Immunofluorescence
IHC	Immunohistochemistry
iPSC	induced pluripotent stem cell
ISC	intestinal stem cell
Jag1	Jagged-1
JAM	junctional adhesion molecule
kDA	kilo Dalton
kHz/Hz	kilohertz/hertz
KRAS	Kirsten rat sarcoma
K. xylinus	Komagataeibacter xylinus
L	liter
Lgr5	leucine-rich repeat-containing G-protein coupled receptor 5
LRC	label-retaining cell
LRP	Frizzled low-density lipoprotein receptor related protein
Lyz	Lysozyme
m	male; mouse/murine; meter; slope
Mam	mitochondria associated membranes
MBV	matrix-bound nanovesicle
Mdr1	multidrug resistance 1
MEK	MAPK/ERK kinase

min	minute(s)
mm	millimeter
mOrg	murine organoid
mRNA	messenger RNA
MRP2	multidrug resistance-associated protein 2
Muc	mucin
mV	millivolt
n	nano
Nanog	homeobox transcription factor Nanog
NEAA	non-essential amino acids
NICD	notch intracellular domain
NP	nanoparticle
NOG	noggin
OCLN	occludin
P	passage
P_{app}	apparent permeability coefficient
PBS	phosphate-buffered saline
PC	polycarbonate
PD/PDL	population doubling/ population doubling level
PDMS	polydimethylsiloxane
PE	polyethylene
Pen/Strep	penicillin-streptomycin
PET	polyethylene terephthalate
PFA	paraformaldehyde
p-gp	*p*-glycoprotein
pH	power of hydrogen
PLGA	poly(lactic-*co*-glycolic acid)

PLO	poly-L-ornithine
pRb	retinoblastoma protein
Raf	rapidly accelerated fibrosarcoma
Ras	rat sarcoma
RBP-J	recombinant signal binding protein for immunoglobulin kappa J (CSL in mouse)
Rex-1	zinc finger protein 42
RNA	ribonucleic acid
Rpl15	ribosomal protein L15
rpm	revolutions per minute
Rps29	ribosomal protein S29
RSPO	R-Spondin
RT	room temperature
RT-qPCR	real-time quantitative polymerase chain reaction
s	second(s)
SC	stem cell
SD	standard deviation
SDS	sodium dodecyl sulfate
SEM	scanning electron microscopy
SGLT	sodium-glucose linked transporter
SIS	small intestinal submucosa
SISmuc	SIS with preserved mucosa
Smad	SMA protein *C. Elegans* and MAD protein *Drosophila*
Sos	son of sevenless
str	surface-structured
t	time
TA	transient amplifying

TAC	transient amplifying cell
TAG/Tag	SV40 large T Antigen
TBS-T	tris-buffered saline and tween 20
TCF4	transcription factor 4
TEER	transepithelial electrical resistance
TEM	transmission electron microscopy
TERM	Tissue Engineering and Regenerative Medicine
TERT	telomerase reverse transcriptase
TFR	terminal restriction fragmentation
TGF-β	transforming growth factor beta superfamily
TiN	titanium-nitride
TJ	tight junction
unmod	unmodified
Vil1	Villin-1
w	weeks
w/o	without or uncoated
Wnt	named after the *Drosophila* segment polarity gene wingless (wingless-type MMTV integration site family member)
y	year(s)
ZEMM	Zentrum für Experimentelle Molekulare Medizin
ZO-1/-2	zonula occludens-1/-2

1. Introduction

1.1. The small intestine

1.1.1. Anatomical and structural organization of the small intestine and its main functions

The gastrointestinal tract (GI) consisting of the esophagus, stomach, small intestine and the large intestine (Figure 1.1A) represents one of the biggest organ systems in humans and rodents [1,2] with a mean length of about 7.62 m [1] and an average mucosal surface area of ~ 32 m² in humans [3]. In comparison, the murine GI tract is about 55.5 cm in length with a surface area of ~ 402.31 cm² [4].

Main functions of the GI tract comprise food uptake, distribution, processing and digestion as well as nutrient and energy absorption [5]. A crucial role in this context plays the small intestine with an average length of 3-5 m in humans [6], where 90% of food digestion occurs by chemical processes using bile acids and digestive enzymes to break down the food into nutrients that can be taken up into circulation [5,7–9].

Anatomically, the small intestine can be separated into three parts: the proximal duodenum, the intermediate jejunum and the distal ileum (Figure 1.1A), each of them characterized by region-specific functions and uptake capacities for distinct nutrients. The proximal duodenum is the shortest section (average length: 20-25 cm [6]) connected to the stomach, the liver and the pancreas being responsible for neutralization of the acidic chyme released from the stomach by secreting bicarbonates into its lumen [6,8]. Further, most of chemical digestion happens in the duodenum to break down the chyme into nutrients that can be absorbed by specialized transport mechanisms. Liver-secreted bile and digestive enzymes released from the pancreas as well as the intestinal epithelium are crucial for this process. In addition, nutrients, electrolytes, water and metal ions are absorbed in the proximal duodenum [8]. The connecting jejunum is around 2.5 m in length, where the largest proportion of nutrients including sugars, amino and fatty acids are absorbed [6]. In contrast, the distal ileum with an average length of 3 m reabsorbs only special nutrients such as vitamin B12, bile salts or non-digested remnants [6,8].

Considering the structural organization, the small intestine is formed as a hollow tube with several tissue layers. The *tunica serosa* as outermost sheet is comprised of connective tissue (*lamina propria serosae*) with intervened vessels and nerve fibers. Adjacent, the *tunica muscularis*, build up of a thin longitudinal and a thick circular muscle layer, both connected with each other via nerve fibers, regulates the direct proximal to distal transport of the chyme through the intestinal tract by initiating peristaltic movements of the gut tube. Between the

muscle layer and the intestinal *mucosa*, a highly vascularized collagen sheet known as the *tela submucosa* ensures a sufficient exchange of nutrients and growth factors. Further, the luminal *mucosa* consists of a thin layer of smooth muscle cells (*lamina muscularis*) covered by connective tissue with incorporated immune cells (*lamina propria*) and a monolayer of epithelial cells [7,10,11] (Figure 1.1B). Together, the *submucosa* and the *mucosa* build protrusions called villi towards the lumen thereby enhancing the apical surface, which implicates an increased nutrient uptake capacity of the epithelium [3,7]. Of note, those villi structures are intermingled by crypt regions representing the germinal zone of the small intestinal epithelium where continuous cell renewal and proliferation occurs (discussed in more detail in the next section).

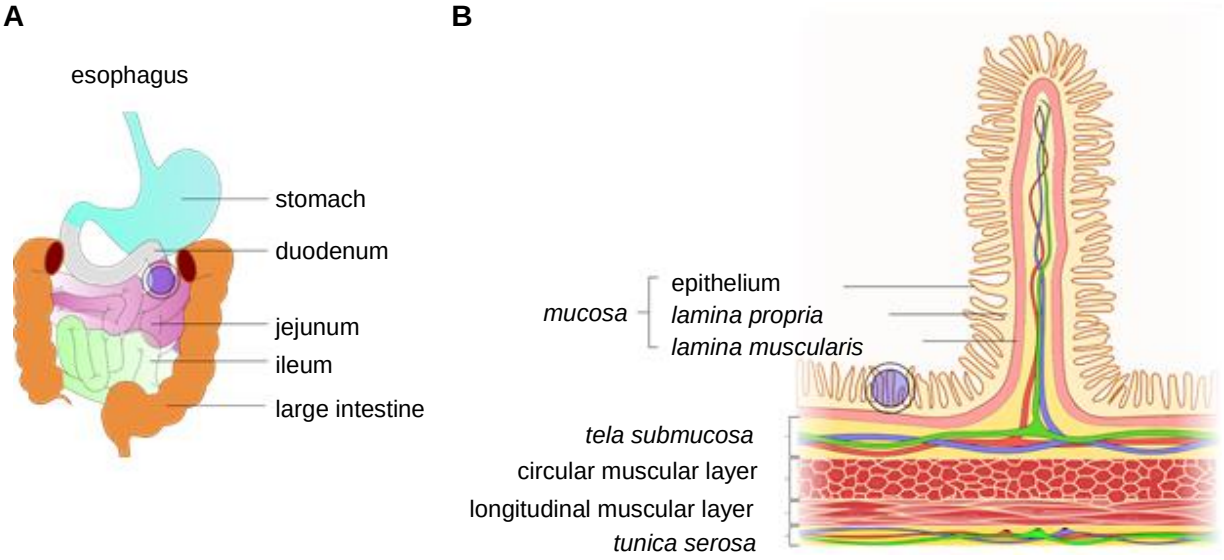

Figure 1.1: Structural organization of the GI tract and the small intestine. Schematic overview of the GI tract including the stomach, the small intestine divided into duodenum, jejunum, ileum and the large intestine **(A)**. Structural organization of the small intestine composed of several tissue layers including the *mucosa* (epithelium, *lamina propria*, *lamina muscularis*), the *tela submucosa*, the *muscularis* (circular and longitudinal muscular layer) and the *tunica serosa* **(B)**. Image adapted and modified from Däullary et al. [7]. GI: gastrointestinal.

The individual villus structures of the small intestine together with the diversity of specifically functionalized cell types ensure food digestion and nutrient absorption with high efficiency. Mucus, enzymes and ions secreted mainly by epithelial cells are essential to break down nutrients such as proteins, lipids or carbohydrates [7,12,13]. The substances resulting from this chemical digestion process like amino acids, glucose or short-chain fatty acids are absorbed or transported across the intestinal epithelium by passive diffusion, active or a

carrier-mediated transport [14,15]. Of note, the diffusion process between neighboring cells of the intestinal epithelium is dynamically regulated via the cytoskeleton by the interaction of junctional complexes (tight junctions, adherens junctions or desmosomes) with the peri-junctional ring of actin and myosin (Figure 1.2). Tight junctions (TJs) consist of two functional protein categories: 1) integral transmembrane proteins such as occludin (OCLN), claudins or junctional adhesion molecules (JAMs) and 2) peripheral membrane proteins such as zonula occludens-1 or -2 (ZO-1 or ZO-2), which seal the intercellular space [16,17] (Figure 1.2). Transmembrane proteins are capable to form size- and charge-selective pores for the permeation of small molecules, water and ions, whereas the peripheral membrane proteins are connected to the cytoskeleton to give the TJ complexes their unique structure and function [18–20]. Strong adhesive bonds formed by desmosomes and adherens junctions (AJs) such as E-Cadherin (ECAD) are located below the TJs, contributing to intestinal barrier integrity [16,18] (Figure 1.2).

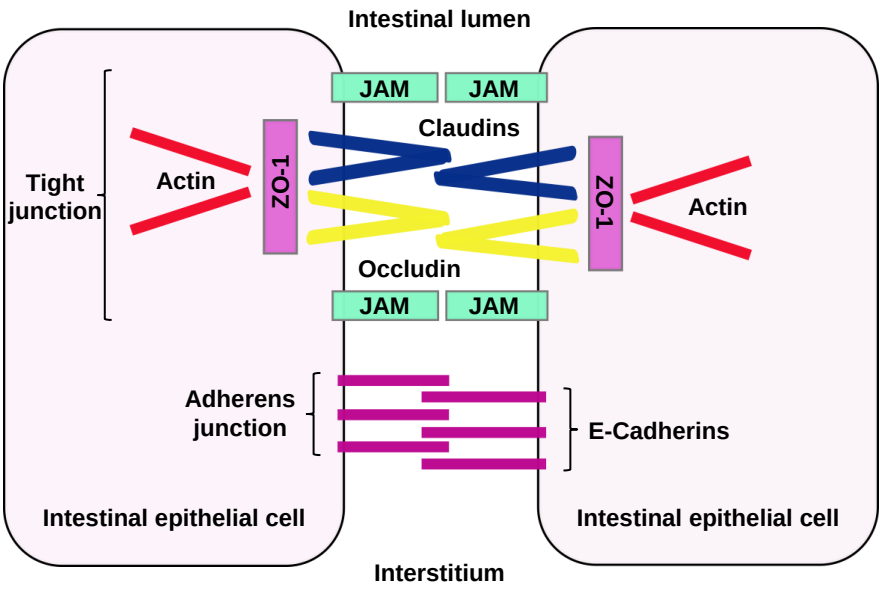

Figure 1.2: Intestinal epithelial-cell junctions important for intestinal barrier integrity. TJs are composed of transmembrane proteins such as different subtypes of Claudins (blue), Occludin (yellow) and diverse JAMs (green) attached to peripheral membrane proteins such as ZO-1 (purple), thereby anchoring TJ proteins to intercellular actin (red). AJs including E-Cadherin (dark purple) further support cell-cell contacts. Image adapted and modified from Hammer et al. [21]. TJs: tight junctions; JAMs: junctional adhesion molecules; ZO-1: zonula occludens-1; AJs: adherens junctions.

1.1.2. Cellular composition of the small intestinal epithelium and molecular regulation of epithelial homeostasis

The small intestinal epithelium, with its rapid turnover rate every 3-5 days [22–24], represents a remarkable microstructure characterized by its separation into crypt-villus-domains (Figure 1.3A). Within these domains, the luminal villus regions are intermingled by tube-shaped invaginations called crypts, that can be separated into the stem cell niche and the transit amplifying (TA) zone (Figure 1.3A). In addition to multipotent intestinal stem cells (ISCs), which are defined by their unlimited self-renewal and potential to differentiate into all epithelial cell types [25–28], the stem cell niche is further constituted by differentiated paneth cells [29,30] and subepithelial myofibroblasts [31,32] (Figure 1.3B), both secreting crucial factors for the maintenance of the stem cell identity or the regulation of ISC differentiation.

In recent years, two types of ISCs have been identified in the crypt: the fast-cycling crypt base columnar (CBC) cells [27] and the slow-cycling +4 label retaining cells (LRCs) (Figure 1.3B) [33]. CBCs marked by the Leucine-rich repeat-containing G-protein coupled receptor 5 (Lgr5) were first reported by Barker et al. [22] as crucial for the regeneration of the epithelium [22,34]. Maintenance of CBC identity in the crypt is ensured by asymmetric cell division with one daughter cell retaining in the crypt, while the other one represents a transient amplifying cell (TAC) that migrates towards the TA region [33,35] (Figure 1.3B). Within the TA region, TACs proliferate and migrate along the villus, thereby differentiating into enterocytes, enteroendocrine cells and goblet cells [36] (Figure 1.3A). In addition, paneth cells, another differentiated cell type present in the small intestine, escape the upward migration process remaining localized within the crypt, where they are of high importance, as they secrete growth factors such as wingless-related integration site (Wnt), the epidermal growth factor (EGF) and the delta like ligand 4 (Dll4), all of them activating stemness-related signaling pathways [37,38]. Further, paneth cells maintain gut homeostasis by secreting a variety of substances, such as antimicrobial peptides, cytokines and proteases to protect the neighboring CBCs from external harmful (*e.g.* pathogenic) influences [39,40] (Figure 1.3B). In addition to CBCs, slow-cycling +4 LRCs, named after their specific position in the crypt, represent the second stem cell type depicted by their quiescent nature and the expression of B lymphoma Mo-MLV insertion region 1 homolog (Bmi1) [24,41,42]. Interestingly, +4 LRCs can revert into mitotically active $Lgr5^{+}$-ISCs after injury of the CBC population [24,42]. In addition, Buczacki et al. provided evidence that these cells function as additional precursors of the secretory-lineage giving rise to paneth cells when the CBC population is injured [43].

In contrast to the crypt, the villus domain represents an elongated structure with differentiated enterocytes as most prominent cell population (Figure 1.3A) that play a major

role in nutrient digestion and nutrient absorption secreting digestive enzymes and presenting specialized transporter proteins for molecule absorption on the apical cell surface, also known as brush border membrane. To increase nutrient absorption and enzyme secretion at the luminal surface, the villus epithelium is further enlarged by microscopic membrane protrusions called microvilli [3,44]. Next to the enterocytes, the villus epithelium contains hormone-secreting enteroendocrine cells (EECs) and mucin-producing goblet cells. Different subpopulations of EECs comprising L-, K- or M-cells fulfill distinct functions after individual nutrient-derived stimulation such as regulation of appetite, gut motility, blood glucose homeostasis or acidity of the stomach-released chyme [7,45] controlled by the release of peptide hormones including somatostatin, glucose-dependent insulino-tropic peptide (GIP) or glucagon-like peptide 1 and 2 (GLP-1, GLP-2) [46] as well as bioactive amines such as serotonin (5-HT) [45,47] (Figure 1.3A). The main function of goblet cells is to synthesize the secretory mucin glycoprotein (mucin 2) and the bioactive membrane-bound mucins (mucin 1, mucin 3) in order to protect the epithelium from pathogenic microbes as well as physical/mechanical stress caused by the passing chyme [48–50] (Figure 1.3A).

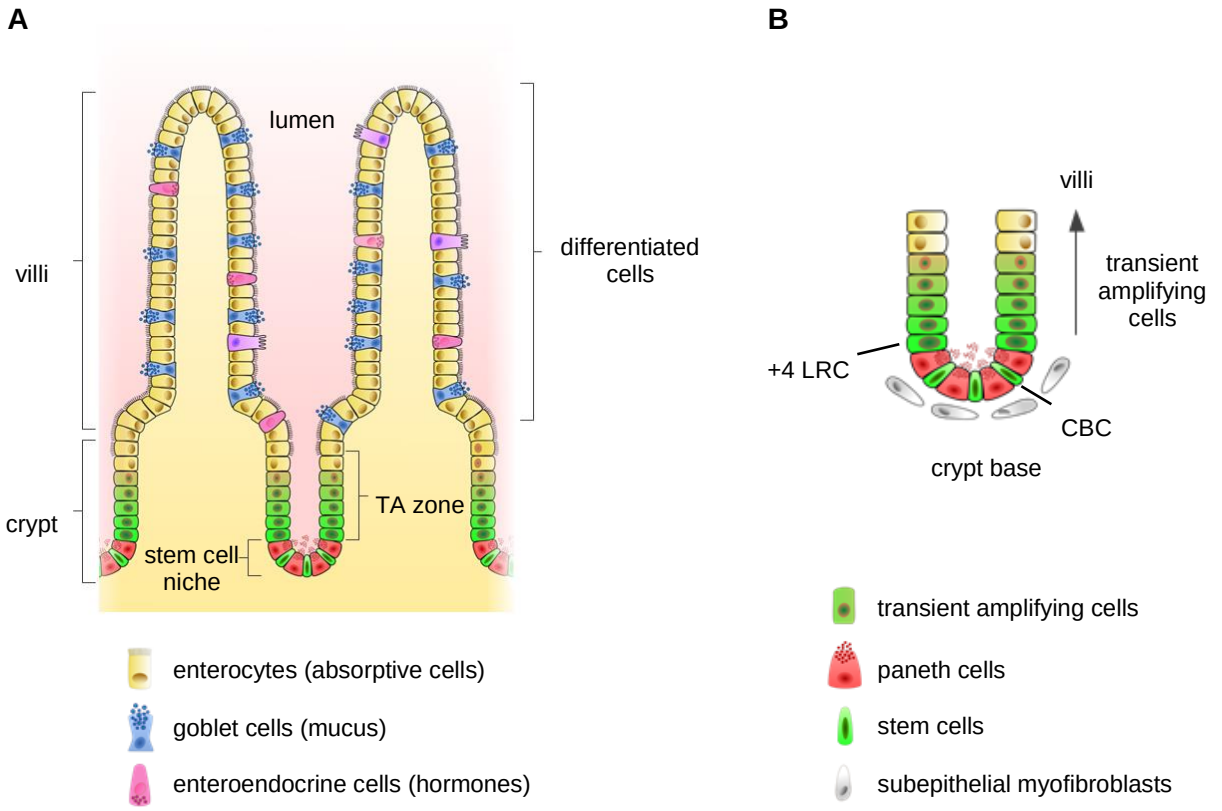

Figure 1.3: Cytomorphology of the intestinal epithelium. Schematic illustration of the crypt-villus organization and cellular composition of the small intestinal mucosa **(A)**. The villus-domains are composed of differentiated cell types such as enterocytes, goblet cells and enteroendocrine cells. The proliferative crypt region is structured into the stem cell niche (crypt base) and the TA zone, in which the main stem cell types categorized as ($Lgr5^{+}$)-CBCs and +4 LRCs are located intermingled by paneth cells at the crypt base, while TACs are located within the TA zone **(B)**. TA: transient amplifying; CBCs: columnar base cells; LRCs: label retaining cells; TACs: transient amplifying cells.

Regeneration of the small intestinal epithelium is driven along the crypt-villus axis by opposing protein gradients of morphogens that regulate ISC proliferation in the crypt and differentiation along the villus [30]. Within the crypt, growth factors and ligands such as Noggin (NOG), R-Spondin (RSPO), EGF and Wnt are key players that are secreted to activate their corresponding signaling cascades to support ISC expansion and stemness (Figure 1.4A). Simultaneously, pro-differentiation pathways such as bone morphogenetic protein (BMP) or hedgehog (HH) signaling are suppressed at the crypt base, while being active along the TA zone and villus region, where increasing gradients of BMP, HH or ephrin B1 (EFNB1) drive differentiation of cells migrating upwards the villus before they undergo apoptosis/anoikis at the villus tip after 3-5 days [7,51] (Figure 1.4A). Hence, stem cell identity and lineage-differentiation in the small intestinal epithelium is tightly regulated by a controlled interplay of distinct signaling cascades [51].

An important pathway that supports ISC identity is the canonical Wnt pathway that is activated by binding of the WNT ligand (secreted by paneth cells in the crypt) to the Frizzled-low-density lipoprotein receptor-related protein 5/6 (LRP5/6) receptor complex, leading to the stabilization of cytoplasmic β-catenin that translocates into the nucleus where it binds to its target genes such as the transcription factor 4 (TCF4). TCF4 is known to contribute to the transcriptional activation of pro-proliferative and anti-differentiation genes in ISCs to maintain their stem cell nature [52,53]. Furthermore, ISC stemness is supported by binding of the Wnt pathway agonist RSPO1 to the LGR4/LGR5 receptor complex which results in an increased phosphorylation of LRP6 [54–56] that leads to the potentiation of cytosolic ß-catenin accumulation [56]. Subsequently, β-catenin is translocated into the nucleus where it binds to TCF4, thereby activating further downstream target genes involved in ISC expansion and maintenance of their stemness (Figure 1.4B).

Further factors such as DII1/4 or Jagged 1 (Jag1), all expressed by paneth cells, act as ligands of the Notch signaling cascade that bind to the transmembrane Notch receptor located in neighboring stem cells to modulate the ISC state. After activation, metalloproteases of the ADAM family and the γ-secretase enzyme lead to the release of the Notch intracellular domain (NICD) from the membrane, which assembles with the DNA-binding protein recombination signal binding protein for immunoglobulin kappa J (RBP-J; also known as CSL) and the co-activator mastermind (Mam) within the nucleus of ISCs to transcriptionally activate the hairy and enhancer of split-1 (Hes1) promoter, thereby preserving the ISC and/or TAC state, while inhibiting differentiation [57–59] (Figure 1.4B).

Next to Wnt/R-Spondin- or Notch-signaling, secretion of EGF by paneth cells supports proliferation as well as migration of ISCs and further inhibits apoptosis of crypt cells [60–62]. Due to binding of EGF to its receptor (EGF receptor; EGF-R), which is located in the ISC membrane, phosphorylation of the terminal proportion of the receptor occurs to provide complex formation with the adaptor proteins growth factor receptor-bound protein 2 (Grb2) and son of sevenless (Sos). Following complex formation, Ras-GDP is recruited, resulting in the activation of the tyrosine kinase cascade Ras/Raf/MEK/ERK [29,60,63]. Finally, the activated kinases are shuttled into the nucleus to phosphorylate specific transcription factors involved in cell proliferation or migration [63] (Figure 1.4B).

In contrast to these stemness-related signaling pathways, BMP secreted by mesenchymal cells regulates the differentiation of $Lgr5^{+}$-ISCs along the crypt-villus axis [64]. To this aim, BMPs and other members of the transforming growth factor-β (TGF-β) family bind to their type II receptor (BMPRII), resulting in phosphorylation and activation of BMPRI, followed by the activation of Smad protein transcription factors (Smad 1, 2, 3, 5 and 8). Together with Co-Smad (Smad 4), the complex translocates into the nucleus to repress stemness-related

genes such as *Lgr5*/*LGR5*. To sustain ISC stemness in the crypt, active BMP signaling is blocked by growth factors such as NOG or gremlin-1/gremlin-2 released by subepithelial myofibroblasts beneath the crypt [65–67] (Figure 1.4B).

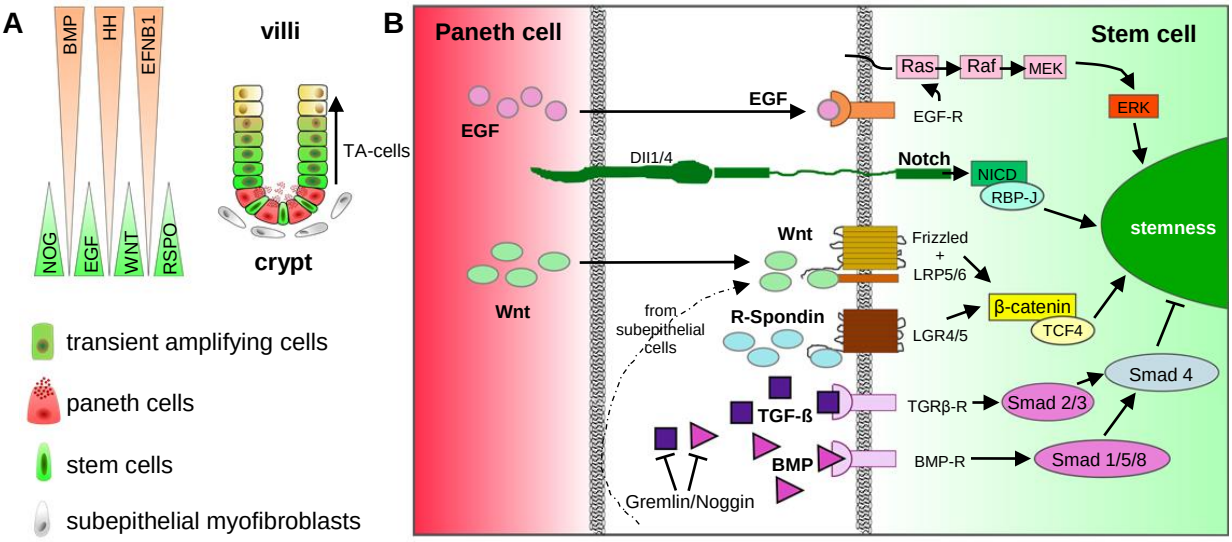

Figure 1.4: Morphogene gradients acting along the crypt-villus axis. Growth factors such as NOG, EGF, WNT and RSPO maintain ISC stemness in the crypt, whereas BMP, HH as well as ENFB1 regulate differentiation of TACs along the villus **(A)**. Scheme of the interplay of important growth factors regulating different signaling pathways within the stem cell niche **(B)**. BMP: bone morphogenetic protein; Dll: delta-like ligand; EGF: epithelial growth factor; EFNB1: ephrin-B1; ERK: extracellular-signal regulated kinase; HH: hedgehog; LGR: leucine-rich repeat-containing G-protein coupled receptor; LRP: Frizzled low-density lipoprotein receptor related protein; MEK: MAPK/ERK kinase; NICD: notch intracellular domain; NOG: noggin; R: receptor; RBP-J: recombinant signal binding protein for immunoglobulin J; Raf: rapidly accelerated fibrosarcoma; Ras: rat sarcoma; RSPO: R-Spondin; Smad: SMA protein *C. Elegans* and MAD protein *Drosophila*; TCF4: transcription factor 4; TGF: transforming growth factor; Wnt: wingless-related integration site. Figure modified from Sato et al. 2011 [30].

1.2. The small intestine as functional barrier

The mucus layer, a gel-like protein sheet covering the intestinal epithelium inside the gut lumen, constitutes a first line physical defense barrier against external molecules and pathogens [68–70]. This layer is formed by highly glycosylated mucin proteins (*e.g.* mucin 1 (MUC1), MUC2, MUC3), secreted and membrane-bound [50], with MUC2 as the most abundant protein in the small intestine that has a complex layered structure, where it is tightly adherent [70–75]. In addition, MUC6 and MUC11 have been reported in the small intestine [76]. Due to the continuously secreted protein layer, everything that aims to reach the intestinal epithelium has to diffuse through the mucus barrier.

In addition to the mucus layer, the epithelium itself represents a highly sophisticated physical barrier [77] based on strong junctional complexes (described above; see Figure 1.2), formed between individual epithelial cells [15,16,78]. Substrate and nutrient transport across this barrier into the interstitium is organized in a tightly regulated manner by three major pathways categorized as transcellular, carrier-mediated and paracellular transport [15,78] (Figure 1.5).

The paracellular transport pathway, considered as passive diffusion process, is controlled by the intercellular space in the most apical part of neighboring cells. Extracellular tight junction proteins, creating narrow water-filled pores between adjacent cells, seal this intercellular gap to form a strong physical barrier. Ions, water and small hydrophilic molecules are allowed to pass the epithelial barrier, depending on the local concentration gradient [15,79], to enter the bloodstream (Figure 1.5B).

The transcellular pathway describes both a passive diffusion process (Figure 1.5A) and an active transport of transporter-specific molecules by co-transporters (Figure 1.5B and C). Therefore, an aligned and polarized epithelial layer with distinct cellular differences in the membrane composition, on the apical or the basolateral cell membrane, is crucial [79]. Passive diffusion via the transcellular pathway is regulated along a concentration gradient either directly through the cell membrane, as it is the case for hydrophobic molecules or by specific transporters, which are selective for only one molecule [79,80]. For instance, fructose as a carbohydrate digestion product is absorbed by the glucose transporter 5 (GLUT5) without energy consumption [80,81]. In comparison, there are also active transport mechanisms such as the transport of glucose across the apical membrane performed by the sodium glucose co-transporter 1 (SGLT1) that transports glucose (Glc) together with sodium (Na^+) into the cell, driven by the Na^+/K^+-ATPase (Figure 1.5B). Therefore, ion pumps located on the basolateral side of the cell such as the Na^+/K^+-ATPase hydrolyze adenosine triphosphate (ATP) to adenosine diphosphate (ADP) by simultaneous replacement of Na^+

ions in the cell with K^+ ions [82]. The exchange of sodium (Na^+) with calcium (Ca^{2+}) is also mediated via an active transcellular transport (Figure 1.5C) under ATP consumption by the transmembrane antiporter termed sodium-calcium-exchanger [83,84].

Efflux-transporters (Figure 1.5C) are located within the apical membrane to actively pump harmful cytotoxic molecules out of the cell towards the intestinal lumen [85,86]. The *P*-glycoprotein (*p*-gp) encoded by the multidrug resistance (*MDR1*) gene belongs to the ATP-binding cassette (ABC) transporter family and is one of the most important efflux-transporters in the intestinal tissue [87,88]. The breast cancer resistance protein (BCRP) as well as the multidrug resistance-associated protein 2 (MRP2) are further members of the ABC-transporter family using a carrier-mediated pathway for eliminating substances like heterocyclic amines, polycyclic aromatic hydrocarbons, glutathione or sulfated and glucuronidated conjugates back into the intestinal lumen [87,89–91]. In general, these transport mechanisms act in an ATP-dependent manner against the concentration gradient driven by the Na^+/K^+-ATPase [87].

In addition, active transport can also occur by internalization of large molecules and particles by the cell membrane, if they cannot be transported across the cellular barrier due to their size, polarity or non-existing transporters [92]. This process is defined as endocytosis and is further divided into phagocytosis and pinocytosis [93]. The former activity binds bacteria or cell debris, resulting in the formation of an intracellular vesicle (phagosome), which fuses with lysosomes to digest these particles. Pinocytosis provides a selective uptake of macromolecules by the invagination of the cell membrane, whereby different budding events have to be distinguished, such as clathrin-mediated [94], caveolae-dependent [95] or flotillin-dependent [96,97] endocytotic pathways. For instance, the clathrin-mediated pathway belongs to the group of receptor-mediated processes where ligands bind to the surface receptors that are located in clathrin-coated pits to form an intracellular clathrin-coated vesicle for trafficking [92,98] through the cell (Figure 1.5D). In contrast to clathrin-mediated pathways, caveolae-dependent processes are driven by integral (caveolins) and peripheral membrane proteins (cavins) which leads to small bulb-shaped plasma membrane invaginations for the transport through the cell [99]. Interestingly, flotillin-mediated endocytosis shows morphological similarities to the caveolae plasma membrane buds; however, flotillin proteins, localized in special microdomains, are involved this process [97].

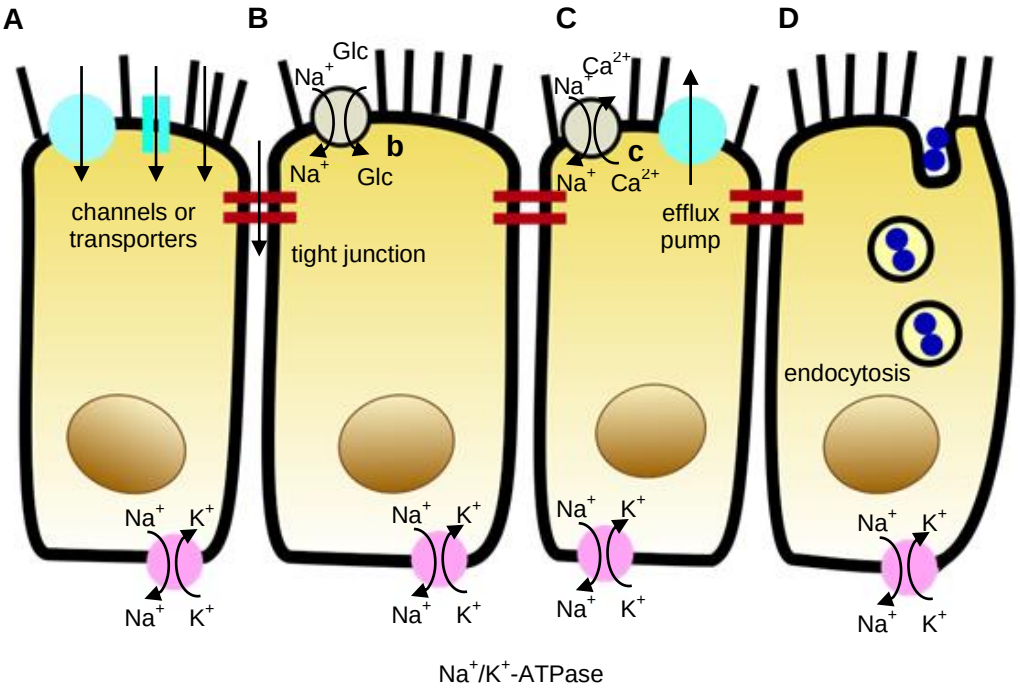

Figure 1.5: Transport mechanisms in the small intestine. Transcellular transport through channels or transporters or directly over the cell membrane **(A)**, transcellular active transport by symporter **(B/b)** or antiporter **(C/c)**, paracellular transport between adjacent cells **(B)**, efflux transport under ATP consumption **(C)** and uptake of substances via vesicles by the endocytotic pathway **(D)**. ATP: Adenosine triphosphate.

1.3. Pre-clinical intestinal model systems

In the past, research on small intestinal biology, physiology and function as well as associated disorders relied on the use of animal models that led to fundamental insights and concepts; however, the use of animal models possesses major limitations including species-specific differences and ethical concerns, as main representatives. To overcome common drawbacks, human *in vitro* models have been established with distinct complexities ranging from simple two-dimensional (2D) cell culture to more complex multicellular three-dimensional (3D) models mimicking *in vivo*-like structural organizations [7]. Those models gain more and more reputation, as they facilitate the study of complex *in vivo* phenomena in a simplified context under standardized and reproducible conditions, while being less expensive, accessible to any laboratory and being conform to the 3Rs (replacement, reduction, refinement) principle [100–102]. Regarding the predictivity and transferability of the achieved data to humans, *in vitro* models of human origin exclude species-specific differences and mimic native cell and tissue function, physiological and metabolic principles in a more precise fashion.

Nowadays, cell-based models of the small intestine are routinely used in fundamental research focusing on general biological principles and mechanisms such as the molecular regulation of cell functions and overall tissue homeostasis or pathophysiological principles of organ-specific disorders as well as to understand host-microbial interactions during tissue infection [103,104]. Additionally, cell-based models gain also more and more interest for pharmaceutical applications including studies on the bioavailability [105,106] and toxicity [107] of drugs. In this context, Kitchens and colleagues demonstrated an enhanced transepithelial transport capacity, and thereby bioavailability of surface-charged polymers that are often used for drug-loading, as diffusion or carrier-mediated transport is simplified due to their surface properties, especially if single drugs cannot properly pass the epithelial barrier [105]. Focusing on translational research, *in vitro* models of the small intestine are interesting in terms of drug screening approaches or cell-based therapies in context of personalized medicine. For example, identification of genetic mutations by genome or transcriptome sequencing combined with clustered regularly interspaced short palindromic repeats/CRISPR-associated protein 9 (CRISPR/Cas9)-based correction of those mutations in *in vitro*-cultured organoids of the small intestine opens the possibility for potential transplantation approaches of the genetically-engineered organoids into diseased regions of the patient's gut. For example, CRISPR/Cas9 technology enabled the targeting of the most frequently mutated genetic hotspots in intestinal stem cells derived from a patient suffering from colorectal cancer [108,109]. Furthermore, artificial introduction of the oncogenic Kirsten rat sarcoma (KRAS) mutation by CRISPR/Cas9 into patient-derived tumor organoids were

recently shown as beneficial to evaluate drug efficacy in a pre-clinical study [110], which proofs the suitability of this experimental procedure in context of patient-specific drug screening approaches.

In the past, *in vitro* models used in preclinical research applications were set up as 2D cell monolayers cultured on flat and rigid plastic until confluence. Such models led to important findings regarding the function of the small intestine as well as the toxicity of applied substances in a standardized and scalable manner [7,111,112]. However, they lack in important cell-cell or cell-matrix interactions [113] and only marginally represent physiological features, thereby being only limited feasible for permeability or bioavailability studies. Further, cellular processes such as proliferation, apoptosis or differentiation as well as gene or protein expression profiles are not fully comparable to the *in vivo* situation [113,114].

Innovative concepts in the last years led to the development of advanced 3D *in vitro* models, which are more representative concerning the physiological and functional aspects of the native organ [112,113,115]. These models are characterized by the use of biological or synthetic scaffolds to culture intestinal cell types in a so-called Transwell®-like setup [116]. Nevertheless, key challenges remain that *in vitro* models meet the requirements to adequately represent the natural situation *in vitro* including the replication of native cytoarchitectural topographies such as a polarized cell-monolayer with formation of a tight epithelial barrier composed of the cellular diversity of the native epithelium. Furthermore, biological features such as tissue homeostasis must be recapitulated *in vitro* to maintain ISC stemness, while simultaneously allowing differentiation. In addition, mechanistic and functional aspects need to be sustained that are regulated by the precise activity of characteristic gene expression profiles, especially those of distinct transporter proteins such as MDR1 or SGLT1. Next to this, the substratum with a 3D structure similar to the native *lamina propria* in terms of chemical composition as well as biochemical properties is of high importance for the recreation of *in vivo*-like conditions in tissue engineering-based concepts [102,117,118]. Furthermore, cells used for the setup of *in vitro* models should be of human origin with the ability of being cultured in the long-term without losing their characteristic features. In the following, the main scaffold materials and cell sources used for current concepts in small intestinal tissue engineering are summarized (Figure 1.6).

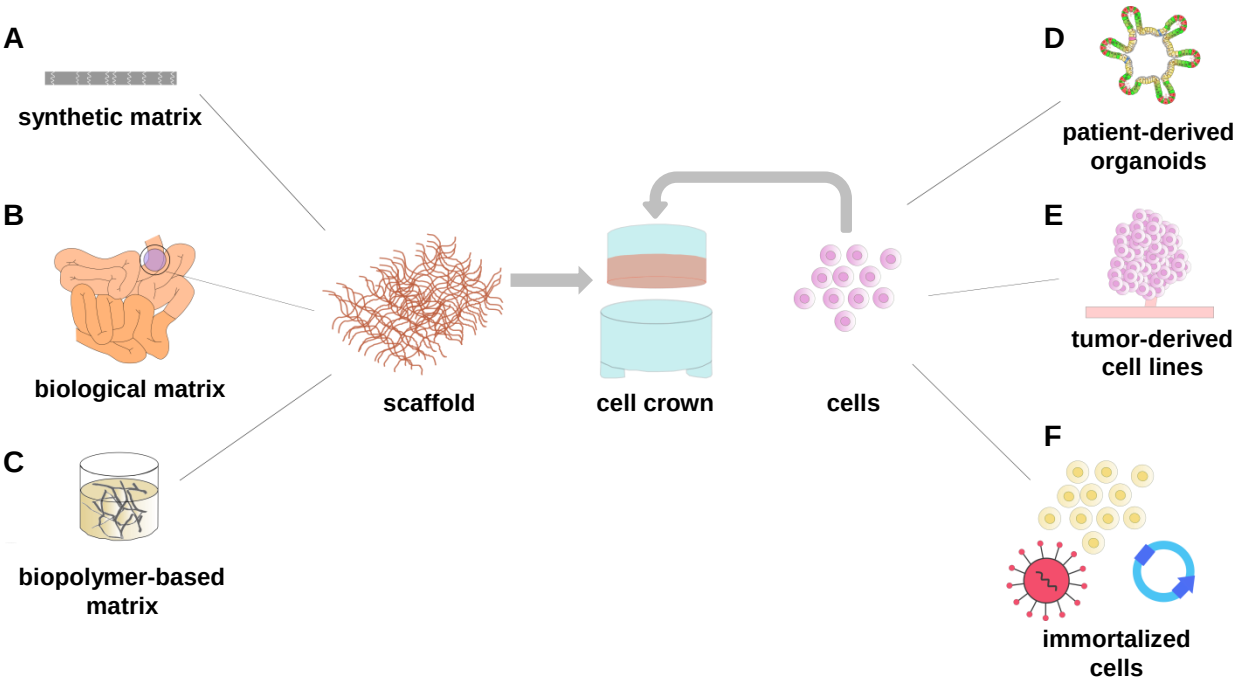

Figure 1.6: Schematic overview on intestinal model systems used in pre-clinical applications. Intestinal Transwell®-like *in vitro* models are composed of a matrix for separation into an apical and a basolateral compartment corresponding to the intestinal epithelium. Synthetic **(A)** or biological matrices **(B)** as well as biopolymer-based scaffolds **(C)** are commonly used for model setup. Primary tissue-derived intestinal organoids **(D)**, tumor-derived intestinal cell lines **(E)** or intestinal immortalized cells **(F)** are seeded on top of the scaffold variants, thereby generating Transwell®-like *in vitro* models.

1.3.1. Scaffold materials in intestinal tissue engineering

Of main importance in tissue engineering is to provide structural support to allow cell attachment within/on the *in vitro* model and a microenvironmental niche to regulate model homeostasis by controlling cell proliferation and survival as well as apoptosis. Nature's blueprint for this is the extracellular matrix (ECM), present in all tissues and organs, which provides structural, biological and physical support to cells during development and throughout life. Interestingly, there is a dynamic crosstalk of the ECM and the resident cells. While the ECM provides signaling cues influencing cell behavior, cells can modify their secreted ECM components in response to alternating microenvironmental stimuli [119].

Although, the 3D network of all ECMs is composed of fibrous proteins such as collagen, fibronectin or laminin together with a mixture of glycosaminoglycans (GAGs), matrix-bound nanovesicles (MBVs) and water, each tissue shows a unique composition and topology [120,121]. Distinct protein compositions thereby facilitate processes like the strength or the load-bearing capability of the ECM and further provides anchoring sites for the cell

membrane to the ECM network by the interaction with collagens and laminins in an organ-specific manner [120]. Within the small intestine, the basement membrane is a specialized ECM surrounding the stem cell niche that is mainly composed of laminins, collagen IV as well as fibronectin [51,122]. Recently, Gjorevski et al. showed in a matrix reconstitution study with intestinal epithelial cells that the biochemical and biophysical characteristics of the ECM influence ISC homeostasis concerning stem cell behavior, maintenance, proliferation and differentiation [123]. Mainly involved in these regulatory processes are the matrix stiffness, the detailed protein composition of the basement membrane and the created reservoirs for soluble factors [51,124]. Considering the characteristic crypt-villus-axis of the small intestine, a few studies [125,126] have also re-created this specific tissue architecture to recapitulate the *in vivo* situation. Therefore, collagen scaffolds are micromolded by 3D printed stamps [125] or hydrogels are directly printed as 3D scaffolds by stereolithography [127] to generate the typical crypt-villus architecture. Next, biological 3D scaffolds with a natural crypt-villus architecture are used in tissue engineering concepts. These scaffolds, obtained by decellularization of the porcine small intestinal tissue, are known as small intestinal submucosa with preserved mucosa (SISmuc) [128]. However, such systems are complex in handling, cost-intensive and high-throughput incompatible, which makes them unsuitable for pre-clinical research approaches.

Given the importance of the ECM *in vivo*, *in vitro* models of the small intestine require a comparable scaffold that was, so far, simulated by mainly artificial matrices to re-create the intestinal barrier *in vitro*. By means of an artificial membrane, a two-compartment system is generated with an apical side corresponding to the intestinal lumen and a basolateral side recapitulating the interstitium. However, these simplified 3D-like systems mimic the *in vivo* epithelium only to some extent. Therefore, decellularized biological scaffolds or biopolymer-based scaffolds are taken into account, to enable a 3D structure for cell adherence that is more *in vivo*-like but still cost-efficient and easy in handling.

1.3.1.1. Artificial scaffolds

Artificial semi-permeable membranes are commonly used to set up Transwell® two compartment cell culture systems (Figure 1.6), as membrane production using a highly standardized process is both simple and cost-efficient. Polycarbonate (PC), polyester (PE) or polyethylene terephthalate (PET) are the most prominent materials implemented in such setups (Figure 1.6A), which are available with different pore sizes and thicknesses as well as at distinct scales [112,129]. However, biological features for sufficient cell-adhesion, cell-survival and cell-proliferation are missing [120]. Therefore, coating procedures with

ECM-related proteins comprising collagen, fibronectin or Matrigel®, with collagen as most widely used one, are routinely performed [116,129]. Nevertheless, cell-matrix interactions are not exhibited as it is known from natural ECM structures [130–132]. Further, artificial polymer-based scaffolds represent an unequal pore distribution, influencing diffusion processes of drugs/compounds, thereby hampering bioavailability studies [105,112]. Although, artificial scaffolds demonstrate some disadvantages, their good accessibility, applicability in high-throughput screenings and compliance to the 3Rs principle ensure a widespread usage, especially in pre-clinical research. In addition to the standard 3D-like PC-, PE- or PET-based inserts, the Alvetex® matrix, a highly porous polystyrene scaffold, enables an adequate alternative membrane with respect to routine 3D-based cell culture, as scanning electron microscopy demonstrates structural characteristics similar to a sponge [133].

1.3.1.2. Biological scaffolds

Natural biological scaffolds exhibit fundamental differences to synthetic scaffolds due to their native 3D-structure and the complex composition of structural proteins, extracellular vesicles and proteoglycans, thereby positively affect cellular behavior [134–136]. Biological scaffolds are derived from a variety of tissues/organs such as dermis, pericardium or small intestine as well as species like humans, pigs or horses [120]. To obtain natural ECM structures (Figure 1.6B), used in tissue engineering concepts, decellularization of the whole organ using mechanical, enzymatic and/or chemical treatment is required for cell removal from source tissues [137,138]. However, all decellularization methods adversely affect the ECM in their composition, architecture or ultrastructural features on the ECM surface, which should be avoided by far [120]. Further, different ECM configurations are known such as powders, hydrogels, multilayer or single-layer sheets, with the porcine SIS as most studied natural single-layer scaffold [116,120,139,140]. Due to its composition and the 3D-like arrangement of dense collagen fibers, the SIS scaffold enables proper cell-ECM as well as cell-cell interactions to form a tight epithelial cell layer together with an improved cell survival, proliferation and differentiation mainly through paracrine and exogenous factors [115,135,141]. Nevertheless, the generation process is barely standardized and therefore batch-to-batch variations cannot be avoided, which limits the application of the SIS matrix as scaffold in context of small intestinal tissue engineering for pre-clinical purposes.

1.3.1.3. Biopolymer-based scaffolds

As shown for artificial and biological scaffolds, limitations concerning the technical and biological aspects highlight the necessity to prove further alternatives for tissue engineering concepts such as biopolymer-based scaffolds. Many of these biopolymers are compounds of the ECM such as heparin sulfate, chondroitin or hyaluronic acid but also polysaccharide derivatives or proteins like alginate, silk or cellulose are used as scaffold material [142]. For instance, cellulose a fibrous, water-insoluble material is considered to be the most abundant biopolymer in this field [143]. Plants or bacteria are used to construct cellulose-based scaffolds, whereby bacterial cellulose is more sustainable and can be manufactured in higher purity [143].

During the fermentation process of species of the genus *Gluconacetobacter* (*Komagataeibacter xylinus; K. xylinus*), glucose monomers polymerize and the secreted cellulose creates a 3D microfibril/nanofibril network [144–146], which assembles as a strong hydrogel. Characteristic features of this scaffold are an excessive water retention capacity, crystallinity and a high mechanical strength. Further, bacterial cellulose (BC), especially bacterial nanocellulose (BNC) (Figure 1.6C), is highly hydrophilic, resistant to enzymatic or chemical hydrolysis, non-toxic, consists of many pores [147,148] and the manufacturing process enables the formation of several shapes, sizes as well as surface structures [149–151]. Given the structural organization and composition of the BNC, comparability with human ECMs [152] is demonstrated by a similar fiber arrangement [151,153], a good mechanical strength [154,155] and a high similarity to the native ECM regarding hydrophilic properties [143]. BNC suitability for modern 3D tissue engineering concepts was already displayed in studies reconstructing the human auricle [156,157], as scaffold stimulating the expansion of mesenchymal stem cells [158] or as surface-structured matrix in epidermal skin models [149]. Of note, surface-structuring of the BNC by guided assembly-based biolithography (GAB) resulted in an aligned fiber structure which further induces an oriented cell polarization and migratory pattern for human dermal fibroblasts and HaCaT cells [149]. In general, epithelial cells respond to distinct topographies by an involved cellular behavior and a better model performance, which makes the surface-structured BNC particularly interesting for the establishment of small intestinal *in vitro* models [159,160].

1.3.2. Cell sources

Functional performance of organs and tissues *in vivo* is mainly driven by their cellular unit that makes it of high importance to mimic all necessary cell types *in vitro*. With regard to the intestinal epithelium, enterocytes, goblet cells, EECs, paneth cells as well as stem cells and

TACs have to be represented in an appropriate *in vitro* model [102]. In addition, the cellular unit should be easy in handling at low costs and provide reproducible and predictive results in pre-clinical studies. Currently, cell lines are used as standard, but primary cells are becoming increasingly interesting due to their high comparability to the *in vivo* situation [102,161].

1.3.2.1. Intestinal cell lines

In the past, most studies were performed with cell lines derived from human colon adenocarcinoma, as they constitute an unlimited cell source, are easy in handling at low costs and are able to differentiate into an enterocyte-like phenotype, representing the small intestinal epithelium, when cultured under specific conditions. HT-29 or Caco-2 cells (Figure 1.6E) are the most widespread human adenocarcinoma cell lines, while the latter are accepted as “gold standard” by the regulatory authorities or the pharmaceutical companies, to set up Transwell®-like models used in bioavailability, toxicity or permeability studies of drugs [111,112]. Caco-2 cells are cultured for 21 days on collagen-coated, semi-permeable, commercially-available Transwell® inserts, thereby displaying physiologically relevant properties, like a polarized epithelial monolayer, adoption of an enterocyte behavior [162] as well as the presentation of an apical brush border with intervened enzymes, transporters and receptors [85,163]. However, important characteristics of the small intestine such as the secretion of mucus or the formation of a corresponding tight junction protein expression profile are not properly mimicked or completely missing [164]. In contrast to Caco-2 cells, HT-29 cells show the ability to differentiate into a goblet cell-specific phenotype but the formation of a tight epithelial barrier is limited [165]. Therefore, Caco-2/HT-29 co-cultures models are set up on Transwell® inserts, demonstrating the formation of a tight monolayer covered by a representative mucus layer [166–169]. In recent years, Caco-2/HT-29-based models were further optimized, but still have limitations in their predictivity due to the development of a very tight or a barely formed barrier, a different expression rate of important transporters and the colon-carcinogenic background [7,170].

Apart from tumor-derived cell lines, there are also primary-derived immortalized cell lines (Figure 1.6F) such as NuLi-1 [171] (lung cell line) or HBEC3-KT [172] (bronchial cell line) available. Although, they have been shown to be physiologically relevant, exhibit a stable genotype *in vitro* and offer an extended proliferative capacity by simultaneous expression of primary-based characteristics [171,173], immortalized cell lines are still rarely used in small intestinal tissue engineering. In respect to the establishment of new test systems for drug developmental studies, these primary-based cell lines are an interesting alternative to the

commonly used Caco-2-based *in vitro* models. Until now, no primary-derived immortalized cell line representing the small intestine was presented with comparable characteristics to *in vivo*.

1.3.2.2. Primary cells - intestinal organoids

Adequate cell-based models closely resembling the human small intestine should mimic the overall cellular diversity of the epithelium and enable long-term culture *in vitro*. In 2009, Sato et al. published for the first time a protocol for the long-term culture of murine intestinal primary epithelial cells, forming so called “mini guts” or organoids *in vitro* [30,174] (Figure 1.6D). These self-organizing 3D-structures, based on primary intestinal crypts, exhibit a multicellular structure reflecting the cellular (stem cells, paneth cells, enterocytes, goblet cells and enteroendocrine cells) and structural organization of the crypt-villus architecture, as it is presented *in vivo*. Long-term cultures were achieved by sustaining of crypts, harboring multipotent ISCs, in a 3D environment using Matrigel®, which provides a complex composition of biomolecules that, to some extent, mimic the precise conditions of the native stem cell niche microenvironment. Matrigel®, derived from mouse tumor cells, is a gelatinous protein mixture composed of laminin, collagen IV and other structural proteins to imitate the intestinal ECM *in vitro* [175]. Next to the ECM-related proteins, growth factors such as EGF, RSPO and NOG are routinely added to the culture medium to maintain the stem cell population *in vitro* [174]. Such factors, contribute to the formation of a symmetric cyst structure from the ISC population that are known as intestinal spheroids. The connection between the ISCs and the ECM-related proteins is essential to prevent extensive anoikis within the spheroids [176] and to support a cyst-like structure with the central lumen surrounded by polarized epithelial cells (apical-basolateral cell polarity) [30,174,177]. With ongoing proliferation and differentiation time in culture, spheroids transform to so-called organoids characterized by symmetry breaks that occur in the spheroid clusters, leading to the formation of bud structures, which resemble the intestinal crypt, while the non-bud areas within the organoid depict the villus epithelium [178,179].

Based on this experimental procedure published in the landmark study by Sato et al. [30,174], primary epithelial cultures were established of different species *e.g.* mouse [174] and human [30] as well as of different health status e.g. healthy, cystic fibrosis [180] or Morbus Crohn [181]. However, factors such as the age, the state of health as well as the time after tissue extraction determine the success of crypt isolation, spheroid expansion and organoid growth [182]. The species used for the establishment of spheroid/organoid cultures leads to further challenges in long-term culture, as the culture medium for murine spheroids/

organoids depends on supplementation of EGF, RSPO and NOG, whereas human spheroid/organoid cultures need a medium formulation supplemented not only of EGF, RSPO and NOG, but also of growth factors such as Wnt3a, nicotinamide (inhibitor for multiple kinases), SB202190 (inhibitor for p38 kinase), LY2157299 (inhibitor for TGF-βR1), A83-01 (inhibitor of Smad signaling) and Leu-Gastrin (supports Lgr5 receptor) [183–187].

Although intestinal spheroids/organoids represent the native tissue to a high degree, they are not easily accessible for each kind of application, as their internal localization of the intestinal lumen together with the internally localized brush border leads to major technical challenges in context of permeability/bioavailability or infection studies that require a direct access of the luminal part of the model *in vitro*. Key challenge thereby is to transfer the substances of interest (*e.g.* drug or pathogen) into the lumen of the spheroid/organoid, which is currently achieved by microinjection, a time-intensive and laboratory method that at least partly disrupts the epithelial barrier [188]. One possibility to overcome this limitation, is the generation of 3D monolayer cultures that have been established by several groups in the past [139,189–191] and are based on primary, tissue-specific spheroids/organoids. In this context, Schweinlin et al. demonstrated that dissociated spheroids/organoids cultured for several days on the biological SIS scaffold, are proliferative and can undergo a spontaneous differentiation into absorptive and secretory lineage cells [139]. Differentiation is supported by medium supplementation with commonly known factors and DAPT [192–194], an inhibitor of the Notch-pathway as well as by a reduced supplementation with Wnt3a-conditioned medium [139].

Another possibility to overcome the drawback of the inside-faced lumen is the generation of so called apical-out spheroids/organoids by simply removing the ECM component from the *in vitro* culture that leads to a polarity switch of the spheroids/organoids, characterized by a flipped structure with the luminal surface at the outside, while the basolateral compartments turned into the inside of the cell cluster [195]. Thereby, an *in vitro* model is created that allows host-pathogen interaction studies without losing the characteristic features of the primary intestinal spheroids/organoids [195]. Nevertheless, primary spheroids/organoids are based on donor tissue, which limits the availability with this specific genetic background, enables the formation of genetically modified cells during long-term culture and complicates the application with regard to standardizability and reproducibility [196,197].

2. Aim of the thesis

To gain more knowledge about biological principles, mechanisms, cellular and molecular regulation of tissue homeostasis but also specialized uptake mechanisms, small intestinal *in vitro* models were established to mimic the *in vivo*-like situation. Routinely, human adeno-carcinoma cell lines, such as Caco-2 or HT-29 are cultured on artificial membranes to establish a Transwell®-based two-compartment system [111,112]. Although such *in vitro* models are standardized, easy in handling and cost-efficient, they lack functional and structural characteristics of the native organ [113,198]. ***Given these main drawbacks and thus the need to improve small intestinal tissue models for pre-clinical applications, the aim of this thesis was to combine different strategies for the establishment of a novel in vitro model.*** In general, the experimental strategy of this work comprises:

1) the use and implementation of alternative ECM scaffolds.
2) the development as well as characterization/validation of a new cell source for intestinal organ modeling.

2.1. Bacterial nanocellulose as biological model scaffold

The most commonly used scaffolds for intestinal organ modeling are composed of PET, a synthetic polymer [111,198]. In recent years, natural ECMs such as decellularized porcine small intestinal tissue termed SIS [116,139,199] offered an alternative structure to mimic a more *in vivo*-like environment. However, both variants do not entirely fulfill the requirements for an improved pre-clinical setup of intestinal *in vitro* models. In the context of pre-clinical models, the most important aspects to be addressed are standardizability, reproducibility, cost-efficiency, easy handling, applicability in a high-throughput approach, no additional barrier formation by the scaffold material and the comparability with results obtained *in vivo* [200]. In view of the advantages and disadvantages of the respective scaffolds, ***I hypothesize BNC as a suitable alternative*** [146,201–203]. Of note, the BNC scaffold used in my studies was either produced with a flat or a surface-structured topography, wherein the latter was generated by GAB technology, hypothesized to result in a better performance in context of cell spreading/adherence and polarization [149].

In this thesis, intestinal *in vitro* models based on Caco-2 cells and primary cells were established on both BNC matrices as well as on the PET and SIS as controls. The use of these cell types was intended to show, whether the surface properties of the BNC are sufficient to enable a proper cell adherence and proliferation capacity. To verify the unmodified and surface-structured BNC as alternative scaffolds for standardized model

setup, histological and structural analyses, expression patterns of corresponding tight/adherens junction proteins and transport activity analyses were performed.

2.2. A primary-cell-derived, immortalized cell line as alternative to intestinal organoids

Next to the scaffold material, the cell source influences the predictivity as well as the functional performance of intestinal *in vitro* models in pre-clinical research approaches. Unlimited availability was presented for cell lines such as the carcinoma-derived Caco-2 cells, but cellular subtypes of the native tissue are not reproduced. Further, their tumor-based background leads to the exhibition of an artificial gene and protein expression profile, which is not compliant with the *in vivo* situation [7,198,204]. In addition to intestinal cell lines such as Caco-2, primary cells isolated from native gut tissue gained recently great attention in intestinal tissue engineering [30,102,139]. In contrast to cell lines, primary cells show a close similarity to the native intestinal tissue in context of cell diversity, genetic features and functionality [7,30,102]. Disadvantages are the need of a human donor, which means that there is only a limited availability of cells with this genetic background and the lack of standardization. Because of their time- and cost-intensive handling in the lab, ***I hypothesize in this work that primary-cell-derived, immortalized intestinal cell lines would enable a standardized and cost-efficient culture, while maintaining cellular diversity.*** Therefore, murine and human intestinal organoids were immortalized in this project by applying the Cl-SCREEN® technology in collaboration with the InSCREENeX GmbH. Immortality was induced by ectopic expression of a 10 (murine cells) or 12 (human cells) gene comprising mixture, identified as cell cycle regulating genes and relevant for the immortalization of intestinal epithelial cells [205] in this study, instead of only one gene, as usual. Oncogenes (*TAg*, *Bmi1*) and others are included in this in total 33-component gene library (Cl-SCREEN® technology) [206,207] to impact on cell proliferation (*c-Myc*), inhibit differentiation (*Nanog*, *Id2*) or apoptosis (*E7*) with simultaneous preservation of the primary cell properties to a particularly high degree, as recently shown for human endothelial cells [208] or alveolar lung cells [209]. This lentivirus-based immortalization strategy was applied to stably integrate foreign DNA into the genome and to allow the transduction of non-replicating cells, which is of special interest when cells isolated from the primary tissue, containing a high cellular diversity, are immortalized [207,210]. Characterization studies of the established murine/human immortalized primary organoid-derived cell lines (cell clones) comprised analyses of intestinal morphology, cellular diversity and function. Besides histological and proliferation rate, intestinal cell type specific gene as well as protein expression patterns

were determined. The formation of a tight and functional epithelial barrier was analyzed by transepithelial electrical resistance (TEER) measurements and transport capacity studies.

Altogether, this work will provide essential new components, structural and cellular, for the establishment of alternative in vitro models of the small intestinal epithelium that enable more reliable drug delivery studies in pre-clinical applications in the future.

3. Materials and Methods

3.1. Materials

3.1.1. Chemicals and Reagents

Product	Company
2-propanol	Carl Roth
BSA	BioFroxx
Cell Recovery Solution	Corning
Citric acid	Sigma Aldrich
Collagen-I (rat-tail)	TERM Würzburg
EDTA	Sigma Aldrich
EGTA	Sigma Aldrich
Ethanol	Sigma Aldrich
FITC-dextran	Sigma Aldrich
Gelatin	Sigma Aldrich
Glutaraldehyde	Sigma Aldrich
Glycine	Carl Roth
Poly-L-ornithine	Sigma Aldrich

3.1.2. Commercial kits

Product	Company
Click-it™ EdU Alexa Fluor™ 647 Flow Cytometry Assay Kit	Invitrogen
iScript™ cDNA Synthesis Kit	Biorad
RNAeasy Micro Kit	QIAGEN
SsoFast™ EvaGreen® Supermix	Biorad

3.1.3. Cell culture

Product	Company
2-mercaptoethanol	Carl Roth
A83-01	Tocris Bioscience
Advanced DMEM/F12	Gibco
Anti-Anti	Gibco
B-27 supplement (without Vitamin A)	Gibco
BNC scaffolds (unmod/str)	JeNaCell
CHIR99021	Biomol
DAPT	Sigma Aldrich
DMEM	Gibco
DMSO	Sigma Aldrich
D-PBS$^-$/PBS$^+$	Gibco
FCS	Bio&Cell
[Leu15]-Gastrin I	Sigma Aldrich
LY2157299	Axon MedChem
Gentamycin	Sigma Aldrich
GlutaMax-I	Gibco
HBSS$^-$	Gibco
HEPES	Gibco
human R-Spondin 1	PeproTech
Jagged-1 peptide	AnaSpec Inc.
Matrigel® Growth Factor Reduced phenol red-free	Corning
human recombinant EGF	PeproTech
mouse recombinant Noggin	PeproTech
N-2 supplement	Gibco
N-Acetylcysteine	Sigma Aldrich
NEAA	Gibco
Nicotinamide	Sigma Aldrich
Pen/Strep	Gibco
PLGA nanoparticles	University of Saarland, AG Prof. Lehr
Rock inhibitor Y-27632	Tocris
SB202190	Sigma Aldrich
Sodium pyruvate	Life Technologies

Product	Company
Trypan Blue, 0.4%	Sigma Aldrich
TrypLE Express	Gibco
Trypsin/EDTA	Gibco
Valproic acid	Sigma Aldrich

3.1.4. Cell culture material and disposable material

Product	Company
Amicon® Ultra 15 mL Filters	Merck Millipore
BRANDplates® 24-well for inserts	BRAND GmbH + Co KG
Cell Crowns	TERM
Centrifuge Tubes PP	Corning
Cryo Tubes	Nunc
Disposable cell culture pipettes CELLSTAR	Greiner Bio-one
Embedding Cassettes	Klinipath
Embedding Filter Paper	Labonord
Parafilm®	Carl Roth
Pasteur Pipettes	Brand
Reaction Tubes	Sarstedt
Standard cell culture material	TPP
Sterile Filter	Sartorius
Syringes	BD
ThinCert™ 24-well inserts	Greiner Bio-one

3.1.5. Cell lines and biological material

Wnt3a-producing cells were obtained from ATCC (ATCC® CRL-2647™) and Caco-2 cells (ACC 169) from DSMZ in Braunschweig. The DSMZ as well as ATCC confirmed the cell identity via Human STR profiling cell authentication service.

Animal research was performed according to the German law and institutional guidelines approved by the Ethics Committee of the District of Unterfranken, Würzburg, Germany (approval number for the generation of porcine SIS 55.2-2532-2-256). The animals received proper attention and humane care in compliance with the Guide for Care and Use of Laboratory Animals published by the National Institute of Health (NIH publication no.85e23, revised 1996) and as approved by the institutional board of animal protection. Organ

explantation occurred according to the German Animal Protection Law (§4 Abs.3) and the institute's animal protection officer regularly informed the responsible authorities.

Porcine jejunum tissue was explanted from 6 week old female pigs provided by the certified pig farm Niedermeyer in Dettelbach, Germany.

Human jejunum tissue was extracted from the surgery unit of PD Dr. med. C. Jurowich at the University Hospital Würzburg with the approval of the Institutional Ethics Committee (number 182/10).

3.1.6. Cell culture media

Crypt medium	Advanced DMEM/F12 1x GlutaMax-I (v/v) 1x Anti-Anti (v/v) 10 mM HEPES 1% (v/v) N-2 supplement 0.5% (v/v) B-27 supplement 1 mM *N*-Acetylcysteine
Murine organoid maintenance medium	Crypt medium 50 ng/mL hEGF 100 ng/mL mNoggin 500 ng/mL hR-Spondin 1 3 µM CHIR99021 1 mM Valproic acid 10 µM Rock inhibitor Y-27632 (after splitting for 2 days)
Murine cell clone expansion medium	Crypt medium 10% FCS 50 ng/mL hEGF 100 ng/mL mNoggin 500 ng/mL hR-Spondin 1 10 µM Rock inhibitor Y-27632

Murine cell clone medium	Crypt medium 10% FCS 50 ng/mL hEGF 100 ng/mL mNoggin 10 µM Rock inhibitor Y-27632
Human organoid maintenance medium (Human proliferation medium)	50% Crypt medium 50% Wnt3a-conditioned medium 50 ng/mL hEGF 100 ng/mL mNoggin 500 ng/mL hR-Spondin1 500 nM A83-01 10 mM Nicotinamid 10 µM SB202190 10 mM Leu-Gastrin 500 mM LY2157299 10 µM Rock inhibitor Y-27632 (after splitting for 2 days) 10 µM JAG-1 (for single cells for 2 days)
Human differentiation medium	75% Crypt medium 25% Wnt3a-conditioned medium 50 ng/mL hEGF 100 ng/mL mNoggin 500 ng/mL hR-Spondin1 500 nM A83-01 10 µM DAPT 10 mM Leu-Gastrin 500 mM LY2157299
Human cell clone medium	80% Crypt medium 20% Wnt3a-conditioned medium 50 ng/mL hEGF 100 ng/mL mNoggin 500 ng/mL hR-Spondin1

Human cell clone medium	500 nM A83-01 10 mM Nicotinamid 10 µM SB202190 10 mM Leu-Gastrin 500 mM LY2157299 10 µM Rock inhibitor Y-27632
Wnt3a cell medium	DMEM 10% (v/v) FCS 1% Sodium pyruvate G-418
Caco-2 cell medium	DMEM 10% (v/v) FCS 1% Sodium pyruvate 1% NEAA 1% Anti-Anti
PBS$^-$/EDTA	500 mL PBS$^-$ 0.5 mM EDTA
Trypsin/EDTA	500 mL PBS-/EDTA 0.5% Trypsin
HBSS$^-$ cell isolation	1% Pen/Strep in HBSS$^-$
Cell freezing medium	90% (v/v) FCS 10% (v/v) DMSO

3.1.7. Mouse strains

Mouse strain	Source and Reference
C57BL6/J (wild type mouse line)	Charles River
B6.129P2-LGR5$^{tm1(cre/ERT2)Cle/J}$ (Lgr5-eGFP mouse line[1])	Jackson Laboratory [22]

[1] Abbreviation for this mouse line in this document. Lgr5-eGFP mice constitutively express the eGFP reporter gene under the control of the murine leucine rich repeat containing G-protein coupled receptor 5 (LGR5) promotor.

3.1.8. Polymerase chain reaction/Primer pairs

Name	5' to 3' Sequence	Source
mRpl15	5'-CTGACCCTGGATGTCTTGGTGC-3' 5'-CCAAGCAGCCACTTCAGTGAACC-3'	NM_025586.3 (housekeeping gene)
mRps29	5'-GTCTGATCCGCAAATACGGG-3' 5'-AGCCTATGTCCTTCGCGTACT-3'	NM_009093 (housekeeping gene)
mLgr5	5'-GGGAAGCGTTCACGGGCCTTC-3' 5'-GGTTGGCATCTAGGCGCAGGG-3'	NM_010195.2
mMuc2	5'-GCTGCATTTGCCGGAACGGG-3' 5'-GGCAGCTAGTGGGACGGGGT-3'	NM_023566.3
mLyz	5'-CCTGACTCTGGGACTCCTCCTGC-3' 5'-CCACGGTTGTAGTTTGTAGCTCGT-3'	NM_017372.3
mVil1	5'-GCAGCATTACCTGCTCTACGTT-3' 5'-GCTTGATAAGCTGATGCTGTAATTT-3'	NM_007127.2
mChga	5'-AGAATTTACTGAAGAAGCTCCAAG-3' 5'-TCCTCTCTTTTCTCCATAACATCC-3'	NM_001275.3
hHPRT1	5'-TGACCTTGATTTATTTTGCATACC-3' 3'-CGAGCAAGACGTTCAGTCCT-3'	NM_000194.2 (housekeeping gene)
hEF1α	5'-AGGTGATTATCCTGAACCATCC-3' 5'-AAAGGTGGATAGTCTGAGAAGC-3'	NM_001402.5 (housekeeping gene)
hMUC2	5'-AGGATCTGAAGAAGTGTGTCACTG-3' 5'-TAATGGAACAGATGTTGAAGTGCT-3'	NM_002457.3
hVIL1	5'-GCAGCATTACCTGCTCTACGTT-3' 5'-GCTTGATAAGCTGATGCTGTAATTT-3'	NM_007127.2

Name	5’ to 3’ Sequence	Source
hCHGA	5‘-AGAATTTACTGAAGAAGCTCCAAG-3‘ 5‘-TCCTCTCTTTTCTCCATAACATCC-3‘	NM_001275.3
hLYZ	5‘-CCGCTACTGGTGTAATGATGG-3‘ 5‘-CATCAGCGATGTTATCTTGCAG-3‘	NM_000239.2
hLGR5	5‘-TCACCTTCCCCAGGCCCCTTC-3‘ 5‘-TGTTCACTGCTGCGATGACCCC-3‘	NM_003667.3

3.1.9. (Immuno-) Histology

3.1.9.1. Material and solutions

Product/buffer	Company/composition
Antibody dilution solution	DCS Innovative Diagnostic-Systems
Citrate buffer pH 4.5	2.5% (w/v) Tri-Sodium-citrate 1.4% (w/v) Citrate 2% (w/v) D (+) Glucose ddH_2O and pH-adjustment
Cover slips for slides	Menzel-Gläser
Donkey serum	Sigma Aldrich
Entellan	Merck Millipore
Eosin	Morphisto
Fluoromount-G™ (with DAPI)	Invitrogen
Glass slides Polysine™	Thermo Fisher
Glass slides SuperFrost® Plus	Langenbrinck
Grease Pencil	Dako
Haematoxylin	Morphisto
Histogel™	VWR
Microtome Blades: Type A35	pfm Medical
Paraffin	Carl Roth
PFA	AppliChem
Roti® Histofix 4%	Carl Roth
TBS-T 0.05 M	100 mL TBS Stock (0.5 M) 5 mL Tween-20 (0.5%) 900 mL Demineralized water
Triton-X 100	Carl Roth
Xylene	Carl Roth

3.1.9.2. Primary antibodies

Antibody	Host	Dilution	Company
anti-Chromogranin A	Rabbit	1:100	Santa Cruz (sc-13090)
anti-Claudin 5	Rabbit	1:100	Abcam (ab15106)
anti-E-Cadherin	Mouse	1:100	BD Biosciences (610181)
anti-Ki-67	Rabbit	1:100	Abcam (ab15580)
anti-Lysozyme	Goat	1:100	Santa Cruz (sc-27958)
anti-Mucin 1	Mouse	1:100	Abcam (ab109185)
anti-Mucin 2	Rabbit	1:100	Santa Cruz (sc-15334)/ Abcam (ab272692)
anti-Occludin	Mouse	1:100	Invitrogen (33-1500)
anti-SGLT1	Rabbit	1:200	Merck Millipore (07-1417)
anti-Villin 1	Goat	1:100	Santa Cruz (sc-7672)
anti-Zonula occludens-1	Rabbit	1:100	Proteintech (21773-1-AP)

3.1.9.3. Secondary antibodies

Antibody	Host	Dilution	Company
anti-mouse Alexa 555	Donkey	1:400	Invitrogen (A-31570)
anti-mouse Alexa 647	Donkey	1:400	Invitrogen (A-31571)
anti-rabbit Alexa 555	Donkey	1:400	Invitrogen (A-31572)
anti-goat Alexa 647	Donkey	1:400	Invitrogen (A-21447)

3.1.10. Software

Product	Company
Bio-Rad CFX Manager 3.1	Biorad
Citavi 6	Swiss Academic Software
FIJI ImageJ	NIH
FlowJo 10.4.1.	FlowJo LLC
GraphPad Prism 7	GraphPad Software Inc.

3.1.11. Microscopes and devices

Product	Company
Aspiration Device (VacuBoy)	Integra Biosciences
BD Accuri C6 Cytometer	BD
Blocking station	Leica
Cell incubator Heraeus	Thermo Scientific
Centrifuge Heraeus Multifuge X1R	Thermo Scientific
CFX96 Touch™ Real-Time PCR Detection System	Biorad
Confocal microscope TCS SP8	Leica Microsystems
Embedding station	Thermo Fisher
EVOS™ XL Core Imaging System	Thermo Fisher
Freezer (-80°C/-20°C)	Thermo Scientific/Liebherr
Freezing Container (Mr. Frosty)	VWR
Inverse Fluorescence Microscope BZ-9000	Keyence
LCR HiTESTER 3522-50	HIOKI E.E. Corp.
Liquid Nitrogen Storage Tank	German-cryo
Millicell ERS-2	Millipore
Neubauer Cell Counting Chamber	Hartenstein
pH meter	Mettler Toledo
TECAN Infinite 200 PRO microplate reader	TECAN
Thermal Cycler C1000	Bio-Rad
Sliding Microtome RM 2255	Leica
Steam Cooker “MultiGourmet”	Braun

3.2. Methods

3.2.1. Preparation and setup of scaffold material for Transwell®-like models

3.2.1.1. Preparation and setup of SIS-based scaffolds

Porcine jejunum tissue was explanted as whole organ at the center for experimental molecular medicine (ZEMM), University Hospital Würzburg in compliant with the German law and institutional guidelines (section 3.1.5). Decellularization of the explanted tissue occurred according to standardized protocols previously published [138,211]. For quality controls of the decellularized tissue, histological analyses and a gallic acid assay were performed. To generate Transwell®-like cell culture systems, SIS matrix was fixed between two plastic cylinders termed 'cell crowns' (self-constructed by the Chair of Tissue Engineering and Regenerative Medicine (TERM), University Hospital Würzburg, Germany).

3.2.1.2. Preparation and setup of BNC-based scaffolds

The BNC scaffolds were provided by the JeNaCell GmbH within a cooperation project. Previously, the preparation and characterization of these scaffolds performed by JeNaCell were published [212]. In brief, bacterial precultures ($1x10^6$ colony forming units per mL) were cultured for 7 days at 28°C in Hestrin-Schramm culture medium. For surface-structured BNC samples, polydimethylsiloxane (PDMS) molds were placed on top of the culture medium. To generate thin membranes with a square of 17 mm x 17 mm, the BNC pellicles were treated with a boiling 0.1 M aqueous sodium hydroxide solution for 30 min, purified with water for neutral pH conditions, followed by manual pressing to a height of 0.5 mm. Finally, the pressed samples were conserved and autoclaved in aluminum pouches. Analyses of the unmodified and surface-structured BNC scaffolds, with regard to structural and biophysical properties, included investigations using scanning electron microscopy, high-performance multiphoton microscopy and the measurement of the water absorption capacity.

To setup BNC Transwell®-like *in vitro* models, the BNC was fixed between cell crowns (described in 3.2.1.1), incubated with 100 µL gelatin solution for 1 h at room temperature (RT) (apical compartment), followed by crosslinking with a 2% glutaraldehyde solution for 15 min at RT. The scaffolds were washed with 70% ethanol for 35 min and washed five times with PBS^- for 5 min each, before the matrices were coated with 2 mM glycine overnight.

3.2.1.3. Setup of PET-based scaffolds

Commercially available polyethylene terephthalate (PET)-membrane-based cell culture inserts (24-well inserts) with a pore size of 1.0 µm were coated with 100 µL of a 0.1 mg/mL collagen-I (rat-tail) solution in 0.1% acetic acid for 15 min at RT. Acetic acid was sucked off and after evaporation of the remaining solution (15 min at RT), inserts were used for model setup.

3.2.2. Cell culture

3.2.2.1. Cell culture conditions

In general, the cells were cultured at 37°C, 5% CO_2 and 95% humidity. A medium change was performed every 2-3 days.

3.2.2.2. Caco-2 cell culture

Caco-2 cells were cultured in Dulbecco's Modified Eagle Medium (DMEM) supplemented with 10% fetal calf serum (FCS), 1% non-essential amino acids (NEAA), 1% sodium pyruvate and 1% antibiotics-antimycotics (Anti-Anti). Passaging of Caco-2 cells (>70% confluence) was performed by cell incubation in 0.5 mM EDTA in 1x PBS^- solution (PBS^-/EDTA) at 37°C for 10 min followed by detaching of cells by administration of 0.5% Trypsin/EDTA solution for 3 min at 37°C (see section 3.1.6). Cells were harvested with a pipette and centrifugation occurred at 1200 rpm for 5 min, RT. In general, cells were split at a ratio of 1:10-1:20.

3.2.2.3. Crypt isolation from B6.129P2-LGR5$^{tm1(cre/ERT2)Cle/J}$ mouse strain (Lgr5-eGFP mouse line) and human biopsies

Crypts were isolated from the following: murine and human tissue. Human jejunum biopsies (two male/two female) were obtained from obese adults during routine stomach bypass operation at the University Hospital Würzburg in collaboration with the surgery unit of PD Dr. med. C. Jurowich (study approval number 182/10) [139]. In advance, patients were informed about using their intestinal biopsies for research purposes. The cryopreserved primary cells, originated from a previous cooperation between the working group of PD Dr. Metzger and PD Dr. med. Jurowich were re-used for this project.

The small intestine of transgenic Lgr5-eGFP mice, 15-27 weeks old (two male/two female), were used to isolate LGR5-$eGFP^+$ crypts as previously described [139,174] according to the

German law and the institutional regulations. The experimental procedure for tissues of both species was as follows: the intestinal tissue was freed from muscle or adipose tissue and villi were scraped off by mechanical force using two glass slides. During tissue incubation in cold Hanks' Balanced Salt Solution ($HBSS^-$) supplemented with 2 mM EDTA for 30 min at 4°C on a rotating shaker, the tight junctions between crypts and the basal membrane were opened. To isolate the crypts, the tissue was transferred into a falcon of cold $HBSS^-$ and shaken several times by hand. After three rounds of shaking the crypt-containing $HBSS^-$ buffers were pooled, centrifuged for 3 min at 350 x g and washed with Advanced DMEM/F12. To seed nearly 1500 crypts per well, the crypts were counted, dissolved in 50 µL/well of Matrigel® and incubated for 10 min to solidify the hydrogel. The droplets were covered with 300 µL organoid maintenance medium (as described in 3.1.6.) supplemented with 10 µM Y-27632 for 2 days, according to the protocols published by Sato et al. [30,174].

3.2.2.4. Primary intestinal organoid cultures

Cells were expanded by dissolving the Matrigel® droplets in 300 µL/well cell recovery solution, incubation for 1 h on ice and centrifugation at 350 x g for 3 min. For single cell suspensions, the spheroids/organoids were resuspended in 1 mL of TrypLE express and incubated at 37°C for 10 min. Incubation times with TrypLE express for 3-4 min occurred, if only spheroid/organoid fragments were used for expansion. In general, TrypLE express is a solution of recombinant cell-dissociation enzymes, which replaces commonly known porcine trypsin. Incubation time in TrypLE express decides with regard to organoid cultures, if cell-cell contacts are completely dissolved as used for single cell expansion or if a partly dissociation in the case of spheroid/organoid fragments takes place. The dissociation reaction was stopped by adding crypt medium, followed by washing of the cell suspension and embedding in Matrigel® (split ratio 1:2 or 1:3) as described in 3.2.2.3. According to spheroid/organoid size and amount per well, this splitting procedure was repeated once or twice a week. Representative images of murine spheroids (short culture time) and human organoids (long culture time) are shown in Figure 3.1A-C.

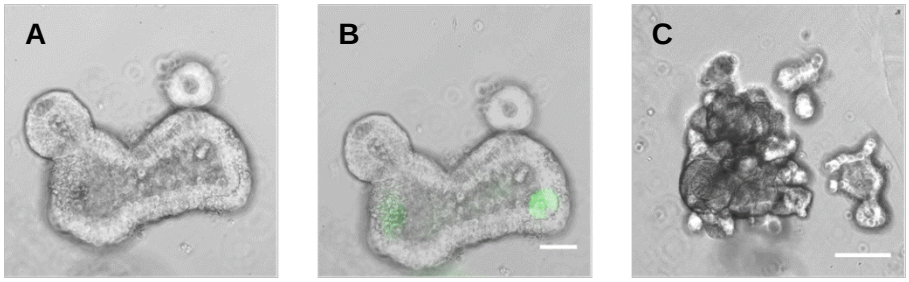

Figure 3.1: Representative images of murine LGR5-eGFP^{+} spheroids and human organoids cultured in Matrigel® droplets. Murine spheroids **(A, B)** and human organoids **(C)** grown in organoid maintenance medium show a characteristic morphology by crypt and villus formation in EVOS bright field images. Murine intestinal stem cells expressing eGFP are displayed in a fluorescence overlay image with the bright field image of the spheroid **(B)**. Scale bar in **A, B** = 50 µm; in **C** = 150 µm.

3.2.2.5. Wnt3a-conditioned medium

Wnt3a-conditioned medium was used for the maintenance of intestinal stem cells in culture. The L-Wnt-3A cell line (ATCC® CRL-2647™) generated from mouse fibroblasts secreted Wnt3a into FCS-containing medium by processing the protocol provided by ATCC. Briefly, cells were cultured in DMEM medium supplemented with G418 (section 3.1.6.) for the selection process of Wnt3a-producing cells. The biological WNT3A protein was secreted into the medium after splitting the cells 1:10 and a culture time for at least 4 days to enable the formation of a confluent cell layer. The next 4 days, the medium was collected and changed every day followed by sterile filtration and pooling of the four medium batches. After the determination of Wnt3a activity of the conditioned medium by performing a Wnt Reporter Activity Assay [213], the samples were stored at -20°C.

3.2.2.6. Lentiviral transduction of intestinal organoids

The generation of immortalized murine/human intestinal cells based on intestinal organoids was performed by the InSCREENex GmbH in Braunschweig, Germany. These partners are specialists in the lentiviral transduction of primary cells and the general procedure was previously described [207]. In brief, HEK293T cells were transfected with a cocktail consisting of four packaging plasmids encoding gagpol, rev, VSC-G and the respective lentiviral vector [214] for 24 h followed by lentivirus containing supernatant collection. Virus was concentrated by using the Lenti-X-concentrator. The virus solution for the immortalization of murine intestinal organoids contains in total 10 genes (bold; Table 3.1) and for human intestinal organoids 12 genes (marked with a star; Table 3.1) based on a gene

pool containing 33 genes (Table 3.1), that are part of the CI-SCREEN® immortalization strategy.

In a next step, 2D- and 3D-cultured primary intestinal epithelial cells were transduced with the concentrated virus solution to optimize the immortalization process as displayed in Figure 3.2. To this aim, 2D-cultured cells were grown on fibronectin/collagen-I pre-coated plates until confluence followed by virus application mixed at a 1:1 ratio of viral supernatant (infection I12 or infection I4) and standard cell culture medium supplemented with 0.25% polybrene to increase the efficiency of the overnight infection. The 3D-cultured cells were transduced under floating-conditions in a falcon and resuspended in Matrigel® on the following day. After a few weeks, immortalized cells sprouted from the Matrigel® droplets and were picked for expansion in 2D on fibronectin/collagen-I pre-coated plates (infection I9).

Table 3.1: Library genes sorted after integration frequency in novel human cell lines. Gene name and categorizing of the frequency rate was adopted from Lipps et al. [207]. Genes used for the immortalization of murine (bold) and human (star) intestinal organoids were marked.

Gene name (high frequency)	Gene name (middle frequency)	Gene name (low frequency)
E7*	***TaG****	*Myb*
Nanog*	***Core****	*HoxA9*
cMyc*	*Yap1*	*Bmi1**
Id2*	*Sox2*	*Klf4*
Fos*	*E6**	*βCat*
Ezh2	*Lmo2*	*NS1*
Id3*	***Rex****	*Jun*
Id1*		*E2F1*
		Bcf2
		PymT
		Oct3
		Nfe2L2
		RhoA
		Gli1
		v-Myc
		Sez12
		ZFP217
		Id4

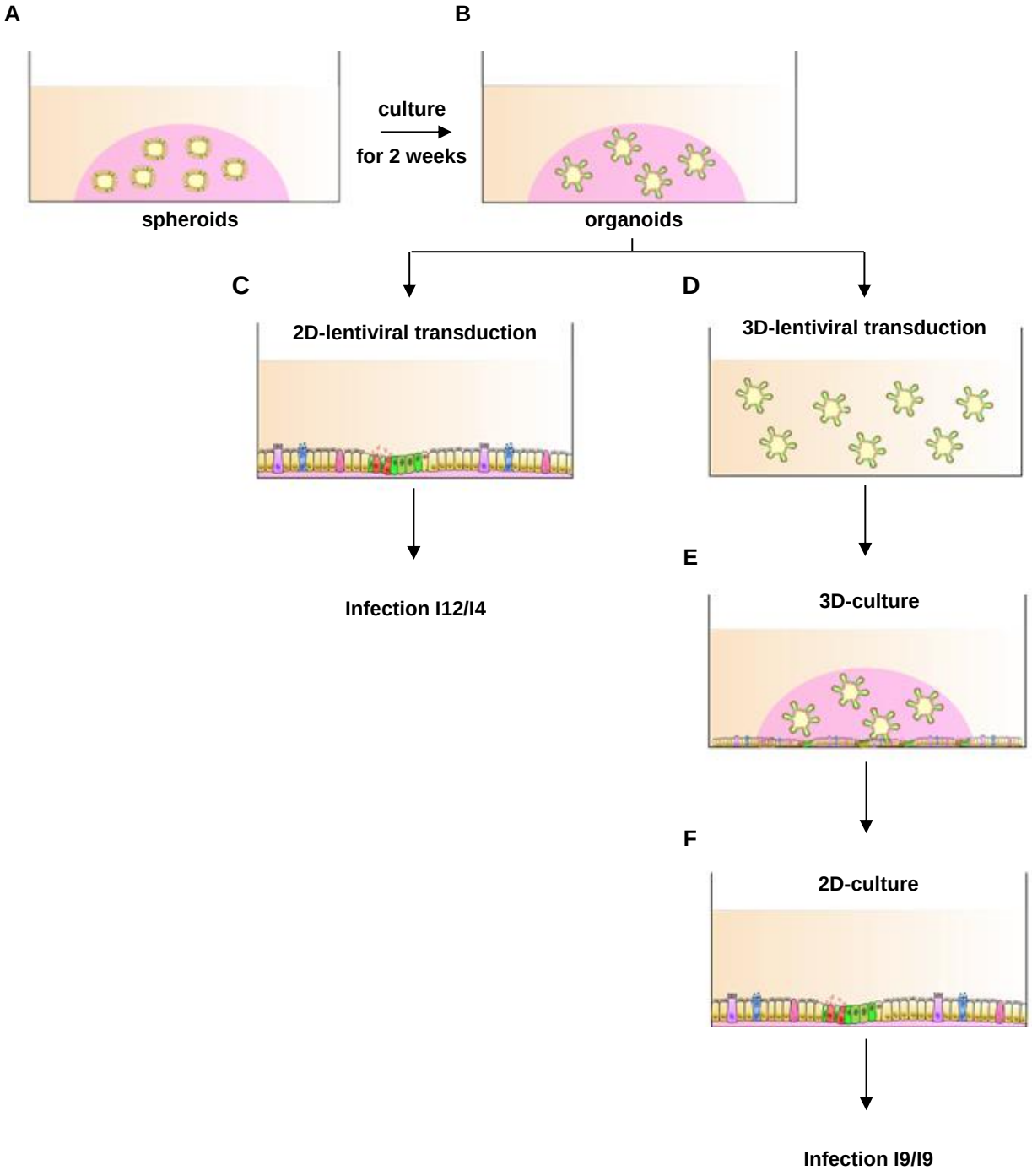

Figure 3.2: Lentiviral transduction of intestinal organoids for the generation of immortalized intestinal epithelial cells. Intestinal primary epithelial cells isolated from biopsies formed spheroids under 3D-culture conditions **(A)** and after prolonged culture (2 weeks) organoids with differentiated cell types are feasible **(B)**. Lentiviral transduction occurred either in 2D **(C)** or in 3D-floating conditions **(D)**. Cells were cultured in Matrigel® after transduction in 3D **(E)**. Cells sprouted from Matrigel® droplets **(E)** and were picked for expansion in 2D **(F)**. The infection in 2D is described as infection I12 for murine cells and as I4 for human cells. Infection in 3D is classified as infection I9 for murine as well as human cells.

3.2.2.7. Culture of immortalized cell clones derived from primary 2D and 3D cell cultures

Immortalized murine cell clones grew on normal cell culture plastic, whereas the immortalized human cell clones needed collagen-I pre-coated cell culture flasks. Therefore, T25 flasks used for human cell clones were pre-coated with collagen-I (rat-tail) acetic acid solution (0.4%) for 30 min and washed with PBS^-. Beforehand different coatings like poly-L-ornithine (only for murine cell clones), collagen-I (0.4%), fibronectin/collagen-I (10 µg/mL) or without coating were tested for both generated cell lines. Further, different medium compositions were used to determine the required growth factors. The final medium consumption is listed in section 3.1.6 for murine as well as human cell clones. Both, murine and human cell lines, were grown until 80-90% confluence and passaged by adding PBS^-/ EDTA for 10 min at 37°C, followed by incubation with 0.5% Trypsin/EDTA for 3 min. For cell harvesting, the cells were transferred to a falcon tube and centrifuged at 300 x g for 3 min. Afterwards, murine cell clones were splitted 1:20 twice a week, whereas human cell clones at a 1:2 ratio once a week. Further, immortalized cell clones were cultured in Matrigel® droplets covered with 300 µL cell clone medium (section 3.1.6). After 24 h of culture in a 3D environment spheroid-like structures were observed. Cell clones with a spheroidal morphology were splitted and expanded as described in section 3.2.2.4.

3.2.2.8. Thawing and freezing of intestinal cells

Cryopreserved cells (spheroids, cell clones) or Caco-2 cells were thawed at 37°C and resuspended in the tenfold quantity of crypt medium or Caco-2 cell culture medium (as described in 3.1.6). Cell suspension was centrifuged for 3 min at 350 x g and supernatant was removed. Intestinal spheroids were dissolved in Matrigel® (50 µL/well) for 3D cell culture and seeded as droplets of 50 µL in a 24-well plate, followed by polymerization for 10 min at 37°C and subsequent administration of 300 µL organoid maintenance medium. Immortalized cell clones or Caco-2 cells were dissolved in cell type-specific medium (as described in 3.1.6.) and transferred to collagen-I pre-coated cell culture flasks for 2D cell culture of human cell clones and non-coated flasks for murine cell clones or Caco-2 cells.

For freezing, organoids were harvested from Matrigel® according to section 3.2.2.4. In general, 6 wells were pooled per cryovial after washing with crypt medium. The pellet was dissolved in 1 mL of cell freezing medium. Immortalized cell clones or Caco-2 cells were trypsinized and $1x10^6$ cells were resuspended in 1 mL of 80% cell maintenance medium or Caco-2 cell culture medium supplemented with 10% DMSO and 10% FCS for freezing. Cells

were stored in Freezing Containers for 24 h at -80°C before being transferred to liquid nitrogen.

3.2.2.9. Cell line-based intestinal tissue models

To set up *in vitro* models of the generated cell clones as well as of the Caco-2 cell line, $5x10^4$ cells were seeded per insert (Figure 3.3). Therefore, SIS- (Figure 3.3C) and BNC-matrices (Figure 3.3B), fixed between cell crowns, as well as commercially available PET- (Figure 3.3A) inserts (Transwells®) were used for Caco-2 *in vitro* models (as described in 3.2.1.). Cell clone-based models were set up only on commercial PET-Transwells® (section 3.2.1.3.; Figure 3.3A). The splitting procedure is described in section 3.2.2.4 and 3.2.2.7. Murine/human cell clones were cultured in murine cell clone medium/human cell clone medium and Caco-2 cells in DMEM as described in 3.1.6, with an apical volume of 300 µL and a basolateral volume of 900 µL. *In vitro* models based on murine cell clones and Caco-2 cells were used for experimental assays after 21 days of static culture and models based on human cell clones after 14 days of static culture.

Furthermore, human primary spheroid/organoid-based *in vitro* models were established on the SIS matrix, the PET membrane and both BNC variants in culture for 9 days in proliferation medium (section 3.1.6), followed by 5 days in differentiation medium (section 3.1.6). Growth factors such as nicotinamide and SB202190 were no longer supplemented, whereas 10 µM DAPT, a γ-secretase inhibitor, was added for spontaneous differentiation towards secretory-lineage-specific cell types.

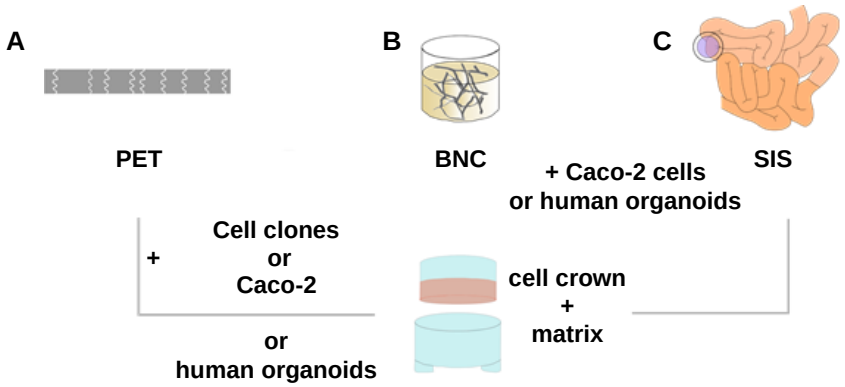

Figure 3.3: Setup of intestinal tissue models. PET-based Transwells® **(A)** were seeded either with murine/human cell clones, Caco-2 cells or human organoids, whereas BNC **(B)** and SIS **(C)** models were set up only with Caco-2 cells and human organoids.

3.2.3. Histology

3.2.3.1. Sample preparation

Intestinal organoids and spheroid-like cell clone-based structures were isolated from Matrigel® as described in section 3.2.2.4, washed in PBS^- and centrifuged at 300 x g for 3 min. The cell pellet, fixed with 4% paraformaldehyde (PFA) for 30 min at 4°C, was washed with PBS^- and resuspended in HistoGel™ to form droplets of 100 µL on a glass slide after solidification.

Caco-2 cells and human primary spheroids cultured as monolayers on PET, SIS or BNC as well as immortalized cell clones cultured as monolayers on either PET membranes or glass slides were washed with PBS^- and fixed with 4% PFA for 1 h at 4°C. HistoGel™ embedding occurred on models set up on PET- or BNC-scaffolds after washing with PBS^-.

Dissected small intestine was fixed in 4% PFA overnight at 4°C, followed by washing in PBS^-. Afterwards, all samples were preserved in paraffin for histological analyses, except the cell-based glass slides for 2D imaging. Caco-2 cell-based Transwell®-like models were used for staining procedures either as paraffin-embedded cross-sections or as top views without any embedding procedure. Paraffin conserved probes were cut into 5 µm slices and mounted on Polysine™ glass slides.

3.2.3.2. Hematoxylin and Eosin (H&E) staining

Slides were incubated at 60°C to melt the paraffin and the remaining residues were removed by two consecutive xylene-washing steps for 10 min each. For rehydration, the probes were dipped three times in a descending ethanol-series (twice 96% EtOH, 70% EtOH, 50% EtOH), stopped in demineralized water (dH_2O) followed by incubation for 6 min in Hematoxylin to stain the cell nuclei. After washing in dH_2O, slices were bathed in floating tap water for 5 min to develop the staining. The extracellular matrix and cytoplasmatic structures were stained in Eosin for 6 min. For dehydration, the samples were dipped twice in 70% EtOH, twice in 96% EtOH, followed by 5 min incubation in isopropanol I, isopropanol II, xylene I and xylene II. Samples were mounted with Entellan and a coverslip.

3.2.3.3. Alcianblue staining

Alcianblue staining was performed to stain acid mucins and therefore mucin producing cells in the intestinal spheroids/organoids or cell clone-based samples. The slices were deparaffinized and rehydrated according to section 3.2.3.2. After the dH_2O bath, the samples were incubated for 3 min in 3% acetic acid to negatively charge the acid mucins. Alcian blue, as positively loaded dye, binds electrostatic to the acid groups of the sample in 30 min. Slices were washed in dH_2O and the cell nuclei as well as the extracellular matrix were stained 5 min with Nuclear fast red. The samples were dehydrated and mounted with Entellan as described in section 3.2.3.2.

3.2.3.4. Immunohistochemistry

Paraffin sections were deparaffinized and rehydrated as described in 3.2.3.2. After boiling samples for 20 min in citrate buffer (pH 6) for heat-mediated antigen retrieval, the sections were marked with a grease pen and washed in PBS^- + 0.5% Tween-20 (PBS-T). A blocking solution (5% donkey serum in PBS^-) was applied for 20 min, followed by incubation with the primary antibody overnight at 4°C. The next day, slices were washed three times in PBS-T for 5 min each, before incubation with the secondary antibody for 60 min, RT in the dark occurred. Samples were washed again three times in PBS-T and mounted with Fluoromount-G™ supplemented with 4',6-diamidino-2-phenylindole (DAPI) for deoxyribonucleic acid (DNA) counterstaining.

Cells cultured on glass slides and Caco-2-based *in vitro* models (imaging top view) were washed with PBS^-, permeabilized with 0.2% Triton-X-100 for 30 min and washed with PBS-T for 5 min on a shaker. To avoid unspecific binding, a blocking solution (5% donkey serum in PBS^-) was applied for 30 min at RT for cells cultured on glass. Caco-2 cell-based models were treated for 2 h with a blocking solution of 5% bovine serum albumin (BSA) in PBS^-. Settled glass slides as well as Caco-2 *in vitro* models were stained with the primary antibody diluted in antibody dilution solution overnight at 4 °C. The following steps were performed according to the normal paraffin sections as described above. Briefly, samples were washed three times with PBS-T, followed by incubation with the secondary antibodies for 60 min at RT in the dark for cells cultured on glass slides and 2 h for Caco-2-based models. Finally, the samples were washed three times with PBS-T and mounted with Fluoromount-G™ supplemented with DAPI for DNA counterstaining.

3.2.3.5. SEM and TEM imaging

Ultrastructural analysis of the Caco-2/cell-clone-based tissue models were performed by transmission (TEM) and scanning electron microscopy (SEM). Samples were washed with PBS^- and fixed in 2.5% glutaraldehyde for TEM imaging and 6.5% glutaraldehyde for SEM imaging. All further steps of processing ultrathin sections and also analyses of the samples were performed at the core facility of Prof. Dr. Stigloher of the University of Würzburg.

3.2.3.6. Microscopy

Histological samples either fluorescence labeled or stained with standard kits were analyzed using the inverse fluorescence microscope BZ-9000 (Keyence) or the confocal microscope TCS SP8 (Leica Microsystems). Image acquisition of cell-clones in 2D/3D and primary organoids was performed with the EVOS™ XL Core Imaging System (Thermo Fisher) for the documentation of cellular morphology.

3.2.4. Flow cytometry

The proliferation rate, as important feature of newly generated cell lines, was measured by flow cytometry analyses via the EdU-Click it® kit. Therefore, the samples were incubated for 2 h with pre-warmed maintenance medium supplemented with 1 mM EdU at 37°C, 5% CO_2, 95% humidity. The cells were harvested according to section 3.2.2.4 and 3.2.2.7 from either Matrigel® droplets or cell culture plastic. Afterwards, samples were washed with PBS^- containing 1% BSA before fixation with 100 µL Click-it fixative for 15 min at RT in the dark. The cell suspension was washed again with 1% BSA in PBS^-, followed by permeabilization (15 min, protected from light, RT) of the cells with the saponin-based buffer as described in the manufacturer instructions. To detect the 5-Ethynyl-2'-deoxyuridine (EdU)-labeled proliferative cells, the Click-it™ Plus reaction cocktail (containing copper sulfate, EdU buffer additive, Alexa Fluor® 647 as fluorescent dye and PBS^-) was added for 30 min at RT. The stained cell pellet, washed twice with the saponin-based buffer, was finally analyzed at the BD FACS Accuri by resuspending the cells in 500 µL saponin-based buffer.

3.2.5. Molecular biological methods

3.2.5.1. RNA isolation

To isolate RNA from 2D-cultured cells or Transwell®-models, samples were lysed with RLT buffer containing 1% 2-mercaptoethanol. For 3D-cultured organoids or spheroid-like cell clone-based structures, Matrigel® droplets were dissolved in Cell Recovery Solution as described in 3.2.2.4 for splitting organoids. The organoid or spheroid-like cell-based pellet was washed with PBS^- and lysed in RLT buffer complemented with 1% 2-mercaptoethanol. Samples were homogenized through a QIAshredder spin column, followed by processing the manufacturer's recommendations of the RNeasy micro Kit including the DNase treatment of 15 min at RT. The amount and quality of RNA was measured at 260 and 280 nm in a NanoDrop plate from Tecan.

3.2.5.2. cDNA synthesis

The isolated RNA was reversely transcribed with the iScript cDNA Synthesis Kit according to the following settings:

5x iScript reaction mix	*4 µL*
iScript Reverse Transcriptase	*1 µL*
1 µg RNA template	*x µL*
Nuclease-free water	*x µL*
Total volume:	*20 µL*

In a 3-step cycler program on the LabCycler48, the reverse transcription was performed according to the protocol: 5 min at 25°C, 30 min at 42°C and 5 min at 85°C. Samples were stored at -20°C for a maximum of two weeks. Long-term storage occurred at -80°C.

3.2.5.3. Real Time quantitative PCR

The messenger ribonucleic acid (mRNA) transcription profile of the generated cell lines was compared to the primary source material, the intestinal organoids. To normalize the amplification signal of the gene of interest, the reference genes *mRpl15* and *mRps29* were used for murine cells, whereas *hHPRT1* and *hEF1α* were used for human cells. The amplification reactions were conducted in duplicates with the following mixture:

SsoFast EvaGreen Supermix	*10 µL*
Forward primer (400 nM)	*2 µL*
Revers primer (400 nM)	*2 µL*
cDNA	*1 µL*
ddH_2O	*5 µL*
Total volume:	*20 µL*

A 2-step quantitative real time polymerase chain reaction (RT-qPCR) protocol was used for the cDNA amplification, which included an initial denaturation (95°C, 3 min) and 40 cycles of the following settings: denaturation at 95°C for 10 s and the annealing/extension period at 60°C for 30 s. The amplicon specificity of the PCR product was verified by an agarose gel. According to the MIQE guidelines [215] [216], the gene expression was calculated by the $2^{-\Delta\Delta CT}$ ($\Delta\Delta$CT) method.

3.2.6. Barrier integrity studies

3.2.6.1. FITC-dextran assay

FITC-dextran is a reference substance for the paracellular transport and therefore allows the characterization of the barrier integrity of intestinal *in vitro* models. The sugar chain is covalently coupled with Fluorescein isothiocyanate (FITC) to enable a fluorescence-based detection method of the transported amount of molecules. Therefore, 4 kDa FITC-dextran was solved in cell type-specific medium at a concentration of 0.04 mg/mL and was centrifuged in Amicon® Ultra size exclusion filters at 4000 x g for 30 min. After sterile filtration of the FITC-dextran solution, 300 µL were added apical balanced by 900 µL cell type specific medium in the basolateral compartment. Samples of 100 µL were drawn basolateral after 1 h of incubation at 37°C and absorption was measured at an excitation wavelength of 490 nm and an emission wavelength of 525 nm with the Tecan infinite 200 plate reader in comparison to an empty insert. The permeability for FITC-dextran was calculated in percentage with regard to the donor solution as 100%.

3.2.6.2. Barrier integrity measurement

To ensure a tight epithelial barrier, TEER measurements were performed on established *in vitro* models. A commercially available hand-electrode was pre-incubated in 70% ethanol for 15 min, followed by cell-specific medium (mentioned in section 3.1.6) for further 15 min. After calibration of the device with a standard resistor, the TEER values of each model were

measured on three different positions of the insert directly after a medium change. For normalization, the TEER values of empty inserts were subtracted and the values obtained are set in relation to the area of the inserts.

Barrier integrity analyses were further determined by an impedance spectrometer with a frequency range from 1 to 100 kHz and a voltage amplitude of 2 mV developed by Schmitz et al. [217] for a more sensitive measurement. Therefore, intestinal models were placed in 24-well plates with 0.3 mL medium in the apical compartment und 1.1 mL medium in the basolateral compartment (cell-specific medium is mentioned in section 3.1.6). After post-incubation of the cleaned nanorough titanium nitride (TiN) electrodes for 60 min at 37°C in the model-containing wells, the impedance-measuring unit was connected and the TEER values were monitored at 12.5 Hz.

3.2.6.3. Transport studies

Functional characterization of the established *in vitro* models based on Caco-2 cells or murine/human cell clones was conducted by epithelial transport studies. The different transport mechanisms were characterized by fluorescein as low-permeable substance for the paracellular transport, propranolol as high-permeable substance for the transcellular transport and rhodamine 123 as substrate for the efflux-transporter *p*-gp. Test substances were solved in cell-specific medium (crypt medium or Caco-2 medium is described in section 3.1.6) and added in a volume of 300 µL in the donor compartment with the following concentrations: 10 µM fluorescein, 100 µM propranolol and 100 µM rhodamine 123. Samples of 100 µL were taken from the acceptor compartment (900 µL) every 15 min for 2 h after application. Propranolol measurements were carried out by HPLC-MS/MS (performed by the external partner Sapiotec GmbH) analysis, whereas fluorescein and rhodamine 123 were determined by analyzing the fluorescence intensity using the Tecan microplate reader. To determine the test substance concentrations after transport, values were compared to a standard curve of the different substances. The apparent permeability coefficient (P_{app}-value) was calculated according to Artursson et al. [111].

3.2.7. Nanoparticle permeation

Nanoparticle permeation was used to characterize physical barriers caused by the pore distribution of the scaffold material (BNC-, SIS- or PET-based models). Coumarin-6 labeled poly($_{D,L}$-lactic-*co*-glycolic acid) (PLGA)-based nanoparticles (NPs), dissolved in Caco-2 cell culture medium, were applied in the apical compartment (1.0 mg/mL, 300 µL) of the

Transwell®-like models. Over a time period of 6 h, samples of 100 µL were retained after 30 min, 1 h, 2 h, 3 h, 4 h, 5 h and 6 h from the basolateral compartment (900 µL) and replaced with fresh medium. The fluorescently labeled NPs as well as a NP standard curve were measured at 450 nm with a Tecan microplate reader to determine the NP concentration.

3.2.8. Permeability assay with EGTA

Caco-2 cell-based *in vitro* models cultured on BNC, PET or SIS were used to prove the formation of an intact barrier and the regeneration capacity of tight junctions after treatment with cell-cell contact disturbing agents. Therefore, Caco-2 based *in vitro* models were treated with 1.5 µL of a 4 M ethylene glycol-bis(β-aminoethyl ether)-*N,N,N',N'*-tetraacetic acid (EGTA) stock solution (final concentration 20 mM EGTA in the apical compartment) after a culture and differentiation time of 21 days. Subsequently, barrier integrity changes were measured at several time points (0/ 5/ 15/ 25/ 35 min) with a chopstick hand-electrode (described in section 3.2.6.2) of treated and non-treated models. For regeneration of the tight junctions, the medium was replaced and the models were cultured for further 24 h at 37°C. In addition to the TEER-values, barrier integrity was measured before and after the regeneration period of EGTA-treated models by FITC-dextran analyses (described in 3.2.6.1). After the regeneration period a treatment for 2 h with sodium dodecyl sulfate (SDS) occurred as negative control, leading to a complete breakdown of the TEER values.

3.2.9. Statistics

Unless otherwise stated all data are presented as means ± standard deviation (SD). Statistical analyses were calculated by one-way ANOVA with Tukey's multiple comparison test for values of three or more. If only two datasets were analyzed, the significance was determined with an unpaired t-test by using the GraphPad Prism 7 Software. The level of statistical significance is hallmarked with an asterisk (*) as follows: *p<0.05, **p<0.01, ***p<0.001.

4. Results

4.1. The BNC as alternative ECM scaffold in intestinal tissue engineering

Artificial synthetic polymers like PET are commonly used as structural scaffolds for intestinal tissue engineering [112,198]. Due to the low porosity or unwanted molecular adhesion effects of synthetic carries [112], natural ECMs were recently highlighted as interesting alternatives. However, major limitations of biological matrices are less well-standardized fabrication processes and the lack of sufficient quantities that need to be produced in large-scale for pre-clinical applications (*e.g.* pharmaceutical drug screenings). Here, I hypothesized that biopolymers such as the BNC could overcome those drawbacks. In this context, the aim of this part of my work was to validate the BNC matrix, unmodified or surface-structured, as suitable scaffold for the standardized setup of intestinal *in vitro* models that display a high *in vitro-in vivo* correlation regarding its functional performance, thereby demonstrating BNC-based models as new alternative for pre-clinical applications. Both versions of the BNC used in this project were provided by the collaboration partner JeNaCell. Of note, parts of the described results were obtained in collaboration with Ms. Jana Betz, a student of biology that performed her bachelor thesis entitled “Establishment of nanocellulose-based *in vitro* test systems” at our institute under my supervision, which was submitted to the University of Würzburg in 2016.

4.1.1. Caco-2 cells cultured on BNC show characteristic tight/adherens junction protein expression profiles

Intestinal *in vitro* models were set up on unmodified or surface-structured BNC scaffolds as well as on SIS or PET matrices as controls. Therefore, both BNC variants and the SIS were fixed between two plastic cylinders, termed cell crowns, to generate a Transwell®-like system, as it is commercially available for PET membranes (Figure 4.1A-C). Within these systems, Caco-2 cells were cultured for up to 21 days on all scaffolds until a confluent cell layer was formed. Immunohistochemistry (IHC) analyses revealed viable Caco-2 cells on all scaffolds at day 21 and further demonstrated the expression of characteristic tight/adherens junction proteins such as ZO-1, OCLN and ECAD in all models, independent from the used scaffold (Figure 4.1D). Furthermore, a continuous allocation of IHC signals was observed indicating a homogenous distribution of corresponding tight/adherens junction proteins among single Caco-2 cells cultured on the unmodified BNC scaffold, the SIS matrix or the PET membrane. In contrast, a more scattered and inhomogeneous expression pattern of all

analyzed tight/adherens junction proteins was revealed for Caco-2 cells cultured on the surface-structured BNC.

In summary, all matrices enabled the formation of a continuous Caco-2 cell layer with characteristic tight/adherens junction expression profiles as indicated by IHC analyses. Comparing all models, the most homogenous expression pattern of all analyzed proteins was observed for Caco-2 cells cultured on the unmodified BNC followed by SIS-, PET- and surface-structured BNC-based models, indicating the unmodified BNC as most beneficial for Caco-2 cells forming a structurally well-defined cell layer *in vitro*.

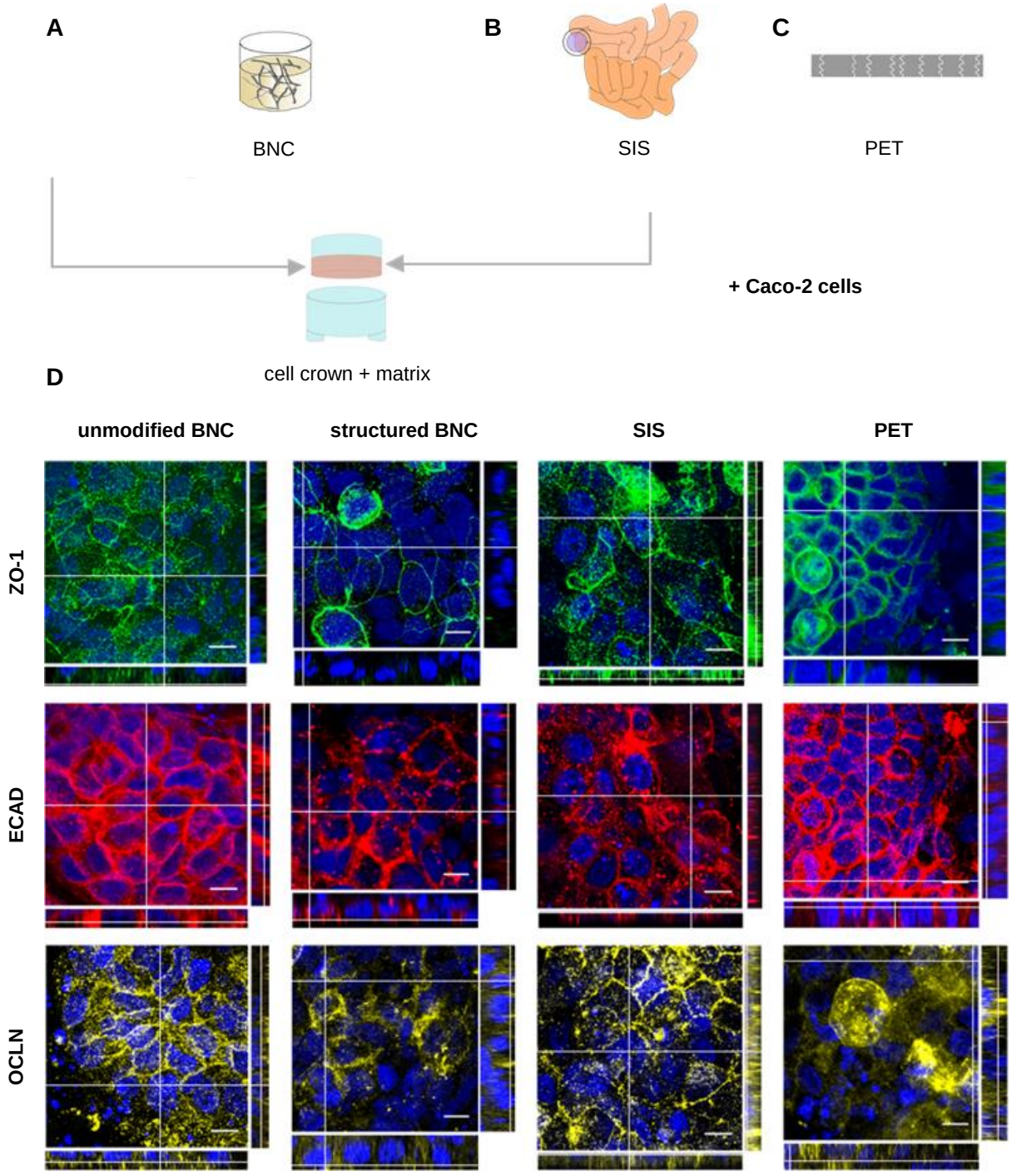

Figure 4.1: Model setup and tight/adherens junction protein expression profiles of Caco-2 cells cultured on unmodified BNC, surface-structured BNC as well as SIS and PET. Caco-2 cells were cultured for 21 days on unmodified or surface-structured BNC **(A)**, SIS **(B)** or PET **(C)**. The expression of the characteristic tight/adherens junction proteins ZO-1 (green), ECAD (red) and OCLN (yellow) analyzed by IHC are shown in representative microscopic images **(D)**. Cell nuclei are counterstained with DAPI (blue). Scale bar = 10 µm; n = 3. ZO-1: zonula occludens-1; ECAD: E-cadherin; OCLN: occludin; BNC: bacterial nanocellulose; SIS: small intestinal submucosa; PET: polyethylene terephthalate; DAPI: 4',6-diamidino-2-phenylindole.

4.1.2. BNC-based Caco-2 models form a tight cell layer

The formation of a tight epithelial barrier as characteristic feature of intestinal *in vitro* models was monitored by histological and ultrastructural analyses as well as by barrier regeneration studies after treatment with EGTA. Representative images of H&E-stained sections of all Caco-2 models revealed the formation of a consistent cell layer with attached cells on all matrix surfaces (Figure 4.2Aa-d). Furthermore, Caco-2 cells showed in all models a so called bi- or multi-layering behavior that depicts a characteristic feature of this cell line [218,219], when cultured under pro-differentiation stimuli *in vitro*. However, Caco-2 models set up on BNC or PET scaffolds showed a flatter cell layer combined with a bright signal of the eosin staining indicating the formation of a compact connective tissue (Figure 4.2Aa-b, d). In contrast, eosin staining in SIS-based models appears lighter suggesting a looser connective tissue within these cell layers.

High-resolution SEM or TEM analyses also confirmed the formation of a consistent cell layer on all matrix surfaces (Figure 4.2e-l). In addition, the presence of characteristic tight junctions (Figure 4.2i-l) as well as a brush border membrane with apical microvilli structures (Figure 4.2e-l) was observed, both representing biological prerequisites for proper cell and therefore model functionality. However, SEM images pointed out that Caco-2 cells cultured on the surface-structured BNC (Figure 4.2f/f_1), the SIS (Figure 4.2g/g_1) or the PET (Figure 4.2h/h_1) contained individual cells without microvilli (marked with a star), whereas a uniform distribution of microvilli-containing cells was shown for *in vitro* models established on the unmodified BNC (Figure 4.2e/e_1).

Next to these (ultra-)structural features, barrier integrity was demonstrated by performing permeability studies with EGTA, a chelating agent that reversibly opens cell-cell contacts by binding extracellular Ca^{2+} ions, which are crucial for the development and stability of tight junction complexes [220–222]. Therefore, EGTA was applied up to 35 min to all models. TEER values were measured before application of EGTA as well as in 5 to 10 min intervals during the time course of 35 min EGTA treatment and after EGTA withdrawal from cultures. TEER values are shown in Figure 4.2B-E and in Table 4.1 in a time-dependent manner for all Caco-2 *in vitro* models. Compared to the TEER values obtained before EGTA application, treatment with EGTA resulted in a 23% reduction of TEER values for models set up on the unmodified BNC, 28% for PET- or structured BNC-based models and 40% for SIS-based models. After a regeneration period of 24 h in exchanged EGTA-free medium, elevated TEER values were measured in all models (Figure 4.2B-E), indicating the reformation of tight junction complexes. Additionally, FITC-dextran transport analyses performed after a regeneration period of 24 h confirmed the data obtained by TEER measurements, as the

comparison between EGTA-treated and EGTA-untreated models showed no significant differences regarding their permeability (Figure 4.2F). To further assess the reformation of an intact barrier on all scaffolds, models were treated for 2 h with SDS leading to the disruption of the cell membrane and therefore barrier breakdown indicated by TEER values of 0 Ω*cm².

In conclusion, H&E stainings revealed differences in connective tissue when cells were cultured on distinct scaffolds. Of note, SIS-cultured Caco-2 layers appeared to have a looser connective tissue compared to those formed by cells cultured on both BNCs and the PET membrane. Furthermore, the data obtained by FITC-dextran or TEER measurements showed a tighter epithelial barrier when Caco-2 cells were cultured on the synthetic PET membrane or both BNC variants. These data together with the observations from the ultrastructural analyses showed that the models set up on the unmodified BNC performed best.

Table 4.1: TEER values of EGTA-treated and untreated models.

Time	**TEER [Ω*cm²]**							
	unmodified BNC		**structured BNC**		**SIS**		**PET**	
	EGTA	**control**	**EGTA**	**control**	**EGTA**	**control**	**EGTA**	**control**
0 min	**212 ± 28**	**224 ± 17**	**176 ± 4**	**224 ± 19**	**125 ± 15**	**126 ± 19**	**140 ± 2**	**165 ± 3**
5 min	**147 ± 1**	**226 ± 12**	**138 ± 15**	**218 ± 13**	**86 ± 22**	**130 ± 24**	**101 ± 12**	**171 ± 2**
15 min	**71 ± 5**	**217 ± 9**	**70 ± 32**	**213 ± 12**	**55 ± 12**	**132 ± 21**	**57 ± 1**	**166 ± 2**
25 min	**49 ± 2**	**219 ± 5**	**50 ± 24**	**209 ± 12**	**54 ± 5**	**135 ± 25**	**44 ± 3**	**164 ± 1**
35 min	**50 ± 1**	**218 ± 9**	**50 ± 23**	**204 ± 17**	**50 ± 9**	**138 ± 22**	**41 ± 1**	**161 ± 9**
24 h	**128 ± 6**	**226 ± 25**	**144 ± 9**	**209 ± 6**	**110 ± 7**	**133 ± 21**	**162 ± 16**	**220 ± 36**
2 h SDS	**0**	**205 ± 23**	**0**	**185 ± 9**	**0**	**129 ± 26**	**0**	**193 ± 17**

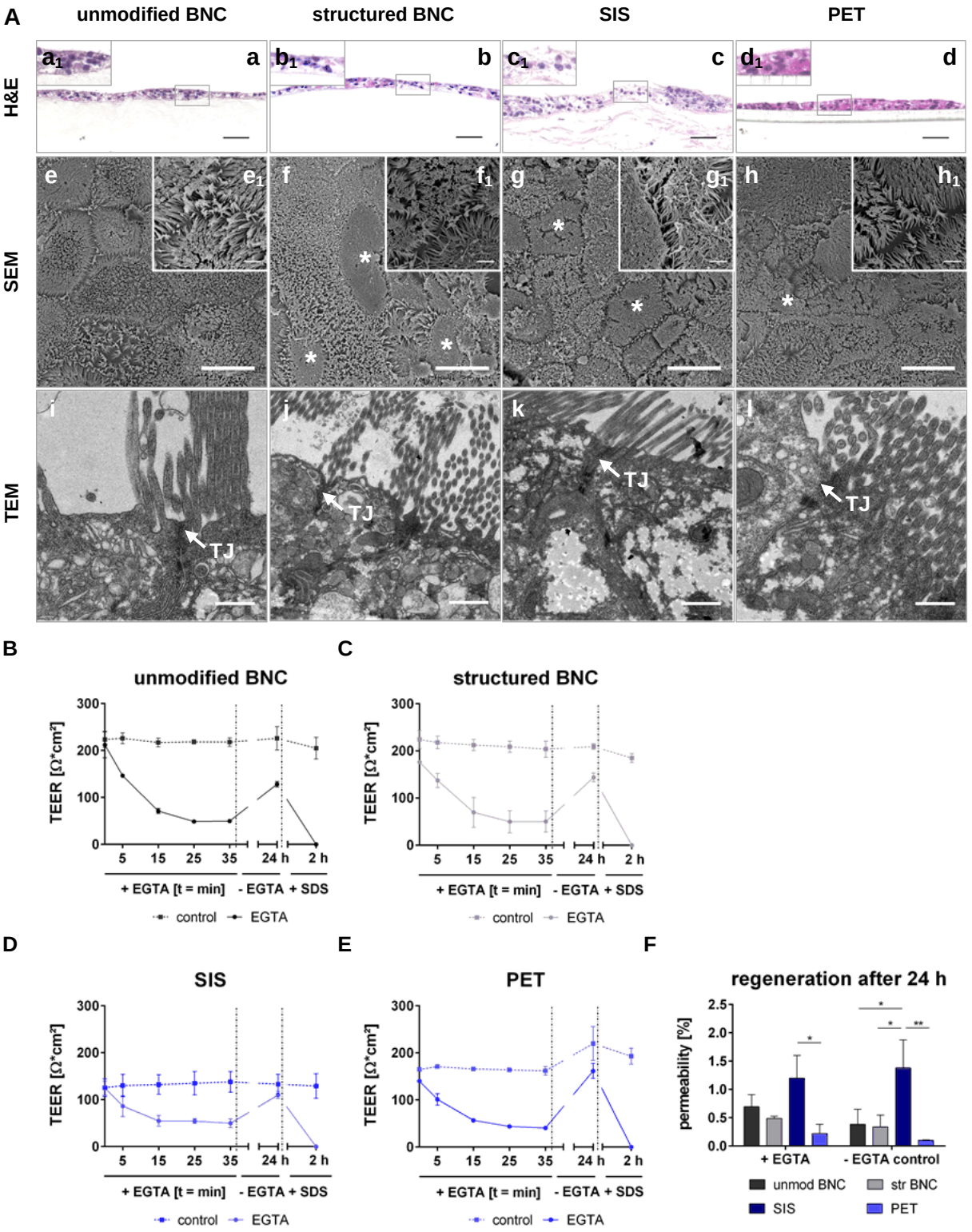

Figure 4.2: Caco-2 cells cultured on the unmodified or structured BNC, SIS as well as PET membrane form a tight epithelial barrier with tight junctions and microvilli. Cross-sectional images of H&E-stained Caco-2 models based on unmodified BNC **(a/a$_1$)**, structured BNC **(b/b$_1$)**, SIS **(c/c$_1$)** or PET **(d/d$_1$)** indicated the formation of a tight epithelial barrier. Representative images obtained from ultrastructural SEM **(e/e$_1$-h/h$_1$)** and TEM **(i-l)** analyses showed a consistent cell layer on all scaffolds, the formation of apical microvilli and tight junctions (TJ; arrow). Single cells without microvilli (marked with a star) were identified in SEM analyses for

structured BNC **(f)**, SIS **(g)** and PET **(h)**. Interruptions in the microvilli formation in TEM images were caused by the refurbishment method of the models. Scale bars = 50 µm (H&E); 10 µm (SEM); 1 µm (SEM magnification); 500 nm (TEM); representative images of n = 3 replicates. Graphs demonstrating TEER values obtained before, during and after EGTA administration (t = 35 min) to assess barrier integrity in models set up on the unmodified BNC **(B)**, the structured BNC **(C)**, the SIS **(D)** as well as the PET **(E)** membrane. Decreasing TEER values indicated barrier break down. After 24 h of regeneration without EGTA treatment, elevated TEER values are shown in the graphs. SDS treatment (t = 2 h) destroyed the cell layer in all models as indicated by the drop of TEER values to 0 Ω*cm². Controls represent untreated (without EGTA and without SDS) Caco-2 models. Regeneration capacity after 24 h was confirmed by FITC-dextran permeability **(F)** for BNC-, SIS- and PET-based models. n = 2 with three technical replicates. Significance was calculated by unpaired t-test. **p<0.05, **p<0.01*. H&E: haematoxylin and eosin; TEM: transmission electron microscopy; SEM: scanning electron microscopy, EGTA: ethylene glycol-bis(β-aminoethyl ether)-*N,N,N',N'*-tetraacetic acid; TEER: transepithelial electrical resistance; SDS: sodium dodecyl sulfate; FITC: fluorescein isothiocyanate; BNC: bacterial nanocellulose; SIS: small intestinal submucosa; PET: polyethylene terephthalate; t: time.

4.1.3. Caco-2-based models show organ-specific transport functions when cultured on BNC scaffolds

The formation of an intact barrier was further determined by non-destructive impedance measurements on individual scaffold-based models started on day 14 up to day 21 of culture. TEER values of Caco-2 cell-based models continuously increased to a mean maximum of 226 ± 14 Ω*cm² on the unmodified BNC, to 243 ± 34 Ω*cm² on the structured BNC, to 191 ± 25 Ω*cm² on the biological SIS matrix and to 194 ± 16 Ω*cm² on the synthetic PET membrane (Figure 4.3A). These data implied a culture time of at least three weeks to establish a tight epithelial barrier on all scaffolds.

Subsequently, FITC-dextran, fluorescein, propranolol and rhodamine 123 were used as reference substances to analyze the transport capacity (Figure 4.3B-E) of the generated *in vitro* models. First, permeability rates of FITC-dextran (zero-permeable substance) were measured to investigate the paracellular transport capacity across a closed cellular barrier. SIS-based Caco-2 models displayed a mean permeability rate for FITC-dextran of 2.4% ± 1.8% to the basolateral compartment, while models established on the unmodified BNC (0.25% ± 0.2%) or surface-structured BNC (0.25% ± 0.3%) as well as PET (0.06% ± 0.1%) showed significantly lower permeability rates (Figure 4.3B). The fluorescein (Figure 4.3C) transport capacity (indicated by the P_{app}-value) was 2.5 times higher for SIS-based models (P_{app}-value of $5.0x10^{-6}$ cm/s) compared to models set up on unmodified BNC (P_{app}-value of $2.0x10^{-6}$ cm/s), structured BNC (P_{app}-value of $1.3x10^{-6}$ cm/s) or PET (P_{app}-value of $2.4x10^{-6}$ cm/s). Together, the results obtained from the FITC-dextran as well as the fluorescein transport assay indicated the formation of a tight epithelial barrier, as the transport of both reference substances is controlled by distinct tight junction proteins [15,223].

Propranolol (Figure 4.3D) was transported to a similar extend in models set up on the unmodified BNC (P_{app}-value of $1.6x10^{-5}$ cm/s) or SIS (P_{app}-value of $2.1x10^{-5}$ cm/s), with a slightly higher P_{app}-value for the SIS-based models. In contrast, models established on the surface-structured BNC (P_{app}-value of $1.4x10^{-5}$ cm/s) or PET (P_{app}-value of $1.0x10^{-5}$ cm/s) showed a 1.5 fold and 2-fold decrease in their transcellular transport capacity, respectively.

The efflux transport studied with rhodamine 123 as representative substrate (Figure 4.3E), is defined as the ratio of basolateral/apical (ba) transport to apical/basolateral (ab) transport. For models set up on both BNCs (ba/ab = 4.0 or 4.9) and the PET (ba/ab = 3.5), a slightly higher efflux was observed, compared to SIS-based models (ba/ab =1.9).

In conclusion, the established models on the unmodified as well as surface-structured BNC demonstrated a tight epithelial barrier with a high applicability in transport studies.

In addition to performing classical transport studies as described above, the nanoparticle uptake capacity by endocytosis was investigated for BNC-based models, as scaffold materials, especially artificial membranes such as PET, often represent an additional physical barrier due to an unequal pore distribution [112,116]. Transport of coumarin-6-labeled PLGA-NPs (1 mg/mL) measured over 6 hours, showed a transfer rate of 1.5% for models set up on the unmodified BNC (Figure 4.3F), 1.3% on the surface-structured BNC (Figure 4.3G), 2.6% on the SIS (Figure 4.3H) and 1.4% on the PET (Figure 4.3I). Within 3-6 hours, the straight slope of the applied straight line is lower in this period for PET-based (slope/m = 0.0013) and unmodified BNC-based (m = 0.0014) models, compared to the models based on structured BNC (m = 0.0017) and SIS (m = 0.0037) (Figure 4.3F-I).

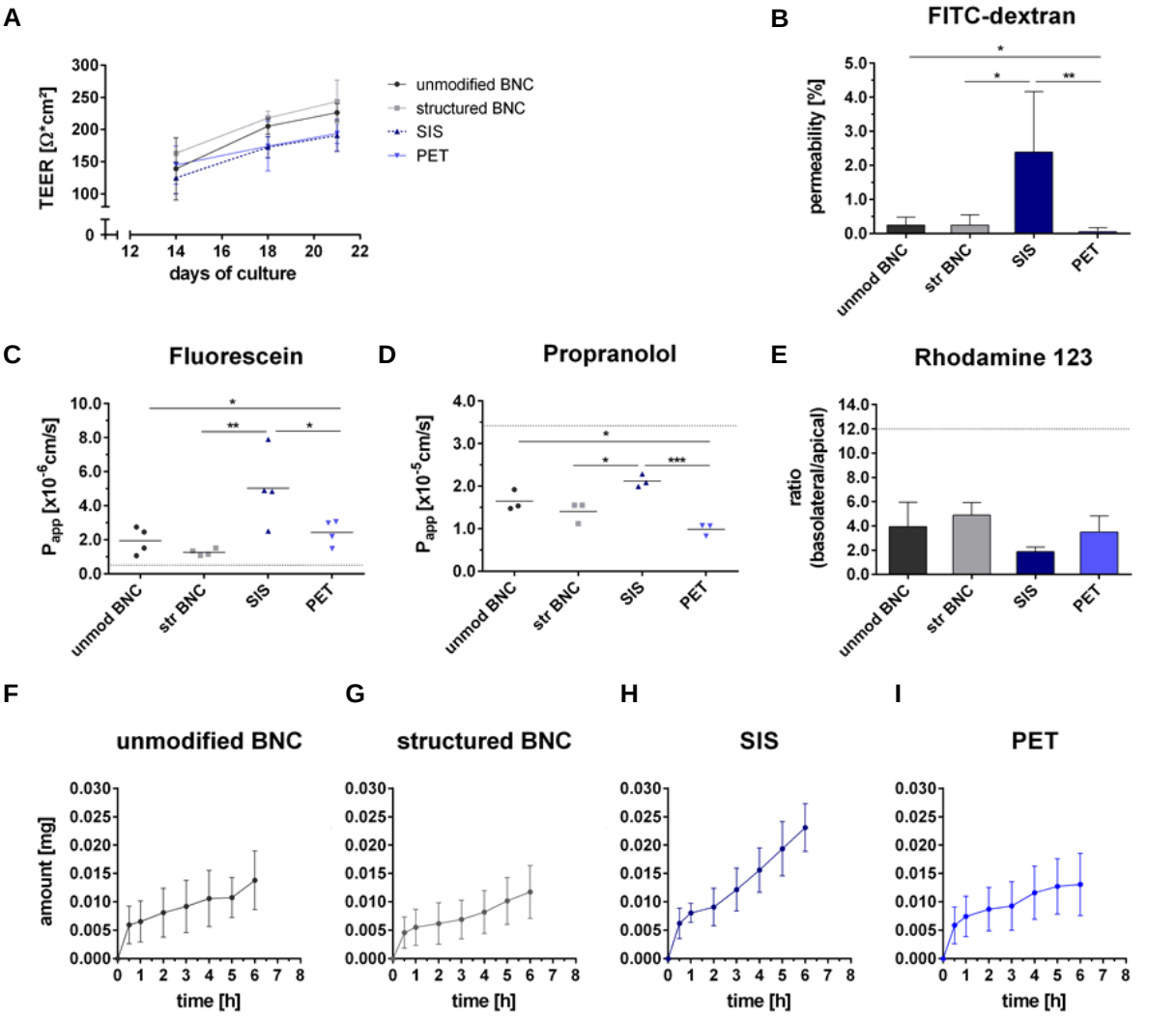

Figure 4.3: BNC-based models form a tight epithelial barrier and display characteristic transport activities. TEER values rose to a similar ratio from day 14 to day 21 in culture **(A)**, but FITC-dextran was transported to a lower extent on BNC- and PET-based models **(B)**. Low-permeable fluorescein **(C)** showed lower and more robust P_{app}-values for models set up on both BNC variants and PET. A reduced transcellular permeability of propranolol **(D)** was measured for models based on surface-structured BNC and PET. The transport activity of rhodamine 123 **(E)** displayed a slight increase in the established models on both BNCs and PET. Transport capacity of Caco-2 Transwell®-models recently reported by Bock et al. [224] is represented as reference value indicated by the dotted line **(C-E)**. Nanoparticle transport was studied up to 6 h on Caco-2 based models established on unmodified BNC **(F)**, surface-structured BNC **(G)**, SIS **(H)** and PET **(I)**. PLGA-NPs (1 mg/mL) were transported to a higher amount on SIS-based models **(H)** compared to the other matrix-based models. Significance was calculated by one-way ANOVA. **p<0.05, **p<0.01, ***p<0.001;* n ≥ 3. TEER: transepithelial electrical resistance; unmod: unmodified; str: structured; BNC: bacterial nanocellulose; SIS: small intestinal submucosa; PET: polyethylene terephthalate; P_{app}: apparent permeability coefficient; PLGA-NPs: poly($_{D,\,L}$-lactic-co-glycolic acid) nanoparticles.

4.1.4. Primary intestinal epithelial cells did not form consistent cell monolayers on both BNC variants

In the studies performed with Caco-2 cells cultured for 21 days on the unmodified BNC, surface-structured BNC as well as SIS or PET as controls, BNC was proven to be a suitable alternative for standardized setup of small intestinal epithelium models, compared to commonly used matrices. To allocate these findings for other cell sources, human primary intestinal organoids were seeded with $4x10^5$ single cells onto the unmodified or structured BNC, the SIS as well as the PET followed by culture of 14 days. Human proliferation medium (section 3.1.6) was applied for 9 days, followed by culture in human differentiation medium (section 3.1.6) for 5 days. Representative images of H&E-stained sections of fixed models showed that Caco-2 cells formed a tight cell layer on all scaffolds (Figure 4.4A-D), while primary organoid cultures formed a highly polarized monolayer only on SIS (Figure 4.4G) and PET (Figure 4.4H) scaffolds. Although primary cells grew on both BNC variants (Figure 4.4E-F), cells did not properly attach to the scaffold. In addition, H&E stainings revealed a fragmentary cell layer on the unmodified (Figure 4.4E) and surface-structured BNC (Figure 4.4F).

Taken together, the unmodified as well as the surface-structured BNC were not suitable for model setup using primary epithelial cells derived from 3D organoid cultures. However, studies in which model setup with Caco-2 cells is preferred, the unmodified BNC represents a new and appropriate scaffold for the generation of robust epithelial cell layers of the small intestine displaying a tight barrier and characteristic transport features.

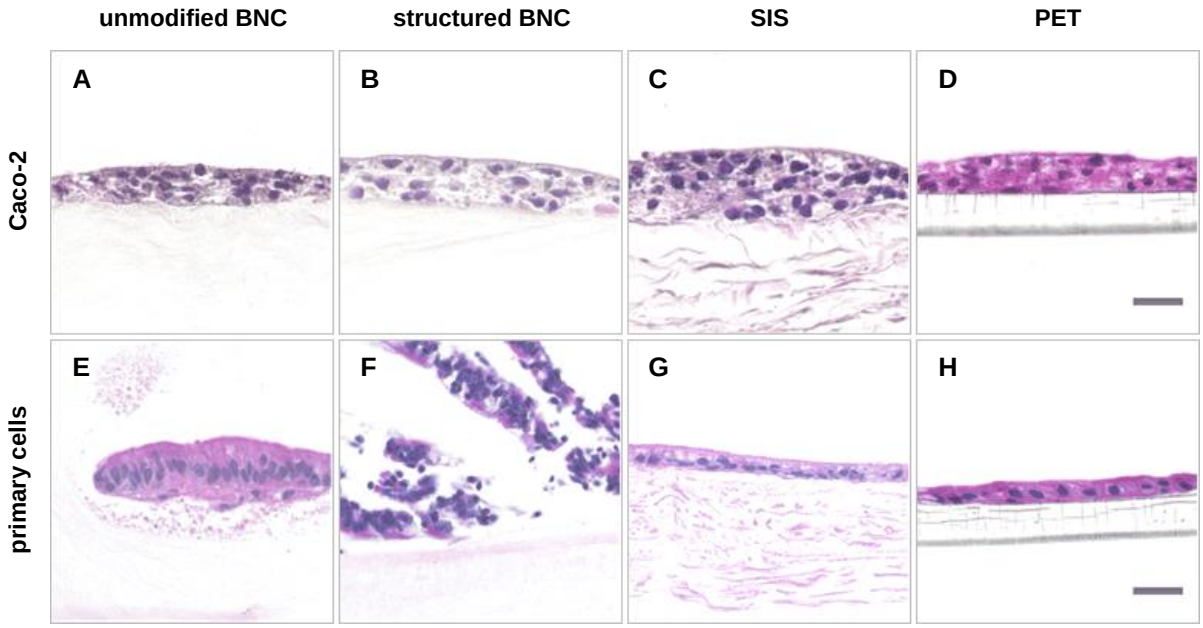

Figure 4.4: Cell morphology of Caco-2 cells and intestinal primary cells cultured on unmodified BNC, structured BNC, SIS and PET. Representative images of H&E stained Caco-2 cells show similar growth characteristics irrespective of the scaffold **(A-D)**. Intestinal primary cells grew as non-confluent, superimposed cell clusters on the unmodified **(E)** and surface-structured BNC **(F)**, whereas the cells formed a 2D monolayer on SIS or PET **(G, H)**. Scale bar = 100 µm; n = 3. BNC: bacterial nanocellulose; SIS: small intestinal submucosa; PET: polyethylene terephthalate.

Due to their animal origin and the manual decellularization process, SIS-based models are less standardized and therefore do not provide ideal conditions for the establishment of pre-clinical test systems. Thus, PET-inserts were chosen as scaffold for all further experiments in order to set up preferably standardized *in vitro* models using the here established immortalized cell clones, which is described in the following part 2 of my work.

4.2. Primary organoid-derived cell lines as alternative cell source

Drug screening [225], bioavailability [105,106] or toxicity studies [107] were mainly performed on Caco-2 *in vitro* models in the past. However, these classical *in vitro* systems represent relevant characteristics of the native tissue only to some extent [112]. Nowadays, primary tissue-derived spheroid/organoid cultures [30,174] gain increasing interest; however, the complex technical conditions and the high costs associated with their *in vitro* culture (*e.g.* Matrigel®, medium supplements) are decisive negative factors for pre-clinical large-scale applications.

To overcome these limitations, I hypothesized together with my collaboration partner InSCREENeX that the immortalization of primary intestinal organoid cultures will result in new cell lines that retain their native cellular features but are technically easy to handle at low costs, thereby representing an interesting alternative for pre-clinical research applications. While immortalization was performed by InSCREENeX, the aim of this part of my thesis was to screen the generated cell lines (cell clones) for their needs in cell culture, to validate their biological and functional properties and to test their capacity to set up an intestinal *in vitro* model applicable in pre-clinical research.

4.2.1. Immortalization of primary organoids by lentiviral transduction with a pool of genes regulating stemness and the cell-cycle

Primary intestinal spheroids used for immortalization were derived from murine and human intestine tissue as previously described [30,174]. Details about murine and human donor tissues are summarized in Table 4.2. After crypt isolation, they were embedded into Matrigel® drops (Figure 4.5A) followed by *in vitro* culture in murine/human organoid maintenance medium (section 3.1.6) until characteristic spheroids formed that developed into organoid structures with ongoing time of culture (Figure 4.5B) [30,174]. Afterwards, organoids were split for subsequent expansion as spheroidal clusters and parts of these cultures were used to establish spheroid biobanks in collaboration with colleagues at the Chair of Tissue Engineering and Regenerative Medicine (TERM/UKW). The proliferative potential of the generated spheroid lines is shown in Figure 4.5C-D depicting cells positive for KI-67 with a mean proliferation rate of 25.5 ± 6.2% for murine and 21.6 ± 6.0% for human spheroids analyzed by an EdU proliferation assay using flow cytometry. In addition, murine and human spheroid/organoid cultures were analyzed for some key features of the native intestinal epithelium before they were transferred to InSCREENeX for immortalization. Alcian blue staining of Histogel®-embedded organoid samples demonstrated the presence of mucus-

producing goblet cells indicated by the blue layer of acid mucin proteins within the intestinal lumen (Figure 4.5C-D). IHC signals for ECAD highlighted the formation of tissue-specific adherens junction proteins between adjacent cells, indicating a tight epithelial barrier (Figure 4.5C-D).

Together, murine and human spheroids of the established biobank showed a tight epithelium with characteristic proliferation rates, suggesting them as suitable for immortalization.

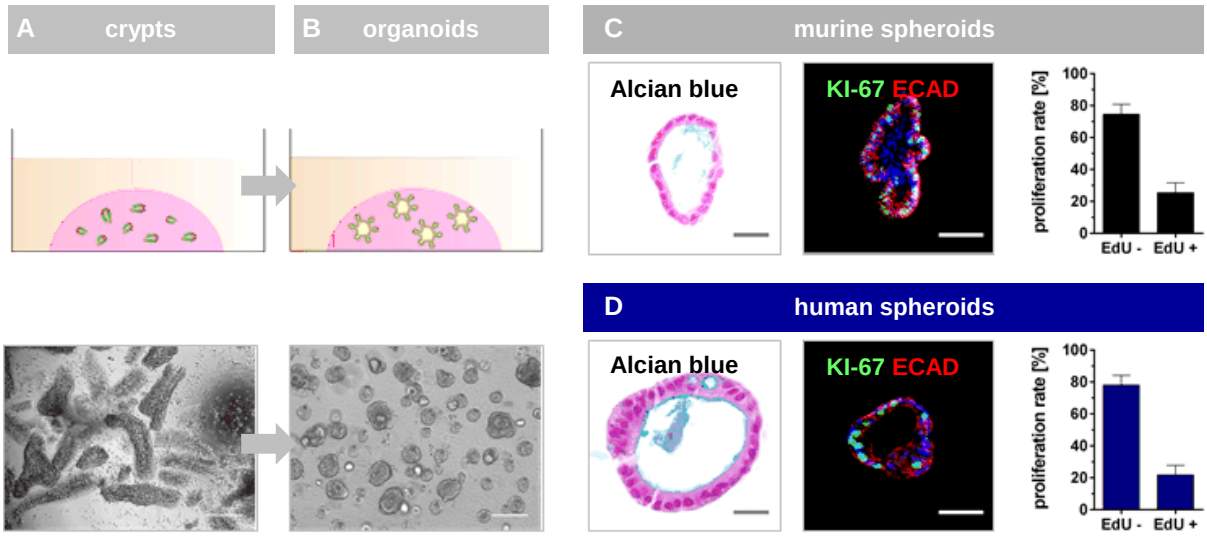

Figure 4.5: Primary tissue-derived spheroids. Schematic representation of crypts embedded in Matrigel® **(A)** and growth into spheroid structures **(B)** of murine and human tissue. Representative microscopic images show the intestinal crypt morphology **(A)** as well as the established spheroid cultures in Matrigel® droplets **(B)**. Alcian blue-stained mucin layer (blue) within the murine **(C)** and human **(D)** spheroid lumen indicative for the presence of differentiated mucus-producing goblet cells. Representative images from Histogel®-embedded spheroids demonstrate proliferative cells by IHC staining for KI-67 **(C-D)**. ECAD (red) as adherens junction marker and DAPI (blue) as cell nuclei marker are stained in parallel **(C-D)**. 25.5 ± 6.2% EdU positive cells for murine spheroids and 21.6 ± 6.0% EdU positive cells for human spheroids were obtained by flow cytometry in a quantitative EdU proliferation assay (n = 3). Scale bar in **A, B** = 200 µm; in **C, D** for Alcian blue = 20 µm and in **C, D** for IHC = 50 µm. ECAD: E-cadherin; EdU: 5-ethynyl-2'-deoxyuridine; DAPI: 4',6-diamidino-2-phenylindole.

Table 4.2: List of murine and human donor tissue biopsies. m/#: murine; h/: human; f: female; m: male; w: weeks; y: years.

Species/Number	Date of Surgery	Segment	Gender	Age
m/#110	25.11.2015	jejunum	m	15 w
m/#9	05.03.2015	jejunum	m	16 w
m/#114	29.02.2016	jejunum	f	27 w
m/#123	08.03.2016	jejunum	f	23 w
h/14-08	10.04.2014	duodenum	f	43 y
h/15-01	28.01.2015	duodenum	m	52 y
h/15-05	23.04.2015	duodenum	m	66 y
h/15-06	16.06.2015	duodenum	f	30 y

Immortalization was performed by the cooperation partner InSCREENeX according to a recently published strategy [205,207,226]. To this aim, the partner differentiated spheroid cultures from four different murine and four distinct human donors (Table 4.2) into organoids via extension of culture time. In contrast to spheroids, which are characterized by mainly proliferative stem and transient amplifying cells, organoids contain an increased amount of differentiated intestinal cells such as secretory and absorptive cells. Lentiviral transduction was performed in two different setups using a 10-component gene pool for murine organoids or a 12-component gene pool for human organoids. These gene pools, selected from the 33-component gene pool (section 3.2.2.6) commonly used by InSCREENeX for similar approaches, were considered to be relevant for the immortalization of primary intestinal organoids [205,207].

First, lentivirus-containing supernatants were applied onto structurally intact organoids cultured under floating conditions in murine cell clone expansion medium/human cell clone medium (section 3.1.6) for 24 h (Figure 4.6A). The next day, virus-treated, floating organoids were embedded in Matrigel® followed by *in vitro* culture and picking of single cells that grew out of the Matrigel® drop (Figure 4.6C). In total, 16 murine (donor m/#123; Table 4.2) and 16 human (donor h/15-06; Table 4.2) individual cell clones were picked and cultured in murine cell clone expansion medium or human cell clone medium (section 3.1.6) under 2D conditions on fibronectin/collagen-I pre-coated plates, representing routinely used tissue culture conditions [30,174,227]. After a defined time in culture monitoring the growth behavior of the picked clones, only two murine (I12K2, I12K9) and two human cell clones (15-06 I4A, 15-06 I4B) could be expanded by InSCREENeX. All four clones were transferred to TERM for further characterization.

In the second experimental setup, viral supernatants were applied to dissociated organoids cultured in 2D on fibronectin/collagen-I pre-coated tissue culture plates for 24 h (Figure 4.6B). The next day, supernatants were removed and cells were cultured in murine cell clone expansion medium or human cell clone medium. In total, lentiviral transduction performed on dissociated primary organoids cultured in 2D resulted in 27 murine (donor m/#123; Table 4.2) and 16 human cell clones established from a single immortalized cell (donor h/15-06; Table 4.2). After several rounds of expansion under standard cell culture conditions, seven murine cell clones (I9K4, I9K6, I9K8, I9K10, I9K11, I9K17, I9K21) and two human cell clones (15-06 I9A, 15-06 I9B) were transferred to TERM for characterization. In general, InSCREENeX analyzed all cell clones for their integrated gene panel, which resulted for all clones in a differently transduced gene pool (data not shown).

Prior to detailed analyses, all transferred cell clones were further expanded on fibronectin/collagen-I pre-coated plates cultured in standard cell clone medium (section 3.1.6) to initially evaluate their morphological characteristics at TERM (Figure 4.6D and E). As the human cell clone 15-06 I4A as well as the murine clones I9K4 and I9K17 showed an inhomogeneous morphology of individual cells (Figure 4.6D and E), these clones were excluded from the characterization panel. Given the organoid-like morphology of the human clone 15-06 I9A (Figure 4.6E), this clone likewise was excluded from further studies. Albeit the murine clone I9K10 (Figure 4.6E) had not shown a typical epithelial morphology, which is one key feature of intestinal epithelial cells, it was included as reference control displaying a non-epithelial-like, but homogenous morphology of individual cells.

In conclusion, a biobank of seven murine and two human organoid-derived cell clones, displaying epithelial-like cell morphologies, was established for further analyses.

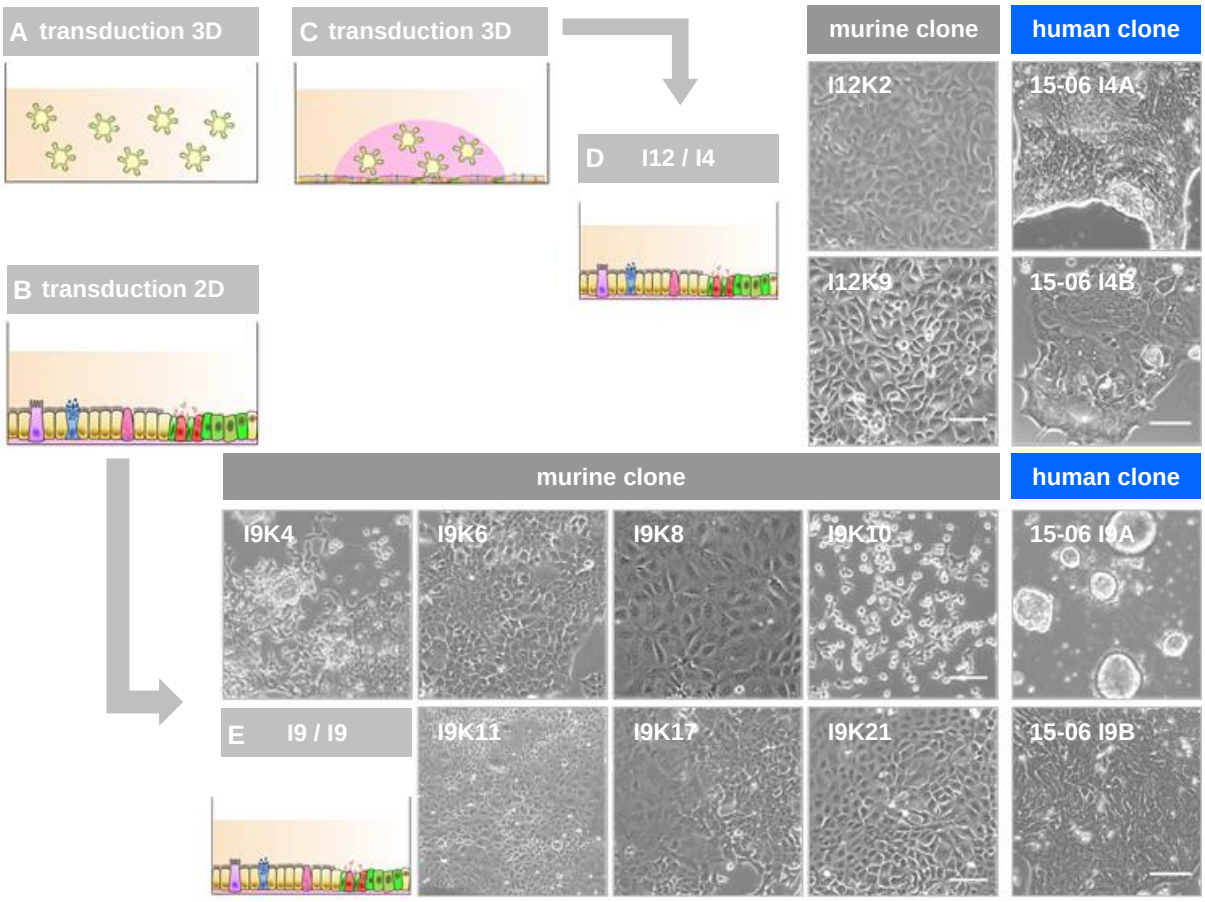

Figure 4.6: Immortalization of intestinal primary organoids by lentiviral transduction. Scheme showing experimental strategy for lentiviral transduction of differentiated organoids cultured under either floating **(A)** or attached conditions **(B)**. Organoids transduced under floating conditions were embedded in Matrigel® after 24 h **(C)**. Transduction strategy performed under 3D culture conditions resulted in two cell clones (I12K2, I12K9) for murine infection I12 **(D)** and likewise two cell clones (15-06 I4A, 15-06 I4B) for human infection I4 **(D)**. Transduction in 2D culture resulted in seven murine (I9) cell clones (I9K4, I9K6, I9K8, I9K10, I9K11, I9K17, I9K21) **(E)** and two human (I4) cell clones (15-06 I9A, 15-06 I9B) **(E)**. Scale bar in **D, E** = 100 µm.

4.2.2. Defined culture conditions for murine cell clones

4.2.2.1. Murine cell clones grew on plastic

Intestinal organoids are routinely cultured in a 3D environment embedded in Matrigel® drops. In this project, we hypothesized that immortalization and thereby generation of cell clones enables a Matrigel®-free, time- and cost-efficient 2D culture, while preserving all characteristic features of the native intestinal epithelium. InSCREENeX already showed in their preliminary studies, that the murine cell clones exponentially grew in a Matrigel®-free environment by culture of these cells on a fibronectin/collagen-I (FN/Col I) pre-coated plastic surface (data not shown).

To simplify the culture conditions further, I analyzed, if the generated murine cell clones are able to grow on uncoated plastic. As controls, cultures set up on the standard FN/Col I coating were used. In addition, poly-L-ornithine (PLO) and collagen-I (Col I) were tested as further alternatives. First, cellular morphology was monitored over 4-5 days. Figure 4.7A summarizes the different cell morphologies of one representative cell clone “I9K6” obtained after 2 and 4 days in culture, depending on the individual coating condition. On day 2, I9K6 cells showed similar morphologies on uncoated, PLO and Col I pre-treated plates with a more roundish and flat cell shape, while cells cultured on FN/Col I were more elongated. Two days later on day 4, I9K6 cultures contained more cells arranged in dense clusters, independent of the coating condition. Of note, cell clusters on PLO plates displayed different cellular morphologies indicating an inhomogeneous cell population. I9K6 cells cultured for 4 days on uncoated, Col I and FN/Col I pre-treated plates were more similar in their cell morphology. Comparable morphological characteristics were observed for the cell clones I12K2, I9K8, I12K9, I9K10, I9K11 and I9K21 (Appendix; Figure A1) when cultured under the same conditions as I9K6 cells.

In addition to monitor cell morphology, cell growth was quantitatively determined for the cell clones I12K2, I9K6, I9K8, I12K9, I9K10, I9K11 and I9K21 (Figure 4.7B-H). For cell growth analyses, the number of cells was counted before seeding and at the time point of analysis (after 4 days in culture for I9K6, I9K8, I12K9; after 5 days in culture for I12K2, I9K10, I9K11, I9K21) to calculate the increase in cell numbers. Given that an uncoated tissue culture plate would be preferred, obtained cell numbers for FN/Col I, Col I and PLO cultures were normalized to the cell growth in uncoated (w/o) plate cultures. As shown in Figure 4.7, all tested murine cell clones grew on uncoated plastic, each of them with individual cell growth capacities when cultured on distinct coatings. While I9K6, I9K8 and I9K11 cells showed similar growth characteristics on all coatings (Figure 4.7B, D and G), I12K2 cells grew better on PLO, Col I or FN/Col I (Figure 4.7C) and I12K9 cultures reached higher cell numbers on uncoated, Col I and FN/Col I coatings (Figure 4.7E). I9K10 cells (Figure 4.7F) showed the highest cell number on FN/Col I pre-treated plates and I9K21 cells (Figure 4.7H) on uncoated plastic.

Taken together, while known coatings such as FN/Col I, Col I and PLO enabled proper cell growth, they were not necessarily important. Instead, all analyzed murine cell clones showed good growth characteristics on uncoated tissue culture plates (Figure 4.7 and Figure A1 in the appendix), representing an important aspect in context of cost-efficient and simplified cell culture.

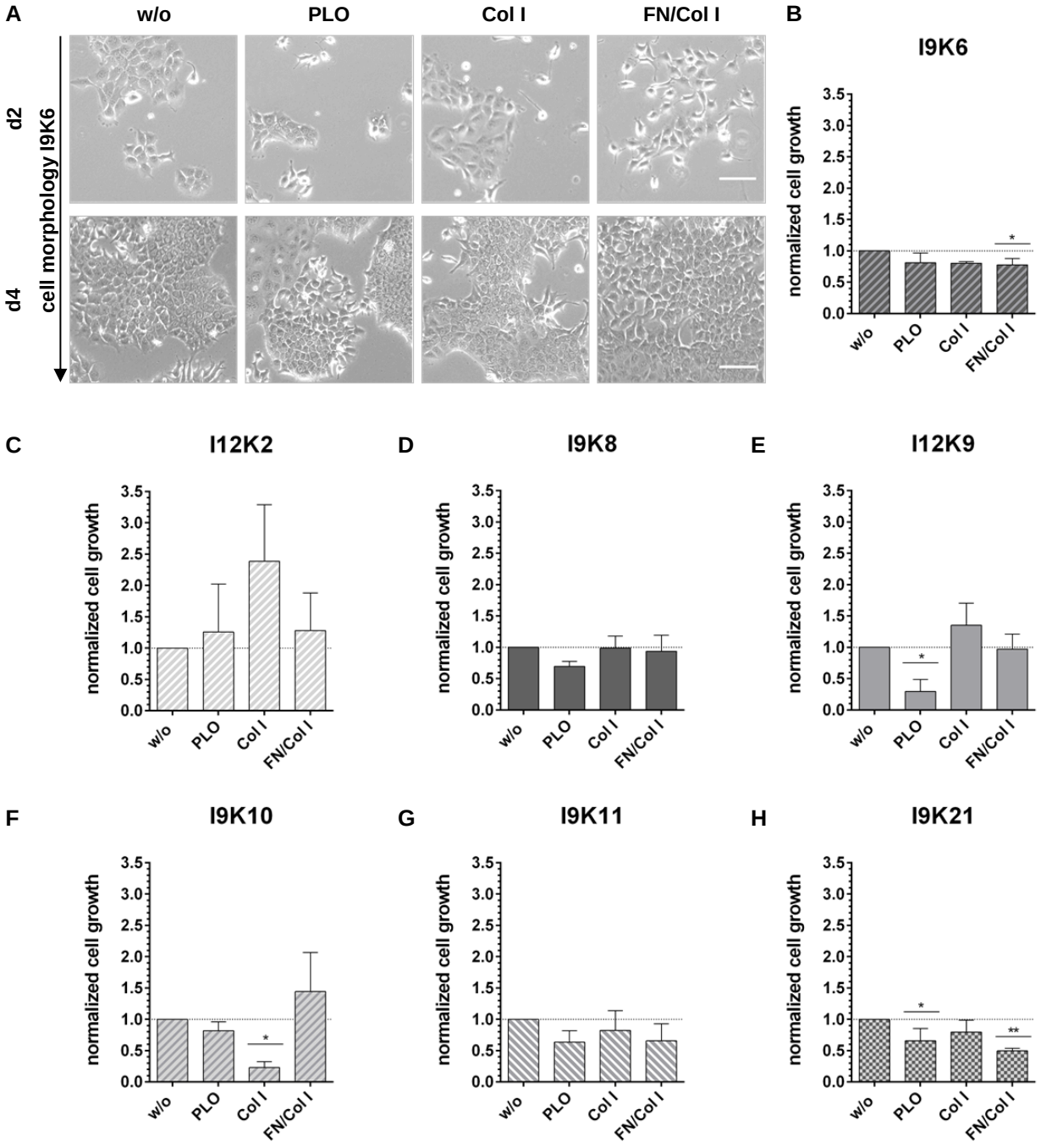

Figure 4.7: Murine cell clones cultured on diverse cell culture coatings. Cell clones were cultured on uncoated (w/o) as well as PLO, Col I or FN/Col I pre-coated plastic for 4-5 days. Cell morphology and cell growth were monitored. Microscope images (n = 3) show the cell morphology of clone I9K6 on d2 and d4 **(A)**, representative for all cell clones that are summarized in Figure A1 of the appendix. Scale bar = 100 µm. Graphs **(B-H)** show the normalized cell growth for I9K6 **(B)**, I9K8 **(D)**, I12K9 **(E)** cells after 4 days of culture and for I12K2 **(C)**, I9K10 **(F)**, I9K11 **(G)**, I9K21 **(H)** cells after 5 days of culture. The increase in cell numbers for FN/Col I, Col I and PLO cultures was normalized to the cell growth in uncoated cultures. Significance was calculated by one-way ANOVA. **p<0.05, **p<0.01;* n = 3. d: day; w/o: uncoated; PLO: poly-L-ornithine; Col I: collagen-I; FN/Col I: fibronectin/collagen-I.

4.2.2.2. Murine cell clones grew without external Wnt pathway activation

Murine intestinal spheroid/organoid cultures depend on growth factor supplementation of the basic cell culture medium with hR-Spondin 1, hEGF, mNoggin and Y-27632 [174]. These growth factors mimic niche conditions to support ISC and TAC proliferation (Wnt signaling/ R-Spondin 1), to regulate cell migration (EGF signaling/EGF), to inhibit differentiation (BMP signaling/Noggin) and to prevent apoptosis (Rho signaling/Y-27632) *in vitro* [7,174,228].

Given the possibility that the immortalized cell clones grew on uncoated plastic, I next investigated, if all niche factors are indeed necessary for proper cell growth or if one or more factors could be removed from the complex and cost-intensive medium composition that is commonly used. To this aim, individual factors were excluded from the supplemented medium and cell morphology as well as cell growth were analyzed after 4 days under the adapted culture conditions. As InSCREENeX supplemented the cell culture medium with 10% FCS for immortalization and cell clone expansion post-transduction, because it is commonly used for routine culture of cell lines [229,230], the requirement for FCS supplementation in a prolonged culture of the generated murine cell clones was further addressed.

Figure 4.8A provides an overview of representative microscope images demonstrating the individual cellular morphologies of I9K6 cells cultured under control conditions (crypt medium supplemented with Y-27632, hEGF, hR-Spondin 1, mNoggin and 10% FCS) compared to in total 5 adapted medium formulations, in which one of the growth factors or FCS was missing. Representative microscope images of all analyzed cell clones are shown in the appendix (Figure A2) or Figure 4.8A for I9K6 cells. I9K6 cells displayed a characteristic epithelial morphology on day 4 when cultured under control conditions (section 3.1.6; murine cell clone expansion medium). Interestingly, similar observations were made for I9K6 cells cultured without hR-Spondin 1 or mNoggin, indicating that both factors were not necessarily required to sustain an epithelial-like identity in I9K6 cultures (Figure 4.8A). I12K2, I9K10 and I9K21 cells (Appendix; Figure A2 A, D, F) showed similar morphological characteristics on day 4 when cultured under the same conditions as I9K6 cells, whereas the murine cell clones I9K8, I12K9 and I9K11 (Appendix; Figure A2 B, C, E) displayed an inhomogeneous morphology of individual cell clusters when one growth factor or FCS was missing in the adapted medium formulations.

Next, cell growth of all clones was quantitatively analyzed by counting the number of cells before seeding and after 4 or 5 days of culture under control or adapted conditions. A culture time of 4-5 days was chosen, as this corresponds to passaging periods applied for murine spheroid/organoid cultures. Together, growth factor supplementation seems to be essential

for all clones strongly depending on Y-27632, hEGF and FCS, as indicated by the reduced cell growth rates under conditions in which these factors were eliminated (Figure 4.8B-H). In addition, graphs in Figure 4.8B-H demonstrated increased or decreased growth rates in individual clone cultures missing mNoggin/hR-Spondin 1 supplementation compared to the control; however, these results did not reach significance in all analyzed cell clones, except of the I9K10 clone (Figure 4.8F).

Therefore, supplementation with mNoggin/hR-Spondin 1 seems to be not required for proper cell growth of the murine cell clones. In contrast, preliminary studies performed by InSCREENeX regarding the medium formulation together with the functional performance of the established murine cell clones, indicated that mNoggin but not hR-Spondin 1 was essential to show a comparable cellular behavior to control conditions.

Taken together, the results achieved in cooperation with InSCREENeX showed for all analyzed murine cell clones, except I9K10, good growth characteristics when cultured under minimal medium conditions composed of crypt medium supplemented with Y-27632, hEGF, mNoggin and 10% FCS (section 3.1.6), as demonstrated in Figure 4.8 and Figure A2 in the appendix, representing thereby an important aspect in context of cost-efficient cell culture.

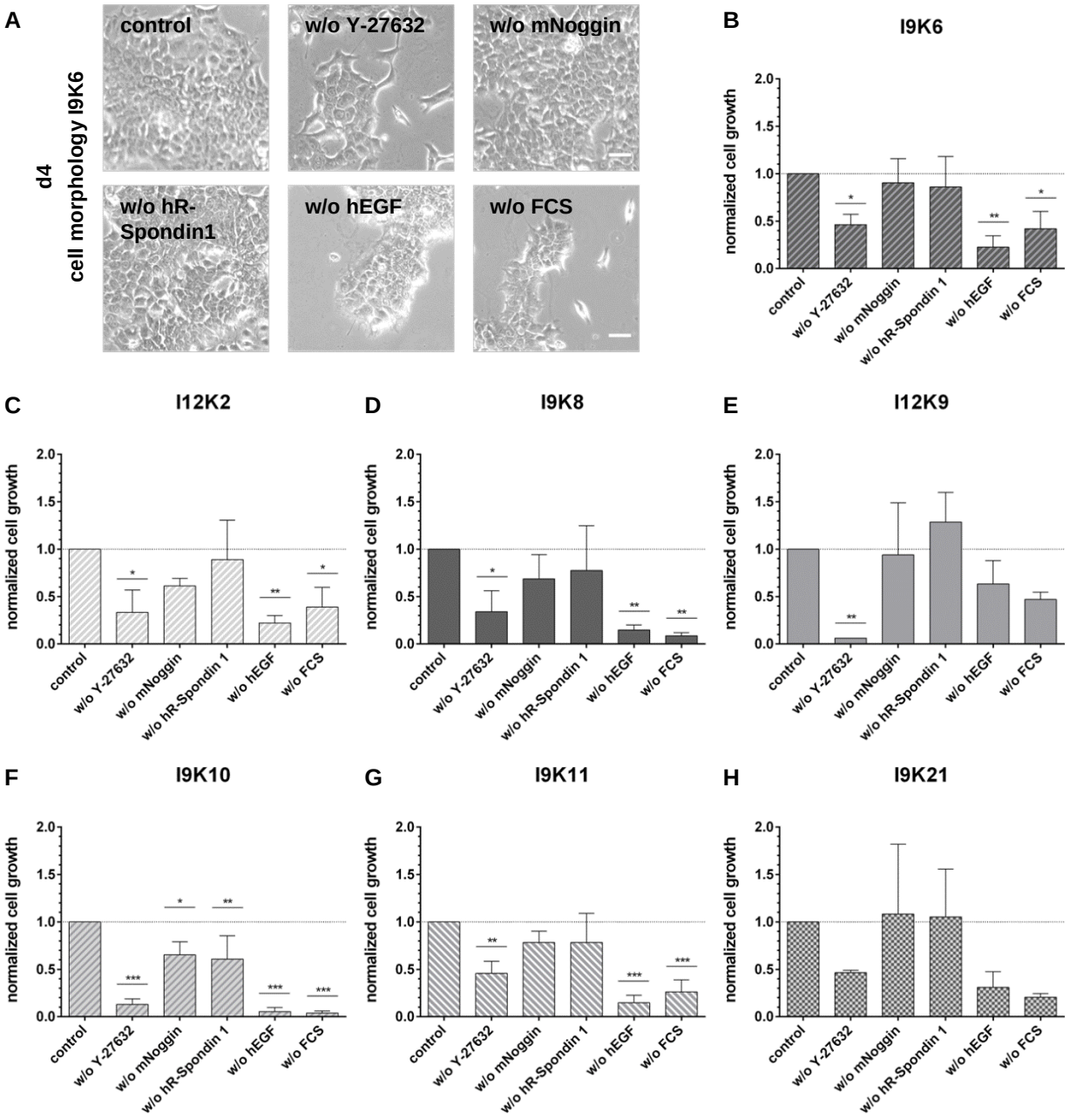

Figure 4.8: Testing appropriate culture conditions for murine cell clones cultured on uncoated plastic. Cell clones were cultured under control conditions and without the essential growth factors for primary murine spheroid/organoid culture such as Y-27632, mNoggin, hR-Spondin 1 or hEGF. FCS (10%) was applied directly after lentiviral transduction, as it is commonly used for culture of cell lines [229,230]. Cell morphology and cell growth were monitored on d4 (I9K6, I9K8, I12K9) or on d5 (I12K2, I9K10, I9K11, I9K12). Representative microscope images (n = 3) of I9K6 cells show a reduced cell density without Y-27632, hEGF and FCS supplementation to the medium **(A)**. Scale bar = 50 µm. Normalized cell growth analyses indicated Y-27632, hEGF and FCS as essential for I9K6 **(B)**, I12K2 **(C)**, I9K8 **(D)**, I12K9 **(E)**, I9K10 **(F)**, I9K11 **(G)** as well as I9K21 **(H)** cells. Significance was calculated by one-way ANOVA. **p<0.05, **p<0.01, ***p<0.001;* n = 3. d: day; FCS: fetal calf serum; hEGF: human epidermal growth factor; w/o: without.

4.2.2.3. Immortalized cell lines displayed individual gene expression profiles and barrier forming capacities

Cell growth, cell type specific gene expression profiles and a tight epithelial barrier are major features to validate the generated cell lines as characteristic intestinal epithelial cells.

After having decided which medium composition will be used in the following analyses, the next step was to compare the growth capacities among all clones (I12K2, I9K6, I9K8, I12K9, I9K10, I9K11 and I9K21). To this aim, individual population doubling levels (PDL) were analyzed on day 5 under the preceding defined culture conditions (Figure 4.9A), as PDL calculations are reported to be the best method to identify cellular alterations and to control experimental processes [231,232]. The mean PDLs of all analyzed murine cell clones varied from PDL 4.3 to PDL 6.9 (Figure 4.9A), which is in line with the PDL of ~ 5 previously reported for other cell lines [233]. Of note, also I9K10 cells displayed appropriate growth rates, albeit not sharing the epithelial-like morphology observed for other clones (Figure 4.9B and Figure 4.6). Therefore, I9K10 cells were chosen as reference control displaying a non-epithelial phenotype for subsequent analyses.

Next, expression of genes representative for the differentiated cell types found in the native intestinal epithelium including *mVil1* for enterocytes, *mMuc2* for goblet cells, *mChga* for enteroendocrine (EE) cells and *mLyz* for paneth cells was investigated for 2D cultured murine cell clones after a culture time of 5 days (Figure 4.9C). Gene expression values were analyzed by RT-qPCR and calculated by the ΔΔCT method with *mRpl15* and *mRps29* as reference genes. Values obtained for murine organoids (mOrg) as controls were set to 1.

As shown in Figure 4.9D, the marker gene *mVil1* is differently expressed in the respective murine cell clones with a higher expression rate in I9K6, I9K8 and I9K11 cells, while expression was lower for I12K9 or I9K21 cells. In line with their non-epithelial-like morphology, I9K10 cells showed one of the lowest *mVil1* expression rates. Surprisingly, no mRNA transcripts for *mVil1* could be detected in I12K2 cultures, albeit these cells displayed an epithelial-like morphology. Values obtained by gene expression analyses for the marker genes *mMuc2* (Figure 4.9E) and *mLyz* (Figure 4.9G) resulted in expression rates, which were similarly low for all analyzed cell clones. However, I12K2 and I9K8 cell clones displayed the most elevated gene expression rates for *mMuc2* (Figure 4.9E), indicating a possible enrichment of goblet cell-like phenotypes in both cultures. Interestingly, the murine cell clones showed no expression of *mChga*, representative of enteroendocrine cells (Figure 4.9F).

Barrier integrity measurements were performed to determine the formation of a consistent cell layer with dense tight junction complexes between adjacent cells in order to reflect the

barrier function of the small intestine and thereby the suitability of the established murine cell clones as an alternative cell source for standardized intestinal tissue modeling. Therefore, murine cell clones were cultured on Col I pre-coated Transwell®-inserts (Figure 4.9H) with a seeding density of $5x10^4$ cells for 21 days under the defined culture conditions followed by TEER measurements on day 21 with a non-destructive hand-electrode, as this experimental procedure is routinely performed for Caco-2 cell-based *in vitro* models. All analyzed clones were categorized into three groups: a high TEER-value group represented by I12K2 (868 ± 163 Ω*cm²), I9K8 (483 ± 81 Ω*cm²) and I12K9 cells (695 ± 125 Ω*cm²), a medium TEER-value group constituted by I9K6 (232 ± 44 Ω*cm²) and I9K21 cells (301 ± 263 Ω*cm²) and a group with low TEER values obtained for I9K10 (22 ± 10 Ω*cm²) or I9K11 (19 ± 8 Ω*cm²) cells when cultured for 21 days on commercially available Transwell®-inserts (Figure 4.9I). Interestingly, the cell morphology of I9K11 cells changed during culture, resulting in a non-epithelial-like phenotype (Figure 4.9B), which was in line with the low TEER values (Figure 4.9I).

In summary, together with the non-epithelial-like I9K10 control, the following cell clones were excluded from further analyses: I9K11, I12K2 and I9K21. I9K11 cells were excluded, as these cells showed the lowest TEER values, characterizing this clone as unsuitable for barrier formation. Further, I12K2 and I9K21 cells were excluded, as these cell clones demonstrated a low or no expression of the marker gene *mVil1*. Additionally, I9K21 cultures displayed high variances in TEER measurements. As the murine cell clones I9K6, I9K8 and I12K9 performed best in these analyses, they were elected for ongoing characterization.

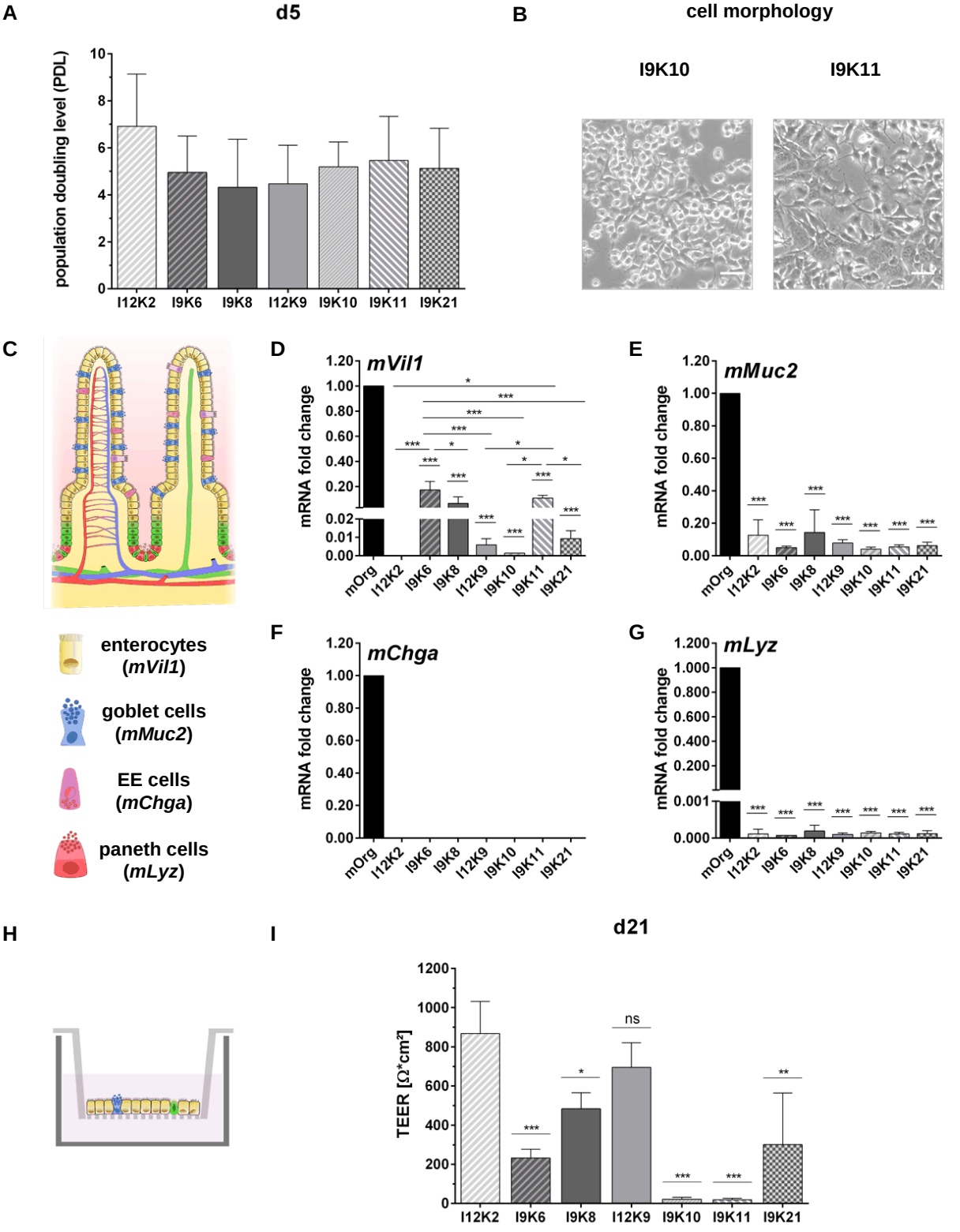

Figure 4.9: I9K6, I9K8 and I12K9 cells perform best in functional analyses. PDL analyses revealed comparable results for all cell clones **(A)**. Representative microscopic images show the roundish cell morphology of I9K10 cells used as reference control in ongoing analyses **(B)** and I9K11 cells demonstrate a non-epithelial-like cellular morphology due to ongoing culture **(B)**. Scale bar = 50 µm. Gene expression values of all murine cell clones were analyzed by ΔΔCT method with *mRpl15* and *mRps29* as reference genes. Values obtained for murine organoids (mOrg) were set to 1. After a culture time of 5 days in 2D, murine cell clones were investigated

for their respective gene expression pattern by RT-qPCR for the intestinal cell type-specific marker genes **(C)**, comprising *mVil1* (enterocytes; **D**), *mMuc2* (goblet cells; **E**), *mChga* (enteroendocrine cells = EE cells; **F**) and *mLyz* (paneth cells; **G**). Barrier integrity was measured by a non-destructive TEER-electrode after 21 days of culture on Col I pre-coated Transwell®-models **(H)**. High TEER-values were observed for I12K2, I9K8 and I12K9 cells, whereas I9K10 and I9K11 cells showed low TEER-values. I9K6 and I9K21 cells demonstrated a group of medium TEER-values. Significances were calculated by one-way ANOVA. **p<0.05, **p<0.01, ***p<0.001;* n = 3. PDL: population doubling level; CT: cycle threshold; m: murine; Rpl15: ribosomal protein L15; Rps29: ribosomal protein S29; RT-qPCR: real-time quantitative polymerase chain reaction; Vil1: villin-1; Muc2: mucin 2; Chga: chromogranin A; Lyz: lysozyme; Col I: collagen I; TEER: transepithelial electrical resistance.

4.2.3. Defined culture conditions for human cell clones

4.2.3.1. Human cell clones depend on collagen coating

Preliminary studies performed by InSCREENeX demonstrated that human cell clone cultures set up on FN/Col I pre-coated plastic grew exponentially and thereby 2D-culture is feasible.

Similar to the test procedures performed for the murine cell clones, I analyzed, if the human cell clones can also grow on uncoated plastic, using standard FN/Col I or Col I coating as controls. First, cellular morphology was monitored over a culture time of 7 days, thereby representing the passaging periods applied for human spheroid/organoid cultures. Microscopic images demonstrating the cell morphology obtained on day 3 and day 7 for the different coating conditions of one representative human cell clone “15-06 I4B” are shown in Figure 4.10A. On day 3, 15-06 I4B cells showed tightly packed colonies in which single cells appeared smaller when cultured on uncoated or FN/Col I pre-coated plastic, whereas cultures set up on Col I coatings displayed less tightly packed colonies (Figure 4.10A). Four days later on day 7, 15-06 I4B cells cultured on Col I and FN/Col I pre-coated plates displayed dense cell clusters, which were more similar in their cell morphology. 15-06 I4B cultures set up on uncoated plastic showed also tightly packed colonies, whereupon these cultures appeared with a less epithelial-like cell morphology (Figure 4.10A). 15-06 I9B cells cultured under the same conditions revealed similar morphological characteristics, as shown in Figure A3 in the appendix.

In a next step, the increase in cell numbers related to the cell number before seeding was determined in 15-06 I4B and 15-06 I9B cultures (Figure 4.10B-C) after a culture time of 7 days on the different coatings. As uncoated cell cultures would be preferred, cell growth of FN/Col I and Col I cultures were normalized to the cell growth in uncoated (w/o) cultures. However, an increased cell growth was observed for both human cell clones when cultured on FN/Col I and Col I pre-coated plates but with individual cell growth capacities

(Figure 4.10B-C). While 15-06 I4B cells (Figure 4.10B) grew best on Col I pre-coated plates, 15-06 I9B cells (Figure 4.10C) reached higher cell numbers on FN/Col I coatings.

In summary, the human cell clones 15-06 I4B and 15-06 I9B showed good growth characteristics on Col I pre-coated culture plates, but not on uncoated plastic. Cultures set up on plastic plates pre-coated with Col I, instead of FN/Col I, still present an advantage in the context of cost-efficient culture conditions, leading to the decision to use Col I pre-coated culture plates for all further analyses with human cell clones.

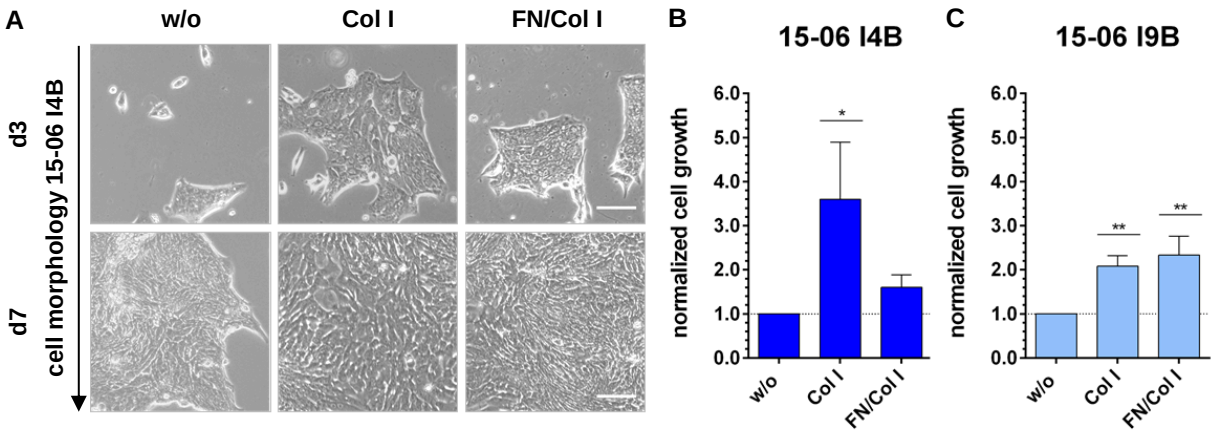

Figure 4.10: Human cell clones cultured on three different cell culture coatings. Cell morphology as well as cell growth were monitored for 15-06 I4B and 15-06 I9B cells cultured on uncoated (w/o), Col I and FN/Col I pre-coated plastic for 7 days. Microscope images (n = 3) show the cell morphology of 15-06 I4B cells **(A)** on d3 and d7. Microscope images displaying the cell morphology of 15-06 I9B cells are summarized in Figure A3 of the appendix. Scale bar = 100 µm. Graphs **(B-C)** demonstrate the normalized cell growth for 15-06 I4B **(B)** and 15-06 I9B **(C)** cells after 7 days of culture. The increase in cell numbers for Col I and FN/Col I cultures was normalized to the cell growth in uncoated cultures. Significance was calculated by one-way ANOVA. **p<0.05, **p<0.01;* n = 3. d: day; w/o: uncoated; Col I: collagen-I; FN/Col I: fibronectin/collagen-I.

4.2.3.2. Human cell clones showed similar growth factor dependencies as human intestinal organoids

Human intestinal spheroid/organoid *in vitro* culture depends on a variety of growth factors supplemented to the basic cell culture medium, thereby regulating different cellular processes. For instance, these growth factors mimic the niche conditions to maintain the stem cell state (Wnt3a, hR-Spondin 1), to inhibit differentiation (mNoggin, LY2157299), to stimulate cell migration (EGF), to prevent apoptosis (Y-27632) and to support conditions needed in the context of long-term *in vitro* culture (Nicotinamide, A83-01) as well as for an increase in culture efficiency (Gastrin, SB202190) [60].

Therefore, immortalized cell clones were analyzed for proper cell growth and altered cell morphology (Figure 4.11) when cultured under control conditions (section 3.1.6; human organoid maintenance medium) and in adapted medium formulations, in which one growth factor was missing. Further, replacement of 20% Wnt3a-conditioned medium with 2% FCS (0% Wnt3a) was analyzed to identify if Wnt3a was essential for the preservation of the cell growth capacities. As the Wnt3a-conditioned medium is composed of standard cell culture medium supplemented with 10% FCS, the 0% Wnt3a medium formulation corresponds to crypt medium supplemented with FCS (2% FCS) to obtain the percentage of FCS, applied under control conditions (section 3.1.6). Next, a medium formulation with 50% Wnt3a-conditioned medium instead of 20% Wnt3a-conditioned medium (control conditions, section 3.1.6) was tested, which corresponds to the culture conditions of human primary spheroids/organoids, as further reference control in the performed cell growth analyses. In addition, a medium formulation based on crypt medium (section 3.1.6), instead of Wnt3a-conditioned medium, supplemented with 10 µM CHIR99021 (GSK-3 inhibitor), a synthetic molecule which could activate the Wnt/β-catenin signaling to a similar level as Wnt plus hR-Spondin 1 as reported by Li et al. [234], was tested in context of cost-efficient culture conditions. Combinations of CHIR99021 with hR-Spondin 1 or FCS were also tested, as hR-Spondin 1 enhances the Wnt/ß-catenin signaling pathway to improve cell growth [234] and FCS, a cocktail of growth factors and proteins, commonly used for routine culture of cell lines [230].

Figure 4.11A provides an overview of representative microscopic images displaying the individual cellular morphologies of 15-06 I4B cells cultured under control conditions compared to the in total 14 adapted medium formulations. 15-06 I4B cells demonstrated a characteristic epithelial morphology on day 7 when cultured under control conditions (section 3.1.6; human cell clone medium). However, cells cultured under adapted medium formulations revealed an altered inhomogeneous morphology, indicating that all growth

factors were essential to sustain an epithelial-like identity in 15-06 I4B cultures (Figure 4.11A). The most important factors to sustain cell proliferation seemed to be LY2157299 (Figure 4.11A/d) and hEGF (Figure 4.11A/i), as only a few cells were observed in representative microscopic images after a culture time of 7 days. Similar morphological characteristics were observed for 15-06 I9B cells (Appendix; Figure A4) on day 7 when cultured under the same conditions as 15-06 I4B cells.

Cell growth of the human cell clones 15-06 I4B (Figure 4.11B) and 15-06 I9B (Figure 4.11C) was quantitatively analyzed by counting the cell number before seeding and after 7 days of culture under control and the adapted conditions. The increase in cell numbers for the individual adapted culture condition was set in relation to the cell growth of the control condition. As shown in Figure 4.11B and C, cultures of the immortalized human cell clones under adapted conditions, resulted in a reduced cell growth, each of the adapted conditions with an individual cell growth capacity compared to the control conditions. These cell growth analyses indicated that all growth factors used for primary human organoid cultures were essential to maintain cell proliferation in the human cell clones. Further, replacement of Wnt3a-conditioned medium by FCS (0% Wnt3a), the increase of Wnt3a-conditioned medium (50% Wnt3a) or the replacement of Wnt3a by CHIR99021 as well as by CHIR99021 with hR-Spondin 1 or FCS, demonstrated also an reduced cell growth capacity in comparison to the control conditions (Figure 4.11B-C).

Together, human cell clones showed good growth characteristics under control conditions but not under the adapted medium formulations, therefore growth factor supplementation seemed to be essential for both clones that strongly depend on A83-01, SB202190, LY2157299, Gastrin, Nicotinamide, hR-Spondin 1, mNoggin, hEGF, Y-27632 and 20% Wnt3a. Given their strong dependence on the supplementation of all growth factors to the basic culture medium, which is commonly used for human spheroid/organoid cultures, the aim of a simplified and cost-efficient cell culture in context of the medium formulation was not obtained. However, human cell clone cultures on Col I pre-coated surfaces offer intensive advantages in terms of reduced costs and handling.

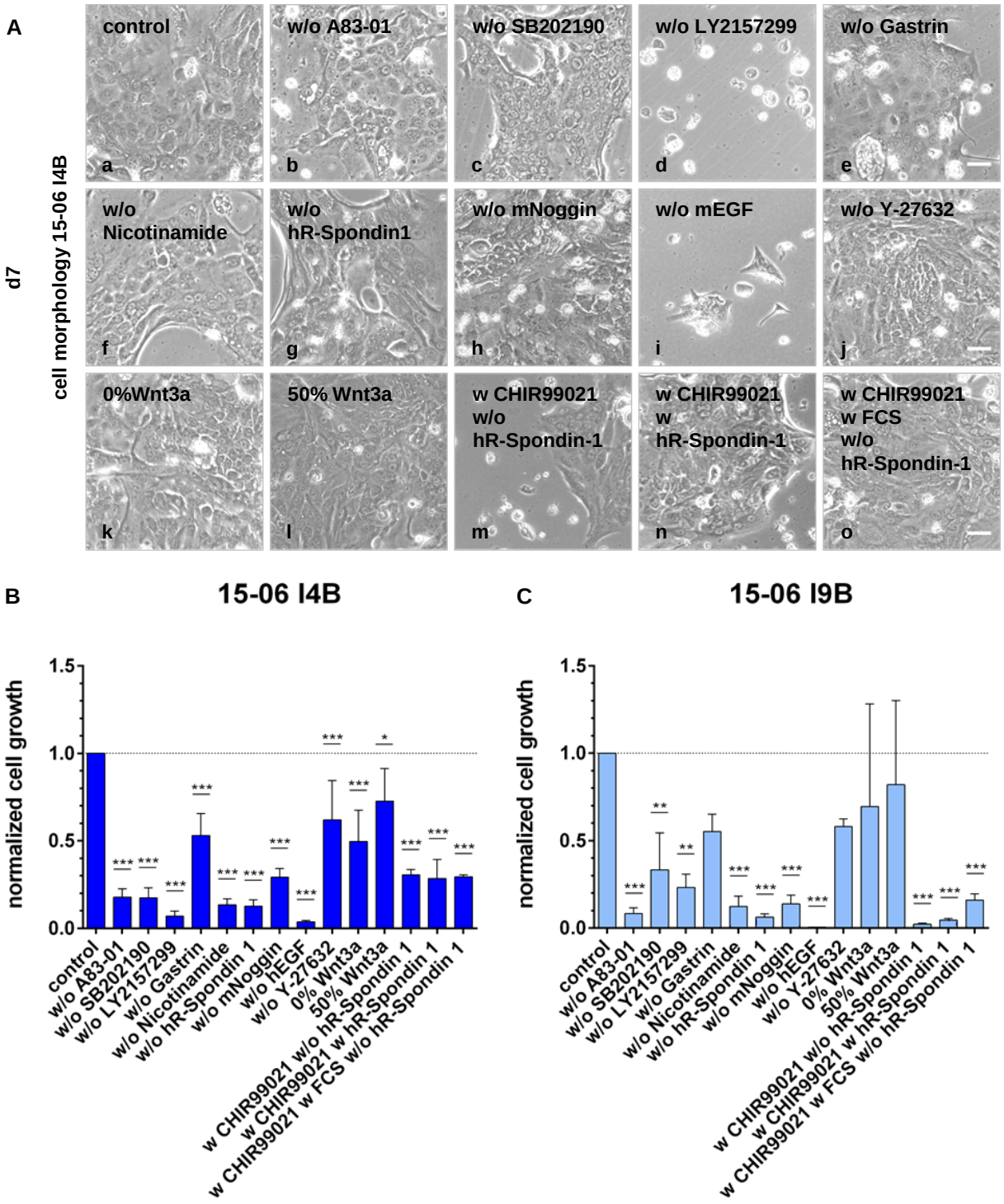

Figure 4.11: Testing appropriate culture conditions for human cell clones cultured on Col I pre-coated plastic. The human cell clones were cultured under control conditions and without the essential growth factors for primary human spheroid/organoid cultures. Further, CHIR99021, a Wnt activator, was tested for standardized model setup instead of supplementation with Wnt3a-conditioned medium. Next to CHIR99021, cell culture medium was supplemented with either hR-Spondin 1 or FCS for a comparative cell growth to control conditions. Cell morphology and cell growth were monitored on d7 for the human cell clones 15-06 I4B and 15-06 I9B. Representative microscope images of 15-06 I4B cells **(A)** show a reduced cell density when cultured under the adapted culture conditions, which was similar for 15-06 I9B cells (Appendix; Figure A4). Scale bar = 50 µm; n = 3.

Normalized cell growth analyses confirmed, that all factors used for human spheroid/organoid cultures were essential for 15-06 I4B **(B)** and 15-06 I9B **(C)** cell cultures and Wnt3a conditioned medium cannot be replaced by CHIR99021 for a more standardized medium formulation. Statistical analyses were carried out by one-way ANOVA. **p<0.05, **p<0.01, ***p<0.001;* n = 3. hEGF: human epidermal growth factor; FCS: fetal calf serum; Wnt: wingless related integration site; w: with; w/o: without.

In addition, cumulative population doubling was analyzed for up to 180 days for the human cell clones 15-06 I4B and 15-06 I9B during cell expansion to validate their immortalized phenotype in long-term [232,235]. As shown in Figure 4.12A, 15-06 I4B cell cultures revealed a linear cell growth over 180 days in culture, suggesting an infinite cell expansion potential depicting these cells as an immortalized cell line derived from human organoids. In contrast, 15-06 I9B cells (Figure 4.12B) could be expanded for 80 days in culture only, which suggests an incomplete immortalization of these cells.

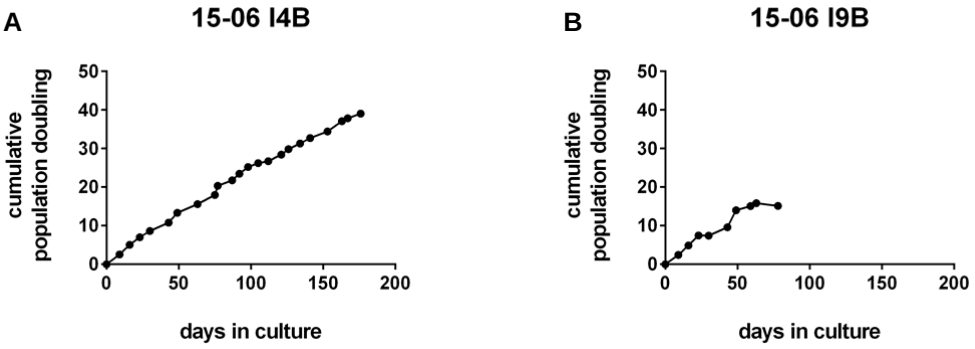

Figure 4.12: Cell growth analyses reveal infinite cell expansion for the human cell clone 15-06 I4B. Cumulative population doubling was measured up to 180 days and showed a linear cell growth for the human cell clone 15-06 I4B **(A)**. In contrast, 15-06 I9B **(B)** cells showed a linear cell growth until day 50. Afterwards cell proliferation stagnated and ended up with the complete detachment of the cells.

In conclusion, growth factor supplementation with all factors regularly applied in human spheroid/organoid cultures seemed to be essential for both human cell clones, as indicated by alterations in the cellular morphology and the reduced cell growth rates under culture conditions, in which single factors were eliminated as shown in Figure 4.11 and Figure A4 in the appendix. Therefore, human cell clones cannot be cultured under cost-efficient conditions in the context of growth factor supplementation to the medium formulation but simplified cell culture was achieved by an Matrigel®-free 2D-culture on Col I pre-coated plates (Figure 4.10). Interestingly, 15-06 I9B cell cultures seemed to be not fully immortalized, as

proliferation stagnated during cell expansion, resulting in the elimination of this cell clone from the characterization panel.

4.2.4. Immortalized cell clones I9K6, I9K8, I12K9 and 15-06 I4B showed infinite cell growth

Lentiviral transduction of organoids with a 10- or 12-component gene pool of immortalization genes (section 3.2.2.6; Table 3.1) resulted in seven murine and two human clones that were pre-screened for mainly their cell culture needs. These pre-screenings revealed three murine (I9K6, I9K8, I12K9) and one human cell clone (15-06 I4B).

Next, cell clones were investigated for their respective genes integrated by lentiviral transduction, outgoing of a gene pool of immortalization genes (section 3.2.2.6; Table 3.1), which was performed by InSCREENeX and is summarized in Table 4.3 for the selected cell clones.

Table 4.3: Genes of the CI-SCREEN® gene bank integrated in the immortalized cell clones I9K6, I9K8, I12K9 and 15-06 I4B.

I9K6	I9K8	I12K9	15-06 I4B
Id1	*Id2*	*Id1*	*Id2*
Id2	*Id3*	*Id2*	*Id3*
Id3	*Fos*	*Id3*	*E7*
cMyc	*Rex*	*cMyc*	*E6*
E7	*Core*	*Fos*	*cMyc*
Rex		*E7*	*Nanog*
Nanog		*Rex*	*Id1*
Core		*Core*	*Fos*
			Core
			Bmi1

To validate the generated cell clones as cell lines with an infinite cell growth, they were analyzed for their respective morphological characteristics and their proliferation rate during long-term culture as well as for their cumulative population doubling for up to 200 days. As controls, murine (Figure 4.13A) as well as human (Figure 4.13B) organoid cultures were used, which demonstrated a typical cellular morphology on day 3 after splitting together with a characteristic mean proliferation rate of 25.5 ± 6.2% for murine (Figure 4.13A) and

21.9 ± 6.0% for human (Figure 4.13B) organoids, investigated by an EdU proliferation assay using flow cytometry.

Cellular morphology of the murine cell clones I9K6, I9K8 and I12K9 (Figure 4.13C) as well as of the human cell clone 15-06 I4B (Figure 4.13D) did not show cellular changes during long-term culture (8-10 passages), as demonstrated in the representative microscopic images of the respective cell clones. The murine cell clones showed a characteristic epithelial morphology during culture (Figure 4.13C). The human cell clone 15-06 I4B appeared as a tightly packed cell cluster with a more elongated cell morphology (Figure 4.13D).

In addition, the mean proliferation rate was determined for the murine cell clones and the human cell clone, using the same method as for the primary organoids, starting from passage 10 of 2D cultured cells, with three independent replicates every 3-5 passages. On day 3 after seeding, a mean proliferation rate of 32.0 ± 8.0% for I9K6 (Figure 4.13E), 21.1 ± 8.5% for I9K8 (Figure 4.13F), 35.2 ± 8.7% for I12K9 (Figure 4.13G) and 19.4 ± 5.3% for 15-06 I4B (Figure 4.13H) cells was observed, thereby demonstrating similar proliferation rates compared to the primary organoids for I9K8 and 15-06 I4B cells, whereas I9K6 and I12K9 cells showed higher proliferation rates.

Next, cumulative population doubling analyses displayed an exponential cell growth during long-term culture for up to 200 days for the murine cell lines I9K6 (Figure 4.13I), I9K8 (Figure 4.13J) and I12K9 (Figure 4.13K), while data achieved for the human cell line 15-06 I4B (Figure 4.13L) resulted in a linear increase.

Taken together, murine (I9K6, I9K8, I12K9) and human (15-06 I4B) cell clones showed an infinite cell growth during long-term culture by simultaneous preservation of their morphological characteristics combined with a representative proliferation rate.

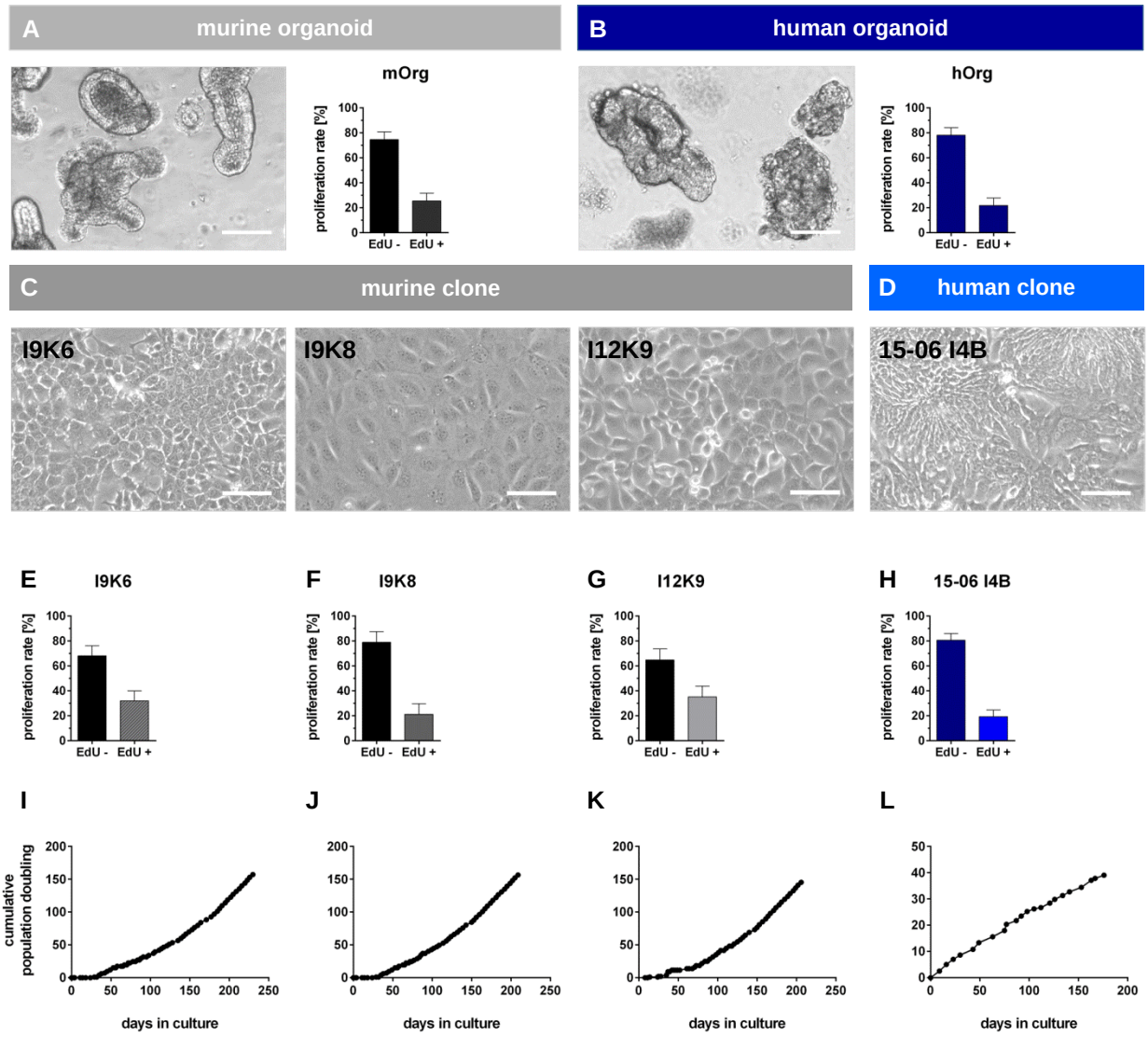

Figure 4.13: Growth characteristics of the generated murine and human cell lines. Murine **(A)** and human **(B)** organoid cultures used as controls were monitored for their proliferation capacity in a quantitative EdU proliferation assay using flow cytometry. Representative microscopic images of the murine cell clones I9K6, I9K8 and I12K9 show an epithelial cell morphology after 8-10 passages in culture **(C)**. The human cell clone 15-06 I4B revealed a more elongated cell morphology **(D)**. Scale bar in **A-D** = 100 µm. Graphs depicting individual clone-specific proliferation rates monitored by EdU flow cytometry assay for the murine cell clones I9K6 **(E)**, I9K8 **(F)** and I12K9 **(G)** as well as for the human cell clone 15-06 I4B **(H)**. n = 3; every 3-5 passages starting with passage 10. Exponential cell growth was observed by cumulative population doubling analyses (> 200 days) for I9K6 **(I)**, I9K8 **(J)** and I12K9 **(K)** cells. Cumulative population doubling curves of murine cell clones were determined by the cooperation partner InSCREENeX and graphs are displayed in a modified form. In contrast to murine cell clones, 15-06 I4B cells **(L)** showed a linear cell growth. mOrg: murine organoids; hOrg: human organoids; EdU: 5-ethynyl-2'-deoxyuridine.

4.2.5. Cell clones expressed marker genes specific for individual cell types localized in the intestinal epithelium

After verifying that the generated murine and human cell clones showed an exponential cell growth in long-term under the defined culture conditions, they were analyzed regarding their specific gene and protein expression profile by RT-qPCR (Figure 4.14) and immuno-fluorescence (IF) (Figure 4.15) characteristic for the cell types localized in the native intestinal tissue (Figure 4.14A). In context of the intestinal epithelium, enterocytes, goblet cells, enteroendocrine cells, paneth cells, TACs as well as stem cells have to be reflected, when cultures of the established cell clones retain their native cellular feature after immortalization.

First, the expression of genes representative for the cell types found in the native epithelium, including the marker genes *mLgr5/hLGR5* (stem cells; SCs), *mLyz/hLYZ* (paneth cells), *mVil1/hVIL1* (enterocytes), *mMuc2/hMUC2* (goblet cells) and *mChga/hCHGA* (entero-endocrine cells; EECs) (Figure 4.14B) were analyzed for 2D cultured murine and human cell clones, together with the reference genes *mRpl15* and *mRps29* for murine cells as well as *hHPRT1* and *hEF1-α* for human cells. As controls, the mRNA transcript levels obtained for the murine (mOrg) and human organoids (hOrg) of the respective marker genes were set to 1 (Figure 4.14C-L).

In general, the murine cell clones I9K6, I9K8 and I12K9 cultured for 5 days on uncoated plastic under the adapted medium formulation showed a reduced mRNA transcript level for all analyzed marker genes in comparison to the murine primary organoids, set as control (Figure 4.14C-G). Further, I9K6 and I9K8 cells demonstrated a higher gene expression rate for *mVil1* (Figure 4.14C) compared to I12K9 cells, while *mChga* (Figure 4.14E) was not expressed in all analyzed murine cell clones. Next, I9K8 cells showed a higher gene expression rate for the marker genes *mMuc2* (Figure 4.14D), *mLyz* (Figure 4.14F) and *mLgr5* (Figure 4.14G) compared to the cell clones I9K6 and I12K9, but with an individual mRNA transcript level for the respective clones in context of the analyzed genes. Interestingly, murine organoids (mOrg) and I9K8 cells showed a similar gene expression rate for *mLgr5* (Figure 4.14G), a specific marker for intestinal stem cells.

In addition, the human cell clone 15-06 I4B (Figure 4.14H-L) cultured for 7 days in 2D was analyzed by RT-qPCR for the same setting of marker genes as the murine cell clones, resulting in a likewise reduced gene expression rate for all analyzed genes in comparison to the human organoid (hOrg) cultures. However, the expression rates observed for the human cell clones seemed to be closer to the control values, as it was shown in the graphs of the murine cell clones (Figure 4.14C-G) and their controls, indicating that the human cell clones

preserved the cellular unit of the organoid cultures better. Of note, the comparison between murine and human cell clones demonstrated that 15-06 I4B cultures express the marker gene *hCHGA* (Figure 4.14J), whereas this marker gene was absent in murine cell clones (Figure 4.14E).

In conclusion, the murine cell clones I9K6, I9K8 and I12K9 as well as the human cell clone 15-06 I4B expressed cell type-specific marker genes, thereby representing the cellular diversity of organoid cultures *in vitro* at least to some extent, even though *mChga* gene expression was not observed in the murine cell cultures under the applied culture conditions.

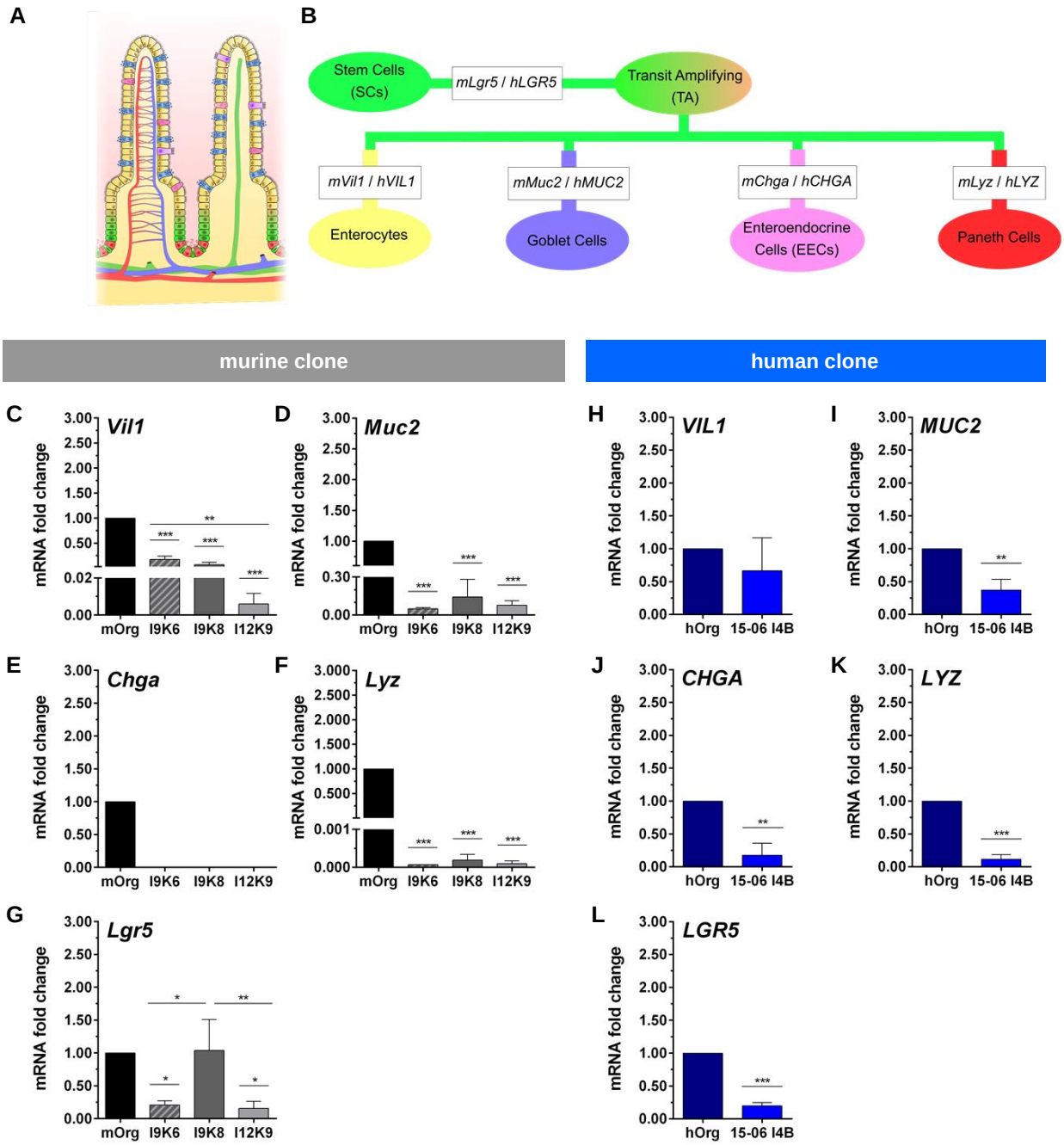

Figure 4.14: Gene expression profile of 2D-cultured murine and human cell clones representing marker genes elected as intestinal cell type-specific genes. The intestinal epithelium **(A)** is structured into villus- and crypt-compartments. Stem cells (*Lgr5/LGR5*) and paneth cells (*Lyz/LYZ*) are located at the crypt base, whereas goblet cells (*Muc2/MUC2*), enterocytes (*Vil1/VIL1*) and enteroendocrine cells (*Chga/CHGA*) are found in the villus compartment **(B)**. Graphs **(C-L)** demonstrate mRNA transcript levels of intestinal cell lineage-specific genes analyzed for murine and human cell clones by RT-qPCR. *Chga* gene expression representative for enteroendocrine cells was absent in murine cell clones **(E)**. Gene expression values were analyzed by ΔΔCT method with *mRpl15*, *mRps29* served as reference genes for murine cells and *hHPRT1*, *hEF1-α* for human cells. Values obtained for murine (mOrg) or human primary organoids (hOrg) were set to 1. Statistical analyses were carried out by one-way ANOVA. **p<0.05, **p<0.01, ***p<0.001;* n = 3. m: murine; h: human; Vil1: villin-1; Muc2: mucin 2; Chga: chromogranin A; Lyz: lysozyme; Lgr5: leucine-rich repeat-containing G-protein coupled receptor 5.

Next, the generated cell clones were analyzed by IF-stainings for their corresponding protein expression pattern when cultured in 2D. Therefore, murine cell clones were cultured for 7 days on uncoated cell culture plastic and human cell clones for 10 days on Col I pre-coated plates until a confluent cell layer was formed. IF analyses (Figure 4.15) revealed signals representative for the proliferation marker KI-67 and demonstrated the expression of characteristic proteins such as LYZ, MUC1, MUC2 and VIL1, which are markers for the different cell types found in the native intestinal epithelium, in all analyzed cell clones. While murine cell clones showed an intense signal for the proliferation marker KI-67, the human cell clone displayed only a few KI-67 positive cells, as demonstrated in the representative microscopic images (Figure 4.15; first panel). Further, protein expression for LYZ was present in all analyzed cell clones, but I9K6 cultures showed more LYZ positive signals compared to the other clones (Figure 4.15; second panel). In addition, the membrane-bound protein MUC1 was observed by IF-stainings in murine as well as human cell clones, while the signal was stronger for cultures based on I9K6 and I12K9 cells (Figure 4.15; third panel). In contrast to MUC1, more MUC2 positive cells were allocated in I9K8 and I12K9 cells compared to I9K6 or 15-06 I4B cultures (Figure 4.15; fourth panel). VIL1 as marker for enterocytes showed in all cell clones only a weak signal (Figure 4.15; fifth panel), but this observation could also be due to the fact, that the detection of apically localized proteins is difficult in 2D-cultures.

In summary, protein expression analyses revealed that the important markers, representing the main cell types of the native epithelium, were present in the immortalized cell lines, indicating that the natural cellular diversity can be reflected after immortalization.

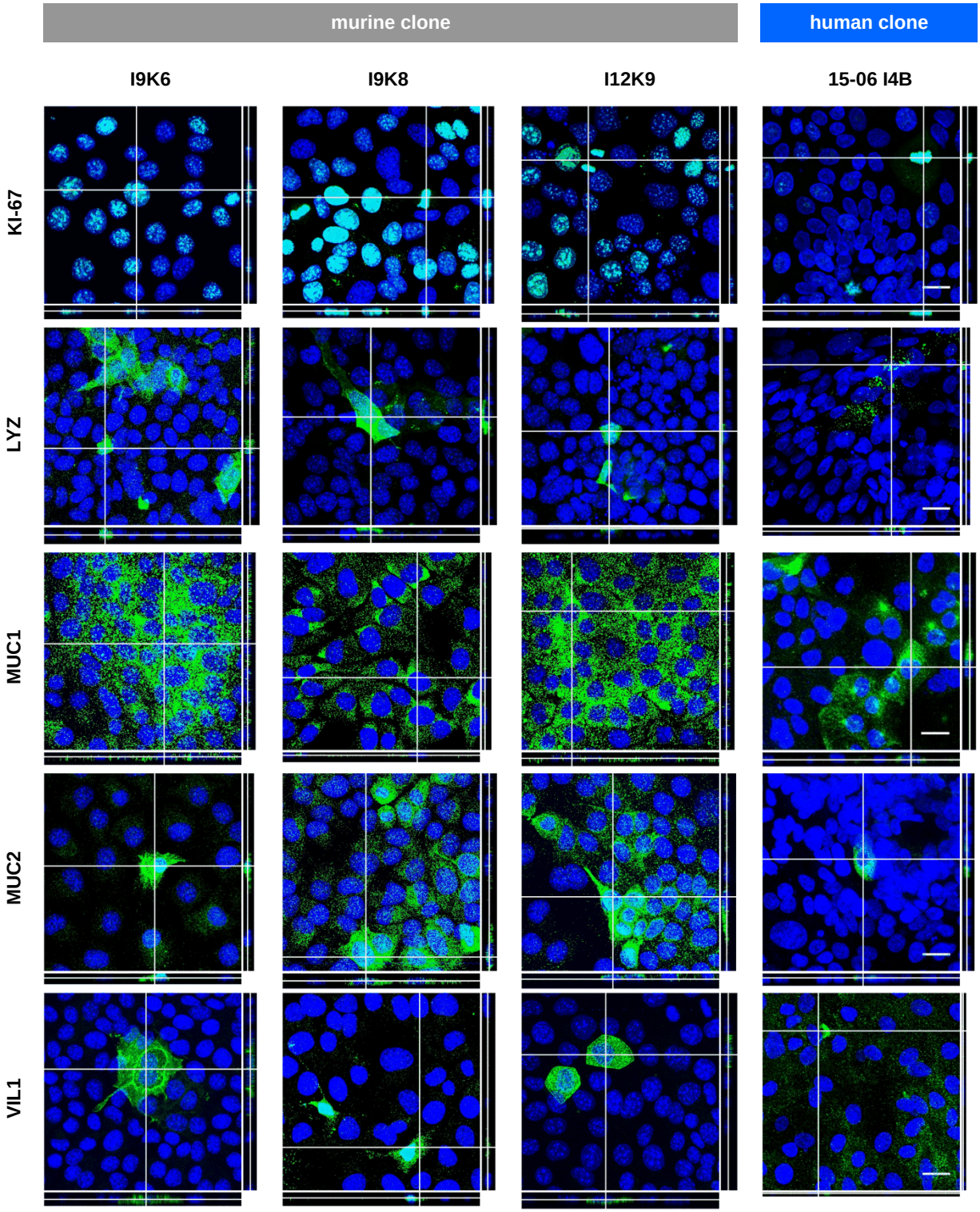

Figure 4.15: Protein expression profile of the generated murine and human cell clones grown in 2D. Murine cell clones (I9K6, I9K8 and I12K9) were cultured for 7 days on uncoated plastic, whereas the human cell clone 15-06 I4B was analyzed after a culture time of 10 days on a Col I pre-coated plate. The 2D-cultures were stained by IF for the proliferation marker KI-67 and the cell type-specific marker LYZ, MUC1, MUC2 as well as VIL1 (green). DAPI staining indicates cell nuclei (blue). Confocal z-stack images show IF signals for the analyzed marker in the investigated 2D-cultures of murine and human cell clones. Scale bar = 20 µm; n = 3.

Col I: collagen-I; LYZ: lysozyme; MUC1: mucin 1; MUC2: mucin 2; VIL1: villin-1; DAPI: 4',6-diamidino-2-phenylindole; IF: immunofluorescence.

4.2.6. Cell clones exhibited the capacity to form spheroid-like 3D structures in Matrigel®

Native intestinal crypt units predominantly composed of ISCs, form so called spheroids under pro-proliferative culture conditions when embedded in Matrigel® drops (Figure 4.16A, C). With ongoing culture time, ISCs differentiate into all cell types of the intestinal epithelium, thereby developing into so called organoids (Figure 4.16B, D) with a crypt-villus-like structural organization *in vitro* [30,174].

Given that differentiated organoid structures were used for immortalization and therefore cell line establishment, next the generated cell clones were analyzed for their capability to re-aggregate into 3D structures, depicting a typical organoid morphology. As shown in Figure 4.16E-H, representative microscopic images demonstrate the capacity of all cell clones (I9K6, I9K8, I12K9 and 15-06 I4B) to aggregate into 3D structures with a more spheroid-like morphological appearance when cultured under pro-proliferative conditions (section 3.1.6; murine/human cell clone medium) embedded in Matrigel® drops. Albeit these cultures survived up to several days, an organoid-like cytoarchitecture with separation into crypt-villus-domains was, however, not observed, also not after extended culture time. Together, this indicates that the cell-aggregates are proliferative but lost their potential to arrange into crypt-villus-domains *in vitro*, a key feature of ISC-containing spheroids that transform into differentiated organoids with extended culture time.

To quantitatively analyze the proliferative capacity of the re-aggregated 3D cell clone cultures, an EdU proliferation assay using flow cytometry was performed. Therefore, spheroids were splitted into single cells followed by re-embedding into Matrigel® drops and expansion culture. On day 3 after splitting, a mean proliferation rate of 8.8 ± 3.1% for I9K6 (Figure 4.16I), 11.6 ± 5.9% for I9K8 (Figure 4.16J), 11.7 ± 0.7% for I12K9 (Figure 4.16K) cell-based spheroid-like structures was observed, while 15-06 I4B cell-based spheroid-like structures (Figure 4.16L) revealed with 15.3 ± 3.2% EdU positive cells a slightly higher mean proliferation rate compared to the murine cell clones. However, in comparison to the mean proliferation rate measured for all cell clones cultured in 2D, a decreased proliferation capacity was induced by culture in a 3D environment, as shown in Table 4.4. While human cell clones cultured in 3D showed only a small reduction in the mean proliferation rate, the decrease for 3D-cultured murine cell clones was even stronger (Table 4.4).

Taken together, the generated murine and human cell clones formed viable and proliferative spheroid-like structures when cultured in 3D, albeit their proliferative capacity was lower compared to cultures set up in 2D. Further, cells were not able to transform from spheroids to organoid-like clusters when the culture time was increased in contrast to primary cells. As the organoid-like cytoarchitecture of primary cultures is mainly driven by their proliferative stem cell compartment together with the first symmetry-breaking event, in which identical cells differentiate into paneth cells [236], thereby generating the stem cell niche with crypt-villus-regions in the 3D clusters *in vitro*, these data indicated the absence of functional ISCs in the immortalized cell lines. This is further supported by the low proliferation values obtained by flow cytometry that rather point out a longer cell cycle, which is characteristic for differentiated cells instead of ISCs that are characterized by a shorter cell cycle length [237]. Together, this supports an immortalized phenotype, which was generated from organoid cultures predominantly consisting of differentiated epithelial cell types rather than ISCs.

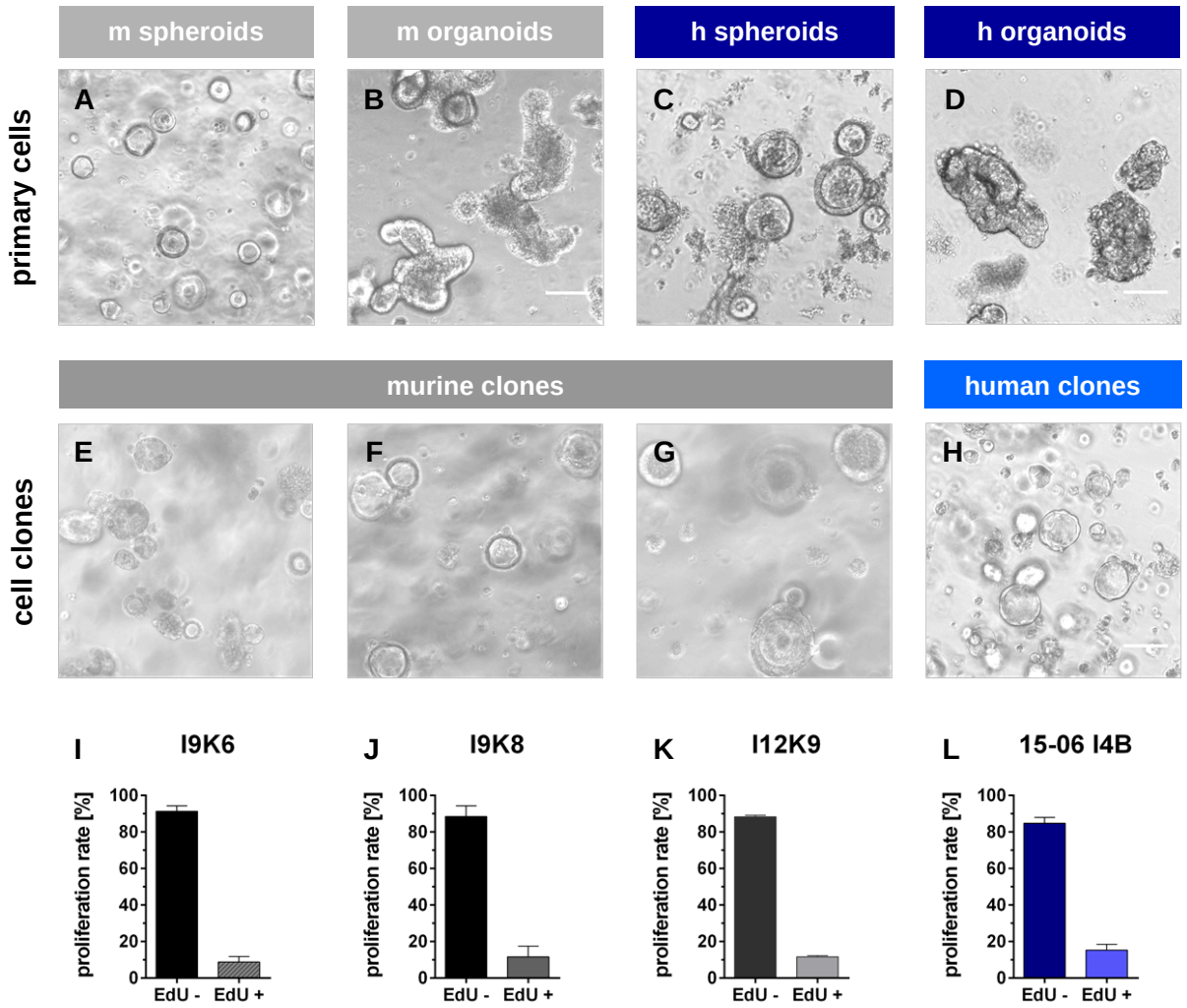

Figure 4.16: Immortalized cell lines form spheroid-like 3D structures in Matrigel® droplets. Representative microscopic images demonstrate the formation of murine spheroids **(A)** and murine organoids **(B)**, when cultured under the respective conditions. In addition, human spheroids **(C)** and human organoids **(D)** are shown in representative microscopic images. Further, representative microscopic images demonstrate the formation of spheroid-like structures by applying the dissociated cell clones I9K6 **(E)**, I9K8 **(F)**, I9K12 **(G)** and 15-06 I4B **(H)** for at least 24 h into a 3D-Matrigel® environment. Scale bar = 100 µm. Proliferation rate was analyzed by flow cytometry after incorporation of EdU into the dividing DNA for 3D-cultured I9K6 **(I)**, I9K8 **(J)**, I12K9 **(K)** and 15-06 I4B **(L)** cells. EdU: 5-ethynyl-2'-deoxyuridine; DNA: deoxyribonucleic acid; m: murine; h: human.

Table 4.4: Proliferation rate in percent of murine and human cell clones. Comparison between cell clones cultured in 2D and 3D.

	Proliferation rate [%] 2D-culture		Proliferation rate [%] 3D-culture	
	EdU -	**EdU +**	**EdU -**	**EdU +**
I9K6	68.0 ± 8.0	32.0 ± 8.0	91.2 ± 3.1	8.8 ± 3.1
I9K8	78.9 ± 8.5	21.1 ± 8.5	88.4 ± 5.9	11.6 ± 5.9
I12K9	64.8 ± 8.7	35.2 ± 8.7	88.3 ± 0.7	11.7 ± 0.7
15-06 I4B	80.6 ± 5.3	19.4 ± 5.3	84.7 ± 3.2	15.3 ± 3.2

To validate the differentiated phenotype of the Matrigel-embedded cell clones, specific gene and protein expression profiles were studied by RT-qPCR (Figure 4.17) and IHC (Figure 4.18). Focus was on marker genes and proteins, which are characteristic for the cell types of the native intestinal epithelium (Figure 4.17A); comprising Vil1 for enterocytes, Muc1/Muc2 for mucin-producing cells (*e.g.* goblet cells), Chga for EE cells and Lyz for paneth cells (Figure 4.17B). Proliferative cells were identified in IHC studies by using KI-67 antibodies (Figure 4.18) and remaining stem cell signatures should be profiled by using Lgr5-specific primer pairs in RT-qPCR analyses (Figure 4.17G, L).

The spheroid-like 3D structures established from the murine cell clones showed reduced gene expression rates for *mVil1* (Figure 4.17C), *mMuc2* (Figure 4.17D), *mChga* (Figure 4.17E) and *mLyz* (Figure 4.17F) compared to primary murine organoids (mOrg) (Figure 4.17C-G). Of note, only I12K9 cells displayed a similar expression rate of *mVil1*, as observed in murine organoid cultures (Figure 4.17C), depicting a predominant epithelial character of I12K9 cultures, possibly composed of enterocytes only. Interestingly, *mLgr5* (Figure 4.17G) was expressed in all murine cell clones at comparable levels to the murine organoid control. Comparing the three murine cell clones among each other, a similar expression rate for *mMuc2*, *mChga*, *mLyz* and *mLgr5* (Figure 4.17D-G) was observed for two lines, while I9K8 cells showed no expression of *mLyz* (Figure 4.17F), indicating that paneth cells were not present in 3D-cultured I9K8 cells.

Next, the spheroidal structures of the human cell clone 15-06 I4B (Figure 4.17H-L) were analyzed for their gene expression profile using the same marker setting as for the spheroidal murine cell clones. In comparison to the control cells (hOrg), a reduced gene expression rate was demonstrated for the genes *hVIL1* (Figure 4.17H), *hMUC2* (Figure 4.17I), *hLYZ* (Figure 4.17J) and *hLGR5* (Figure 4.17L), while *hCHGA* (Figure 4.17K) expression was absent in the 3D-cultured human cell clone. Of note, the expression rates observed for the 3D-cultured human cell clone (Figure 4.17H-L) seemed to be closer to the control values, except of the *hCHGA* expression rate, which indicates that the cellular

composition of the primary human organoids was better preserved in the immortalized human cells, compared to the murine cell clones (Figure 4.17C-G). Interestingly, the murine cell clones showed a similar *mLgr5* expression compared to the mRNA transcript level of the control cells when cultured in 3D (Figure 4.17G), which was not observed for the human cell clone cultured under the same conditions (Figure 4.17L).

Together, all three 3D-cultured murine cell lines formed spheroid-like 3D clusters but they did not form any organoid-like morphology, therefore they are hypothesized to bear no functional stem cell unit. Furthermore, all three lines individually expressed specific marker genes characteristic of the intestinal epithelium, albeit at distinct and drastically reduced levels when compared to primary organoid cultures. While I9K8 cultures seemed to lack in paneth cells, I12K9 cultures seemed to be predominantly composed of *mVil1*-expressing enterocytes.

Similarly, 3D-cultures generated from the human cell clone were able to proliferate as spheroidal clusters without transmitting into organoid cytoarchitectures after prolonged culture time. Together with the drastically reduced *hLGR5* expression values, this indicated an immortalized phenotype of mainly differentiated cell types or TACs instead of ISCs. Additionally, comparable to the murine cell lines, also the human cell clone displayed gene expression profiles characteristic for the intestinal epithelium, albeit at drastically reduced levels. Of note, there was no *hCHGA* expression detectable, indicating the lack in EE cell identities.

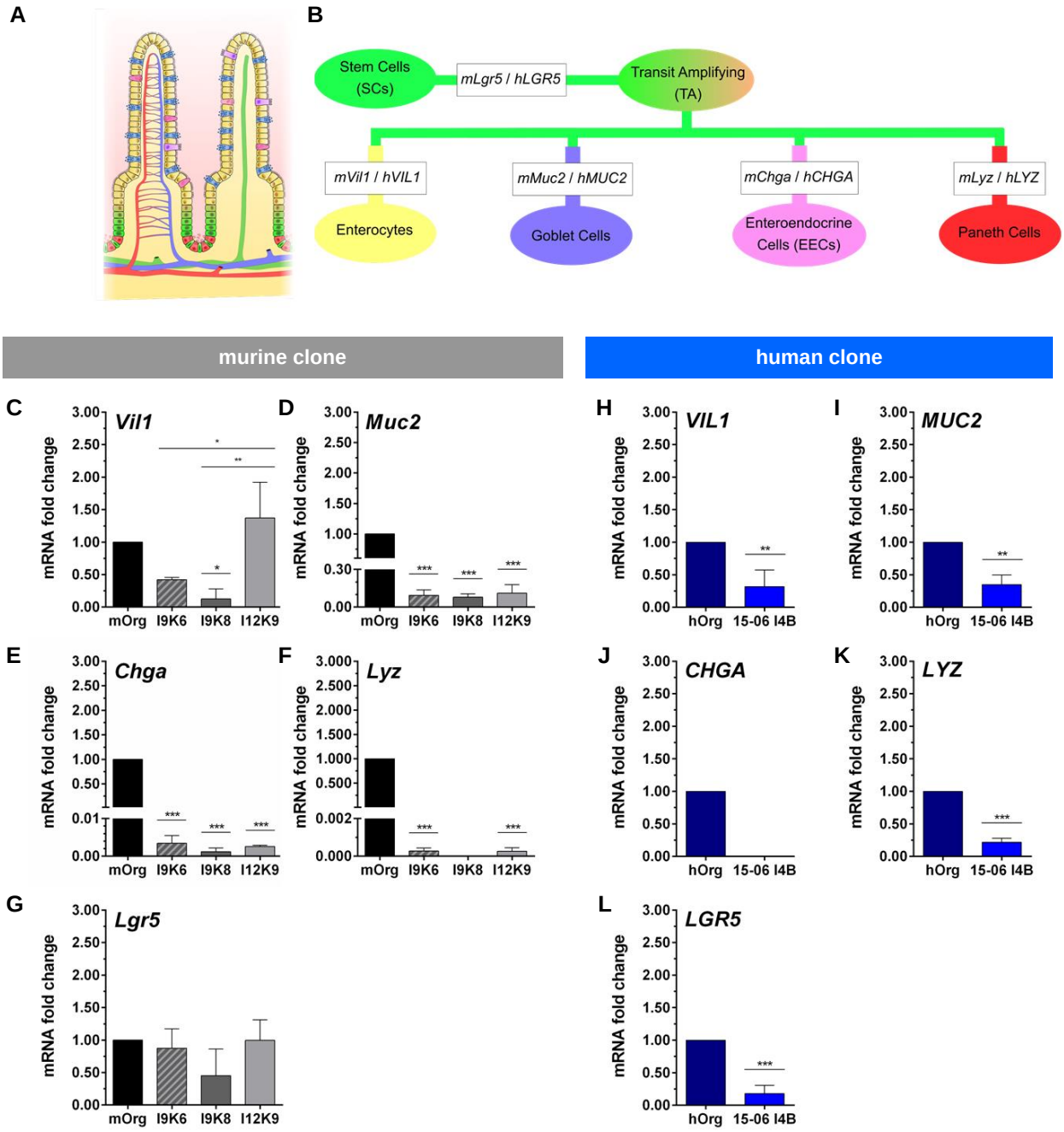

Figure 4.17: Gene expression profile of murine and human cell clones grown in a 3D-Matrigel® environment. Villus- and crypt-specific cell types of the intestinal epithelium **(A)** such as enterocytes, goblet cells, enteroendocrine cells, paneth cells as well as stem cells **(B)** were analyzed for their specific marker gene using RT-qPCR. Graphs **(C-L)** demonstrate the mRNA transcript level of the intestinal cell lineage-specific genes *Vil1/VIL1*, *Muc2/MUC2*, *Chga/CHGA*, *Lyz/LYZ* and *Lgr5/LGR5* for murine and human cell clones. *CHGA* gene expression representative for enteroendocrine cells was absent in human cell clones **(J)**. Values obtained for murine (mOrg) and human organoids (hOrg) were set to 1. Gene expression values were analyzed by ΔΔCT method with *mRpl15*, *mRps29* served as reference genes for murine cells and *hHPRT1*, *hEF1-α* for human cells. Significance calculated by one-way ANOVA is indicated by asterisks. **p<0.05, **p<0.01, ***p<0.001;* n = 3. m: murine; h: human; Vil1: villin-1; Muc2: mucin 2; Chga: chromogranin A; Lyz: lysozyme; Lgr5: leucine-rich repeat-containing G-protein coupled receptor 5.

In addition to gene expression profiles, corresponding protein expression patterns were studied in the spheroid-like 3D structures by IF analyses (Figure 4.18). In line with their previously shown proliferative capacity determined by quantitative EdU analyses, IF analyses revealed KI-67 positive cells within these spheroidal structures (Figure 4.18; first panel). Further, IHC-staining of Histogel®-embedded sections of cell clone-based spheroids, showed signals for LYZ (Figure 4.18; second panel), MUC1 (Figure 4.18; third panel), MUC2 (Figure 4.18; fourth panel) and VIL1 (Figure 4.18; fifth panel) with individual signal intensities in the analyzed cell lines. Interestingly, spheroids of the respective cell clones showed partly an outward-facing staining for the marker VIL1, MUC2 and MUC1, instead of the commonly known internal protein expression pattern in primary organoids, which indicates that spheroid-like 3D structures of the murine and human cell clones have lost their polarization towards the internal lumen. In this context, the protein expression pattern of SGLT1, a transporter localized in the internal lumen of primary organoids, was further analyzed in the respective cell-clone based spheroids, in order to determine whether these spheroids had lost their polarization under these culture conditions. As shown in Figure 4.18 (last panel), the staining for SGLT1 demonstrated a positive signal on the apical and basolateral side of the cell clone-based spheroids, indicating that the cells were not polarized.

In conclusion, cell clones cultured in Matrigel® drops was sufficient to induce the formation of spheroid-like structures, albeit an organoid-like formation was not observed under the applied culture conditions. Further, gene as well as protein expression analyses confirmed the presence of specific intestinal cell types and turned out, that these spheroid-like 3D structures did not show a polarized epithelial cell layer.

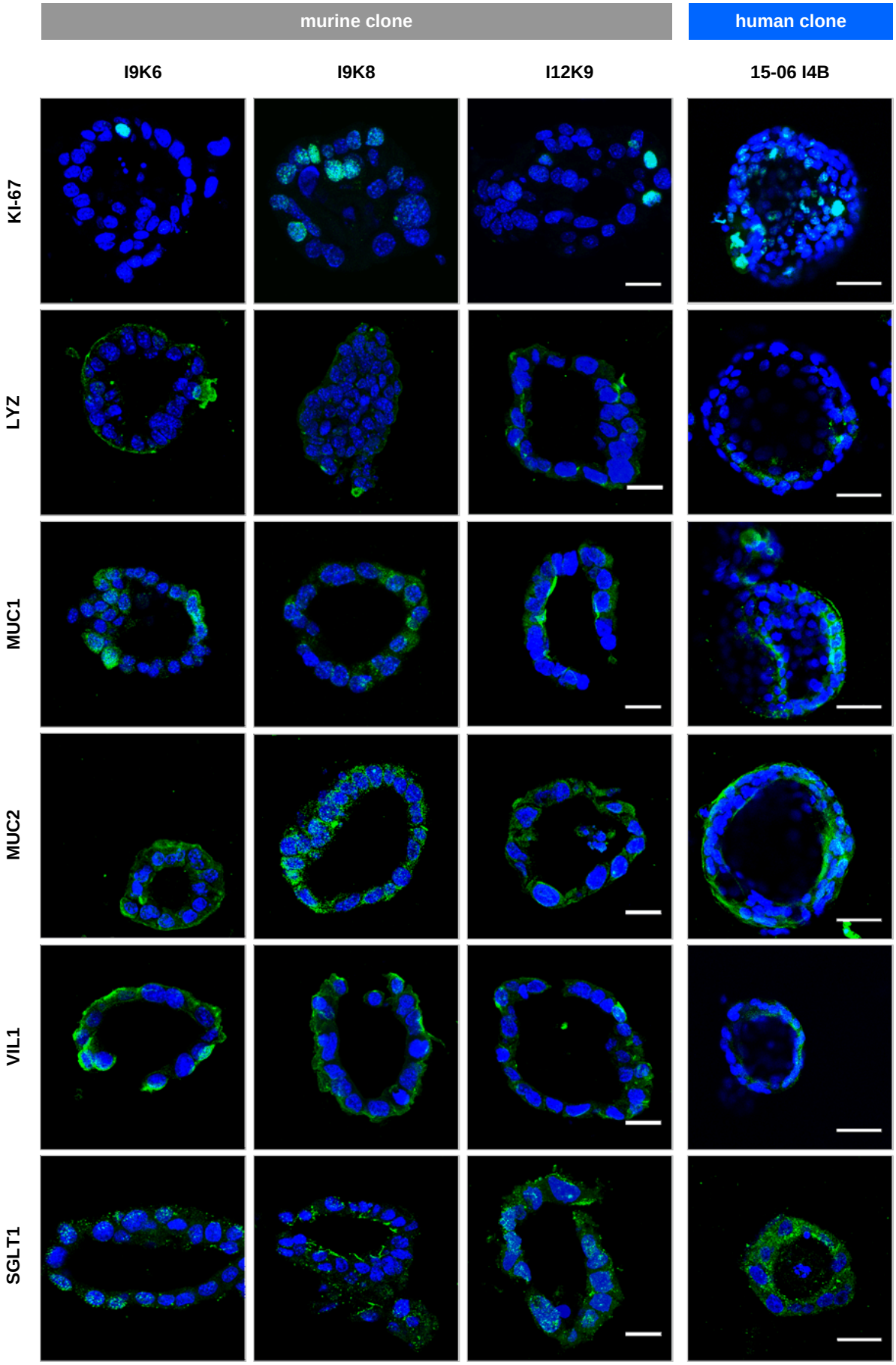
murine clone
human clone
I9K6
I9K8
I12K9
15-06 I4B
KI-67
LYZ
MUC1
MUC2
VIL1
SGLT1

Figure 4.18: Protein expression profile of the established murine and human cell clones cultured as spheroid-like structures. Cell clones were cultured for 5-7 days in Matrigel® drops to form spheroid-like structures. IHC-stained Histogel®-embedded sections were analyzed for the proliferation marker KI-67 and the intestinal cell type-specific marker such as LYZ, MUC1, MUC2 as well as VIL1 (green). Cell nuclei are counterstained with DAPI (blue). Representative confocal images show that some spheroids changed their orientation (apical-basolateral side) resulting in so called apical-out spheroids for murine and human cell clones. Therefore spheroid structures were not fully polarized structures. Scale bar for murine clones = 20 µm, for human clones = 50 µm; n = 3. LYZ: lysozyme; MUC1: mucin 1; MUC2: mucin 2; VIL1: villin-1; SGLT1: sodium glucose linked transporter 1; DAPI: 4',6-diamidino-2-phenylindole.

4.2.7. Immortalized cell lines showed characteristic tight/adherens junction expression patterns

One major characteristic of intestinal *in vitro* models is the formation of a tight epithelial barrier, which can be demonstrated by the expression of corresponding tight or adherens junction proteins such as ZO-1, Claudin-5 (CLDN5) or ECAD. Therefore, murine cell clones (I9K6, I9K8 and I12K9) were cultured for 5 days on uncoated plastic and the human cell clone (15-06 I4B) for 7 days on Col I pre-coated plates, until a confluent cell layer was formed. IHC analyses revealed the expression of the characteristic tight/adherens junction proteins ZO-1, CLDN5 and ECAD in all cultures, except of CLDN5 in cultures based on 15-06 I4B cells, indicating that CLDN5 expression is abrogated after immortalization in these cells (Figure 4.19). Furthermore, a continuous allocation of IHC signals was observed for all analyzed cell clones regarding the tight/adherens junction proteins ZO-1 and ECAD, thereby indicating a homogenous distribution of these tight/adherens junction proteins (Figure 4.19). In contrast, a more scattered and inhomogeneous expression pattern of the tight junction protein CLDN5 was revealed for I9K8 and I12K9 cultures, while I9K6 cells demonstrated a continuous homogenous IHC signal of CLDN5 (Figure 4.19).

In summary, a characteristic tight/adherens junction protein expression profile as indicated by IHC analyses was observed for ZO-1 and ECAD for all cell clones, while the protein signal of CLDN5 appeared inhomogeneous or was not identified at all, as shown for I9K8, I12K9 and 15-06 I4B cells.

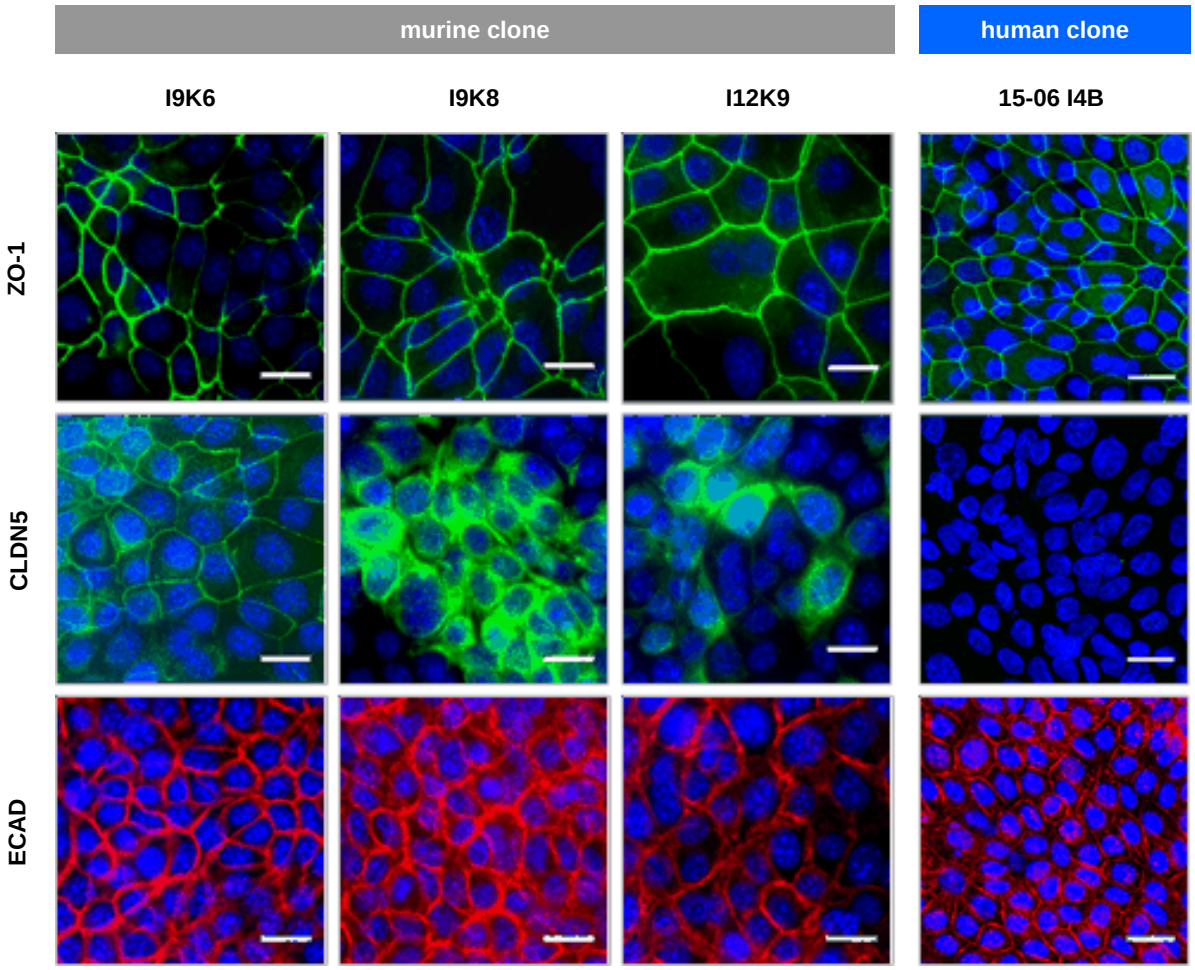

Figure 4.19: Tight junction protein expression profile of murine and human cell clones. Murine cell clones (I9K6, I9K8 and I12K9) were cultured for 5 days on uncoated plastic until a confluent cell layer was formed; while the human cell clone (15-06 I4B) was cultured for 7 days on Col I pre-coated plastic. Representative microscopic images (Keyence or Leica Confocal) show an equal expression of the tight/adherens junction proteins ZO-1 (green; first panel), CLDN5 (green; second panel) and ECAD (red) by IF-staining. Cell nuclei are counterstained with DAPI (blue). Scale bar = 20 µM; n = 3. IF: immunofluorescence; ZO-1: zonula occludens-1; ECAD: E-cadherin; CLDN5: Claudin-5; DAPI: 4,6'-diamidino-2-phenylindole; Col I: collagen-I.

4.2.8. Cell clones formed a tight cell layer representing a characteristic protein expression profile

Routinely, Caco-2 cells cultured for 21 days on Transwell® inserts are used in pre-clinical research to study bioavailability or toxicity of drugs [111]. To validate the capacity of the established murine and human cell clones for the setup of intestinal *in vitro* models used for pre-clinical applications, cell clones with a seeding density of $5x10^4$ cells/ 24-well insert were cultured on Col I pre-coated PET membranes until a confluent cell layer was formed, as this corresponds to the culture conditions applied for Caco-2 Transwell® models [112,224,238]. The formation of a tight epithelial barrier is one important characteristic feature of intestinal *in vitro* models, which was depicted by histological and ultrastructural analyses.

Representative microscopic images of H&E-stained sections (Figure 4.20A-D/a-d) of Transwell®-models based on the murine cell clones (I9K6, I9K8 and I12K9) revealed the formation of a dense cell-monolayer after a culture time of 21 days, while the human cell clone (15-06 I4B) implied a culture time of 14 days to establish a consistent cell layer, when the respective cell clones were cultured under the defined conditions (section 3.1.6; murine/human cell clone medium). Further, the murine cell clones I9K6 (Figure 4.20A/a), I9K8 (Figure 4.20B/b) and I12K9 (Figure 4.20C/c) demonstrated a flat, elongated cell layer together with a weak eosin staining, indicating that these cells form a less compact connective tissue. In contrast, models based on the human cell clone 15-06 I4B (Figure 4.20D/d) showed likewise a flat cell layer, but the formation of a densely packed cell cluster, surrounded by a compact connective tissue was observed for this cell clone.

In addition to the H&E-stained sections, high-resolution SEM and TEM analyses (Figure 4.20E-L) of the generated murine and human cell clones cultured on Transwell®-inserts, provided evidence for the formation of a consistent cell layer. Furthermore, these ultrastructural analyses presented characteristic TJs (Figure 4.20I-L) as well as a brush border membrane with apical microvilli (Figure 4.20E-H/e-h). However, murine cell clone based models (Figure 4.20E-G/e-g) demonstrated a cell layer with less densely packed microvilli, which are further rather short in length (Figure 4.20I-K), whereas models based on the human cell clone showed longer microvilli together with a tight distribution on the apical cell surface (Figure 4.20H/h and L).

In conclusion, Transwell®-models based on 15-06 I4B cells formed a compact connective tissue and showed a uniform as well as tight distribution of microvilli on the cell surface, which is similar to the *in vivo* structure of the intestinal epithelium. In contrast, models based on murine cell clones demonstrated cells with a less tight distribution of microvilli on the cell surface.

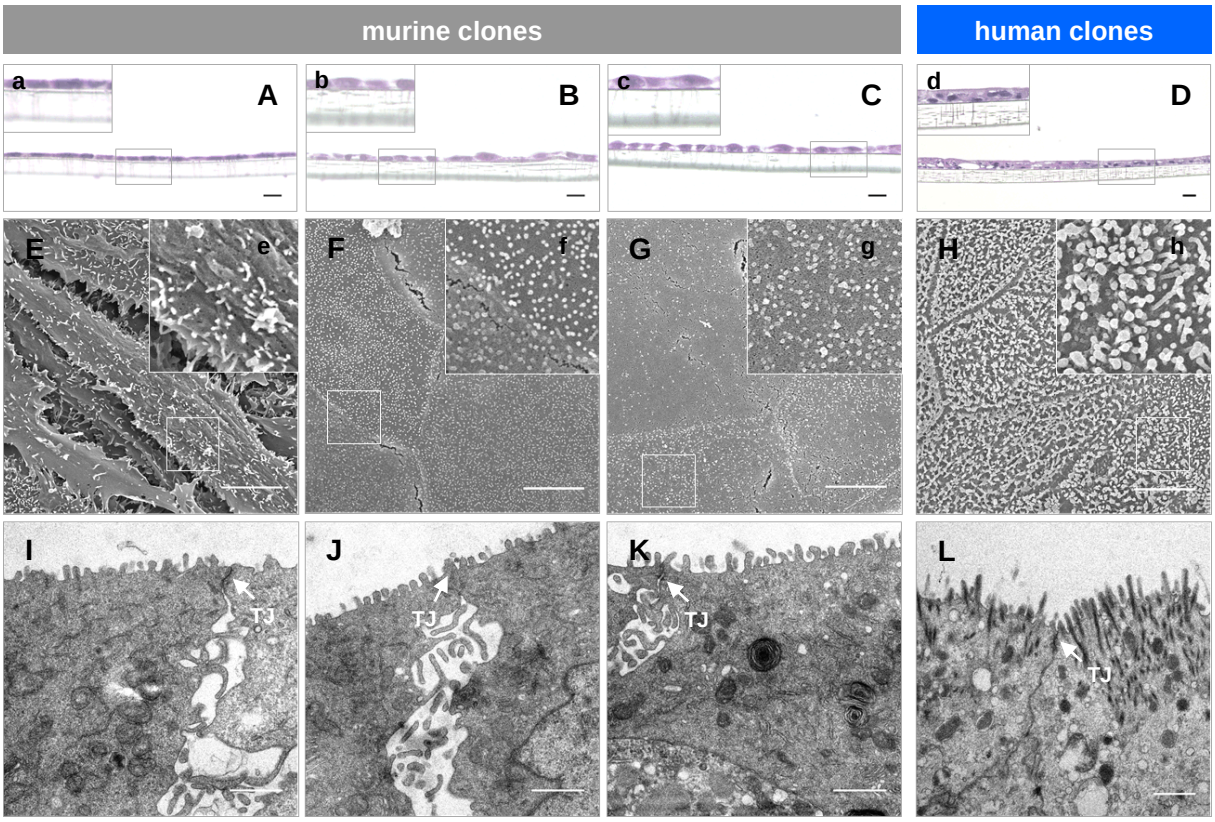

Figure 4.20: Murine and human cell clones cultured on the PET membrane form a tight epithelial layer with tight junctions and microvilli. The formation of a tight cell layer was observed in cross-sectional images of H&E-stained models based on I9K6 **(A/a)**, I9K8 **(B/b)**, I12K9 **(C/c)** cells after a culture time of 21 days and on 15-06 I4B **(D/d)** cells after a culture time of 14 days. Representative images received from SEM **(E/e-H/h)** and TEM **(I-L)** analyses confirmed the formation of a consistent cell layer with apical microvilli and tight junctions (TJ; arrow). Scale bar in **A-C** = 20 µm; in **D** = 200 µm; in **E-H** = 5 µm; in **I-L** = 1 µm; representative of n = 3 biological replicates. The image E/e was provided by InSCREENeX. H&E: haematoxylin and eosin; SEM: scanning electron microscopy; TEM: transmission electron microscopy.

Further, intestinal *in vitro* models based on murine and human cell clones were analyzed for cell type-specific protein expression patterns (VIL1, SGLT1, MUC2, MUC1, CHGA, LYZ) by IHC staining of the respective tissue sections (Figure 4.21). In this context, the intestinal cell type-specific marker LYZ and CHGA were not at all observed in Transwell®-models based on the generated cell clones. As controls, IHC stainings of the native tissue were performed with the same marker setting, as shown in Figure 4.21. While VIL (Figure 4.21A), MUC1 (Figure 4.21K) and SGLT1 (Figure 4.21P) appeared as protein layer covering the epithelial cell sheet, the MUC2 (Figure 4.21F) protein formed spots in direct contact to the cell, which secrets the MUC2 protein. As shown in Figure 4.21B-E, models based on murine and human cell clones also demonstrated a small layer of VIL1 covering the epithelial cells, thereby indicating a polarized epithelial monolayer. These observations were confirmed by the IHC

staining for SGLT1 (Figure 4.21P-T), as this transporter likewise showed a protein sheet on the apical side of the cell layer. In addition, IHC stainings of the protein MUC2 (Figure 4.21G-J) depicted some positive spots of MUC2 in all analyzed cell clone-based models, while the membrane-bound MUC1 (Figure 4.21L-O) protein appeared as small layer covering the epithelial cells. ECAD and DAPI were stained in parallel to investigate the cell borders (red) as well as the cell nuclei (blue) in the respective tissue sections.

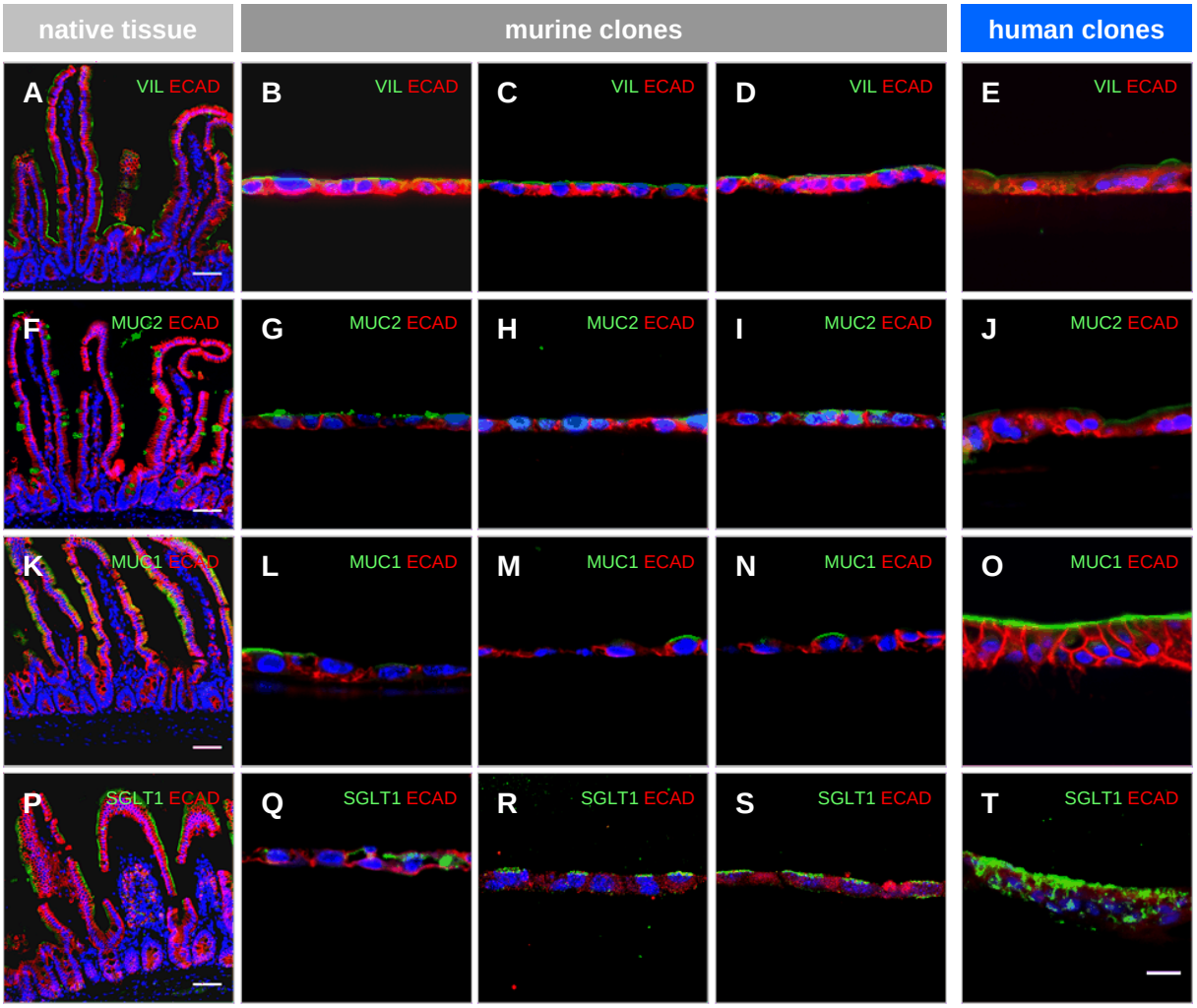

Figure 4.21: IHC analyses of Transwell®-models based on murine and human cell clones. Representative microscopic images obtained by IHC staining of sections of the cell clone-based models show the protein expression profile of intestinal cell type-specific marker proteins (green) such as VIL **(A-E)** or SGLT1 **(P-T)** for enterocytes and MUC2 **(F-J)** or MUC1 **(K-O)** for mucin-producing cells (*e.g.* goblet cells). ECAD (red) and DAPI (blue) are stained to identify cell borders and the cell nuclei (blue). Scale bar in **A**, **F**, **K**, **P** = 50 µm; **B-E**, **G-J**, **L-O**, **Q-T** = 20 µm. representative of n = 3 biological replicates. VIL: villin-1; SGLT1: sodium glucose linked transporter 1; MUC2: mucin 2; MUC1: mucin 1; ECAD: E-cadherin; DAPI: 4,6'-diamidino-2-phenylindole.

Next, the gene expression profiles of the murine and human cell clones, cultured for 21 days (murine) or respectively 14 days (human) on PET-membranes under the preceding defined culture conditions, were analyzed for the same marker setting (*Vil1/VIL1*, *Muc2/MUC2*, *Chga/CHGA*, *Lyz/LYZ* and *Lgr5/LGR5*) as already described for 2D- or 3D-cultured cell clones (section 4.2.5 and 4.2.6) by RT-qPCR (Figure 4.22).

In general, the Transwell®-models based on the murine cell clones I9K6, I9K8 and I12K9 showed a reduced mRNA transcript level for all analyzed marker genes compared to the murine organoids (Figure 4.22C-G), except of the expression of *mMuc2* in I12K9 cell-based models (Figure 4.22D). Further, I9K8 and I12K9 cell-based models demonstrated a higher *mVil1* (Figure 4.22C), *mMuc2* (Figure 4.22D) and *mLyz* (Figure 4.22F) expression compared to I9K6 cell-based models, although *mLyz* was not at all expressed by I9K6 cells in this experimental setting (Figure 4.22F). Values obtained for *mLgr5* (Figure 4.22G) were expressed to a higher degree in models based on I9K6 and I9K8 cells compared to I12K9 cell-based models. However, in comparison to 2D- and 3D-cultured murine cell clones (section 4.2.5 and 4.2.6); the mRNA transcript level was reduced in cultures setup on PET-membranes. Interestingly, *mChga* (Figure 4.22E) was not at all expressed in murine cell clone based Transwell®-models.

In addition, the human cell clone-based Transwell®-models were analyzed for the same marker genes, resulting likewise in a reduced gene expression rate for *hMUC2* (Figure 4.22I), *hLYZ* (Figure 4.22K) and *hLGR5* (Figure 4.22L) compared to the control cells (hOrg), while *hVIL1* expression was increased as shown in Figure 4.22H. Further, 15-06 I4B cell-based models showed for *hLGR5* (Figure 4.22L) a lower expression compared to cultures set up in 2D (section 4.2.5) or 3D (section 4.2.6). As already demonstrated for murine cell clones (Figure 4.22E), also for the Transwell®-models based on 15-06 I4B cells no expression of *hCHGA* was obtained (Figure 4.22J).

In summary, cell clones cultured on Transwell®-inserts showed a slight increase in the mRNA transcript level of some differentiation genes related to the absorptive- and secretory-lineage as demonstrated by gene and protein analyses, but in general a mixture of proliferation- and differentiation-related genes was preserved during culture on Transwell®-inserts.

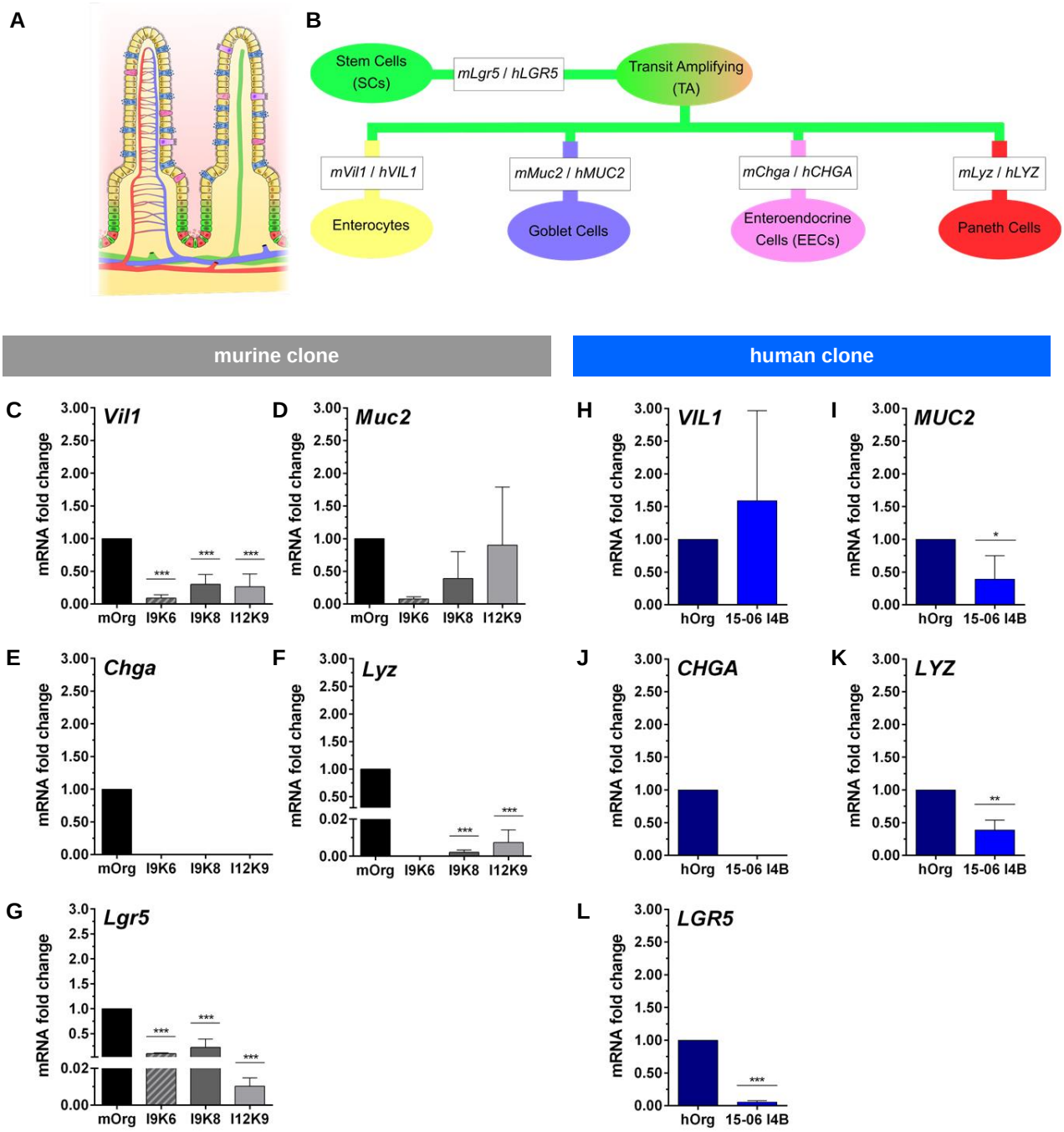

Figure 4.22: Gene expression profile of Transwell®-models based on murine and human cell clones. The intestinal epithelium **(A)** is represented by several cell types and their specific marker genes **(B)** such as *Vil1/VIL1* (enterocytes), *Muc2/MUC2* (goblet cells), *Chga/CHGA* (enteroendocrine cells), *Lyz/LYZ* (paneth cells) and *Lgr5/LGR5* (stem cells). Graphs **(C-L)** demonstrate the gene expression rate of intestinal cell lineage-specific genes analyzed for Transwell®-models based on murine and human cell clones by RT-qPCR. *mRpl15, mRps29* served as reference genes for murine cells and *hHPRT1, hEF1-α* for human cells. Values obtained for murine (mOrg) and human (hOrg) organoids were set to 1. Statistical analyses were carried out by one-way ANOVA. **p<0.05, **p<0.01, ***p<0.001;* n = 3. m: murine; h: human; Vil1: villin-1; Muc2: mucin 2; Chga: chromogranin A; Lyz: lysozyme; Lgr5: leucine-rich repeat-containing G-protein coupled receptor 5.

4.2.9. Immortalized cell clones showed organ-specific transport functions

Based on the observations that cell clone-based Transwell®-models showed a polarized epithelial monolayer together with a characteristic tight/adherens junction protein expression profile, I analyzed, if the generated cell clones also formed an intact as well as functional barrier. In first line, TEER values were measured periodically with a non-destructive TEER electrode every 2-3 days. While the TEER values (Figure 4.23A) continuously increased between day 3 and day 21 to a mean maximum of 232 ± 44 Ω*cm² for I9K6 and 483 ± 81 Ω*cm² for I9K8 cells, I12K9 cells (mean maximum 727 ± 143 Ω*cm²) showed high TEER values during culture of 21 days. In comparison, a tight barrier was determined for models based on the human cell clone 15-06 I4B after 14 days with a mean TEER value of 253 ± 47 Ω*cm² (Figure 4.23B). These data demonstrated a culture time of at least 21 days for murine cell clone-based *in vitro* models and 14 days for models based on the human cell clone, to establish a tight barrier.

In addition, transport capacity was measured by applying reference substances characterizing the paracellular-, the transcellular- and the efflux-transport of the established cell clone-based *in vitro* models to identify their functional performance. In a first step, permeability of 4 kDa FITC-dextran molecules (paracellular transport) was observed to be lower in models set up of 15-06 I4B (0.06 ± 0.05%) cells as well as of the murine cell clones I9K6 (0.32 ± 0.37%) or I9K8 (0.86 ± 0.57%), in comparison to I12K9 (1.26 ± 0.83) cell-based models (Figure 4.23C). Of note, permeability rates were below 2% for all models, which supports the formation of a tight epithelial barrier.

Fluorescein (Figure 4.23D) transport studies (low-permeable reference substance) revealed for I9K6 cell-based models (P_{app}-value of $1.6x10^{-6}$ cm/s) an almost 6-times higher permeability matched to 15-06 I4B (P_{app}-value of $2.5x10^{-7}$ cm/s) or I9K8 (P_{app}-value of $3.2x10^{-7}$ cm/s) *in vitro* models and a 2-times higher permeability compared to models set up of I12K9 (P_{app}-value of $7.5x10^{-7}$ cm/s) cells. Transcellular transport investigated by propranolol (Figure 4.23E) showed a similar permeability for models based on I9K6 (P_{app}-value of $1.9x10^{-5}$ cm/s), I9K8 (P_{app}-value of $1.7x10^{-5}$ cm/s) and I12K9 (P_{app}-value of $1.9x10^{-5}$ cm/s) cells. In contrast, propranolol transport in human cell clone-based (15-06 I4B) models (P_{app}-value of $1.1x10^{-5}$ cm/s) was significantly decreased. The efflux transport mechanism, described as basolateral/apical ratio (ba/ab = basolateral-apical/apical-basolateral) was studied by applying the reference substance rhodamine 123 either to the apical or the basolateral compartment of the established Transwell®-models. As shown in Figure 4.23F, efflux transport was similar for models based on I9K6 or I12K9 cells (ba/ab = 2.5), whereas it was slightly decreased in I9K8 cell based models (ba/ab = 1.5). Of note,

human cell clone based models showed with a ba/ab ratio of 5.1 the highest efflux transport (Figure 4.23F).

In conclusion, these data indicated the formation of a tight epithelial barrier for all cell clone-based models with partly improved transport functions compared to the “gold standard” Caco-2 Transwell®-models. Results observed for Caco-2 *in vitro* models are depicted as dotted line in the respective transport capacity studies, as shown in Figure 4.23D-F.

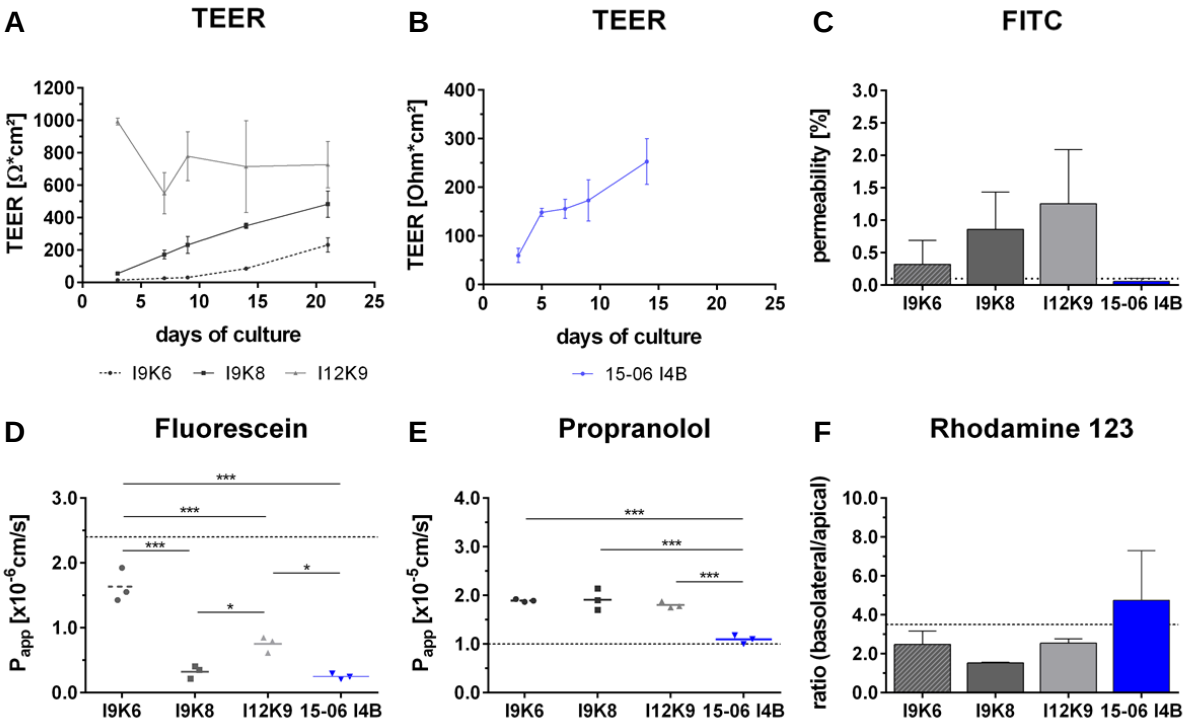

Figure 4.23: Cell clones cultured on Transwell® inserts form a tight epithelial barrier and show characteristic transport activities. TEER values of I9K6 and I9K8 cells increased from day 3 to day 21 in culture **(A)**. In contrast, I12K9 cells **(A)** showed high TEER values already after 3 days, which remained at a similar high level over the culture time of 21 days. TEER values of 15-06 I4B cell-based models rose from day 3 to day 14, indicating a tight cell layer **(B)**. FITC-dextran was transported to a lower extent in 15-06 I4B cell-based models compared to models set up of I9K6, I9K8 or I12K9 cells **(C)**. I9K8 and 15-06 I4B cell-based models showed a lower permeability for the paracellular transport of fluorescein **(D)**. An increased transport of propranolol was measured for Transwell®-models based on murine cell clones **(E)**. The efflux-transport investigated by rhodamine 123, as reference substance, displayed an enlarged permeability for models set up of 15-06 I4B cells, while murine cell clone-based models showed a rather similar permeability ratio **(F)**. Transport capacities of Caco-2 Transwell®-models recently reported by Fey et al. [212] are presented as reference values (dotted line; **D-F**). Significance was calculated by one-way ANOVA. **p<0.05, **p<0.01, ***p<0.001;* n = 3. TEER: transepithelial electrical resistance; FITC: Fluorescein isothiocyanate; P_{app}: apparent permeability coefficient.

5. Discussion

The small intestine represents one of the most important contact surfaces to our environment with important physiological functions like the absorption of nutrients, water and vitamins as well as the protection from toxic xenobiotics and pathogens at the same time [15,161].

Orally applied drugs move through the digestive tract, followed by transport across the intestinal epithelium and pass the liver before circulation via the bloodstream to reach its target site. This drug administration route is the most convenient, safest and cost-efficient way [239,240], as patient compliance is given due to an easy ingestion and pain avoidance. Further, the pharmaceutical industry benefits, as pills can be easily produced in a computer-assisted 3D printing process with a high versatility (same manufacturing process for different drugs) [239]. The small intestine represents a strong barrier separating the lumen from circulation and is therefore significantly involved in the absorption and transport of drugs, thereby determining their bioavailability [3,7]. In the context of drug design, pharmaceutical research is mainly concerned with effectiveness and toxicity, which both requires predictive pre-clinical models.

In first line, high-throughput screenings (HTS) were performed on behalf of cell line-based models cultured in 2D on plastic surfaces to gain more knowledge about effective dosing or toxicity of the applied drugs, followed by animal studies to identify systemic effects under physiological conditions *in vivo* [241]. Nevertheless, high failure rates were observed in drug discovery, which is largely attributed to the culture conditions in cell-based HTS, as most of the classical cell models were not representative of the native intestinal epithelium and due to species-specific differences [242]. Therefore, 3D cell culture technologies, closely resembling the *in vivo* cell environment, are of high interest, as they are expected to show a better predictivity in pre-clinical research applications [240,241]. Standard intestinal 3D-like *in vitro* models are represented by cell lines (*e.g.* Caco-2) cultured on artificial PET membranes to screen the developed drugs for toxicity or bioavailability, however they lack in important cell-ECM interactions as well as corresponding protein expression profiles, limiting the *in vitro-in vivo* correlation [85,111,112]. Decellularized natural ECM scaffolds such as the SIS [116,139,140] overcome these limitations due to their structural, biochemical and biophysical features [120,135]. However, the production of native ECM structures is time- and cost-consuming with a varying batch to batch quality; therefore the application in pre-clinical research is limited and economically inefficient.

Of note, Sato and colleagues reported in 2009 a protocol for the long-term culture of primary intestinal spheroids/organoids embedded in Matrigel® as alternative cell source to cell lines, as they show a high comparability to the *in vivo* situation and therefore positively influence

the predictivity in the conducted studies. Nevertheless, spheroid/organoid cultures in Matrigel®, an undefined mixture of ECM-related proteins, is not standardized, high-throughput incompatible, more complex in handling and associated with high costs.

Taken together, an intestinal *in vitro* model used in pre-clinical research applications should satisfy a variety of requirements such as presenting a standardized and well-defined system, high-throughput qualified, reveal a high *in vitro-in vivo* correlation, while being easy in handling under cost-efficient conditions. To achieve this, alternative cell sources and scaffolds are central to establish standardized functional intestinal *in vitro* models with a better performance in drug delivery studies.

Therefore the aim of this thesis was to prove the suitability of two versions of BNC, unmodified and surface-structured, as biological model scaffolds to generate a functional intestinal barrier. Furthermore, a primary-cell-derived immortalized cell line was tested as alternative to intestinal organoids to enable the design and development of time- and cost-efficient in vitro models of the small intestinal epithelium.

5.1. Bacterial nanocellulose as scaffold for standardized model setup

The first goal of this thesis was ***to prove two variants of BNC, unmodified and surface-structured, as suitable bioscaffolds for a standardized setup of tissue engineered intestinal organ models***, demonstrating an overall good performance regarding their predictivity and functionality. Caco-2 cells considered as “gold standard” in intestinal tissue engineering concepts were used to establish Transwell®-like *in vitro* models on BNC scaffolds with PET as well as the biological SIS as controls [111,112]. The results obtained for the BNC-based Caco-2 models demonstrated an overall good performance, as a characteristic tight/adherens junction protein expression pattern together with a representative transport capacity of several reference substances was observed. Further, the production of the BNC scaffold is cost-efficient under standardized conditions, is highly flexible as different surface topographies can be implemented, is easy in handling and fits the 3Rs principle. Together, this indicates the BNC matrix as alternative scaffold for standardized and reproducible model setup at least for cell lines such as Caco-2, as dissociated primary organoids did not show a good cell adherence under the applied conditions. However, the flexibility of the BNC production method and therefore the surface properties indicates that an adapted surface topography or composition will enable an improved cell adherence for each cell type/cell source.

5.1.1. The BNC - a natural scaffold with moldable matrix properties

As scaffold materials in intestinal tissue engineering concepts, artificial membranes based on PET or natural decellularized ECM scaffolds such as the porcine SIS are currently used. Especially, decellularized ECM matrices are of high interest, as the cellular behavior mainly depends on the micro- and ultrastructural features of a scaffold material, which synthetic polymers (*e.g.* PET) cannot provide [7,120]. Further, the single continuous fiber arrangement, the hydrophilic properties and the matrix composition, enhancing cell-ECM interactions, support the preferred use of natural ECM scaffolds [115,135,141]. However, their production is barely standardized as well as time- and cost-intensive, which limits the application of SIS matrices in pre-clinical research. In this context, the BNC scaffold offers an interesting alternative, as the production is highly standardized at low costs. Further, the BNC scaffold demonstrates features comparable to natural ECMs such as a similar fiber arrangement and the hydrophilic properties [146,243].

Versatile application fields including the biomedical area like wound healing, tissue engineering, medical implants or drug delivery demonstrated the BNC matrix, produced by bacterial strains, as bioscaffold of high interest, also in the context of novel intestinal tissue engineering concepts [244]. Thus, many efforts for a better procurement of the BNC have been undertaken to improve the yield and purity in BNC production as well as the overall BNC performance defined by its mechanical, physical and biological properties. For instance, post-treatment of the BNC material with alkaline solutions led to alterations in pore size and porosity of the BNC-based scaffold due to an improved binding capacity of acetic acid, resulting in bigger ice crystals during freeze-drying and therefore better porous features [245]. Further, genetically manipulated bacteria strains used for the fermentation process of the BNC material can reveal enlarged pores, which influences cell adhesion and proliferation [244]. Next, thickness, surface-structure or size of the BNC scaffold can be easily adapted and optimized through the manufacturing process [149,246]. Recently, Bottan et al. reported an elegant method to structure the BNC surface by GAB technology, resulting in BNC scaffolds with an aligned fiber arrangement due to structured PDMS stamps, which further leads to a better cell adherence of human dermal fibroblasts together with a higher cellular density compared to the flat controls [149]. In general, the GAB technology describes a molding methodology, in which structured PDMS stamps are placed into the gas-liquid interface of bacterial strain cultures to transfer on-demand functional topographies to the surface of the generated scaffolds [149]. The surface-structured BNC scaffolds obtained by GAB were also used in the current study next to the unmodified BNC scaffolds with a rather smooth surface, as modulation of the surface topography is known to induce distinct cellular responses [149,159,160]. However, models set up on the surface-structured BNC did not

show advantages compared to the unmodified BNC in the current study with Caco-2 cells. In general, the surface-structured BNC can be generated with different grating depth as demonstrated in the study of Bottan et al., which resulted in 10 µm depth gratings that are closely located to each other by using the PDMS mold “P10”, while PDMS mold “P100” based scaffolds showed less gratings related to the same area [149]. Further, Bottan et al. demonstrated that human dermal fibroblasts performed better in the applied analyses compared to HaCaT cells and in comparison between the different molded structures, as improved characteristics were observed for cultures setup on scaffolds with an increased grating depth [149]. For the current study surface-structured BNC scaffolds with a “P10” PDMS mold were used, which could be too small to enable good culture conditions for Caco-2 cells, as *in vivo* crypt structures are deeper and exhibit a spacing of 50 µm [247]. In future studies, different grating depth could be tested for an improved model setup for Caco-2 cells. Here, both BNCs, unmodified and surface-structured, were used to demonstrate their applicability as alternative scaffolds in intestinal tissue engineering purposes.

5.1.2. Caco-2 cells adhere and differentiate properly when cultured on the BNC scaffolds

To test both BNC variants as alternative scaffolds for a standardized setup of intestinal *in vitro* models, the commonly used human adenocarcinoma cell line Caco-2 [102,111] was cultured for 21 days on the BNC scaffolds as well as on the PET and SIS matrix as controls. The results obtained by histological analyses showed Caco-2 models with a good cellular adhesion and growth on all scaffold as well as the formation of a bi- or multi-layering of Caco-2 cells, a characteristic feature of differentiated Caco-2 cells and therefore indicative for a proper cellular behavior on the BNC scaffolds [218,219]. Interestingly, the SIS-based models demonstrated an eosin staining, which appears lighter compared to the other scaffold-based models, suggesting a looser connective tissue within these cells. Properly, the tumorigenic cell line Caco-2 cultured on the SIS scaffolds leads to a remodeling of the biological matrix, which resulted in the less compact connective tissue between adjacent cells. This phenomenon is known *in vivo*, as the formation of colorectal cancer leads to changes in the ECM regarding an increased stiffness and degradation of the matrix [248,249]. As the PET membrane and both BNC variants do not enable or need this remodeling due to their higher stiffness as well as their compact structure compared to the SIS, these matrices are more suitable for a standardized model setup with Caco-2 cells. However, in context of tumor research the SIS-based models would be preferred [128].

A key feature of intestinal *in vitro* models with respect to drug bioavailability studies is the formation of a tight epithelial cell layer. Ultrastructural and histological analyses revealed the formation of a tight cell layer with a homogenous tight/adherens junction protein expression pattern when cultured on the unmodified BNC. In contrast, models set up on the surface-structured BNC, SIS or PET showed a less homogenous protein expression pattern for the intracellular proteins ZO-1 and OCLN, while the protein expression pattern of ECAD an adherens junction protein was well established. These intracellular proteins connected to the cytoskeleton of the cells are mainly influenced by changes in the local environment, suggesting surface-properties on the structured BNC that are not ideally for an entire maturation of the Caco-2 cells [250]. However, corresponding TEER values and the low permeability rates for FITC-dextran confirmed that cells cultured on both BNC variants formed a tight epithelial cell layer. Of note, SIS-based models demonstrated a higher permeability for FITC-dextran together with a high variance in the obtained results, which can properly be attributed to the batch to batch variations of the matrix but also to the less compact connective tissue between the Caco-2 cells.

As proof of concept, that Caco-2 cell adherence is properly accomplished on both BNC scaffolds, treatment with the chelating agent EGTA occurred, as thereby tight junction complexes between adjacent cells are reversibly opened with respect to changes in the colocalization maxima of different TJ pairs such as ZO-1/occludin or E-cadherin/claudin-1 [220,251]. The TEER-values decreased rapidly in the first 10-15 min after EGTA was applied into the apical compartment of all established models, as it was previously demonstrated by Ma and colleagues [252]. With ongoing time a minimum TEER-value was reached, where only the resistance of the cell layer was measured [217,252]. After a regeneration period of 24 h in exchanged EGTA-free medium, increased TEER-values are indicative for closed tight junctions, as cell-cell contacts were interrupted but not cell-matrix contacts, demonstrating that both BNC matrices enable a good cell adhesion. In addition, FITC-dextran transport measured before and after EGTA treatment, as an indication of a tight epithelial barrier [79,223], showed a comparable low permeability, to further support the good performance of the BNC-based models in this study. The good cellular adhesion to the BNC scaffold as well as cell differentiation is in line with results observed for mesenchymal stem cells [158] and human dermal fibroblasts [149] cultured on BNC-based scaffolds, which further enhances this scaffold material as adequate alternative to the commonly known artificial and biological matrices.

In addition, the models displayed a uniform distribution of microvilli on the cell surface, indicating a proper Caco-2 cell differentiation towards mature enterocytes and thereby representing epithelial cells of the small intestinal epithelium to some extent [111,253] when

cultured on the unmodified BNC. In contrast, a few Caco-2 cells without microvilli on the cell surface were observed for surface-structured BNC-, PET- and SIS-based models. With regard to the microvilli height, similar observations were made for all scaffold-based Caco-2 models in ultrastructural analyses, which is in line with other Caco-2 cell based models with a microvilli height about 1.19 ± 0.16 µm [253] as well as to the *in vivo* situation with a microvilli height of 1-3 µm on the apical cell-surface of enterocytes [254]. Further, a uniform and pronounced formation of microvilli on the cell surface could influence transport capacity studies, which is why the unmodified BNC-based models could show a better model performance.

5.1.3. Caco-2 cells cultured on BNC scaffolds perform well in drug transport studies relative to controls

Routinely, Caco-2 cell-based *in vitro* models set up on synthetic PET membranes are used to study toxicity or transport across the epithelial barrier of orally applied drugs [111,112]. Therefore, Caco-2 *in vitro* models established on both variants of the BNC were investigated in the context of characteristic transport mechanisms known from the native intestinal tissue. The paracellular-, transcellular- and efflux-transport are the main transport routes in the intestinal epithelium, which are characterized by reference substances such as fluorescein, propranolol and rhodamine 123 [15,78,223]. Paracellular transport of fluorescein was limited in both BNC-based models compared to the models established on the synthetic PET or the biological SIS matrix, underlining the formation of a tighter epithelial barrier. This finding is in line with the results observed for TEER measurements and the permeability of FITC-dextran for BNC-based models compared to PET- or SIS-based models.

The activity of the transcellular pathway is of high interest for drug delivery studies in pharmaceutical research, as some drugs are transcellularly transported across the epithelial cell layer, which is strongly dependent on the appropriate expression of specialized proteins located in the apical brush border membrane and on a polarized epithelial cell layer [79]. In this context, unmodified BNC-based models showed a higher permeability for the reference substance propranolol compared to models set up on the surface-structured BNC, indicating an altered protein expression profile due to the modulation of the surface topography. In line with this, Li et al. and Gasiorowski et al. demonstrated a significantly altered gene expression pattern when mesenchymal stem cells [255] or human vascular endothelial cells [256] were cultured on distinct surface topographies; however, these effects of the surface topography are individual for each cell type [257]. In addition, the models set up as controls demonstrated for SIS-based models an even higher permeability compared to Caco-2 *in vitro*

models established on the unmodified BNC, while PET-based models showed the lowest permeability rate among all cell-based models in this study, indicating that unmodified BNC-based models performed well in the context of transcellular transport mechanism.

In addition to the paracellular or the transcellular route, the efflux transport pathway, mediated by the transporter *e.g. p*-gp located in the apical brush border, is of high interest for pharmaceutical research, as drugs like digoxin, paclitaxel or indinavir will be transported back into the intestinal lumen by this special transporter, which leads to a decreased transport rate across the epithelial barrier and therefore a low efficiency of the respective drug [258]. Given a high comparability of the established *in vitro* models to the *in vivo* situation, the value for the efflux-transport (basolateral/apical ratio) is high [85,87,89], whereby a value of at least 2 should be reached according to 'food and drug administration' (FDA) regulations [224]. In the current study, the efflux transport was investigated by the reference substance rhodamine 123, which revealed an improved efflux transport in unmodified (ba/ab = 4.0) and surface-structured BNC-based models (ba/ab = 4.9) compared to PET- (ba/ab = 3.5) or SIS-based models (ba/ab = 1.9), indicating an increased expression of the *p*-gp transporter of BNC-based models and therefore a better model performance. In future studies, differences in the expression rate of the *p*-gp transporter or the other efflux associated transporters such as MRP2 or BCRP could be analyzed by western blotting to validate an increased/reduced value for the efflux transport [87].

Taken together, Caco-2 models cultured on BNC scaffolds showed an overall good performance in transport capacity studies. In comparison to previously published transport rates of Caco-2 models established on PET membranes (P_{app}-value fluorescein: $0.5x10^{-6}$ cm/s; P_{app}-value propranolol: $3.4x10^{-5}$ cm/s; ba/ab rhodamine 123: 12) [224], the PET-based models in the current study demonstrated a decreased transport activity, which is possible due to different culture conditions and different passage numbers of the used Caco-2 cell line, a common phenomenon among various laboratories [164]. Further, studies regarding the fluorescein transport capacity of rat jejunum tissue with a P_{app}-value of $6.9 \pm 2.35 x10^{-6}$ cm/s show a less tight barrier, indicating that the results obtained in the current study are more similar to the *in vivo* situation [259]. In contrast, the transport capacity of propranolol is ~ 10 times lower for models setup on all scaffold materials compared to the human jejunal tissue with a permeability rate of $2.9 \pm 2.2 x10^{4}$ cm/s [260], indicating a reduced expression of specific transporters on the cell surface. With regard to the efflux ration of 6.88 for rhodamine 123 *in vivo* (rat intestinal tissue), models established in the current study demonstrated a slightly decreased efflux ratio, in which BNC-based models showed a higher comparability to the *in vivo* situation [261]. However, according to the regulations of the FDA new model systems have to be screened for a much broader range of known substances classified in

the Biopharmaceutics Classification System, which originally demonstrates human jejunal permeability rates, to validate novel model systems for their use in pre-clinical research purposes [262].

To support the relevance of the established BNC-based models with regard to their use in pre-clinical research, the endocytotic pathway as one of the main transport routes of formulated drugs across the epithelial barrier [92], was further investigated in these studies. This pathway enables the transport of particles, in which pharmacological agents are often shuttled to improve their biodistribution and bioavailability, as the agent alone cannot pass the intestinal barrier due to size, positive/negative charge or composition [263]. Further, PET membranes with an unequally pore distribution used for model setup were described to negatively affect the transport of individual nanoparticles by creating a physical barrier [112,116], which would result in a reduced efficiency of the analyzed drug and therefore a limited predictivity, as *in vivo* the natural ECM would not harbor such an additional physical barrier. In this context, coumarin-6-labeled PLGA-NPs with a particle size of 200 nm, thereby ensuring an endocytotic particle uptake [264,265], were used in this study. PLGA belongs to the mainly used polymers in cell-based studies, as this polymer is biocompatible and encapsulation of fluorescence emitting substances *e.g.* coumarin-6, for an easier detection, is possible [265,266]. In addition, these NPs demonstrate an almost neutral charge together with hydrophobic properties and therefore intensive sticking of PLGA to the hydrophilic matrix proteins should be avoided [265]. Caco-2 cells cultured on SIS scaffolds showed an overall good performance in the PLGA nanoparticle transport over a time period of 6 h, while both BNC-based models and the PET-based models revealed a retarded permeability, indicating that the BNC variants also form a physical barrier for particle transport similar to the PET membrane. In a comparable study with Caco-2 cells cultured on PET-based Transwell®-inserts with a pore size of 3.0 µm demonstrated an increased permeability for PLGA-NPs around 18.5 ± 2.39% [267], which is 7-14 times the amount of transported particles compared to models established for the current study, indicating a strong dependence on the pore size. However, matrix thickness besides pore size could be a preliminary factor for a reduced particle transport, which was recently reported by Vllasaliu et al. as influencing factor in nanoparticle permeability studies [227]. Therefore, model functionality in BNC-based models could be improved in future studies, when matrix thickness, pore size and pore distribution of the developed BNC scaffolds will be adopted. In addition, sticking of nanoparticles to the scaffold could be tested in a cell-free assay by detection of the recovery rate in combination with ultrastructural analyses to identify the impact of the used scaffold.

5.1.4. Primary intestinal epithelial cells might need special surface properties for a good cellular adhesion on the BNC scaffolds

The overall goal in small intestinal tissue engineering is the establishment of a highly standardized *in vitro* model, which is easy in handling at low costs and applicable for high-throughput screenings, while representing the cellular and functional diversity of the native intestinal epithelium. As the BNC was proven as suitable alternative scaffold in the preceding analyses with Caco-2 cells, the cellular complexity of BNC-based models was increased by using primary human intestinal organoids. Therefore, primary intestinal organoids were dissociated to single cells and cultured for 14 days on both BNC variants according to culture conditions previously defined by Schweinlin et al. [139]. However, a good cellular adhesion of the primary cells was not observed on the two versions of BNC.

In general, the ECM protein composition, the integrin repertoire and the localization of E-Cadherin are changed in epithelial cells of the villus-domain compared to the crypt-domain in the native intestinal epithelium, which allows cells, especially enterocytes, to glide over the basement membrane to reach the tip of the villus without losing their important cell-cell interactions [268]. The established primary cell culture models undergo likewise a differentiation process *in vitro*, as they were cultured in differentiation medium for 5 days. H&E-stained tissue sections of these models set up on both BNC variants demonstrated a detached cell layer, which could be due to a similar process as *in vivo*, if the cell-matrix interaction has to be loosened to enable a proper cell differentiation [268]. In this context, the E-Cadherin/actin colocalization was demonstrated to be an important factor for a good cell-matrix interaction [268], which could be investigated in future studies by IF-stainings for E-Cadherin in combination with actin. Further, if the adhesion of primary cells is disturbed directly from the beginning, cellular adhesion experiments could be performed by seeding of the cells on all matrices, followed by an incubation time of 3 h and a staining with crystal violet to measure the optical density with regard to the amount of cells [269].

For this study BNC matrices were coated with gelatin, a mixture of proteins produced by partial hydrolysis of collagen [270], whereas hydrolyzed collagen alone seems to be not suitable for a proper cell adherence for primary cells. In contrast, models established on Col I pre-coated PET membranes showed good cellular adhesion characteristics. These differences can be attributed to different integrin-dependent adhesion processes, as it is known that cells can express on the surface Col-binding integrins (*e.g.* α2β1), gelatin-binding integrins (*e.g.* α5β1) or both [271]. A study performed by Hernandez-Gordillo demonstrated that Col-binding integrins are more important for a proper organoid cell growth compared to gelatin-binding integrins [272], which could lead also to the better performance of the primary

organoid cultures on the Col I pre-coated PET-based inserts. The SIS scaffold already exhibits in the basal lamina the necessary components for a good cellular behavior, which is further supported by the natural ECM environment [120]. Therefore, a coating strategy with a mixture of collagen/fibronectin or collagen/laminin could improve the cellular adhesion and behavior of primary cells on the BNC scaffolds, as fibronectin or laminin are mainly involved in cell adhesion processes *in vivo* [120]. Furthermore, the surface-topography, the pore structure or the matrix stiffness, influencing factors for cell adhesion, could be adopted in future studies.

Taken together, both BNC scaffolds were not suitable for the establishment of intestinal organoid-based *in vitro* models. In contrast, the SIS-based models showed a good cellular behavior, but these models are less standardized. Thus, PET-inserts were chosen as scaffold for further experiments to enable a standardized model setup, which is important in the context of pre-clinical research purposes.

5.2. A primary-cell-derived immortalized cell line as alternative cell source for intestinal organ modeling

In view of the potential of primary intestinal organoids, representing a close similarity to the native intestinal epithelium in the context of cellular diversity and functionality [7,30,102], together with the need of a more predictive cell line in pre-clinical research purposes, ***the aim of this part of the thesis was to establish a primary-derived cell line***, which shows an improved performance in functional assays compared to the commonly used Caco-2 cell-based models. Murine and human intestinal organoids were used for the lentivirus-based immortalization strategy in cooperation with InSCREENeX, which resulted in several organoid-derived cell lines (cell clones) established from a single immortalized cell. Preceding analyses revealed that three murine cell clones and one human cell clone demonstrated features characteristic for the intestinal epithelium such as the formation of a tight epithelial barrier, *in vivo*-like transport mechanisms and a gene as well as protein expression pattern representative for the cellular unit, at least to some extent.

5.2.1. Lentivirus-based immortalization strategy to establish primary-derived cell clones

A major limitation for pre-clinical research applications is the availability of expandable cell cultures derived from tissues with an individual background, thereby representing the cellular complexity of the native tissue, while being easy in handling at low costs. Primary cells or pluripotent stem cells (embryonic/induced pluripotent (iP)) demonstrate cell sources with an individual tissue background, but the low proliferation capacity of primary cell cultures and the immature, fetal-like phenotype of differentiated iPS-derived cells [273–275] are obvious drawbacks for the routine use. In contrast, cell lines such as the colorectal adenocarcinoma Caco-2 cells are routinely used in pharmaceutical research, as they are easy in handling under cost-efficient conditions. Given the limitations of an adequate expression pattern resembling the cellular diversity of the intestinal epithelium, Caco-2 cells do not entirely fulfill the requirements for pre-clinical research purposes. Therefore, together with the cooperation partner InSCREENeX, I hypothesized that primary-derived immortalized cell lines could represent an interesting alternative cell source.

In general, the cell cycle and thus the cell proliferation are controlled and regulated by a number of cellular processes. For instance, the Hayflick limit is accomplished when a certain number of cell divisions occurred and therefore a critical telomere length is reached, which results in cell senescence and finally cell death [276–279]. In contrast, immortalized cells do

not have this limitation in the number of cell divisions, therefore they propagate indefinitely. The tumor suppressor protein p53 or the retinoblastoma protein (pRb) are mainly involved in processes controlling the cellular proliferation [280,281]. To trigger immortality and likewise cell proliferation, the replication limits have to be removed or intervened in cells to be immortalized. In the past, immortalization was achieved by manipulating the cells genome through the transfection with viral oncogenes/oncoproteins [282–286] or with the telomerase reverse transcriptase (TERT) protein [287–289]. Viral oncogenes/oncoproteins such as the simian virus 40 large T antigen (TAG) [290–292], E6 or E7 from the human papillomavirus [293,294] and E1A or E1B from the adenovirus [295,296] are able to inactivate both, pRb and p53, to overcome cell senescence. The pRb is known to regulate cell cycle processes in the cell [281,297], while p53 is more responsible for the repair of cellular DNA or elimination of damaged cells [280,298,299]. It was shown that pRb inactivation results in continues activation of the G1 checkpoint and therefore entry into the S-phase of the cell cycle inducing cell division [297]. Next, inactive p53 results in ongoing activation, instead of repression of target genes implicated in apoptosis (*e.g. noxa, bax*), senescence (*e.g. pai-1*) and cell cycle control (*e.g. p21*) [300]. However, such strong oncogenes/oncoproteins often display cell degeneration leading to a dramatic change in their phenotype and therefore they are no longer physiologically relevant [207]. Tumorigenic characteristics, limited ability for maturation and altered cellular functions are the most common cellular changes due to immortalization [276].

For the current study the Cl-SCREEN® immortalization technology patented by InSCREENeX was used. This method is based on vectors containing a gene pool of 33 genes which are relevant for the generation of long-term proliferating cell lines independent of their cell type [207]. Furthermore, this lentivirus-based immortalization strategy induces immortality in dividing as well as non-dividing cells [207,210,301] and demonstrated that immortalization results in cell populations with preserved primary cell-based properties to a particularly high degree [206,207], as recently shown for human endothelial cells [208], murine embryonic intestinal epithelial cells [205] or alveolar lung cells [209]. For instance, Heiss et al. demonstrated that immortalized human endothelial cells, used in spheroid-based angiogenesis assays, provided a sensitive and versatile tool to screen potential pro- and antiangiogenic compounds in the context of pre-clinical studies under cost-efficient conditions, while primary endothelial cell-based assays were affected by passage number and donor variability [208]. Kuehn et al. showed the generation of a novel human alveolar epithelial cell line representing type I-like characteristics that exhibited functional tight junctions to study the absorption and toxicity of inhaled substances (*e.g.* drugs, chemicals, nanomaterials), which was only insufficiently implemented with other lung-based cell lines

such as A549 [209]. Studies by Schwerk et al. showed a reproducible method to generate intestinal epithelial cell lines from wild type or transgenic embryonic mice to study the cellular responses to type I and III interferon in the context of mucosal immunology after an innate immune stimuli [205]. In the current study a pre-selected 10- (murine) or 12-component (human) gene pool was used for the generation of the murine and human cell clones based on primary organoids generated of murine/human intestinal tissue, as in a previous study performed by InSCREENeX and partners, a distinct set of genes was already identified for embryonic intestinal epithelial cells [205], which was thought to be an ideal combination also in this context.

Within this project the 10-component gene pool used for murine organoids included the immortalization genes *Id1*, *Id2*, *Id3*, *c-Myc*, *Fos*, *E7*, *Rex-1*, *Nanog*, *Core* and *TAg*, whereas a 12-component gene pool was used for the human organoids composed of *ID1*, *ID2*, *ID3*, *E6*, *E7*, *C-MYC*, *FOS*, *REX-1*, *NANOG*, *CORE*, *TAG* and *BMI1*. In Table 4.3 the panel of integrated genes for selected murine (I9K6, I9K8 and I12K9) and human (15-06 I4B) cell clones is shown, as these clones fit best to the requirements of this study. The ectopically expressed genes of the respective clones were identified by InSCREENeX. Interestingly, the most well-known immortalization genes *TAg/TAG* and *E7* were proven in only a few cell clones such as I9K6, I12K9 and 15-06 I4B, while *TAg/TAG* was not at all integrated into the cells genome of murine or human cell clones. In contrast, the genes *Id2/ID2*, *Id3/ID3* and *Core/CORE* were identified in all analyzed clones. Russel et al. showed that Id2/ID2 prevents tumor formation in the intestinal epithelium as a pRb binding protein [302] and Cao et al. further demonstrated the importance of Id2/ID2 as a suppressor of the TGF-β signaling pathway [303], thereby inhibiting the cell cycle control and apoptosis. Id2/ID2 belongs to the protein family of inhibitors of DNA binding and cell differentiation (Id) [304], whereof further members such as the *Id3/ID3* and the *Id1/ID1* gene were also integrated in the established cell clones, whereas *Id1* was not identified in the genome of I9K8 cells. Further, Id1/ID1 was described in other studies as relevant for maintenance of stemness and thus the suppression of epithelial cell differentiation [305], which could result in immortalized cell populations with cellular characteristics representing a stem cell or progenitor cell fate. In addition, *Core/CORE* was identified to be integrated in the cells genome of all clones, which is involved in p53- and pRb-related pathways to overcome cell senescence, as demonstrated in a study by Basu et al. for the immortalization of human hepatocytes [306].

The integration of *c-Myc/C-MYC* was observed in all clones except of I9K8, where *c-Myc* is known to positively influence proliferation-specific genes through binding enhancer box sequences (E-boxes) and recruitment of histone acetyltransferases to induce transcription of various target genes such as cyclin D2 which are involved in cell cycle control mechanisms

[307]. Further, c-Myc was found to be localized in the transient-amplifying domain of intestinal crypts, as it was implicated as a target of the canonical Wnt-pathway [308]. Another immortalization gene is *Rex-1/REX-1*, a zinc-finger protein which is mainly expressed in undifferentiated stem cells. *REX-1* knockout showed in hiPS-derived cells a decreased expression of genes associated to cell cycle control, cell growth and proliferation (*e.g. Gbp2*, *E2F5*), thus identifies it as a crucial factor in influencing the cell cycle control signaling pathways, as demonstrated in a study by Scotland et al. [309]. Interestingly, this gene was integrated in all murine cell clones but not in the human cell clone, where *REX-1* together with *TAG* were the only genes that could not be successfully transduced into the human cell clone from the original gene pool. In total, several genes were identified to be integrated into the generated cell clones to trigger immortality, which are described in the context of cell-cycle control or the stem cell state/behavior. However, the murine cell clone I9K8 showed the biggest differences regarding the transduced genes compared to the other cell clones.

Next to the strategy and the ectopic expression of a gene pool used for immortalization, the cell culture conditions contribute to an efficient immortalization process. With regard to the immortalization of primary organoids, which are routinely cultured in a 3D-Matrigel®-based environment [30,174], genetic manipulation of 3D-cultured cells could be inefficient as already demonstrated by Onuma et al. for murine primary intestinal cells [310]. Therefore, InSCREENeX established a protocol also for the lentiviral transduction of 2D-cultured primary organoids. In order to improve the immortalization process further, differentiated primary organoid cultures achieved by the extension of culture time were used, as these 3D-structures present the cellular composition of the native intestinal epithelium to a higher degree [29,177], which means that enterocytes, goblet cells, enteroendocrine cells, paneth cells, TACs and SCs can be evidenced. Lindeboom and colleagues have shown in multi-omics analyses of differentiated organoids induced by prolonged culture, that marker genes/proteins representing SCs and TACs are further prominent in these cultures [311].

Finally, differentiated murine and human organoids were either cultured in 2D as single cells on FN/Col I pre-coated plates or cultured as floating organoids for the lentiviral transduction process, as the physiological environment of the primary organoids is thereby represented to a higher degree, which could enable the generation of cell lines with improved characteristic features. Both transduction strategies resulted in several cell populations, which were picked and cultured in the following on FN/Col I pre-coated plates. In total, the 3D-transduction revealed in 16 murine and 16 human cell clones, whereas the 2D-transduction resulted in 27 murine and 16 human cell clones, indicating a higher transduction efficiency when cultured in 2D due to a better accessibility for the lentivirus-based gene pool [312].

In this context, it was further demonstrated that the immortalization process of human primary organoid cultures in 2D as well as in 3D was more difficult compared to murine primary cells. In general, human primary organoids showed a slightly lower proliferation capacity and a lower cellular turnover together with the need for a more complex composition of external growth factors to sustain their cellular diversity *in vitro*, indicating different intrinsic signalling pathways between these species [313], which could be a first hint for these difficulties in the immortalization process. Finally, immortalization of intestinal organoid cultures of only one human donor was successfully achieved, whereby this donor was comparatively young in age. It could be possible that cells of different stages of age will have varying abilities to integrate foreign DNA, as it was assumed for cells at different passages [314].

In general, the proof of a successful immortalization should be presented in subsequent studies, which would refer to the maintenance of a short telomere length and simultaneously high activity [315,316] either by telomerase or alternative lengthening of telomeres (ALT) [317]. Several detection methods are available, with the terminal restriction fragmentation (TFR) analyses as the most common one, which provides advantages in the context of comparability to other studies [318].

5.2.2. Immortalized intestinal cell clones needed a special micro-environment supported by extracellular matrix proteins or/and growth factors

In this study, intestinal murine and human organoids were immortalized to generate the primary-derived cell lines, whereupon a suitable platform for the culture and expansion of these novel cell lines has to be evaluated. Culture conditions that are time- and cost-efficient are preferred to establish an alternative cell source for pre-clinical research purposes, which cannot be provided by primary organoid cultures.

In general, intestinal spheroids/organoids are cultured in a 3D-Matrigel®-based environment and a cell culture medium supplemented with a variety of growth factors for generating crypt-villus-units *in vitro*. These growth factors mimic niche conditions to maintain the stem cell state (Wnt3a, hR-Spondin 1), to inhibit differentiation (mNoggin, LY2157299), to stimulate cell migration (hEGF), to prevent apoptosis (Y-27632) and to support conditions needed in the context of long-term *in vitro* culture (Nicotinamide, A83-01) as well as for an increase in culture efficiency (Gastrin, SB202190) [60]. This medium composition was reported by Sato et al. with respect to human organoids [30], while murine organoids only need the supplementation of hEGF, mNoggin, hR-Spondin-1 and Y-27632 [174]. As the culture in a 3D environment and supplementation with the mentioned factors is time- and cost-intensive,

we hypothesized that immortalized primary-derived cell clones are no longer dependent on these factors to accomplish more efficient culture conditions. In addition, batch to batch variations and the composition of unknown substances together with the tumorigenic origin of Matrigel® are further disadvantages [175].

To this aim, a Matrigel®-free 2D-culture should be established for the generated murine and human cell clones. Preliminary studies performed by InSCREENeX resulted in cultures based on FN/Col I pre-coated plastic; however, a more simplified culture on uncoated surfaces was favored. While the coating with FN/Col I was used as control condition, PLO and Col I coating was tested additionally, whereas PLO coating was only used for cultures of murine cell clones. Cell growth analyses revealed that murine cell clones showed good growth characteristics on uncoated plastic; while the human cell clone demonstrated a dependency for Col I pre-coated surfaces for a likewise good growth. Collagen I as well as fibronectin are both important components in the small intestinal ECM, whereby collagen provides structural support and fibronectin supports cell adhesion processes, therefore these proteins are also widespread in cultures setup on epithelial cells for an improved cellular behavior [319–321]. With regard to cell adhesion, Liu et al. reported that hTERT or hTERTmut overexpressing cell lines revealed changes in cell adhesion-related genes [322], indicating that a different gene pool has versatile influences. Therefore, an altered expression of cell adhesion-related genes due to the different setting of immortalization genes in human cell clone cultures could result in the dependency on Col I pre-coated surfaces.

In addition to the Matrigel®-free culture conditions of the generated cell clones, a growth factor reduced medium formulation compared to the medium composition used for primary organoid cultures was tested. Based on the cell growth analyses of the murine cell clones, the growth factors Y-27632, hEGF and 10% FCS were identified as essential for the culture and expansion of the cells. However, preliminary studies performed by InSCREENeX revealed that mNoggin has to be supplemented additionally to the standard medium to sustain the cellular behavior in culture, whereupon all analyses with murine cell clones were carried out in a medium formulation supplemented with mNoggin. Interestingly, Lindeboom et al. demonstrated organoid cultures enriched for mature enterocytes when cultured in differentiation medium composed of hEGF and mNoggin [311], although mNoggin acts as inhibitor of the BMP pathway and thus suppresses stem cell differentiation [65,66]. Of note, cell growth analyses of the cell clone I9K10, used as reference control due to its non-epithelial morphology, demonstrated reduced growth rates if any of the growth factors was missing, indicating that this cell population showed a higher similarity to stem cells, as mNoggin and hR-Spondin are important for maintenance of stemness [60]. Nevertheless, the

dependency of supplementation with mNoggin to the medium formulation for all murine cell clone cultures should be tested again with regard to cell growth and gene expression analyses.

Next, cell growth analyses of the human cell clones revealed that the medium supplementation with all growth factors known from primary human organoid cultures was essential to maintain the cell growth capacity. In general, it is known that the intrinsic signaling pathways in murine and human tissues differs and therefore also in the established organoid cultures [313], which is indicative also for a different need of growth factor supplementation in the generated immortalized cell clones. Further, an inefficient or not completed immortalization process would result in necessity of the growth factors hR-Spondin 1 and mNoggin, as these factors are important for maintaining stemness in the native intestinal tissue [60]. In general, a immortalization process has to overcome two phases of cell senescence before the cells are stable immortalized, which can take up to 300 days depending on cell type and immortalization strategy [323].

Further, a medium formulation supplemented with Y-27632 used for all cell clones is not advantageous, as this factor suppresses apoptosis, which could be an indication that the cell clones may have not been fully immortalized and therefore stem cells are still present in these cultures.

FCS, a complex cocktail of proteins, hormones and growth factors is often used for long-term culture of cells *in vitro*. Cell adherence, proliferation, migration and differentation are cellular processes, which can be influenced by supplementation of FCS to the culture medium [324]. However, the use of FCS is controversial as unborn calves suffer from serum collection and batch-to-batch variations cannot be avoided, therefore reproducibility of the obtained results is sometimes difficult. Nevertheless, FCS supplementation was necessary in this project for cultures setup of murine and human cell clones, as investigations concerning the medium composition demonstrated a reduced cell growth capacity.

5.2.3. Some clones did not show good characteristics with respect to the establishment of a cell line representing the small intestine

A cell line, representing the small intestine *in vitro* should be easily expandable, result in reproducible experimental data, demonstrate a homogenous epithelial morphology and a representative population doubling level (PDL), while presenting a primary-like phenotype and being applicable for multiple purposes.

In the context of a homogenous epithelial morphology, the murine cell clones I9K4 and I9K17 (of in total nine clones) as well as the human cell clones 15-06 I4A and 15-06 I9A (of in total four clones) were excluded from the further characterization panel, as they did not fulfill this prerequisite. An inhomogeneous cell morphology could indicate an incomplete immortalization, as Li et al. demonstrated a likewise inhomogeneous morphology of immortalized nasopharyngeal epithelial cells during the first stage of senescence, which revealed in a homogenous morphology after 85 population doublings (PD) [315,323] or a completely inefficient immortalization. In addition, the cell clone I9K10 exhibited a non-epithelial but homogenous morphology, which defines this clone as reference control in further analyses.

In addition, the PDLs of the remaining murine clones showed no significant differences between the clones and the obtained values reached from a PDL 4.3 to a PDL 6.9, which is in line with the recently published PDLs of ~ 5 for other cell lines [233]. Further, the cumulative PDL over a period of up to 180 days was determined for the human cell clones, which revealed that the human clone 15-06 I9B reached cell senescence and finally cell death after 80 days in culture, indicating an instable transduction of the immortalization genes. To identify an instable transduction, the cell clone 15-06 I9B should be analyzed at different passages of cryopreserved samples of this clone for changes in the ectopic expression of genes used for immortalization or for an instable telomere length as well as low telomere activity. Therefore, the human cell clone 15-06 I4B was the only human cell clone, which remained in the ongoing analyses.

Next, the gene expression profile of the established murine cell clones represented only to some extent a primary cell-like phenotype, as demonstrated by the mRNA transcript level of cell type-specific marker genes such as *mVil1*, *mMuc2*, *mChga* and *mLyz*. In general, all analyzed murine cell clones revealed a dramatically reduction of the expression rates compared to murine primary organoid cultures, which is possibly a negative side effect due to the applied immortalization strategy, as these decreased expression rates were also observed for immortalized human alveolar epithelial cells, which were immortalized in the same way [209]. Further, it is also feasible that mainly TACs were immortalized, however this cell type, present above the stem cell niche in the native crypt, was not detected in the current study. In addition, *mChga* expression representing an enteroendocrine cell identity was not at all detectable in any murine cell clone, while a low mRNA transcript level for *mLyz* and *mMuc2* was observed for all murine cell clones.

However, in the context of cell lines representing the primary cell phenotype, the most prominent marker gene is *mVil1* that is specific for enterocytes, which represent with 80% the majority of cells in the intestinal epithelium [9]. First, the cell clone I9K10 elected as reference

control in these studies demonstrated a low expression of the enterocyte marker gene *mVil1* that resulted also in low TEER values, thereby representing a non-epithelial phenotype. Next to I9K10 cells, I9K11 cultures showed low TEER values, however a higher expression of *mVil1* was observed, whereas I12K2 cells demonstrated the complete opposite of this, with high TEER values and no expression of *mVil1*. The expression of villin-1 together with a tight epithelial barrier indicated by high TEER values, are major characteristics for the enterocyte cell phenotype. Of note, also other immortalized epithelial cells demonstrated such findings as shown by Nossol et al. for porcine immortalized cells (IPEC-1; IPEC-J2) [325]. For instance, the IPEC-1 cell line showed no expression of *Vil1*, however a high TEER value of 7.0 ± 1.2 kΩ*cm² was measured with a non-destructive handelectrode [325]. Further, in a previous study they demonstrated that the *Vil1* expression of the IPEC-1 cells changes due to other culture conditions with the highest mRNA transcript level for *Vil1* in Transwell®-based cultures [326]. The murine cell clones I9K6, I9K8, I12K9 and I9K21 revealed individual TEER values together with individual *mVil1* expression rates, depicting these cells as interesting newly generated cell lines. However, for the clone I9K21 TEER values with high variances in three independent experiments were observed, which excludes this cell clone also from further analyses, as achieving reproducible results is an essential prerequisite for cell lines.

Taken together, the cellular features depicted by barrier integrity measurements and RT-qPCR analyses led to the exclusion of I12K2, I9K10, I9K11 and I9K21 cells from further characterization, while I9K4 and I9K17 cells were excluded due to their non-epithelial morphology. In addition, a non-epithelial like morphological as observed for 15-06 I4A and 15-06 I9A cells or an infinite cell growth of 15-06 I9B cells led to the exclusion of these human cell clones. Finally, the three murine cell clones I9K6, I9K8 and I12K9 as well as the human cell clone 15-06 I4B showed good growth characteristics combined with an epithelial cell morphology and features thereby representing the primary cell phenotype to some extent at least for murine cell clones, depicting these clones as alternative cell source to commonly used Caco-2 cells.

5.2.4. Growth characteristics of immortalized epithelial cells

Immortalized cell lines are hallmarked to proliferate indefinitely without lingering in cellular senescence when cultured under adequate conditions. Cumulative PDL analyses over a culture time of up to 200 days, proliferation rate analyses and IF-stainings to identify KI-67 positive cells are common methods, depicting the proliferative potential of newly generated cell lines.

A study characterizing immortalized human esophageal squamous cells demonstrated that non-immortalized cells show a linear cell growth in the first 30-40 population PDs followed by a constant doubling rate due to cell senescence, while for immortalized cells an exponential cell growth was observed [316]. In line with this also the murine cell clones demonstrated an exponential cell growth in cumulative PDL analyses for up to 180 days, while similar analyses regarding the human cell clone revealed in a linear cell growth; however without reaching cell senescence during this culture time. These findings could be due to an incomplete immortalization or this could give a hint for a not yet completed selection process of the human cell clone, which is essential to establish an immortalized cell line as shown by Li and colleagues [323]. In contrast, primary organoids dissociated to single cells can be cultured on pre-coated surfaces; however, splitting and expansion of these cells is not feasible (data not shown), which favors an incomplete selection process towards only immortalized cells in the human cell clone cultures.

Considering the native intestinal epithelium, SCs and TACs represent the proliferative cell populations, whereas TACs demonstrate a higher cell division rate [327]. In line with this are the findings of Tian et al., as this group reported that EdU positive cells in the intestinal epithelium are mostly detected near the border of the stem cell compartment and in the TA zone [286]. Primary intestinal organoids, demonstrating a high similarity to the *in vivo* situation, revealed a proliferation rate of 25% for murine and 21% for human organoids in an EdU assay performed by flow cytometry, whereas the gut crypt demonstrates a proliferation rate of 10-16% in a comparable assay with ^{3}H-thymidine as labeling reagent [328]. In contrast, Caco-2 cells showed a proliferation capacity of 70% in BrdU analyses of Wayakanon et al., which is comparable to the EdU assay in the current studies [329], while other tissue culture cell lines demonstrate a proliferation capacity of ~ 40% [328]. The murine cell clones I9K6 and I12K9 demonstrated with about 32% and 35% EdU positive cells a higher proliferation capacity compared to primary organoids, while I9K8 and 15-06 I4B cells revealed proliferation rates similar to primary organoids. In summary, the proliferation capacity of the established cell clones is in line with results reported for primary organoid cultures and other cell lines, except of Caco-2 cells. In addition, the proliferation capacity was also measured by an EdU assay, when the murine cell clones and the human cell clone were cultured in a 3D Matrigel®-based environment to identify if the cell clones can form proliferative 3D cell aggregates depicting a typical organoid morphology, as differentiated organoids were used for the immortalization. However, no organoid morphology was observed but spheroid-like structures, which are proliferative, as within 24 h these spheroids were formed from single cells, but proliferation capacity is lower compared to 2D-cultured cells and revealed only 9-15% EdU positive cells for all clones. Therefore I hypothesize that

no functional stem cells are present in these cultures after immortalization and their proliferative behavior is based on the immortalized differentiated cell populations.

In general, the EdU assay detects the proliferation capacity of cells in the S-phase instead of the complete cell cycle; therefore differences in the cell cycle length of the S-phase were determined in this assay [330]. In contrast, IF-stainings with the antibody for the proliferation marker KI-67 demonstrate the complete cell cycle at a certain time point. As shown by Tian et al. also KI-67 positive cells, next to EdU positive cells, were mainly found above the stem cell compartment, thereby demonstrating the proliferation capacity of the TACs [286]. In the current study, KI-67 positive cells were observed for all analyzed cell clones when cultured in 2D or 3D; however, the staining patterns are indicative for a reduced proliferation rate in 3D-cultures compared to 2D-cultures, which would be in line with the results of the quantitative proliferation rate analyses by flow cytometry. Interestingly, I9K8 2D-cultures seem to exhibit a higher amount of KI-67 positive cells compared to the other murine cell clones, while the EdU assay detects the lowest proliferation capacity within the murine cell clone cultures, thereby indicating that this cell clone could have a longer S-phase of the cell cycle detected by the EdU assay and shorter cell cycle phases for G1, G2 and M which were identified due to antigen binding by the proliferation marker KI-67 [331].

Taken together, the reduced proliferation capacity of all cell clones when cultured in 3D indicates that no longer functional stem cells are present in these immortalized cultures, however the cell clones cultured in 2D showed good growth characteristics with a representative proliferation capacity.

5.2.5. Varying expression of intestinal cell type specific marker might display intermediate cell identities for the immortalized epithelial cells

An important characteristic feature that would identify the murine and human cell clones as very different from commonly used Caco-2 cells in terms of their applicability and predictivity is mimicking the cellular diversity of the native intestinal epithelium, which was hypothesized to be reached by the immortalization of primary organoids. Therefore the murine and human cell clones were analyzed for their specific gene as well as protein expression profile with regard to the main marker genes/proteins representing the most important cell types of organoid cultures such as enterocytes (Vil1, SGLT1), goblet cells (Muc1, Muc2), enteroendocrine cells (ChgA), paneth cells (Lyz) and stem cells (Lgr5).

As demonstrated in the current study, the established cell clones showed a slightly different gene expression profile when cultured in 2D, 3D or on Transwell®-inserts, thereby indicating a kind of differentiation potential due to tight cell-cell contacts or cell-matrix interactions,

although a cellular composition of mainly differentiated cells was used for immortalization. Similar observations were published for the cell line Caco-2 with a changing gene expression pattern during Caco-2 cell differentiation due to tighter cell-cell interactions, thereby demonstrating a more enterocyte-like phenotype [332,333].

In comparison with the gene expression profile of murine/human organoid cultures, the established cell clones showed dramatically reduced values for all analyzed genes, which could be due to the immortalization strategy as also reduced values were demonstrated for other generated cell lines [209] or due to the possibility that mostly TACs were immortalized. However, the *mVil1/hVIL1* expression was mostly dominant, as enterocytes are the main cell type found in the intestinal epithelium and therefore also in the organoid cultures, whereby the proportion of *mVil1/hVIL1* expressing cells should also be the highest in a representative cell line [9]. Interestingly, cell clone-based Transwell®-models demonstrated the highest *mVil1/hVIL1* expression rate compared to the other culture conditions. In line with this, also a slightly higher *mMuc2/hMUC2* transcript level was observed in the Transwell®-models, which could enable a good performance in drug transport studies, as enterocytes and mucin-producing cells are mostly involved in the predictivity of these studies. Cells expressing *mChga/hCHGA* seemed to be not present in these cell clone-based cultures and *mLyz/hLYZ* have to be rather low, which depicts all cell clones as cells representing the native intestinal epithelium only to some extent. In addition, remaining stem cell potential was identified by the gene expression profile of *mLgr5/hLGR5*, which revealed a low mRNA transcript level when cultured in 2D and on Transwell®-inserts, while a similar expression rate to murine organoids was observed for all murine cell clones cultured in 3D, which depicts the established cell clones as immortalized cells based on differentiated organoids. However, for human cell clones cultured in 3D the *hLGR5* expression rate was even lower compared to human organoid cultures.

In addition, cell type specific markers were also analyzed in IHC stainings, which revealed a low expression for all markers when cultured in 2D and the formation of a polarized cell layer when cultured on Transwell®-inserts with a apical protein expression pattern for VIL1, SGLT1, MUC1 and MUC2, thereby identifying enterocytes and mucin-producing cell types in all cell clone-based model setups. However, no positive signal for CHGA was observed in any of the culture conditions, while positive signals for LYZ were identified in 2D- and 3D-cultures of all cell clones.

In order to identify functional and proliferative stem cells in the respective cell clone cultures, they were cultured for several days in Matrigel® drops like primary organoids, followed by analyses of their growth behavior and gene as well as protein expression profile. It was demonstrated that all analyzed cell clones formed spheroid-like structures with an internal

lumen but no budding into organoid-like structures was observed. These findings could indicate that functional stem cells are no longer present, which would identify the generated cell clones as immortalized cells representing a cell population of mainly differentiated cell types of the absorptive or secretory lineage. However, also the absence of paneth cells could result in these spheroid-like structures, as Serra et al. demonstrated the necessity of paneth cells to enable the first symmetry break to yield in the formation of a organoid structure [236]. In the current study the *mLyz/hLYZ* mRNA transcript level, representing paneth cells, was rather low when cultured in 2D, 3D or on Transwell®-inserts. In comparison, Caco-2 cells cultured in Matrigel®-based cultures or in round bottom plates also aggregate to spheroid-like structures, however centrifugation steps are essential to form these cell-aggregates [334,335] followed by embedding in Matrigel® drops. In addition, the formation of these spheroidal structures with a centralized lumen surrounded by a polarized monolayer of cells was observed for the first time after a culture time of 5 days [334], instead of 24 h as it was demonstrated in the current study for cell clone-based 3D structures (data not shown). Further, the spheroid-like structures based on the established cell clones were set up as single cells directly in Matrigel® drops, as it is known for 3D primary cell cultures, which indicates a different proliferative behavior as well as cellular composition of these spheroid-like structures compared to Caco-2 aggregates [236].

Studies regarding the protein expression pattern of VIL1, SGLT1 specific for enterocytes and MUC1 specific for mucin-producing cells were indicative for the formation of non-polarized cell clone-based spheroids. Compared to sections of Histogel® embedded primary spheroid/organoid cultures stained for the same marker panel this results in a small layer of VIL1, SGLT1 and MUC1 localized in the internal lumen of these polarized spheroids/ organoids [30,174,336]. In contrast, also apical-out spheroids were established recently, which demonstrated a positive signal for these markers on the outside of the spheroid thus the signal direction has changed due to altered culture conditions [195]. As the spheroid structures formed in this study demonstrated within the same cultures, spheroids with an internal staining and also with a staining on the outside, all cell clone cultures revealed a non-polarized spheroid structure. Further, the SGLT1 staining pattern demonstrated a diffuse signal on both sides of the cell layer, which underlines the formation of non-polarized 3D-spheroids. However, cell clone-based Transwell®-models showed a polarized cell layer that identifies the established cell clones as feasible for drug transport studies.

5.2.6. Immortalized primary-derived epithelial cells showed organ-specific functions in drug transport studies

Drug transport and uptake studies based on Caco-2 Transwell®-models are standard, but the lack of a mucus layer covering the epithelial cell layer and a reduced expression pattern of specific transporter proteins in the apical brush border are indicative for an insufficient predictivity [111,112].

To identify the generated murine and human cell clones as alternative cell sources in terms of transport capacity, the formation of a tight as well as functional barrier of the established cell clone-based Transwell®-models is mandatory. Therefore, cell clone-based models were investigated for their barrier integrity by TEER measurement and FITC-dextran as well as for their performance in characteristic transport mechanisms of the intestinal epithelium. Another criterion for representative models is the presentation of microvilli on the cell surface of enterocytes and the formation of tight junction complexes between adjacent cells.

In first line, cell clone-based models set up on Transwell®-inserts with a seeding density of $5x10^4$ cells/insert were analyzed by histological and ultrastructural analyses. Within 21 days murine cell clones and 14 days for the human cell clone, the formation of a consistent cell layer was observed in H&E-stained tissue sections, when cultured under pro-proliferative conditions. In addition, different seeding densities were tested without demonstrating differences in the culture time until a consistent cell layer was formed or in the corresponding TEER values (data not shown). In comparison, Caco-2 cell-based models require likewise 3 weeks of culture to form a consistent cell layer [111,212], whereas primary-based models need only 14 days. Of note, primary-based models were set up and cultured according to a protocol published by Schweinlin et al., where culture conditions, using proliferation medium is followed by differentiation medium, to enable the formation of a cell monolayer with representative features comparable to the native intestinal epithelium [139].

Next to the H&E-stained tissue sections, immunohistological analyses regarding a corresponding tight junction protein expression pattern revealed the formation of a consistent cell layer with tight cell-cell interactions in stainings with antibodies for ZO-1 and ECAD for all analyzed cell clones. Interestingly, the protein expression pattern for CLDN5 was homogenous only for the murine cell clone I9K6, while I9K8 and I12K9 cultures demonstrated an inhomogeneous tight junction protein expression pattern and 15-06 I4B cells showed completely no protein expression for CLDN5. The transmembrane protein CLDN5 is mostly relevant in the context of creating the intercellular barrier together with occludin and thereby contributing to the paracellular transport route of molecules [337]. However, barrier integrity measurements did not demonstrate increased paracellular

permeability, whereupon the tight epithelial barrier in the respective clones must probably be maintained by occludin or other claudins. Down regulation of especially CLDN5 was described in the context of colon cancer and epithelial dysfunction [338], whereas dysfunction also results in an reduced barrier resistance, which could indicate that the human cell clone shows tumorigenic characteristics due to an inefficient immortalization [276,339]. In addition, tight junction complexes were also identified in the corresponding ultrastructural TEM analyses of all cell clones.

Ultrastructural analyses further revealed less densely-packed microvilli-containing cells in models based on murine cell clones compared to human cell clone-based models together with short microvilli, indicating not functionally differentiated enterocytes in the established models. In contrast, differentiated Caco-2 cell-based models showed at day 16 a microvilli height about 1.19 ± 0.16 µm [253], which was more similar to the microvilli height of 1-3 µm of enterocytes in the native small intestinal epithelium [254]. Interestingly, Mustata et al. showed in ultrastructural analyses of primary spheroid structures, microvilli-containing cells, even if these are only a few and short microvilli [340]. Compared to the ultrastructural analyses of the cell clone-based models regarding the microvilli-containing cells, similarities were observed, which is further indicative that mostly TACs were immortalized, if not the immortalization process causes this negative effect on the ultrastructural characteristics, as spheroids are mainly composed of SCs and TACs [340].

Next, immunohistological stainings for the marker MUC2, MUC1, VIL1 and SGLT1 demonstrated the formation of a polarized cell layer for the established cell clone-based models, as the protein expression pattern was orientated to the apical cell surface and therefore indicating a proper functional and biological performance of the models. Further, these markers are representative for enterocytes and goblet cells, specific cell types of the native intestinal tissue, thereby contributing to the barrier formation of intestinal *in vitro* models. Histological analyses of primary-based *in vitro* models established by Schweinlin et al. showed a similar protein expression pattern with respect to MUC2, MUC1 and VIL1 as in the current study [139].

The formation of an intact cell layer was investigated by TEER and FITC-dextran measurements. In the current study, Caco-2 Transwell®-models demonstrated TEER values of about 194 Ω*cm², while other studies have shown values between 1100-1350 Ω*cm², in which the used Transwell®-inserts, the passage of cells and the temperature strongly influences the obtained results [341]. In addition, also for primary-cell based models a huge variance in TEER values were published in recent years with 40 Ω*cm² [139], 400 Ω*cm² [342] and > 1500 Ω*cm² [190], which can be attributed to the use of different cell sources and cell culture protocols. In comparison, the primary-derived cell clone based models

established in this study showed with values of 232 Ω*cm² for I9K6, 483 Ω*cm² for I9K8, 727 Ω*cm² for I12K9 and 253 Ω*cm² for 15-06 I4B cells a similarly pronounced barrier integrity. Nevertheless, the small intestine *in vivo* revealed in measurements with the Ussing chamber TEER values of 50-100 Ω*cm² [341], which is lower compared to the results achieved here for primary-derived cell clone-based *in vitro* models. The permeability of FITC-dextran revealed likewise a tight epithelial barrier for all established cell clone-based Transwell®-models, as the amount of transported FITC-dextran is lower than 2% [223].

In the context of characteristic transport mechanism, the paracellular, the transcellular and the efflux route [15,223] were investigated for all generated cell clones set up on the PET membrane. The paracellular transport of fluorescein confirmed the formation of a tight epithelial barrier for all models; however I9K8 and 15-06 I4B cells showed an even lower permeability rate for fluorescein. These findings were in line with the results obtained by TEER and FITC-dextran permeability rate measurements.

The transcellular pathway is of special interest for drug delivery studies, as some drugs use this transport route to reach its target side, but an appropriate expression of these transporter proteins is crucial for an high efficacy of the drug [79]. For murine cell clone-based models a similar permeability rate for propranolol, a reference substance for the transcellular transport mechanism, was observed, while models based on the human cell clone showed a lower permeability for propranolol, which is comparable to the permeability in Caco-2 cell-based models [212].

In addition, the efflux transport pathway, mediated by the transporter *p*-gp is of high interest in the context of *in vitro* models used in pre-clinical research applications, as drugs can be transported back into the lumen by this special transporter [258] and therefore *in vitro* models should represent this transport mechanism to a high degree for an efficient efficacy testing of the applied drugs [87,224]. In the current study the efflux transport mechanism was investigated by the reference substance rhodamine 123, which revealed a slightly improved efflux transport in models set up of the human cell clone compared to the murine cell clone-based models, indicating a higher expression of *p*-gp or other efflux transporter proteins in the apical cell surface of human cell clone cultures and therefore a better model performance with respect to *in vivo*-like conditions. In comparison to Caco-2 *in vitro* models, all cell clone-based models demonstrated a similar ratio of basolateral/apical transport for rhodamine 123 [212].

Taken together, the primary-derived cell clone-based models demonstrated advantages in the context of an easier and more flexible model setup compared to primary cell-based models, as a pro-proliferative medium composition together with an adequate culture time to

form a consistent and functional cell monolayer on PET-based Transwell®-inserts was established in this study. In future studies, the BNC matrix used for the first part of this thesis, could enable an even better predictivity in transport capacity studies when murine and human cell clone-based models would be set up on both BNC variants or adapted versions of these scaffolds.

5.3. Conclusion

Central aspect of this thesis was to combine different strategies for the establishment of an alternative *in vitro* model and thereby demonstrating the importance of the used scaffold as well as cell source to enable a better model performance regarding predictivity and reproducibility in drug delivery studies. In terms of the scaffold material, the BNC matrix was presented as interesting alternative with comparable properties to natural ECMs, but with benefits regarding standardizability, being conform to the 3Rs principle and an easy as well as cost-efficient manufacturing process. The good performance of the BNC-based Caco-2 models is summarized in Figure 5.1 in comparison to the PET- and SIS-based *in vitro* models used as controls in the current study.

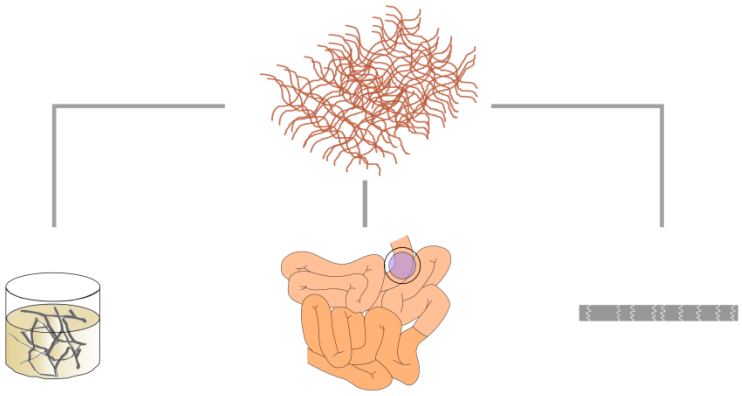

	unmod BNC	struc BNC	SIS	PET
Manufacturing process	fermentation of *Komagataeibacter xylinus*		decellularization of porcine small intestinal submucosa	polymerization of ethylene glycol and terephthalic acid
Costs per insert	0.05 €		12.50 €	3.19 €
standardization	+	+	-	0
3D topography	yes		SIS and SISmuc (mucosa)	no
Protein expression pattern	+	0	+	0
Connective tissue	0	0	-	0
Ultrastructural features	+	-	-	0
Barrier integrity	+	+	0	0
Transport activity of reference drugs				
Fluorescein	0	0	-	0
Propranolol	+	+	+	0
Rhodamine123	+	+	-	0
Unwanted molecular adhesion	0	0	+	0

Figure 5.1: Comparison of matrix-based Caco-2 models. Two versions of BNC, unmodified and surface-structured, and the commonly used scaffolds SIS and PET were investigated in this study for their functional

performance in a 3D-like Transwell®-system with Caco-2 cells. The results obtained for PET-based models were set as standard in this scoring system. No improvement = 0, inferior to standard = -, superior to standard = +. BNC: bacterial nanocellulose; SIS: small intestinal submucosa; PET: polyethylene terephthalate.

In addition to the used scaffold, the cellular unit is mainly involved in the predictivity of drug delivery studies within the used *in vitro* models. Immortalization of primary organoid cultures was hypothesized to sustain the cellular diversity of these cells, while establishing a cell culture population, which is easy in handling at low costs to fulfill the requirements for pre-clinical research purposes. The performance of the established immortalized primary-derived cell clones of murine and human origin in the applied assays, which characterizes the cellular behavior in 2D-, 3D- and Transwell®-based cultures, is summarized in Table 5.2.

Taken together, the murine and human cell clone cultures demonstrated a more progenitor-specific phenotype, as a reduced mRNA transcript level was observed for all analyzed marker genes, which are specific for the differentiated cell types found in the native epithelium. Furthermore, a slightly different gene expression profile was identified for the respective cell clones when cultured in 2D, 3D or on Transwell®-inserts, indicating that the different culture conditions induce differentiation inside the immortalized cell population. Nevertheless, these newly generated cell lines provide an alternative cell source to the commonly used Caco-2 cell line for drug delivery studies, as these cells show a polarized cell layer with a tight and functional barrier covered by a mucus protein sheet to reflect also the physical barrier present in the native intestinal epithelium. Further, these cells can be easily expanded under more cost-efficient conditions compared to primary organoid cultures and set up as Transwell®-models, thereby being eligible for transport capacity studies due to the expression of important transporters on the cell surface.

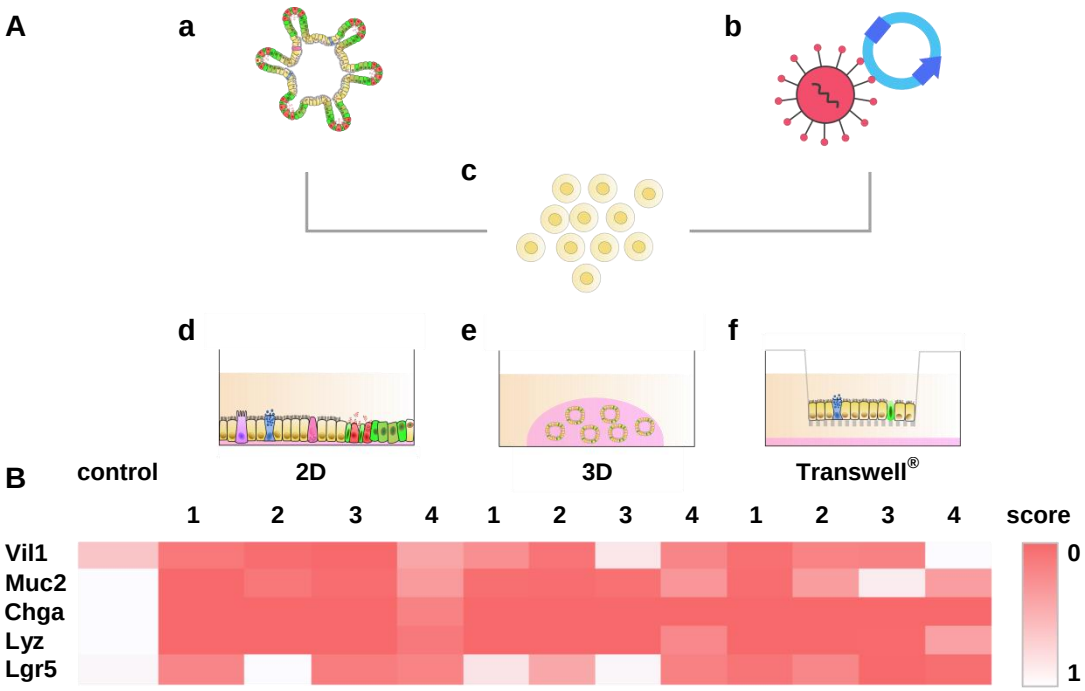

	murine cell clones			human cell clone
Identification	**I9K6**	**I9K8**	**I12K9**	**15-06 I4B**
Proliferation in 2D	+	0	+	0
Cumulative PDL	+	+	+	0
Protein expression pattern in 2D	0	+	+	-
Spheroid-like 3D structure	0	+	0	+
Protein expression pattern in 3D	0	+	0	-
Tight junction protein expression pattern	+	0	0	-
Ultrastructural features	-	0	-	+
Protein expression pattern Transwell®	+	+	+	+
Barrier integrity	0	+	-	+
Transport activity of reference drugs				
Fluorescein	-	+	0	+
Propranolol	+	+	+	0
Rhodamine123	0	-	0	+

Figure 5.2: Comparison between the generated murine and human immortalized primary-derived cell clones. Schematic setup of immortalized primary-derived cell clones **(A)**. Primary organoids **(a)** used for the lentivirus-based immortalization strategy **(b)** resulted in several cell populations **(c)**. Established cell clones were characterized in 2D- **(d)**, 3D- **(e)** and Transwell®-based **(f)** cultures. Respective characterization panel of the

murine (I9K6, I9K8 and I12K9) clones as well as the human cell clone (15-06 I4B) **(B)**. 1 = I9K6, 2 = I9K8, 3 = I12K9 and 4 = 15-06 I4B. Adequate cellular behavior = 0, inferior cellular behavior = -, superior cellular behavior = +. Vil1 = Villin-1; Muc2 = Mucin-2; Chga = Chromogranin A; Lyz = Lysozyme; Lgr5 = Leucine-rich repeat-containing G protein-coupled receptor 5.

References

[1] J.S. Schwegler, Der Mensch - Anatomie und Physiologie im Bild: Abbildungen für Unterricht und Vorlesung ; aktuell zur 4. Auflage ; Grafik-CD ; Lehrprogramm gemäss §14 JuSchG, 2nd ed., Thieme, Stuttgart, 2007.

[2] M. Jalali (Ed.), Basic science methods for clinical researchers, 2017.

[3] H.F. Helander, L. Fändriks, Surface area of the digestive tract – revisited, Scandinavian Journal of Gastroenterology 49 (2014) 681–689.https://doi.org/10.3109/00365521.2014.898326.

[4] C. Casteleyn, A. Rekecki, A. van der Aa, P. Simoens, W. van den Broeck, Surface area assessment of the murine intestinal tract as a prerequisite for oral dose translation from mouse to man, Laboratory animals 44 (2010) 176–183. https://doi.org/10.1258/la.2009.009112.

[5] J. Beumer, H. Clevers, Regulation and plasticity of intestinal stem cells during homeostasis and regeneration, Development (Cambridge, England) 143 (2016) 3639–3649. https://doi.org/10.1242/dev.133132.

[6] J.T. Collins, A. Nguyen, M. Badireddy, StatPearls: Anatomy, Abdomen and Pelvis, Small Intestine, Treasure Island (FL), 2020.

[7] T. Däullary, C. Fey, C. Berger, M. Metzger, D. Zdzieblo, 11 - Bioartificial gut—current state of small intestinal tissue engineering, in: N.E. Vrana, H. Knopf-Marques, J. Barthes (Eds.), Biomaterials for Organ and Tissue Regeneration Woodhead Publishing Series in Biomaterials, Woodhead Publishing, 2020, pp. 273–297.

[8] A. Benninghoff, D. Drenckhahn, Anatomie: Makroskopische Anatomie, Histologie, Embriologie, Zellbiologie, 17th ed., Urban und Fischer, München, Jena, 2008.

[9] H. Gehart, H. Clevers, Tales from the crypt: new insights into intestinal stem cells, Nature reviews. Gastroenterology & hepatology 16 (2019) 19–34. https://doi.org/10.1038/s41575-018-0081-y.

[10] P.A. Blaker, P. Irving, Physiology and function of the small intestine, 2014.

[11] M. Schünke, E. Schulte, U. Schumacher, Prometheus LernAtlas der Anatomie: Innere Organe, 5th ed., 2018.

[12] S. Kong, Y.H. Zhang, W. Zhang, Regulation of Intestinal Epithelial Cells Properties and Functions by Amino Acids, BioMed research international 2018 (2018) 2819154. https://doi.org/10.1155/2018/2819154.

[13] R. Okumura, K. Takeda, Roles of intestinal epithelial cells in the maintenance of gut homeostasis, Experimental & Molecular Medicine 49 (2017) e338. https://doi.org/10.1038/emm.2017.20.

[14] B.E. Goodman, Insights into digestion and absorption of major nutrients in humans, Advances in physiology education 34 (2010) 44–53. https://doi.org/10.1152/advan.00094.2009.

[15] C. Chelakkot, J. Ghim, S.H. Ryu, Mechanisms regulating intestinal barrier integrity and its pathological implications, Experimental & Molecular Medicine 50 (2018) 103. https://doi.org/10.1038/s12276-018-0126-x.

[16] B. Lee, K.M. Moon, C.Y. Kim, Tight Junction in the Intestinal Epithelium: Its Association with Diseases and Regulation by Phytochemicals, J Immunol Res 2018 (2018) 2645465. https://doi.org/10.1155/2018/2645465.

[17] S.R. Hwang, Y. Byun, Advances in oral macromolecular drug delivery, Expert opinion on drug delivery 11 (2014) 1955–1967. https://doi.org/10.1517/17425247.2014.945420.

[18] S. Citi, The mechanobiology of tight junctions, Biophysical reviews 11 (2019) 783–793. https://doi.org/10.1007/s12551-019-00582-7.

[19] S. Varadarajan, R.E. Stephenson, A.L. Miller, Multiscale dynamics of tight junction remodeling, Journal of cell science 132 (2019). https://doi.org/10.1242/jcs.229286.

[20] S. Lechuga, A.I. Ivanov, Actin cytoskeleton dynamics during mucosal inflammation: a view from broken epithelial barriers, Current Opinion in Physiology 19 (2021) 10–16. https://doi.org/10.1016/j.cophys.2020.06.012.

[21] A.M. Hammer, N.L. Morris, Z.M. Earley, M.A. Choudhry, The First Line of Defense: The Effects of Alcohol on Post-Burn Intestinal Barrier, Immune Cells, and Microbiome, Alcohol Research Current Reviews 37 (2015) 209–222.
[22] N. Barker, van Es, Johan H., J. Kuipers, P. Kujala, van den Born, Maaike, M. Cozijnsen, A. Haegebarth, J. Korving, H. Begthel, P.J. Peters, H. Clevers, Identification of stem cells in small intestine and colon by marker gene Lgr5, Nature 449 (2007) 1003–1007. https://doi.org/10.1038/nature06196.
[23] A.S. Darwich, U. Aslam, D.M. Ashcroft, A. Rostami-Hodjegan, Meta-analysis of the turnover of intestinal epithelia in preclinical animal species and humans, Drug metabolism and disposition: the biological fate of chemicals 42 (2014) 2016–2022. https://doi.org/10.1124/dmd.114.058404.
[24] H. Tian, B. Biehs, S. Warming, K.G. Leong, L. Rangell, O.D. Klein, F.J. de Sauvage, A reserve stem cell population in small intestine renders Lgr5-positive cells dispensable, Nature 478 (2011) 255–259. https://doi.org/10.1038/nature10408.
[25] T. Chatterjee, R.S. Sarkar, P.S. Dhot, S. Kumar, V.K. Kumar, Adult Stem Cell Plasticity: Dream or Reality?, Med J Armed Forces India 66 (2010) 56–60. https://doi.org/10.1016/S0377-1237(10)80095-4.
[26] S. Umar, Intestinal stem cells, Curr Gastroenterol Rep 12 (2010) 340–348. https://doi.org/10.1007/s11894-010-0130-3.
[27] H. Cheng, C.P. Leblond, Origin, differentiation and renewal of the four main epithelial cell types in the mouse small intestine. V. Unitarian Theory of the origin of the four epithelial cell types, The American journal of anatomy 141 (1974) 537–561. https://doi.org/10.1002/aja.1001410407.
[28] L.W. Peterson, D. Artis, Intestinal epithelial cells: regulators of barrier function and immune homeostasis, Nature reviews. Immunology 14 (2014) 141–153. https://doi.org/10.1038/nri3608.
[29] H. Clevers, The intestinal crypt, a prototype stem cell compartment, Cell 154 (2013) 274–284. https://doi.org/10.1016/j.cell.2013.07.004.
[30] T. Sato, D.E. Stange, M. Ferrante, Vries, Robert G J, van Es, Johan H, Van den Brink, Stieneke, Van Houdt, Winan J, A. Pronk, J. van Gorp, P.D. Siersema, H. Clevers, Long-term expansion of epithelial organoids from human colon, adenoma, adenocarcinoma, and Barrett's epithelium, Gastroenterology 141 (2011) 1762–1772. https://doi.org/10.1053/j.gastro.2011.07.050.
[31] C. Kosinski, V.S.W. Li, A.S.Y. Chan, J. Zhang, C. Ho, W.Y. Tsui, T.L. Chan, R.C. Mifflin, D.W. Powell, S.T. Yuen, S.Y. Leung, X. Chen, Gene expression patterns of human colon tops and basal crypts and BMP antagonists as intestinal stem cell niche factors, Proceedings of the National Academy of Sciences of the United States of America 104 (2007) 15418–15423. https://doi.org/10.1073/pnas.0707210104.
[32] D.W. Powell, I.V. Pinchuk, J.I. Saada, X. Chen, R.C. Mifflin, Mesenchymal cells of the intestinal lamina propria, Annual review of physiology 73 (2011) 213–237. https://doi.org/10.1146/annurev.physiol.70.113006.100646.
[33] C.S. Potten, M. Loeffler, Stem cells: attributes, cycles, spirals, pitfalls and uncertainties. Lessons for and from the crypt, Development (Cambridge, England) 110 (1990) 1001–1020.
[34] B.S. Sailaja, X.C. He, L. Li, The regulatory niche of intestinal stem cells, J Physiol 594 (2016) 4827–4836. https://doi.org/10.1113/JP271931.
[35] S. Goulas, R. Conder, J.A. Knoblich, The Par complex and integrins direct asymmetric cell division in adult intestinal stem cells, Cell stem cell 11 (2012) 529–540. https://doi.org/10.1016/j.stem.2012.06.017.
[36] van der Flier, Laurens G, H. Clevers, Stem cells, self-renewal, and differentiation in the intestinal epithelium, Annual review of physiology 71 (2009) 241–260. https://doi.org/10.1146/annurev.physiol.010908.163145.
[37] F. Kuhnert, C.R. Davis, H.-T. Wang, P. Chu, M. Lee, J. Yuan, R. Nusse, C.J. Kuo, Essential requirement for Wnt signaling in proliferation of adult small intestine and colon revealed by adenoviral expression of Dickkopf-1, Proceedings of the National

Academy of Sciences of the United States of America 101 (2004) 266–271. https://doi.org/10.1073/pnas.2536800100.
[38] A.J. Ouellette, Chapter 44 - Paneth Cells, in: L.R. Johnson, F.K. Ghishan, J.D. Kaunitz, J.L. Merchant, H.M. Said, J.D. Wood (Eds.), Physiology of the Gastrointestinal Tract (Fifth Edition), Academic Press, Boston, 2012, pp. 1211–1228.
[39] S. Bel, M. Pendse, Y. Wang, Y. Li, K.A. Ruhn, B. Hassell, T. Leal, S.E. Winter, R.J. Xavier, L.V. Hooper, Paneth cells secrete lysozyme via secretory autophagy during bacterial infection of the intestine, Science (New York, N.Y.) 357 (2017) 1047–1052. https://doi.org/10.1126/science.aal4677.
[40] M.K. Holly, J.G. Smith, Paneth Cells during Viral Infection and Pathogenesis, Viruses 10 (2018). https://doi.org/10.3390/v10050225.
[41] N. Barker, A. van Oudenaarden, H. Clevers, Identifying the stem cell of the intestinal crypt: strategies and pitfalls, Cell stem cell 11 (2012) 452–460. https://doi.org/10.1016/j.stem.2012.09.009.
[42] E. Sangiorgi, M.R. Capecchi, Bmi1 is expressed in vivo in intestinal stem cells, Nature Genetics 40 (2008) 915–920. https://doi.org/10.1038/ng.165.
[43] S.J.A. Buczacki, H.I. Zecchini, A.M. Nicholson, R. Russell, L. Vermeulen, R. Kemp, D.J. Winton, Intestinal label-retaining cells are secretory precursors expressing Lgr5, Nature 495 (2013) 65–69. https://doi.org/10.1038/nature11965.
[44] P.R. Kiela, F.K. Ghishan, Physiology of Intestinal Absorption and Secretion, Best practice & research. Clinical gastroenterology 30 (2016) 145–159. https://doi.org /10.1016/j.bpg.2016.02.007.
[45] J.J. Worthington, F. Reimann, F.M. Gribble, Enteroendocrine cells-sensory sentinels of the intestinal environment and orchestrators of mucosal immunity, Mucosal immunology 11 (2018) 3–20. https://doi.org/10.1038/mi.2017.73.
[46] K.L. Egerod, M.S. Engelstoft, K.V. Grunddal, M.K. Nøhr, A. Secher, I. Sakata, J. Pedersen, J.A. Windeløv, E.-M. Füchtbauer, J. Olsen, F. Sundler, J.P. Christensen, N. Wierup, J.V. Olsen, J.J. Holst, J.M. Zigman, S.S. Poulsen, T.W. Schwartz, A major lineage of enteroendocrine cells coexpress CCK, secretin, GIP, GLP-1, PYY, and neurotensin but not somatostatin, Endocrinology 153 (2012) 5782–5795. https://doi.org /10.1210/en.2012-1595.
[47] M.S. Engelstoft, K.L. Egerod, M.L. Lund, T.W. Schwartz, Enteroendocrine cell types revisited, Current opinion in pharmacology 13 (2013) 912–921. https://doi.org/ 10.1016/j.coph.2013.09.018.
[48] Y.S. Kim, S.B. Ho, Intestinal goblet cells and mucins in health and disease: recent insights and progress, Curr Gastroenterol Rep 12 (2010) 319–330. https://doi.org/ 10.1007/s11894-010-0131-2.
[49] M.A. McGuckin, S.K. Lindén, P. Sutton, T.H. Florin, Mucin dynamics and enteric pathogens, Nature reviews. Microbiology 9 (2011) 265–278. https://doi.org/10.1038/ nrmicro2538.
[50] G.M.H. Birchenough, M.E.V. Johansson, J.K. Gustafsson, J.H. Bergström, G.C. Hansson, New developments in goblet cell mucus secretion and function, Mucosal immunology 8 (2015) 712–719. https://doi.org/10.1038/mi.2015.32.
[51] Y. Wang, R. Kim, S.S. Hinman, B. Zwarycz, S.T. Magness, N.L. Allbritton, Bioengineered Systems and Designer Matrices That Recapitulate the Intestinal Stem Cell Niche, Cellular and molecular gastroenterology and hepatology 5 (2018) 440-453.e1. https://doi.org/10.1016/j.jcmgh.2018.01.008.
[52] Y. Komiya, R. Habas, Wnt signal transduction pathways, Organogenesis 4 (2008) 68–75. https://doi.org/10.4161/org.4.2.5851.
[53] H. Clevers, R. Nusse, Wnt/β-catenin signaling and disease, Cell 149 (2012) 1192–1205. https://doi.org/10.1016/j.cell.2012.05.012.
[54] K.S. Carmon, X. Gong, Q. Lin, A. Thomas, Q. Liu, R-spondins function as ligands of the orphan receptors LGR4 and LGR5 to regulate Wnt/beta-catenin signaling, Proceedings of the National Academy of Sciences of the United States of America 108 (2011) 11452–11457. https://doi.org/10.1073/pnas.1106083108.

[55] W. de Lau, N. Barker, T.Y. Low, B.-K. Koo, V.S.W. Li, H. Teunissen, P. Kujala, A. Haegebarth, P.J. Peters, van de Wetering, Marc, D.E. Stange, J.E. van Es, D. Guardavaccaro, R.B.M. Schasfoort, Y. Mohri, K. Nishimori, S. Mohammed, A.J.R. Heck, H. Clevers, Lgr5 homologues associate with Wnt receptors and mediate R-spondin signalling, Nature 476 (2011) 293–297. https://doi.org/10.1038/nature10337.

[56] K. Nagano, R-spondin signaling as a pivotal regulator of tissue development and homeostasis, The Japanese dental science review 55 (2019) 80–87. https://doi.org/10.1016/j.jdsr.2019.03.001.

[57] D. Henrique, F. Schweisguth, Mechanisms of Notch signaling: a simple logic deployed in time and space, Development (Cambridge, England) 146 (2019). https://doi.org/10.1242/dev.172148.

[58] L. Pellegrinet, V. Rodilla, Z. Liu, S. Chen, U. Koch, L. Espinosa, K.H. Kaestner, R. Kopan, J. Lewis, F. Radtke, Dll1- and dll4-mediated notch signaling are required for homeostasis of intestinal stem cells, Gastroenterology 140 (2011) 1230-1240.e1-7. https://doi.org/10.1053/j.gastro.2011.01.005.

[59] M. Kitagawa, Notch signalling in the nucleus: roles of Mastermind-like (MAML) transcriptional coactivators, Journal of biochemistry 159 (2016) 287–294. https://doi.org/10.1093/jb/mvv123.

[60] F.E. Holmberg, J.B. Seidelin, X. Yin, B.E. Mead, Z. Tong, Y. Li, J.M. Karp, O.H. Nielsen, Culturing human intestinal stem cells for regenerative applications in the treatment of inflammatory bowel disease, EMBO molecular medicine 9 (2017) 558–570. https://doi.org/10.15252/emmm.201607260.

[61] A. Suzuki, S. Sekiya, E. Gunshima, S. Fujii, H. Taniguchi, EGF signaling activates proliferation and blocks apoptosis of mouse and human intestinal stem/progenitor cells in long-term monolayer cell culture, Laboratory investigation; a journal of technical methods and pathology 90 (2010) 1425–1436. https://doi.org/10.1038/labinvest.2010.150.

[62] M.R. Frey, R.S. Dise, K.L. Edelblum, D.B. Polk, p38 kinase regulates epidermal growth factor receptor downregulation and cellular migration, The EMBO journal 25 (2006) 5683–5692. https://doi.org/10.1038/sj.emboj.7601457.

[63] M. Scaltriti, J. Baselga, The epidermal growth factor receptor pathway: a model for targeted therapy, Clinical cancer research an official journal of the American Association for Cancer Research 12 (2006) 5268–5272. https://doi.org/10.1158/1078-0432.CCR-05-1554.

[64] R.N. Wang, J. Green, Z. Wang, Y. Deng, M. Qiao, M. Peabody, Q. Zhang, J. Ye, Z. Yan, S. Denduluri, O. Idowu, M. Li, C. Shen, A. Hu, R.C. Haydon, R. Kang, J. Mok, M.J. Lee, H.L. Luu, L.L. Shi, Bone Morphogenetic Protein (BMP) signaling in development and human diseases, Genes & diseases 1 (2014) 87–105. https://doi.org/10.1016/j.gendis.2014.07.005.

[65] L.E. Batts, D.B. Polk, R.N. Dubois, H. Kulessa, Bmp signaling is required for intestinal growth and morphogenesis, Developmental dynamics an official publication of the American Association of Anatomists 235 (2006) 1563–1570. https://doi.org/10.1002/dvdy.20741.

[66] B.A. Auclair, Y.D. Benoit, N. Rivard, Y. Mishina, N. Perreault, Bone morphogenetic protein signaling is essential for terminal differentiation of the intestinal secretory cell lineage, Gastroenterology 133 (2007) 887–896. https://doi.org/10.1053/j.gastro.2007.06.066.

[67] F. Maloum, J.M. Allaire, J. Gagné-Sansfaçon, E. Roy, K. Belleville, P. Sarret, J. Morisset, J.C. Carrier, Y. Mishina, K.H. Kaestner, N. Perreault, Epithelial BMP signaling is required for proper specification of epithelial cell lineages and gastric endocrine cells, American Journal of Physiology - Gastrointestinal and Liver Physiology 300 (2011) G1065-79. https://doi.org/10.1152/ajpgi.00176.2010.

[68] J.R. Turner, Intestinal mucosal barrier function in health and disease, Nature reviews. Immunology 9 (2009) 799–809. https://doi.org/10.1038/nri2653.

[69] T. Pelaseyed, J.H. Bergström, J.K. Gustafsson, A. Ermund, Birchenough, George M H, A. Schütte, van der Post, Sjoerd, F. Svensson, A.M. Rodríguez-Piñeiro, Nyström, Elisabeth E L, C. Wising, Johansson, Malin E V, G.C. Hansson, The mucus and mucins of the goblet cells and enterocytes provide the first defense line of the gastrointestinal tract and interact with the immune system, Immunological reviews 260 (2014) 8–20. https://doi.org/10.1111/imr.12182.

[70] M. Vancamelbeke, S. Vermeire, The intestinal barrier: a fundamental role in health and disease, Expert Rev Gastroenterol Hepatol 11 (2017) 821–834. https://doi.org/10.1080/17474124.2017.1343143.

[71] Van der Sluis, Maria, De Koning, Barbara A E, De Bruijn, Adrianus C J M, A. Velcich, Meijerink, Jules P P, Van Goudoever, Johannes B, H.A. Büller, J. Dekker, I. van Seuningen, I.B. Renes, Einerhand, Alexandra W C, Muc2-deficient mice spontaneously develop colitis, indicating that MUC2 is critical for colonic protection, Gastroenterology 131 (2006) 117–129. https://doi.org/10.1053/j.gastro.2006.04.020.

[72] Johansson, Malin E. V., Larsson, Jessica M. Holmén, G.C. Hansson, The two mucus layers of colon are organized by the MUC2 mucin, whereas the outer layer is a legislator of host–microbial interactions, Proc Natl Acad Sci USA 108 (2011) 4659. https://doi.org/10.1073/pnas.1006451107.

[73] C. Atuma, V. Strugala, A. Allen, L. Holm, The adherent gastrointestinal mucus gel layer: thickness and physical state in vivo, American Journal of Physiology - Gastrointestinal and Liver Physiology 280 (2001) G922-9. https://doi.org/10.1152/ajpgi.2001.280.5.G922.

[74] A. Macierzanka, A.R. Mackie, L. Krupa, Permeability of the small intestinal mucus for physiologically relevant studies: Impact of mucus location and ex vivo treatment, Sci Rep 9 (2019) 17516. https://doi.org/10.1038/s41598-019-53933-5.

[75] A.N. Round, N.M. Rigby, A. La Garcia de Torre, A. Macierzanka, E.N.C. Mills, A.R. Mackie, Lamellar structures of MUC2-rich mucin: a potential role in governing the barrier and lubricating functions of intestinal mucus, Biomacromolecules 13 (2012) 3253–3261. https://doi.org/10.1021/bm301024x.

[76] A.P. Corfield, N. Myerscough, R. Longman, P. Sylvester, S. Arul, M. Pignatelli, Mucins and mucosal protection in the gastrointestinal tract: new prospects for mucins in the pathology of gastrointestinal disease, Gut 47 (2000) 589–594. https://doi.org/10.1136/gut.47.4.589.

[77] S.'a.Y. Salim, J.D. Söderholm, Importance of disrupted intestinal barrier in inflammatory bowel diseases, Inflammatory bowel diseases 17 (2011) 362–381. https://doi.org/10.1002/ibd.21403.

[78] K.R. Groschwitz, S.P. Hogan, Intestinal barrier function: molecular regulation and disease pathogenesis, The Journal of allergy and clinical immunology 124 (2009) 3-20; quiz 21-2. https://doi.org/10.1016/j.jaci.2009.05.038.

[79] K.L. Edelblum, J.R. Turner, Chapter 12 - Epithelial Cells: Structure, Transport, and Barrier Function, in: J. Mestecky, W. Strober, M.W. Russell, B.L. Kelsall, H. Cheroutre, B.N. Lambrecht (Eds.), Mucosal Immunology (Fourth Edition), Academic Press, Boston, 2015, pp. 187–210.

[80] R.P. Ferraris, Nutrient Transport, Regulation of, in: L.R. Johnson (Ed.), Encyclopedia of gastroenterology, Elsevier, 2004, pp. 754–759.

[81] R.P. Ferraris, J.-Y. Choe, C.R. Patel, Intestinal Absorption of Fructose, Annual review of nutrition 38 (2018) 41–67. https://doi.org/10.1146/annurev-nutr-082117-051707.

[82] E.M. Wright, D.D.F. Loo, B.A. Hirayama, Biology of human sodium glucose transporters, Physiological reviews 91 (2011) 733–794. https://doi.org/10.1152/physrev.00055.2009.

[83] S. Saksena, M.S. Ammar, S. Tyagi, A. Elsharydah, R.K. Gill, K. Ramaswamy, P.K. Dudeja, Mechanisms of calcium transport in human colonic basolateral membrane vesicles, Digestive diseases and sciences 47 (2002) 2306–2315. https://doi.org/10.1023/a:1020151730940.

[84] Q.-S. Liao, Q. Du, J. Lou, J.-Y. Xu, R. Xie, Roles of Na(+)/Ca(2+) exchanger 1 in digestive system physiology and pathophysiology, World J Gastroenterol 25 (2019) 287–299. https://doi.org/10.3748/wjg.v25.i3.287.
[85] P.V. Balimane, S. Chong, Cell culture-based models for intestinal permeability: A critique, Drug Discovery Today 10 (2005) 335–343. https://doi.org/10.1016/S1359-6446(04)03354-9.
[86] H. Singh, S. Velamakanni, M.J. Deery, J. Howard, S.L. Wei, van Veen, Hendrik W., ATP-dependent substrate transport by the ABC transporter MsbA is proton-coupled, Nature Communications 7 (2016) 12387. https://doi.org/10.1038/ncomms12387.
[87] D. Epel, T. Luckenbach, C.N. Stevenson, L.A. Macmanus-Spencer, A. Hamdoun, T. Smital, Efflux transporters: newly appreciated roles in protection against pollutants, Environ Sci Technol 42 (2008) 3914–3920. https://doi.org/10.1021/es087187v.
[88] R.H. Stephens, C.A. O'Neill, A. Warhurst, G.L. Carlson, M. Rowland, G. Warhurst, Kinetic profiling of P-glycoprotein-mediated drug efflux in rat and human intestinal epithelia, The Journal of pharmacology and experimental therapeutics 296 (2001) 584–591.
[89] M. Takano, R. Yumoto, T. Murakami, Expression and function of efflux drug transporters in the intestine, Pharmacology & therapeutics 109 (2006) 137–161. https://doi.org/10.1016/j.pharmthera.2005.06.005.
[90] T. Nakanishi, D.D. Ross, Breast cancer resistance protein (BCRP/ABCG2): its role in multidrug resistance and regulation of its gene expression, Chinese journal of cancer 31 (2012) 73–99. https://doi.org/10.5732/cjc.011.10320.
[91] H.E. Karpen, S.J. Karpen, Bile Acid Metabolism During Development, in: R.A. Polin, S.H. Abman, D. Rowitch, W.E. Benitz (Eds.), Fetal and Neonatal Physiology, 5th ed., Elsevier Health Care - Major Reference Works, s.l., 2017, 913-929.e4.
[92] G.J. Doherty, H.T. McMahon, Mechanisms of endocytosis, Annual review of biochemistry 78 (2009) 857–902. https://doi.org/10.1146/annurev.biochem.78.081307.110540.
[93] G.M. Cooper, R.E. Hausman, The cell: A molecular approach, 3rd ed., ASM Press, Washington, DC, 2004.
[94] M. Kaksonen, A. Roux, Mechanisms of clathrin-mediated endocytosis, Nature Reviews Molecular Cell Biology 19 (2018) 313–326. https://doi.org/10.1038/nrm.2017.132.
[95] R.G. Parton, K. Simons, The multiple faces of caveolae, Nature reviews. Molecular cell biology 8 (2007) 185–194. https://doi.org/10.1038/nrm2122.
[96] O.O. Glebov, N.A. Bright, B.J. Nichols, Flotillin-1 defines a clathrin-independent endocytic pathway in mammalian cells, Nature cell biology 8 (2006) 46–54. https://doi.org/10.1038/ncb1342.
[97] M. Frick, N.A. Bright, K. Riento, A. Bray, C. Merrified, B.J. Nichols, Coassembly of flotillins induces formation of membrane microdomains, membrane curvature, and vesicle budding, Current biology CB 17 (2007) 1151–1156. https://doi.org/10.1016/j.cub.2007.05.078.
[98] A. Sorkin, Cargo recognition during clathrin-mediated endocytosis: a team effort, Current opinion in cell biology 16 (2004) 392–399. https://doi.org/10.1016/j.ceb.2004.06.001.
[99] O. Kovtun, V.A. Tillu, N. Ariotti, R.G. Parton, B.M. Collins, Cavin family proteins and the assembly of caveolae, Journal of cell science 128 (2015) 1269–1278. https://doi.org/10.1242/jcs.167866.
[100] A. Cencic, T. Langerholc, Functional cell models of the gut and their applications in food microbiology--a review, International journal of food microbiology 141 Suppl 1 (2010) S4-14. https://doi.org/10.1016/j.ijfoodmicro.2010.03.026.
[101] R.G.W. Kirk, Recovering The Principles of Humane Experimental Technique: The 3Rs and the Human Essence of Animal Research, Sci Technol Human Values 43 (2018) 622–648. https://doi.org/10.1177/0162243917726579.

[102] J. Costa, A. Ahluwalia, Advances and Current Challenges in Intestinal in vitro Model Engineering: A Digest, Frontiers in bioengineering and biotechnology 7 (2019) 144. https://doi.org/10.3389/fbioe.2019.00144.
[103] M. Gagnon, A. Zihler Berner, N. Chervet, C. Chassard, C. Lacroix, Comparison of the Caco-2, HT-29 and the mucus-secreting HT29-MTX intestinal cell models to investigate Salmonella adhesion and invasion, Journal of microbiological methods 94 (2013) 274–279. https://doi.org/10.1016/j.mimet.2013.06.027.
[104] K. Todoriki, T. Mukai, S. Sato, T. Toba, Inhibition of adhesion of food-borne pathogens to Caco-2 cells by Lactobacillus strains, Journal of applied microbiology 91 (2001) 154–159. https://doi.org/10.1046/j.1365-2672.2001.01371.x.
[105] K.M. Kitchens, R.B. Kolhatkar, P.W. Swaan, N.D. Eddington, H. Ghandehari, Transport of poly(amidoamine) dendrimers across Caco-2 cell monolayers: Influence of size, charge and fluorescent labeling, Pharmaceutical research 23 (2006) 2818–2826. https://doi.org/10.1007/s11095-006-9122-2.
[106] S. Yamashita, Y. Tanaka, Y. Endoh, Y. Taki, T. Sakane, T. Nadai, H. Sezaki, Analysis of drug permeation across Caco-2 monolayer: implication for predicting in vivo drug absorption, Pharmaceutical research 14 (1997) 486–491. https://doi.org/10.1023/a:1012103700981.
[107] K. Gerloff, C. Albrecht, A.W. Boots, I. Förster, Schins, Roel P. F., Cytotoxicity and oxidative DNA damage by nanoparticles in human intestinal Caco-2 cells, Nanotoxicology 3 (2009) 355–364. https://doi.org/10.3109/17435390903276933.
[108] J. Drost, R.H. van Jaarsveld, B. Ponsioen, C. Zimberlin, R. van Boxtel, A. Buijs, N. Sachs, R.M. Overmeer, G.J. Offerhaus, H. Begthel, J. Korving, van de Wetering, Marc, G. Schwank, M. Logtenberg, E. Cuppen, H.J. Snippert, J.P. Medema, G.J.P.L. Kops, H. Clevers, Sequential cancer mutations in cultured human intestinal stem cells, Nature 521 (2015) 43–47. https://doi.org/10.1038/nature14415.
[109] M. Matano, S. Date, M. Shimokawa, A. Takano, M. Fujii, Y. Ohta, T. Watanabe, T. Kanai, T. Sato, Modeling colorectal cancer using CRISPR-Cas9-mediated engineering of human intestinal organoids, Nature Medicine 21 (2015) 256–262. https://doi.org/10.1038/nm.3802.
[110] C.S. Verissimo, R.M. Overmeer, B. Ponsioen, J. Drost, S. Mertens, I. Verlaan-Klink, B. van Gerwen, M. van der Ven, M. de van Wetering, D.A. Egan, R. Bernards, H. Clevers, J.L. Bos, H.J. Snippert, Targeting mutant RAS in patient-derived colorectal cancer organoids by combinatorial drug screening, eLife 5 (2016). https://doi.org/10.7554/eLife.18489.
[111] P. Artursson, K. Palm, K. Luthman, Caco-2 monolayers in experimental and theoretical predictions of drug transport, Advanced drug delivery reviews 46 (2001) 27–43. https://doi.org/10.1016/s0169-409x(00)00128-9.
[112] B. Sarmento, F. Andrade, da Silva, Sara Baptista, F. Rodrigues, J. das Neves, D. Ferreira, Cell-based in vitro models for predicting drug permeability, Expert opinion on drug metabolism & toxicology 8 (2012) 607–621. https://doi.org/10.1517/17425255.2012.673586.
[113] R. Edmondson, J.J. Broglie, A.F. Adcock, L. Yang, Three-dimensional cell culture systems and their applications in drug discovery and cell-based biosensors, Assay and drug development technologies 12 (2014) 207–218. https://doi.org/10.1089/adt.2014.573.
[114] J. Bourgine, I. Billaut-Laden, M. Happillon, J.-M. Lo-Guidice, V. Maunoury, M. Imbenotte, F. Broly, Gene expression profiling of systems involved in the metabolism and the disposition of xenobiotics: comparison between human intestinal biopsy samples and colon cell lines, Drug metabolism and disposition: the biological fate of chemicals 40 (2012) 694–705. https://doi.org/10.1124/dmd.111.042465.
[115] E. Cukierman, R. Pankov, D.R. Stevens, K.M. Yamada, Taking cell-matrix adhesions to the third dimension, Science (New York, N.Y.) 294 (2001) 1708–1712. https://doi.org/10.1126/science.1064829.

[116] J. Pusch, M. Votteler, S. Göhler, J. Engl, M. Hampel, H. Walles, K. Schenke-Layland, The physiological performance of a three-dimensional model that mimics the microenvironment of the small intestine, Biomaterials 32 (2011) 7469–7478. https://doi.org/10.1016/j.biomaterials.2011.06.035.
[117] R.W. Stidham, J. Xu, L.A. Johnson, K. Kim, D.S. Moons, B.J. McKenna, J.M. Rubin, P.D.R. Higgins, Ultrasound elasticity imaging for detecting intestinal fibrosis and inflammation in rats and humans with Crohn's disease, Gastroenterology 141 (2011) 819-826.e1. https://doi.org/10.1053/j.gastro.2011.07.027.
[118] D.C. Stewart, D. Berrie, J. Li, X. Liu, C. Rickerson, D. Mkoji, A. Iqbal, S. Tan, A.L. Doty, S.C. Glover, C.S. Simmons, Quantitative assessment of intestinal stiffness and associations with fibrosis in human inflammatory bowel disease, PLOS ONE 13 (2018) e0200377. https://doi.org/10.1371/journal.pone.0200377.
[119] C.M. Nelson, M.J. Bissell, Of extracellular matrix, scaffolds, and signaling: tissue architecture regulates development, homeostasis, and cancer, Annual review of cell and developmental biology 22 (2006) 287–309. https://doi.org/10.1146/annurev.cellbio.22.010305.104315.
[120] A. Costa, J.D. Naranjo, R. Londono, S.F. Badylak, Biologic Scaffolds, Cold Spring Harbor perspectives in medicine 7 (2017). https://doi.org/10.1101/cshperspect.a025676.
[121] C. Frantz, K.M. Stewart, V.M. Weaver, The extracellular matrix at a glance, Journal of cell science 123 (2010) 4195–4200. https://doi.org/10.1242/jcs.023820.
[122] L. Meran, A. Baulies, V.S.W. Li, Intestinal Stem Cell Niche: The Extracellular Matrix and Cellular Components, Stem cells international 2017 (2017) 7970385. https://doi.org/10.1155/2017/7970385.
[123] N. Gjorevski, N. Sachs, A. Manfrin, S. Giger, M.E. Bragina, P. Ordóñez-Morán, H. Clevers, M.P. Lutolf, Designer matrices for intestinal stem cell and organoid culture, Nature 539 (2016) 560–564. https://doi.org/10.1038/nature20168.
[124] D.A.C. Walma, K.M. Yamada, The extracellular matrix in development, Development (Cambridge, England) 147 (2020). https://doi.org/10.1242/dev.175596.
[125] Y. Wang, D.B. Gunasekara, M.I. Reed, M. DiSalvo, S.J. Bultman, C.E. Sims, S.T. Magness, N.L. Allbritton, A microengineered collagen scaffold for generating a polarized crypt-villus architecture of human small intestinal epithelium, Biomaterials 128 (2017) 44–55. https://doi.org/10.1016/j.biomaterials.2017.03.005.
[126] Y. Wang, R. Kim, D.B. Gunasekara, M.I. Reed, M. DiSalvo, D.L. Nguyen, S.J. Bultman, C.E. Sims, S.T. Magness, N.L. Allbritton, Formation of Human Colonic Crypt Array by Application of Chemical Gradients Across a Shaped Epithelial Monolayer, Cellular and molecular gastroenterology and hepatology 5 (2018) 113–130. https://doi.org/10.1016/j.jcmgh.2017.10.007.
[127] J. Creff, R. Courson, T. Mangeat, J. Foncy, S. Souleille, C. Thibault, A. Besson, L. Malaquin, Fabrication of 3D scaffolds reproducing intestinal epithelium topography by high-resolution 3D stereolithography, Biomaterials 221 (2019) 119404. https://doi.org/10.1016/j.biomaterials.2019.119404.
[128] S. Nietzer, F. Baur, S. Sieber, J. Hansmann, T. Schwarz, C. Stoffer, H. Häfner, M. Gasser, A.M. Waaga-Gasser, H. Walles, G. Dandekar, Mimicking Metastases Including Tumor Stroma: A New Technique to Generate a Three-Dimensional Colorectal Cancer Model Based on a Biological Decellularized Intestinal Scaffold, Tissue engineering. Part C, Methods 22 (2016) 621–635. https://doi.org/10.1089/ten.TEC.2015.0557.
[129] M.J. Mondrinos, Y.-S. Yi, N.-K. Wu, X. Ding, D. Huh, Native extracellular matrix-derived semipermeable, optically transparent, and inexpensive membrane inserts for microfluidic cell culture, Lab on a chip 17 (2017) 3146–3158. https://doi.org/10.1039/c7lc00317j.
[130] P. Bruckner, Suprastructures of extracellular matrices: paradigms of functions controlled by aggregates rather than molecules, Cell and tissue research 339 (2010) 7–18. https://doi.org/10.1007/s00441-009-0864-0.

[131] L. Bruckner-Tuderman, K. von der Mark, T. Pihlajaniemi, K. Unsicker, Cell interactions with the extracellular matrix, Cell and tissue research 339 (2010) 1–5. https://doi.org/10.1007/s00441-009-0891-x.
[132] M.W. Tibbitt, K.S. Anseth, Hydrogels as extracellular matrix mimics for 3D cell culture, Biotechnology and bioengineering 103 (2009) 655–663. https://doi.org/10.1002/bit.22361.
[133] E. Knight, B. Murray, R. Carnachan, S. Przyborski, Alvetex®: polystyrene scaffold technology for routine three dimensional cell culture, Methods in molecular biology (Clifton, N.J.) 695 (2011) 323–340. https://doi.org/10.1007/978-1-60761-984-0_20.
[134] D.M. Faulk, J.D. Wildemann, S.F. Badylak, Decellularization and cell seeding of whole liver biologic scaffolds composed of extracellular matrix, Journal of clinical and experimental hepatology 5 (2015) 69–80. https://doi.org/10.1016/j.jceh.2014.03.043.
[135] S.D. Sackett, D.M. Tremmel, F. Ma, A.K. Feeney, R.M. Maguire, M.E. Brown, Y. Zhou, X. Li, C. O'Brien, L. Li, W.J. Burlingham, J.S. Odorico, Extracellular matrix scaffold and hydrogel derived from decellularized and delipidized human pancreas, Scientific reports 8 (2018) 10452. https://doi.org/10.1038/s41598-018-28857-1.
[136] A.D. Theocharis, S.S. Skandalis, C. Gialeli, N.K. Karamanos, Extracellular matrix structure, Advanced drug delivery reviews 97 (2016) 4–27. https://doi.org/10.1016/j.addr.2015.11.001.
[137] P.M. Crapo, T.W. Gilbert, S.F. Badylak, An overview of tissue and whole organ decellularization processes, Biomaterials 32 (2011) 3233–3243. https://doi.org/10.1016/j.biomaterials.2011.01.057.
[138] J. Schanz, J. Pusch, J. Hansmann, H. Walles, Vascularised human tissue models: a new approach for the refinement of biomedical research, Journal of biotechnology 148 (2010) 56–63. https://doi.org/10.1016/j.jbiotec.2010.03.015.
[139] M. Schweinlin, S. Wilhelm, I. Schwedhelm, J. Hansmann, R. Rietscher, C. Jurowich, H. Walles, M. Metzger, Development of an Advanced Primary Human In Vitro Model of the Small Intestine, Tissue engineering. Part C, Methods 22 (2016) 873–883. https://doi.org/10.1089/ten.TEC.2016.0101.
[140] J.S. Woo, M.C. Fishbein, B. Reemtsen, Histologic examination of decellularized porcine intestinal submucosa extracellular matrix (CorMatrix) in pediatric congenital heart surgery, Cardiovascular pathology the official journal of the Society for Cardiovascular Pathology 25 (2016) 12–17. https://doi.org/10.1016/j.carpath.2015.08.007.
[141] G. Totonelli, P. Maghsoudlou, M. Garriboli, J. Riegler, G. Orlando, A.J. Burns, N.J. Sebire, V.V. Smith, J.M. Fishman, M. Ghionzoli, M. Turmaine, M.A. Birchall, A. Atala, S. Soker, M.F. Lythgoe, A. Seifalian, A. Pierro, S. Eaton, P. de Coppi, A rat decellularized small bowel scaffold that preserves villus-crypt architecture for intestinal regeneration, Biomaterials 33 (2012) 3401–3410. https://doi.org/10.1016/j.biomaterials.2012.01.012.
[142] J. Velema, D. Kaplan, Biopolymer-Based Biomaterials as Scaffolds for Tissue Engineering, in: K. Lee, D. Kaplan (Eds.), Tissue Engineering I, Springer Berlin Heidelberg, Berlin, Heidelberg, 2006, pp. 187–238.
[143] J.D.P. de Amorim, K.C. de Souza, C.R. Duarte, I. da Silva Duarte, F. de Assis Sales Ribeiro, G.S. Silva, P.M.A. de Farias, A. Stingl, A.F.S. Costa, G.M. Vinhas, L.A. Sarubbo, Plant and bacterial nanocellulose: production, properties and applications in medicine, food, cosmetics, electronics and engineering. A review, Environ Chem Lett 18 (2020) 851–869. https://doi.org/10.1007/s10311-020-00989-9.
[144] A. Dufresne, J.-Y. Cavaill, M.R. Vignon, Mechanical behavior of sheets prepared from sugar beet cellulose microfibrils, J. Appl. Polym. Sci. 64 (1997) 1185–1194. https://doi.org/10.1002/(SICI)1097-4628(19970509)64:6<1185:AID-APP19>3.0.CO;2-V.
[145] D. Klemm, B. Heublein, H.-P. Fink, A. Bohn, Cellulose: fascinating biopolymer and sustainable raw material, Angewandte Chemie (International ed. in English) 44 (2005) 3358–3393. https://doi.org/10.1002/anie.200460587.

[146] D. Klemm, E.D. Cranston, D. Fischer, M. Gama, S.A. Kedzior, D. Kralisch, F. Kramer, T. Kondo, T. Lindström, S. Nietzsche, K. Petzold-Welcke, F. Rauchfuß, Nanocellulose as a natural source for groundbreaking applications in materials science: Today's state, Materials Today 21 (2018) 720–748. https://doi.org/10.1016/j.mattod.2018.02.001.
[147] D. Klemm, D. Schumann, U. Udhardt, S. Marsch, Bacterial synthesized cellulose — artificial blood vessels for microsurgery, Progress in Polymer Science 26 (2001) 1561–1603. https://doi.org/10.1016/S0079-6700(01)00021-1.
[148] M. Osorio, P. Fernández-Morales, P. Gañán, R. Zuluaga, H. Kerguelen, I. Ortiz, C. Castro, Development of novel three-dimensional scaffolds based on bacterial nanocellulose for tissue engineering and regenerative medicine: Effect of processing methods, pore size, and surface area, Journal of biomedical materials research. Part A 107 (2019) 348–359. https://doi.org/10.1002/jbm.a.36532.
[149] S. Bottan, F. Robotti, P. Jayathissa, A. Hegglin, N. Bahamonde, J.A. Heredia-Guerrero, I.S. Bayer, A. Scarpellini, H. Merker, N. Lindenblatt, D. Poulikakos, A. Ferrari, Surface-structured bacterial cellulose with guided assembly-based biolithography (GAB), ACS nano 9 (2015) 206–219. https://doi.org/10.1021/nn5036125.
[150] M. Zaborowska, A. Bodin, H. Bäckdahl, J. Popp, A. Goldstein, P. Gatenholm, Microporous bacterial cellulose as a potential scaffold for bone regeneration, Acta biomaterialia 6 (2010) 2540–2547. https://doi.org/10.1016/j.actbio.2010.01.004.
[151] F. Dourado, M. Gama, S. Bielecki (Eds.), Bacterial nanocellulose: From biotechnology to bio-economy, Elsevier, Amsterdam, Netherlands, 2016.
[152] F. Lina, Z. Yue, Z. Jin, Y. Guang, Bacterial Cellulose for Skin Repair Materials, in: R. Fazel-Rezai (Ed.), Biomedical engineering: Frontiers and challenges, InTech, Rijeka, Croatia, 2011.
[153] C. Brackmann, M. Zaborowska, J. Sundberg, P. Gatenholm, A. Enejder, In situ imaging of collagen synthesis by osteoprogenitor cells in microporous bacterial cellulose scaffolds, Tissue engineering. Part C, Methods 18 (2012) 227–234. https://doi.org/10.1089/ten.TEC.2011.0211.
[154] C. Castro, A. Vesterinen, R. Zuluaga, G. Caro, I. Filpponen, O.J. Rojas, G. Kortaberria, P. Gañán, In situ production of nanocomposites of poly(vinyl alcohol) and cellulose nanofibrils from Gluconacetobacter bacteria: effect of chemical crosslinking, Cellulose 21 (2014) 1745–1756. https://doi.org/10.1007/s10570-014-0170-1.
[155] M.A. Osorio, D. Restrepo, J.A. Velásquez-Cock, R.O. Zuluaga, U. Montoya, O. Rojas, P.F. Gañán, D. Marin, C.I. Castro, Synthesis of Thermoplastic Starch-Bacterial Cellulose Nanocomposites via in situ Fermentation, Journal of the Brazilian Chemical Society. https://doi.org/10.5935/0103-5053.20140146.
[156] E.-M. Feldmann, J.F. Sundberg, B. Bobbili, S. Schwarz, P. Gatenholm, N. Rotter, Description of a novel approach to engineer cartilage with porous bacterial nanocellulose for reconstruction of a human auricle, Journal of biomaterials applications 28 (2013) 626–640. https://doi.org/10.1177/0885328212472547.
[157] W. Czaja, A. Krystynowicz, M. Kawecki, K. Wysota, S. Sakiel, P. Wróblewski, J. Glik, M. Nowak, S. Bielecki, Biomedical Applications of Microbial Cellulose in Burn Wound Recovery, in: R.M. Brown, I.M. Saxena (Eds.), Cellulose: Molecular and Structural Biology, Springer Netherlands, Dordrecht, 2007, pp. 307–321.
[158] M. Vielreicher, D. Kralisch, S. Völkl, F. Sternal, A. Arkudas, O. Friedrich, Bacterial nanocellulose stimulates mesenchymal stem cell expansion and formation of stable collagen-I networks as a novel biomaterial in tissue engineering, Scientific reports 8 (2018) 9401. https://doi.org/10.1038/s41598-018-27760-z.
[159] C.J. Bettinger, R. Langer, J.T. Borenstein, Engineering substrate topography at the micro- and nanoscale to control cell function, Angewandte Chemie (International ed. in English) 48 (2009) 5406–5415. https://doi.org/10.1002/anie.200805179.
[160] J.P. Spatz, B. Geiger, Molecular Engineering of Cellular Environments: Cell Adhesion to Nano-Digital Surfaces, in: Y.-l. Wang, D.E. Discher (Eds.), Cell mechanics, Elsevier Academic Press, Amsterdam, 2007, pp. 89–111.

[161] S. Gordon, M. Daneshian, J. Bouwstra, F. Caloni, S. Constant, D.E. Davies, G. Dandekar, C.A. Guzman, E. Fabian, E. Haltner, T. Hartung, N. Hasiwa, P. Hayden, H. Kandarova, S. Khare, H.F. Krug, C. Kneuer, M. Leist, G. Lian, U. Marx, M. Metzger, K. Ott, P. Prieto, M.S. Roberts, E.L. Roggen, T. Tralau, C. van den Braak, H. Walles, C.-M. Lehr, Non-animal models of epithelial barriers (skin, intestine and lung) in research, industrial applications and regulatory toxicology, ALTEX 32 (2015) 327–378. https://doi.org/10.14573/altex.1510051.

[162] Y. Sambuy, I. de Angelis, G. Ranaldi, M.L. Scarino, A. Stammati, F. Zucco, The Caco-2 cell line as a model of the intestinal barrier: influence of cell and culture-related factors on Caco-2 cell functional characteristics, Cell Biology and Toxicology 21 (2005) 1–26. https://doi.org/10.1007/s10565-005-0085-6.

[163] I. Hubatsch, E.G.E. Ragnarsson, P. Artursson, Determination of drug permeability and prediction of drug absorption in Caco-2 monolayers, Nature protocols 2 (2007) 2111–2119. https://doi.org/10.1038/nprot.2007.303.

[164] D. Swiatecka, A. Mackie, The Impact of Food Bioactives on Health: In Vitro and Ex Vivo Models: Caco-2 Cell Line, Springer, [Erscheinungsort nicht ermittelbar], 2015.

[165] P.G.M. Jochems, J. Garssen, A.M. van Keulen, R. Masereeuw, P.V. Jeurink, Evaluating Human Intestinal Cell Lines for Studying Dietary Protein Absorption, Nutrients 10 (2018). https://doi.org/10.3390/nu10030322.

[166] D. Antoine, Y. Pellequer, C. Tempesta, S. Lorscheidt, B. Kettel, L. Tamaddon, V. Jannin, F. Demarne, A. Lamprecht, A. Béduneau, Biorelevant media resistant co-culture model mimicking permeability of human intestine, International journal of pharmaceutics 481 (2015) 27–36. https://doi.org/10.1016/j.ijpharm.2015.01.028.

[167] F. Pan, L. Han, Y. Zhang, Y. Yu, J. Liu, Optimization of Caco-2 and HT29 co-culture in vitro cell models for permeability studies, International journal of food sciences and nutrition 66 (2015) 680–685. https://doi.org/10.3109/09637486.2015.1077792.

[168] A. Ferraretto, M. Bottani, P. de Luca, L. Cornaghi, F. Arnaboldi, M. Maggioni, A. Fiorilli, E. Donetti, Morphofunctional properties of a differentiated Caco2/HT-29 co-culture as an in vitro model of human intestinal epithelium, Bioscience Reports 38 (2018). https://doi.org/10.1042/BSR20171497.

[169] C. Hilgendorf, H. Spahn-Langguth, C.G. Regårdh, E. Lipka, G.L. Amidon, P. Langguth, Caco-2 versus Caco-2/HT29-MTX Co-cultured Cell Lines: Permeabilities Via Diffusion, Inside- and Outside-Directed Carrier-Mediated Transport, Journal of Pharmaceutical Sciences 89 (2000) 63–75. https://doi.org/10.1002/(SICI)1520-6017(200001)89:1<63:AID-JPS7>3.0.CO;2-6.

[170] I. Lozoya-Agullo, F. Araújo, I. González-Álvarez, M. Merino-Sanjuán, M. González-Álvarez, M. Bermejo, B. Sarmento, Usefulness of Caco-2/HT29-MTX and Caco-2/HT29-MTX/Raji B Coculture Models To Predict Intestinal and Colonic Permeability Compared to Caco-2 Monoculture, Molecular pharmaceutics 14 (2017) 1264–1270. https://doi.org/10.1021/acs.molpharmaceut.6b01165.

[171] J. Zabner, P. Karp, M. Seiler, S.L. Phillips, C.J. Mitchell, M. Saavedra, M. Welsh, A.J. Klingelhutz, Development of cystic fibrosis and noncystic fibrosis airway cell lines, American journal of physiology. Lung cellular and molecular physiology 284 (2003) L844-54. https://doi.org/10.1152/ajplung.00355.2002.

[172] R.D. Ramirez, S. Sheridan, L. Girard, M. Sato, Y. Kim, J. Pollack, M. Peyton, Y. Zou, J.M. Kurie, J.M. Dimaio, S. Milchgrub, A.L. Smith, R.F. Souza, L. Gilbey, X. Zhang, K. Gandia, M.B. Vaughan, W.E. Wright, A.F. Gazdar, J.W. Shay, J.D. Minna, Immortalization of human bronchial epithelial cells in the absence of viral oncoproteins, Cancer research 64 (2004) 9027–9034. https://doi.org/10.1158/0008-5472.CAN-04-3703.

[173] E. Ramboer, T. Vanhaecke, V. Rogiers, M. Vinken, Immortalized Human Hepatic Cell Lines for In Vitro Testing and Research Purposes, Methods in molecular biology (Clifton, N.J.) 1250 (2015) 53–76. https://doi.org/10.1007/978-1-4939-2074-7_4.

[174] T. Sato, R.G. Vries, H.J. Snippert, van de Wetering, Marc, N. Barker, D.E. Stange, van Es, Johan H, A. Abo, P. Kujala, P.J. Peters, H. Clevers, Single Lgr5 stem cells build

crypt-villus structures in vitro without a mesenchymal niche, Nature 459 (2009) 262–265. https://doi.org/10.1038/nature07935.
[175] C.S. Hughes, L.M. Postovit, G.A. Lajoie, Matrigel: a complex protein mixture required for optimal growth of cell culture, Proteomics 10 (2010) 1886–1890. https://doi.org/10.1002/pmic.200900758.
[176] M.A. Loza-Coll, S. Perera, W. Shi, J. Filmus, A transient increase in the activity of Src-family kinases induced by cell detachment delays anoikis of intestinal epithelial cells, Oncogene 24 (2005) 1727–1737. https://doi.org/10.1038/sj.onc.1208379.
[177] S. Date, T. Sato, Mini-gut organoids: reconstitution of the stem cell niche, Annual review of cell and developmental biology 31 (2015) 269–289. https://doi.org/10.1146/annurev-cellbio-100814-125218.
[178] O. Basak, J. Beumer, K. Wiebrands, H. Seno, A. van Oudenaarden, H. Clevers, Induced Quiescence of Lgr5+ Stem Cells in Intestinal Organoids Enables Differentiation of Hormone-Producing Enteroendocrine Cells, Cell stem cell 20 (2017) 177-190.e4. https://doi.org/10.1016/j.stem.2016.11.001.
[179] M. Fujii, M. Matano, K. Toshimitsu, A. Takano, Y. Mikami, S. Nishikori, S. Sugimoto, T. Sato, Human Intestinal Organoids Maintain Self-Renewal Capacity and Cellular Diversity in Niche-Inspired Culture Condition, Cell stem cell 23 (2018) 787-793.e6. https://doi.org/10.1016/j.stem.2018.11.016.
[180] J.F. Dekkers, C.L. Wiegerinck, H.R. de Jonge, I. Bronsveld, H.M. Janssens, K.M. de Winter-de Groot, A.M. Brandsma, N.W.M. de Jong, M.J.C. Bijvelds, B.J. Scholte, E.E.S. Nieuwenhuis, Van den Brink, Stieneke, H. Clevers, C.K. van der Ent, S. Middendorp, J.M. Beekman, A functional CFTR assay using primary cystic fibrosis intestinal organoids, Nature Medicine 19 (2013) 939–945. https://doi.org/10.1038/nm.3201.
[181] M. Meir, J. Salm, C. Fey, M. Schweinlin, C. Kollmann, F. Kannapin, C.-T. Germer, J. Waschke, C. Beck, N. Burkard, M. Metzger, N. Schlegel, Enteroids generated from patients with severe inflammation in Crohn's disease maintain alterations of junctional proteins, Journal of Crohn's & colitis. https://doi.org/10.1093/ecco-jcc/jjaa085.
[182] M.R. Aberle, R.A. Burkhart, H. Tiriac, S.W.M. Olde Damink, C.H.C. Dejong, D.A. Tuveson, R.M. van Dam, Patient-derived organoid models help define personalized management of gastrointestinal cancer, The British journal of surgery 105 (2018) e48-e60. https://doi.org/10.1002/bjs.10726.
[183] Y. Meng, Z. Ren, F. Xu, X. Zhou, C. Song, V.Y.-F. Wang, W. Liu, L. Lu, J.A. Thomson, G. Chen, Nicotinamide Promotes Cell Survival and Differentiation as Kinase Inhibitor in Human Pluripotent Stem Cells, Stem Cell Reports 11 (2018) 1347–1356. https://doi.org/10.1016/j.stemcr.2018.10.023.
[184] Ş.A. Düzgün, A. Yerlikaya, S. Zeren, Z. Bayhan, E. Okur, İ. Boyacı, Differential effects of p38 MAP kinase inhibitors SB203580 and SB202190 on growth and migration of human MDA-MB-231 cancer cell line, Cytotechnology 69 (2017) 711–724. https://doi.org/10.1007/s10616-017-0079-2.
[185] Q. Zhang, X. Hou, B.J. Evans, J.L. VanBlaricom, S.J. Weroha, W.A. Cliby, LY2157299 Monohydrate, a TGF-βR1 Inhibitor, Suppresses Tumor Growth and Ascites Development in Ovarian Cancer, Cancers 10 (2018). https://doi.org/10.3390/cancers10080260.
[186] M. Tojo, Y. Hamashima, A. Hanyu, T. Kajimoto, M. Saitoh, K. Miyazono, M. Node, T. Imamura, The ALK-5 inhibitor A-83-01 inhibits Smad signaling and epithelial-to-mesenchymal transition by transforming growth factor-beta, Cancer science 96 (2005) 791–800. https://doi.org/10.1111/j.1349-7006.2005.00103.x.
[187] A. Fatehullah, S.H. Tan, N. Barker, Organoids as an in vitro model of human development and disease, Nature cell biology 18 (2016) 246–254. https://doi.org/10.1038/ncb3312.
[188] I.A. Williamson, J.W. Arnold, L.A. Samsa, L. Gaynor, M. DiSalvo, J.L. Cocchiaro, I. Carroll, M.A. Azcarate-Peril, J.F. Rawls, N.L. Allbritton, S.T. Magness, A High-Throughput Organoid Microinjection Platform to Study Gastrointestinal Microbiota and

Luminal Physiology, Cellular and molecular gastroenterology and hepatology 6 (2018) 301–319. https://doi.org/10.1016/j.jcmgh.2018.05.004.
[189] L.N. Schulte, M. Schweinlin, A.J. Westermann, H. Janga, S.C. Santos, S. Appenzeller, H. Walles, J. Vogel, M. Metzger, An Advanced Human Intestinal Coculture Model Reveals Compartmentalized Host and Pathogen Strategies during Salmonella Infection, mBio 11 (2020). https://doi.org/10.1128/mBio.03348-19.
[190] A.L. Kauffman, A.V. Gyurdieva, J.R. Mabus, C. Ferguson, Z. Yan, P.J. Hornby, Alternative functional in vitro models of human intestinal epithelia, Frontiers in Pharmacology 4 (2013) 79. https://doi.org/10.3389/fphar.2013.00079.
[191] T. Takenaka, N. Harada, J. Kuze, M. Chiba, T. Iwao, T. Matsunaga, Human small intestinal epithelial cells differentiated from adult intestinal stem cells as a novel system for predicting oral drug absorption in humans, Drug metabolism and disposition: the biological fate of chemicals 42 (2014) 1947–1954. https://doi.org/10.1124/dmd.114.059493.
[192] van Es, Johan H., M.E. van Gijn, O. Riccio, van den Born, Maaike, M. Vooijs, H. Begthel, M. Cozijnsen, S. Robine, D.J. Winton, F. Radtke, H. Clevers, Notch/gamma-secretase inhibition turns proliferative cells in intestinal crypts and adenomas into goblet cells, Nature 435 (2005) 959–963. https://doi.org/10.1038/nature03659.
[193] S. Ogaki, N. Shiraki, K. Kume, S. Kume, Wnt and Notch signals guide embryonic stem cell differentiation into the intestinal lineages, Stem cells (Dayton, Ohio) 31 (2013) 1086–1096. https://doi.org/10.1002/stem.1344.
[194] J. Milano, J. McKay, C. Dagenais, L. Foster-Brown, F. Pognan, R. Gadient, R.T. Jacobs, A. Zacco, B. Greenberg, P.J. Ciaccio, Modulation of notch processing by gamma-secretase inhibitors causes intestinal goblet cell metaplasia and induction of genes known to specify gut secretory lineage differentiation, Toxicological sciences an official journal of the Society of Toxicology 82 (2004) 341–358. https://doi.org/10.1093/toxsci/kfh254.
[195] J.Y. Co, M. Margalef-Catala, X. Li, A.T. Mah, C.J. Kuo, D.M. Monack, M.R. Amieva, Controlling Epithelial Polarity: A Human Enteroid Model for Host-Pathogen Interactions, Cell reports 26 (2019) 2509-2520.e4. https://doi.org/10.1016/j.celrep.2019.01.108.
[196] M. Huch, J.A. Knoblich, M.P. Lutolf, A. Martinez-Arias, The hope and the hype of organoid research, Development (Cambridge, England) 144 (2017) 938–941. https://doi.org/10.1242/dev.150201.
[197] J.S. Dutton, S.S. Hinman, R. Kim, Y. Wang, N.L. Allbritton, Primary Cell-Derived Intestinal Models: Recapitulating Physiology, Trends in biotechnology 37 (2019) 744–760. https://doi.org/10.1016/j.tibtech.2018.12.001.
[198] T. Langerholc, P.A. Maragkoudakis, J. Wollgast, L. Gradisnik, A. Cencic, Novel and established intestinal cell line models - An indispensable tool in food science and nutrition, Trends in food science & technology 22 (2011) S11-S20. https://doi.org/10.1016/j.tifs.2011.03.010.
[199] K. Lindberg, S.F. Badylak, Porcine small intestinal submucosa (SIS): a bioscaffold supporting in vitro primary human epidermal cell differentiation and synthesis of basement membrane proteins, Burns 27 (2001) 254–266. https://doi.org/10.1016/S0305-4179(00)00113-3.
[200] E. Martinez, J.-P. St-Pierre, F. Variola, Advanced bioengineering technologies for preclinical research, Advances in Physics: X 4 (2019) 1622451. https://doi.org/10.1080/23746149.2019.1622451.
[201] I. Anton-Sales, U. Beekmann, A. Laromaine, A. Roig, D. Kralisch, Opportunities of Bacterial Cellulose to Treat Epithelial Tissues, Current drug targets 20 (2019) 808–822. https://doi.org/10.2174/1389450120666181129092144.
[202] I. Sulaeva, U. Henniges, T. Rosenau, A. Potthast, Bacterial cellulose as a material for wound treatment: Properties and modifications. A review, Biotechnology advances 33 (2015) 1547–1571. https://doi.org/10.1016/j.biotechadv.2015.07.009.
[203] R.M. Brown, I.M. Saxena, Cellulose: Molecular and structural biology selected articles on the synthesis, structure, and applications of cellulose, Springer, Dordrecht, 2007.

[204] I.J. Hidalgo, J. Li, Carrier-mediated transport and efflux mechanisms in Caco-2 cells, Cell Culture to Assess Drug Transport and Metabolism 22 (1996) 53–66. https://doi.org/10.1016/S0169-409X(96)00414-0.
[205] J. Schwerk, M. Köster, H. Hauser, M. Rohde, M. Fulde, M.W. Hornef, T. May, Generation of Mouse Small Intestinal Epithelial Cell Lines That Allow the Analysis of Specific Innate Immune Functions, PLOS ONE 8 (2013) e72700. https://doi.org/10.1371/journal.pone.0072700.
[206] F. Klein, innovative Strategie zur Etablierung physiologisch relevanter Säugerzelllinien, 2012.
[207] C. Lipps, F. Klein, T. Wahlicht, V. Seiffert, M. Butueva, J. Zauers, T. Truschel, M. Luckner, M. Köster, R. MacLeod, J. Pezoldt, J. Hühn, Q. Yuan, P.P. Müller, H. Kempf, R. Zweigerdt, O. Dittrich-Breiholz, T. Pufe, R. Beckmann, W. Drescher, J. Riancho, C. Sañudo, T. Korff, B. Opalka, V. Rebmann, J.R. Göthert, P.M. Alves, M. Ott, R. Schucht, H. Hauser, D. Wirth, T. May, Expansion of functional personalized cells with specific transgene combinations, Nature Communications 9 (2018) 994. https://doi.org/10.1038/s41467-018-03408-4.
[208] M. Heiss, M. Hellström, M. Kalén, T. May, H. Weber, M. Hecker, H.G. Augustin, T. Korff, Endothelial cell spheroids as a versatile tool to study angiogenesis in vitro, The FASEB Journal 29 (2015) 3076–3084. https://doi.org/10.1096/fj.14-267633.
[209] A. Kuehn, S. Kletting, de Souza Carvalho-Wodarz, Cristiane, U. Repnik, G. Griffiths, U. Fischer, E. Meese, H. Huwer, D. Wirth, T. May, N. Schneider-Daum, C.-M. Lehr, Human alveolar epithelial cells expressing tight junctions to model the air-blood barrier, ALTEX 33 (2016) 251–260. https://doi.org/10.14573/altex.1511131.
[210] D. Escors, K. Breckpot, Lentiviral Vectors in Gene Therapy: Their Current Status and Future Potential, Archivum Immunologiae et Therapiae Experimentalis 58 (2010) 107–119. https://doi.org/10.1007/s00005-010-0063-4.
[211] H. Mertsching, J. Schanz, V. Steger, M. Schandar, M. Schenk, J. Hansmann, I. Dally, G. Friedel, T. Walles, Generation and Transplantation of an Autologous Vascularized Bioartificial Human Tissue, Transplantation 88 (2009).
[212] C. Fey, J. Betz, C. Rosenbaum, D. Kralisch, M. Vielreicher, O. Friedrich, M. Metzger, D. Zdzieblo, Bacterial nanocellulose as novel carrier for intestinal epithelial cells in drug delivery studies, Materials Science and Engineering: C 109 (2020) 110613. https://doi.org/10.1016/j.msec.2019.110613.
[213] C. Zhao, Wnt Reporter Activity Assay, BIO-PROTOCOL 4 (2014). https://doi.org/10.21769/BioProtoc.1183.
[214] T. May, L. Eccleston, S. Herrmann, H. Hauser, J. Goncalves, D. Wirth, Bimodal and Hysteretic Expression in Mammalian Cells from a Synthetic Gene Circuit, PLOS ONE 3 (2008) e2372. https://doi.org/10.1371/journal.pone.0002372.
[215] J. Vandesompele, K. de Preter, F. Pattyn, B. Poppe, N. van Roy, A. de Paepe, F. Speleman, Accurate normalization of real-time quantitative RT-PCR data by geometric averaging of multiple internal control genes, Genome biology 3 (2002) RESEARCH 0034. https://doi.org/10.1186/gb-2002-3-7-research0034.
[216] S.A. Bustin, V. Benes, J.A. Garson, J. Hellemans, J. Huggett, M. Kubista, R. Mueller, T. Nolan, M.W. Pfaffl, G.L. Shipley, J. Vandesompele, C.T. Wittwer, The MIQE guidelines: minimum information for publication of quantitative real-time PCR experiments, Clinical chemistry 55 (2009) 611–622. https://doi.org/10.1373/clinchem.2008.112797.
[217] T. Schmitz, M. Schweinlin, R.T. Kollhoff, L. Engelhardt, C. Lotz, F. Groeber-Becker, H. Walles, M. Metzger, J. Hansmann, Nanostructured TiN-Coated Electrodes for High-Sensitivity Noninvasive Characterization of in Vitro Tissue Models, ACS Appl. Nano Mater. 1 (2018) 2284–2293. https://doi.org/10.1021/acsanm.8b00345.
[218] L.R. Madden, T.V. Nguyen, S. Garcia-Mojica, V. Shah, A.V. Le, A. Peier, R. Visconti, E.M. Parker, S.C. Presnell, D.G. Nguyen, K.N. Retting, Bioprinted 3D Primary Human Intestinal Tissues Model Aspects of Native Physiology and ADME/Tox Functions, iScience 2 (2018) 156–167. https://doi.org/10.1016/j.isci.2018.03.015.

[219] J.D. Patient, H. Hajiali, K. Harris, B. Abrahamsson, C. Tannergren, L.J. White, A.M. Ghaemmaghami, P.M. Williams, C.J. Roberts, Rose, Felicity R. A. J., Nanofibrous Scaffolds Support a 3D in vitro Permeability Model of the Human Intestinal Epithelium, Frontiers in Pharmacology 10 (2019) 456. https://doi.org/10.3389/fphar.2019.00456.
[220] S. Tria, L.H. Jimison, A. Hama, M. Bongo, R.M. Owens, Sensing of EGTA Mediated Barrier Tissue Disruption with an Organic Transistor, Biosensors 3 (2013) 44–57. https://doi.org/10.3390/bios3010044.
[221] L. Gonzalez-Mariscal, R.G. Contreras, J.J. Bolívar, A. Ponce, B. Chávez De Ramirez, M. Cereijido, Role of calcium in tight junction formation between epithelial cells, The American journal of physiology 259 (1990) C978-86. https://doi.org/10.1152/ajpcell.1990.259.6.C978.
[222] M.A. Deli, Potential use of tight junction modulators to reversibly open membranous barriers and improve drug delivery, Biochimica et biophysica acta 1788 (2009) 892–910. https://doi.org/10.1016/j.bbamem.2008.09.016.
[223] P. Artursson, S. Neuhoff, P. Matsson, S. Tavelin, Passive Permeability and Active Transport Models for the Prediction of Oral Absorption, in: J.B. Taylor, D.J. Triggle (Eds.), Comprehensive medicinal chemistry II, Elsevier, Amsterdam, London, 2007, pp. 259–278.
[224] U. Bock, T. Flototto, E. Haltner, Validation of cell culture models for the intestine and the blood-brain barrier and comparison of drug permeation, ALTEX 21 Suppl 3 (2004) 57–64.
[225] T. Sergent, N. Piront, J. Meurice, O. Toussaint, Y.-J. Schneider, Anti-inflammatory effects of dietary phenolic compounds in an in vitro model of inflamed human intestinal epithelium, Chemico-biological interactions 188 (2010) 659–667. https://doi.org/10.1016/j.cbi.2010.08.007.
[226] R. Schucht, D. Wirth, T. May, Precise regulation of transgene expression level and control of cell physiology, Cell Biology and Toxicology 26 (2010) 29–42. https://doi.org/10.1007/s10565-009-9135-9.
[227] D. Vllasaliu, F.H. Falcone, S. Stolnik, M. Garnett, Basement membrane influences intestinal epithelial cell growth and presents a barrier to the movement of macromolecules, Experimental cell research 323 (2014) 218–231. https://doi.org/10.1016/j.yexcr.2014.02.022.
[228] T. Takahashi, A. Shiraishi, Stem Cell Signaling Pathways in the Small Intestine, International journal of molecular sciences 21 (2020). https://doi.org/10.3390/ijms21062032.
[229] K. Hashimoto, M. Shimizu, Epithelial properties of human intestinal Caco-2 cells cultured in a serum-free medium, Cytotechnology 13 (1993) 175–184. https://doi.org/10.1007/bf00749813.
[230] M. Baker, Reproducibility: Respect your cells!, Nature 537 (2016) 433–435. https://doi.org/10.1038/537433a.
[231] M.M. Bonab, K. Alimoghaddam, F. Talebian, S.H. Ghaffari, A. Ghavamzadeh, B. Nikbin, Aging of mesenchymal stem cell in vitro, BMC cell biology 7 (2006) 14. https://doi.org/10.1186/1471-2121-7-14.
[232] J. Lo Surdo, S.R. Bauer, Quantitative approaches to detect donor and passage differences in adipogenic potential and clonogenicity in human bone marrow-derived mesenchymal stem cells, Tissue engineering. Part C, Methods 18 (2012) 877–889. https://doi.org/10.1089/ten.TEC.2011.0736.
[233] S. Wray, M. Self, P.A. Lewis, J.-W. Taanman, N.S. Ryan, C.J. Mahoney, Y. Liang, M.J. Devine, U.-M. Sheerin, H. Houlden, H.R. Morris, D. Healy, J.-F. Marti-Masso, E. Preza, S. Barker, M. Sutherland, R.A. Corriveau, M. D'Andrea, A.H.V. Schapira, R.J. Uitti, M. Guttman, G. Opala, B. Jasinska-Myga, A. Puschmann, C. Nilsson, A.J. Espay, J. Slawek, L. Gutmann, B.F. Boeve, K. Boylan, A.J. Stoessl, O.A. Ross, N.J. Maragakis, J. van Gerpen, M. Gerstenhaber, K. Gwinn, T.M. Dawson, O. Isacson, K.S. Marder, L.N. Clark, S.E. Przedborski, S. Finkbeiner, J.D. Rothstein, Z.K. Wszolek, M.N. Rossor, J. Hardy, Creation of an open-access, mutation-defined fibroblast resource for

neurological disease research, PloS one 7 (2012) e43099. https://doi.org/10.1371/journal.pone.0043099.
[234] Y. Li, Y. Liu, B. Liu, J. Wang, S. Wei, Z. Qi, S. Wang, W. Fu, Y.-G. Chen, A growth factor-free culture system underscores the coordination between Wnt and BMP signaling in Lgr5+ intestinal stem cell maintenance, Cell discovery 4 (2018) 49. https://doi.org/10.1038/s41421-018-0051-0.
[235] A.G. Bodnar, M. Ouellette, M. Frolkis, S.E. Holt, C.P. Chiu, G.B. Morin, C.B. Harley, J.W. Shay, S. Lichtsteiner, W.E. Wright, Extension of life-span by introduction of telomerase into normal human cells, Science (New York, N.Y.) 279 (1998) 349–352. https://doi.org/10.1126/science.279.5349.349.
[236] D. Serra, U. Mayr, A. Boni, I. Lukonin, M. Rempfler, L. Challet Meylan, M.B. Stadler, P. Strnad, P. Papasaikas, D. Vischi, A. Waldt, G. Roma, P. Liberali, Self-organization and symmetry breaking in intestinal organoid development, Nature 569 (2019) 66–72. https://doi.org/10.1038/s41586-019-1146-y.
[237] S. Dalton, Linking the Cell Cycle to Cell Fate Decisions, Trends in cell biology 25 (2015) 592–600. https://doi.org/10.1016/j.tcb.2015.07.007.
[238] I.D. Angelis, L. Turco, Caco-2 Cells as a Model for Intestinal Absorption, Current Protocols in Toxicology 47 (2011) 20.6.1-20.6.15. https://doi.org/10.1002/0471140856.tx2006s47.
[239] S.V. Sastry, J.R. Nyshadham, J.A. Fix, Recent technological advances in oral drug delivery – a review, Pharmaceutical Science & Technology Today 3 (2000) 138–145. https://doi.org/10.1016/S1461-5347(00)00247-9.
[240] J. Zhang, Z. Xie, N. Zhang, J. Zhong, Chapter 13 - Nanosuspension drug delivery system: preparation, characterization, postproduction processing, dosage form, and application, in: E. Andronescu, A.M. Grumezescu (Eds.), Nanostructures for Drug Delivery Micro and Nano Technologies, Elsevier, 2017, pp. 413–443.
[241] S.A. Langhans, Three-Dimensional in Vitro Cell Culture Models in Drug Discovery and Drug Repositioning, Frontiers in Pharmacology 9 (2018) 6. https://doi.org/10.3389/fphar.2018.00006.
[242] R.L. Perlman, Mouse models of human disease: An evolutionary perspective, Evolution, medicine, and public health 2016 (2016) 170–176. https://doi.org/10.1093/emph/eow014.
[243] M. Gama, P. Gatenholm, D. Klemm, Bacterial NanoCellulose, CRC Press, 2016.
[244] C. Sharma, N.K. Bhardwaj, Bacterial nanocellulose: Present status, biomedical applications and future perspectives, Materials science & engineering. C, Materials for biological applications 104 (2019) 109963. https://doi.org/10.1016/j.msec.2019.109963.
[245] Y. Hu, J.M. Catchmark, Effect of freeze-drying behavior on the density and structure of bacterial cellulosic films by different acidic and alkaline treatments, in: 2009 Reno, Nevada, June 21 - June 24, 2009, American Society of Agricultural and Biological Engineers, St. Joseph, MI.
[246] P. Jacek, M. Ryngajłło, S. Bielecki, Structural changes of bacterial nanocellulose pellicles induced by genetic modification of Komagataeibacter hansenii ATCC 23769, Applied microbiology and biotechnology 103 (2019) 5339–5353. https://doi.org/10.1007/s00253-019-09846-4.
[247] L. Wang, S.K. Murthy, W.H. Fowle, G.A. Barabino, R.L. Carrier, Influence of micro-well biomimetic topography on intestinal epithelial Caco-2 cell phenotype, Biomaterials 30 (2009) 6825–6834. https://doi.org/10.1016/j.biomaterials.2009.08.046.
[248] C. Liu, H. Pei, F. Tan, Matrix Stiffness and Colorectal Cancer, OncoTargets and therapy 13 (2020) 2747–2755. https://doi.org/10.2147/OTT.S231010.
[249] V. Gkretsi, T. Stylianopoulos, Cell Adhesion and Matrix Stiffness: Coordinating Cancer Cell Invasion and Metastasis, Frontiers in oncology 8 (2018) 145. https://doi.org/10.3389/fonc.2018.00145.
[250] M. Ölander, J.R. Wiśniewski, P. Matsson, P. Lundquist, P. Artursson, The Proteome of Filter-Grown Caco-2 Cells With a Focus on Proteins Involved in Drug Disposition,

Journal of Pharmaceutical Sciences 105 (2016) 817–827. https://doi.org/10.1016/j.xphs.2015.10.030.
[251] B. Rothen-Rutishauser, F.K. Riesen, A. Braun, M. Günthert, H. Wunderli-Allenspach, Dynamics of tight and adherens junctions under EGTA treatment, The Journal of membrane biology 188 (2002) 151–162. https://doi.org/10.1007/s00232-001-0182-2.
[252] T.Y. Ma, D. Tran, N. Hoa, D. Nguyen, M. Merryfield, A. Tarnawski, Mechanism of extracellular calcium regulation of intestinal epithelial tight junction permeability: Role of cytoskeletal involvement, Microsc. Res. Tech. 51 (2000) 156–168. https://doi.org/10.1002/1097-0029(20001015)51:2<156:AID-JEMT7>3.0.CO;2-J.
[253] I.J. Hidalgo, T.J. Raub, R.T. Borchardt, Characterization of the human colon carcinoma cell line (Caco-2) as a model system for intestinal epithelial permeability, Gastroenterology 96 (1989) 736–749.
[254] S.W. Crawley, M.S. Mooseker, M.J. Tyska, Shaping the intestinal brush border, The Journal of cell biology 207 (2014) 441–451. https://doi.org/10.1083/jcb.201407015.
[255] Q. Li, B. Zhang, N. Kasoju, J. Ma, A. Yang, Z. Cui, H. Wang, H. Ye, Differential and Interactive Effects of Substrate Topography and Chemistry on Human Mesenchymal Stem Cell Gene Expression, International journal of molecular sciences 19 (2018). https://doi.org/10.3390/ijms19082344.
[256] J.Z. Gasiorowski, S.J. Liliensiek, P. Russell, D.A. Stephan, P.F. Nealey, C.J. Murphy, Alterations in gene expression of human vascular endothelial cells associated with nanotopographic cues, Biomaterials 31 (2010) 8882–8888. https://doi.org/10.1016/j.biomaterials.2010.08.026.
[257] M.S. Lord, M. Foss, F. Besenbacher, Influence of nanoscale surface topography on protein adsorption and cellular response, Nano Today 5 (2010) 66–78. https://doi.org/10.1016/j.nantod.2010.01.001.
[258] L. Zhang, J.M. Strong, W. Qiu, L.J. Lesko, S.-M. Huang, Scientific perspectives on drug transporters and their role in drug interactions, Molecular pharmaceutics 3 (2006) 62–69. https://doi.org/10.1021/mp050095h.
[259] K. Berginc, S. Zakelj, L. Levstik, D. Ursic, A. Kristl, Fluorescein transport properties across artificial lipid membranes, Caco-2 cell monolayers and rat jejunum, European journal of pharmaceutics and biopharmaceutics official journal of Arbeitsgemeinschaft fur Pharmazeutische Verfahrenstechnik e.V 66 (2007) 281–285. https://doi.org/10.1016/j.ejpb.2006.10.023.
[260] S. Winiwarter, N.M. Bonham, F. Ax, A. Hallberg, H. Lennernäs, A. Karlén, Correlation of human jejunal permeability (in vivo) of drugs with experimentally and theoretically derived parameters. A multivariate data analysis approach, Journal of medicinal chemistry 41 (1998) 4939–4949. https://doi.org/10.1021/jm9810102.
[261] W. Zhao, S. Uehera, K. Tanaka, S. Tadokoro, K. Kusamori, H. Katsumi, T. Sakane, A. Yamamoto, Effects of Polyoxyethylene Alkyl Ethers on the Intestinal Transport and Absorption of Rhodamine 123: A P-glycoprotein Substrate by In Vitro and In Vivo Studies, Journal of Pharmaceutical Sciences 105 (2016) 1526–1534. https://doi.org/10.1016/j.xphs.2016.01.020.
[262] C.A. Larregieu, L.Z. Benet, Drug discovery and regulatory considerations for improving in silico and in vitro predictions that use Caco-2 as a surrogate for human intestinal permeability measurements, The AAPS journal 15 (2013) 483–497. https://doi.org/10.1208/s12248-013-9456-8.
[263] L. Kou, Y.D. Bhutia, Q. Yao, Z. He, J. Sun, V. Ganapathy, Transporter-Guided Delivery of Nanoparticles to Improve Drug Permeation across Cellular Barriers and Drug Exposure to Selective Cell Types, Frontiers in Pharmacology 9 (2018) 27. https://doi.org/10.3389/fphar.2018.00027.
[264] E. Roger, S. Kalscheuer, A. Kirtane, B.R. Guru, A.E. Grill, J. Whittum-Hudson, J. Panyam, Folic acid functionalized nanoparticles for enhanced oral drug delivery, Molecular pharmaceutics 9 (2012) 2103–2110. https://doi.org/10.1021/mp2005388.
[265] R.B. Baleeiro, M. Schweinlin, R. Rietscher, A. Diedrich, J.A. Czaplewska, M. Metzger, C.M. Lehr, R. Scherlieb, A. Hanefeld, M. Gottschaldt, P. Walden, Nanoparticle-Based

Mucosal Vaccines Targeting Tumor-Associated Antigens to Human Dendritic Cells, Journal of biomedical nanotechnology 12 (2016) 1527–1543. https://doi.org/10.1166/jbn.2016.2267.

[266] F. Danhier, E. Ansorena, J.M. Silva, R. Coco, A. Le Breton, V. Préat, PLGA-based nanoparticles: an overview of biomedical applications, Journal of controlled release official journal of the Controlled Release Society 161 (2012) 505–522. https://doi.org/10.1016/j.jconrel.2012.01.043.

[267] R. Ismail, A. Bocsik, G. Katona, I. Gróf, M.A. Deli, I. Csóka, Encapsulation in Polymeric Nanoparticles Enhances the Enzymatic Stability and the Permeability of the GLP-1 Analog, Liraglutide, Across a Culture Model of Intestinal Permeability, Pharmaceutics 11 (2019). https://doi.org/10.3390/pharmaceutics11110599.

[268] C. Schreider, G. Peignon, S. Thenet, J. Chambaz, M. Pinçon-Raymond, Integrin-mediated functional polarization of Caco-2 cells through E-cadherin—actin complexes, Journal of cell science 115 (2002) 543.

[269] L. Sigurdson, D.E. Carney, Y. Hou, L. Hall, R. Hard, W. Hicks, F.V. Bright, J.A. Gardella, A comparative study of primary and immortalized cell adhesion characteristics to modified polymer surfaces: toward the goal of effective re-epithelialization, Journal of biomedical materials research 59 (2002) 357–365. https://doi.org/10.1002/jbm.1252.

[270] V.S. Kulkarni, C. Shaw, Chapter 5 - Use of Polymers and Thickeners in Semisolid and Liquid Formulations, in: V.S. Kulkarni, C. Shaw (Eds.), Essential Chemistry for Formulators of Semisolid and Liquid Dosages, Academic Press, Boston, 2016, pp. 43–69.

[271] N. Davidenko, C.F. Schuster, D.V. Bax, R.W. Farndale, S. Hamaia, S.M. Best, R.E. Cameron, Evaluation of cell binding to collagen and gelatin: a study of the effect of 2D and 3D architecture and surface chemistry, Journal of materials science. Materials in medicine 27 (2016) 148. https://doi.org/10.1007/s10856-016-5763-9.

[272] V. Hernandez-Gordillo, T. Kassis, A. Lampejo, G. Choi, M.E. Gamboa, J.S. Gnecco, A. Brown, D.T. Breault, R. Carrier, L.G. Griffith, Fully synthetic matrices for in vitro culture of primary human intestinal enteroids and endometrial organoids, Biomaterials 254 (2020) 120125. https://doi.org/10.1016/j.biomaterials.2020.120125.

[273] J.R. Spence, C.N. Mayhew, S.A. Rankin, M.F. Kuhar, J.E. Vallance, K. Tolle, E.E. Hoskins, V.V. Kalinichenko, S.I. Wells, A.M. Zorn, N.F. Shroyer, J.M. Wells, Directed differentiation of human pluripotent stem cells into intestinal tissue in vitro, Nature 470 (2011) 105–109. https://doi.org/10.1038/nature09691.

[274] K.W. McCracken, J.C. Howell, J.M. Wells, J.R. Spence, Generating human intestinal tissue from pluripotent stem cells in vitro, Nature protocols 6 (2011) 1920–1928. https://doi.org/10.1038/nprot.2011.410.

[275] A. Mithal, A. Capilla, D. Heinze, A. Berical, C. Villacorta-Martin, M. Vedaie, A. Jacob, K. Abo, A. Szymaniak, M. Peasley, A. Stuffer, J. Mahoney, D.N. Kotton, F. Hawkins, G. Mostoslavsky, Generation of mesenchyme free intestinal organoids from human induced pluripotent stem cells, Nat Commun 11 (2020) 215. https://doi.org/10.1038/s41467-019-13916-6.

[276] Frappart, David de Semir, R. Maurisse, E.H. Vock, D.C. Gruenert, Immortalization Strategies for Epithelial Cells in Primary Culture, in: C. Ehrhardt, K.-J. Kim (Eds.), Drug Absorption Studies: In Situ, In Vitro and In Silico Models, Springer US, Boston, MA, 2008, pp. 616–639.

[277] L. HAYFLICK, THE LIMITED IN VITRO LIFETIME OF HUMAN DIPLOID CELL STRAINS, Experimental cell research 37 (1965) 614–636. https://doi.org/10.1016/0014-4827(65)90211-9.

[278] L. HAYFLICK, A brief history of the mortality and immortality of cultured cells, The Keio journal of medicine 47 (1998) 174–182. https://doi.org/10.2302/kjm.47.174.

[279] L. HAYFLICK, P.S. MOORHEAD, The serial cultivation of human diploid cell strains, Experimental cell research 25 (1961) 585–621. https://doi.org/10.1016/0014-4827(61)90192-6.

[280] B.J. Aubrey, G.L. Kelly, A. Janic, M.J. Herold, A. Strasser, How does p53 induce apoptosis and how does this relate to p53-mediated tumour suppression?, Cell Death & Differentiation 25 (2018) 104–113. https://doi.org/10.1038/cdd.2017.169.
[281] R.J. Duronio, Y. Xiong, Signaling pathways that control cell proliferation, Cold Spring Harb Perspect Biol 5 (2013) a008904. https://doi.org/10.1101/cshperspect.a008904.
[282] K. Münger, W.C. Phelps, V. Bubb, P.M. Howley, R. Schlegel, The E6 and E7 genes of the human papillomavirus type 16 together are necessary and sufficient for transformation of primary human keratinocytes, J Virol 63 (1989) 4417–4421.
[283] D. Song, F. Zhang, R.R. Reid, J. Ye, Q. Wei, J. Liao, Y. Zou, J. Fan, C. Ma, X. Hu, X. Qu, L. Chen, L. Li, Y. Yu, X. Yu, Z. Zhang, C. Zhao, Z. Zeng, R. Zhang, S. Yan, T. Wu, X. Wu, Y. Shu, J. Lei, Y. Li, W. Zhang, J. Wang, M.J. Lee, J.M. Wolf, D. Huang, T.-C. He, BMP9 induces osteogenesis and adipogenesis in the immortalized human cranial suture progenitors from the patent sutures of craniosynostosis patients, J Cell Mol Med 21 (2017) 2782–2795. https://doi.org/10.1111/jcmm.13193.
[284] A. Houghton, B.O. Oyajobi, G.A. Foster, R.G. Russell, B.M. Stringer, Immortalization of human marrow stromal cells by retroviral transduction with a temperature sensitive oncogene: identification of bipotential precursor cells capable of directed differentiation to either an osteoblast or adipocyte phenotype, Bone 22 (1998) 7–16. https://doi.org/10.1016/s8756-3282(97)00229-9.
[285] J. Gil, P. Kerai, M. Lleonart, D. Bernard, J.C. Cigudosa, G. Peters, A. Carnero, D. Beach, Immortalization of primary human prostate epithelial cells by c-Myc, Cancer research 65 (2005) 2179–2185. https://doi.org/10.1158/0008-5472.CAN-03-4030.
[286] H. Tian, B. Biehs, C. Chiu, C.W. Siebel, Y. Wu, M. Costa, de Sauvage, Frederic J, O.D. Klein, Opposing activities of Notch and Wnt signaling regulate intestinal stem cells and gut homeostasis, Cell reports 11 (2015) 33–42. https://doi.org/10.1016/j.celrep. 2015.03.007.
[287] N.S. Roy, T. Nakano, H.M. Keyoung, M. Windrem, W.K. Rashbaum, M.L. Alonso, J. Kang, W. Peng, M.K. Carpenter, J. Lin, M. Nedergaard, S.A. Goldman, Telomerase immortalization of neuronally restricted progenitor cells derived from the human fetal spinal cord, Nature Biotechnology 22 (2004) 297–305. https://doi.org/10.1038/nbt944.
[288] C.-J. Hung, C.-L. Yao, F.-C. Cheng, M.-L. Wu, T.-H. Wang, S.-M. Hwang, Establishment of immortalized mesenchymal stromal cells with red fluorescence protein expression for in vivo transplantation and tracing in the rat model with traumatic brain injury, Cytotherapy 12 (2010) 455–465. https://doi.org/10.3109/1465324 0903555827.
[289] S.L. Piper, M. Wang, A. Yamamoto, F. Malek, A. Luu, A.C. Kuo, H.T. Kim, Inducible immortality in hTERT-human mesenchymal stem cells, Journal of orthopaedic research official publication of the Orthopaedic Research Society 30 (2012) 1879–1885. https://doi.org/10.1002/jor.22162.
[290] T.M. Bryan, R.R. Reddel, SV40-induced immortalization of human cells, Critical reviews in oncogenesis 5 (1994) 331–357. https://doi.org/10.1615/critrevoncog. v5.i4.10.
[291] H.L. Ozer, S.S. Banga, T. Dasgupta, J. Houghton, K. Hubbard, K.K. Jha, S.-H. Kim, M. Lenahan, Z. Pang, J.R. Pardinas, P.C. Patsalis, SV40-mediated immortalization of human fibroblasts, In Memory of Samuel Goldstein 1938-1994 31 (1996) 303–310. https://doi.org/10.1016/0531-5565(95)00024-0.
[292] Alwin Prem Anand, A., S. Gowri Sankar, V. Kokila Vani, Immortalization of neuronal progenitors using SV40 large T antigen and differentiation towards dopaminergic neurons, J. Cell. Mol. Med. 16 (2012) 2592–2610. https://doi.org/10.1111/j.1582-4934.2012.01607.x.
[293] C.L. Halbert, G.W. Demers, D.A. Galloway, The E6 and E7 genes of human papillomavirus type 6 have weak immortalizing activity in human epithelial cells, J Virol 66 (1992) 2125–2134.
[294] A. Yamamoto, S.-i. Kumakura, M. Uchida, J.C. Barrett, T. Tsutsui, Immortalization of normal human embryonic fibroblasts by introduction of either the human papillomavirus

type 16 E6 or E7 gene alone, International journal of cancer 106 (2003) 301–309. https://doi.org/10.1002/ijc.11219.
[295] T. Speiseder, H. Hofmann-Sieber, E. Rodríguez, A. Schellenberg, N. Akyüz, J. Dierlamm, T. Spruss, C. Lange, T. Dobner, Efficient Transformation of Primary Human Mesenchymal Stromal Cells by Adenovirus Early Region 1 Oncogenes, J Virol 91 (2016) e01782-16. https://doi.org/10.1128/JVI.01782-16.
[296] S. Gopalakrishnan, J.L. Douglas, M.P. Quinlan, Immortalization of primary epithelial cells by E1A 12S requires late, second exon-encoded functions in addition to complex formation with pRB and p300, Cell growth & differentiation the molecular biology journal of the American Association for Cancer Research 8 (1997) 541–551.
[297] C. Giacinti, A. Giordano, RB and cell cycle progression, Oncogene 25 (2006) 5220–5227. https://doi.org/10.1038/sj.onc.1209615.
[298] S. Haupt, M. Berger, Z. Goldberg, Y. Haupt, Apoptosis - the p53 network, J. Cell Sci. 116 (2003) 4077. https://doi.org/10.1242/jcs.00739.
[299] E. Wawryk-Gawda, P. Chylinska-Wrzos, M. Lis-Sochocka, K. Chlapek, K. Bulak, M. Jedrych, B. Jodlowska-Jedrych, P53 protein in proliferation, repair and apoptosis of cells, Protoplasma 251 (2014) 525–533. https://doi.org/10.1007/s00709-013-0548-1.
[300] A.H. Stegh, Targeting the p53 signaling pathway in cancer therapy - the promises, challenges and perils, Expert opinion on therapeutic targets 16 (2012) 67–83. https://doi.org/10.1517/14728222.2011.643299.
[301] T. Sakuma, M.A. Barry, Y. Ikeda, Lentiviral vectors: basic to translational, The Biochemical journal 443 (2012) 603–618. https://doi.org/10.1042/BJ20120146.
[302] R.G. Russell, A. Lasorella, L.E. Dettin, A. Iavarone, Id2 drives differentiation and suppresses tumor formation in the intestinal epithelium, Cancer research 64 (2004) 7220–7225. https://doi.org/10.1158/0008-5472.CAN-04-2095.
[303] Y. Cao, X. Liu, W. Zhang, X. Deng, H. Zhang, Y. Liu, L. Chen, E.A. Thompson, C.M. Townsend, T.C. Ko, TGF-beta repression of Id2 induces apoptosis in gut epithelial cells, Oncogene 28 (2009) 1089–1098. https://doi.org/10.1038/onc.2008.456.
[304] C. Roschger, C. Cabrele, The Id-protein family in developmental and cancer-associated pathways, Cell communication and signaling CCS 15 (2017) 7. https://doi.org/10.1186/s12964-016-0161-y.
[305] N. Zhang, R.K. Yantiss, H.-S. Nam, Y. Chin, X.K. Zhou, E.J. Scherl, B.P. Bosworth, K. Subbaramaiah, A.J. Dannenberg, R. Benezra, ID1 is a functional marker for intestinal stem and progenitor cells required for normal response to injury, Stem Cell Reports 3 (2014) 716–724. https://doi.org/10.1016/j.stemcr.2014.09.012.
[306] A. Basu, K. Meyer, R.B. Ray, R. Ray, Hepatitis C virus core protein is necessary for the maintenance of immortalized human hepatocytes, Virology 298 (2002) 53–62. https://doi.org/10.1006/viro.2002.1460.
[307] O. Zaytseva, L.M. Quinn, Controlling the Master: Chromatin Dynamics at the MYC Promoter Integrate Developmental Signaling, Genes 8 (2017). https://doi.org/10.3390/genes8040118.
[308] M.D. Bettess, N. Dubois, M.J. Murphy, C. Dubey, C. Roger, S. Robine, A. Trumpp, c-Myc is required for the formation of intestinal crypts but dispensable for homeostasis of the adult intestinal epithelium, Molecular and cellular biology 25 (2005) 7868–7878. https://doi.org/10.1128/MCB.25.17.7868-7878.2005.
[309] K.B. Scotland, S. Chen, R. Sylvester, L.J. Gudas, Analysis of Rex1 (zfp42) function in embryonic stem cell differentiation, Developmental dynamics an official publication of the American Association of Anatomists 238 (2009) 1863–1877. https://doi.org/10.1002/dvdy.22037.
[310] K. Onuma, M. Ochiai, K. Orihashi, M. Takahashi, T. Imai, H. Nakagama, Y. Hippo, Genetic reconstitution of tumorigenesis in primary intestinal cells, Proceedings of the National Academy of Sciences of the United States of America 110 (2013) 11127–11132. https://doi.org/10.1073/pnas.1221926110.
[311] R.G. Lindeboom, L. van Voorthuijsen, K.C. Oost, M.J. Rodríguez-Colman, M.V. Luna-Velez, C. Furlan, F. Baraille, P.W. Jansen, A. Ribeiro, B.M. Burgering, H.J. Snippert, M.

Vermeulen, Integrative multi-omics analysis of intestinal organoid differentiation, Molecular systems biology 14 (2018) e8227. https://doi.org/10.15252/msb.20188227.
[312] Y. Maru, K. Orihashi, Y. Hippo, Lentivirus-Based Stable Gene Delivery into Intestinal Organoids, Methods in molecular biology (Clifton, N.J.) 1422 (2016) 13–21. https://doi.org/10.1007/978-1-4939-3603-8_2.
[313] J. Kim, B.-K. Koo, J.A. Knoblich, Human organoids: model systems for human biology and medicine, Nature Reviews Molecular Cell Biology. https://doi.org/10.1038/s41580-020-0259-3.
[314] R. Maurisse, D. de Semir, H. Emamekhoo, B. Bedayat, A. Abdolmohammadi, H. Parsi, D.C. Gruenert, Comparative transfection of DNA into primary and transformed mammalian cells from different lineages, BMC biotechnology 10 (2010) 9. https://doi.org/10.1186/1472-6750-10-9.
[315] Z.-Y. Shen, L.-Y. Xu, E.-M. Li, W.-J. Cai, M.-H. Chen, J. Shen, Y. Zeng, Telomere and telomerase in the initial stage of immortalization of esophageal epithelial cell, World J Gastroenterol 8 (2002) 357–362. https://doi.org/10.3748/wjg.v8.i2.357.
[316] C.P. Morales, K.G. Gandia, R.D. Ramirez, W.E. Wright, J.W. Shay, S.J. Spechler, Characterisation of telomerase immortalised normal human oesophageal squamous cells, Gut 52 (2003) 327–333. https://doi.org/10.1136/gut.52.3.327.
[317] M.A. Cerone, C. Autexier, J.A. Londoño-Vallejo, S. Bacchetti, A human cell line that maintains telomeres in the absence of telomerase and of key markers of ALT, Oncogene 24 (2005) 7893–7901. https://doi.org/10.1038/sj.onc.1208934.
[318] A.J. Montpetit, A.A. Alhareeri, M. Montpetit, A.R. Starkweather, L.W. Elmore, K. Filler, L. Mohanraj, C.W. Burton, V.S. Menzies, D.E. Lyon, C.K. Jackson-Cook, Telomere length: a review of methods for measurement, Nursing research 63 (2014) 289–299. https://doi.org/10.1097/NNR.0000000000000037.
[319] J.-F. Groulx, D. Gagné, Y.D. Benoit, D. Martel, N. Basora, J.-F. Beaulieu, Collagen VI is a basement membrane component that regulates epithelial cell-fibronectin interactions, Matrix biology journal of the International Society for Matrix Biology 30 (2011) 195–206. https://doi.org/10.1016/j.matbio.2011.03.002.
[320] K. Lam, L. Zhang, K.M. Yamada, R.M. Lafrenie, Adhesion of epithelial cells to fibronectin or collagen I induces alterations in gene expression via a protein kinase C-dependent mechanism, J. Cell. Physiol. 189 (2001) 79–90. https://doi.org/10.1002/jcp.1142.
[321] D.F. Sweeney, R.Z. Xie, M.D.M. Evans, A. Vannas, S.D. Tout, H.J. Griesser, G. Johnson, J.G. Steele, A comparison of biological coatings for the promotion of corneal epithelialization of synthetic surface in vivo, Investigative ophthalmology & visual science 44 (2003) 3301–3309. https://doi.org/10.1167/iovs.02-0561.
[322] H. Liu, Q. Liu, Y. Ge, Q. Zhao, X. Zheng, Y. Zhao, hTERT promotes cell adhesion and migration independent of telomerase activity, Sci Rep 6 (2016) 22886. https://doi.org/10.1038/srep22886.
[323] H.M. Li, C. Man, Y. Jin, W. Deng, Y.L. Yip, H.C. Feng, Y.C. Cheung, K.W. Lo, P.S. Meltzer, Z.G. Wu, Y.L. Kwong, A.P.W. Yuen, S.W. Tsao, Molecular and cytogenetic changes involved in the immortalization of nasopharyngeal epithelial cells by telomerase, International journal of cancer 119 (2006) 1567–1576. https://doi.org/10.1002/ijc.22032.
[324] J. van der Valk, D. Brunner, K. de Smet, A. Fex Svenningsen, P. Honegger, L.E. Knudsen, T. Lindl, J. Noraberg, A. Price, M.L. Scarino, G. Gstraunthaler, Optimization of chemically defined cell culture media--replacing fetal bovine serum in mammalian in vitro methods, Toxicology in vitro an international journal published in association with BIBRA 24 (2010) 1053–1063. https://doi.org/10.1016/j.tiv.2010.03.016.
[325] C. Nossol, A. Barta-Böszörményi, S. Kahlert, W. Zuschratter, H. Faber-Zuschratter, N. Reinhardt, S. Ponsuksili, K. Wimmers, A.-K. Diesing, H.-J. Rothkötter, Comparing Two Intestinal Porcine Epithelial Cell Lines (IPECs): Morphological Differentiation, Function and Metabolism, PloS one 10 (2015) e0132323. https://doi.org/10.1371/journal.pone.0132323.

[326] C. Nossol, A.-K. Diesing, N. Walk, H. Faber-Zuschratter, R. Hartig, A. Post, J. Kluess, H.-J. Rothkötter, S. Kahlert, Air-liquid interface cultures enhance the oxygen supply and trigger the structural and functional differentiation of intestinal porcine epithelial cells (IPEC), Histochemistry and cell biology 136 (2011) 103–115. https://doi.org/10.1007/s00418-011-0826-y.
[327] E. Rangel-Huerta, E. Maldonado, Transit-Amplifying Cells in the Fast Lane from Stem Cells towards Differentiation, Stem cells international 2017 (2017) 7602951. https://doi.org/10.1155/2017/7602951.
[328] T.J. Mitchison, The proliferation rate paradox in antimitotic chemotherapy, Molecular biology of the cell 23 (2012) 1–6. https://doi.org/10.1091/mbc.E10-04-0335.
[329] K. Wayakanon, K. Rueangyotchanthana, P. Wayakanon, C. Suwannachart, The inhibition of Caco-2 proliferation by astaxanthin from Xanthophyllomyces dendrorhous, Journal of medical microbiology 67 (2018) 507–513. https://doi.org/10.1099/jmm.0.000710.
[330] P.D. Pereira, A. Serra-Caetano, M. Cabrita, E. Bekman, J. Braga, J. Rino, R. Santus, P.L. Filipe, A.E. Sousa, J.A. Ferreira, Quantification of cell cycle kinetics by EdU (5-ethynyl-2'-deoxyuridine)-coupled-fluorescence-intensity analysis, Oncotarget 8 (2017) 40514–40532. https://doi.org/10.18632/oncotarget.17121.
[331] T. Scholzen, J. Gerdes, The Ki-67 protein: From the known and the unknown, J. Cell. Physiol. 182 (2000) 311–322. https://doi.org/10.1002/(SICI)1097-4652(200003)182:3<311:AID-JCP1>3.0.CO;2-9.
[332] C.P. Landowski, P. Anderle, D. Sun, W. Sadee, G.L. Amidon, Transporter and ion channel gene expression after caco-2 cell differentiation using 2 different microarray technologies, The AAPS journal 6 (2004) 35–44. https://doi.org/10.1208/aapsj060321.
[333] G. Dalmasso, H.T.T. Nguyen, Y. Yan, H. Laroui, S. Srinivasan, S.V. Sitaraman, D. Merlin, MicroRNAs determine human intestinal epithelial cell fate, Differentiation; research in biological diversity 80 (2010) 147–154. https://doi.org/10.1016/j.diff.2010.06.005.
[334] K.E. Samy, E.S. Levy, K. Phong, B. Demaree, A.R. Abate, T.A. Desai, Human intestinal spheroids cultured using Sacrificial Micromolding as a model system for studying drug transport, Sci Rep 9 (2019) 9936. https://doi.org/10.1038/s41598-019-46408-0.
[335] M. Zoetemelk, M. Rausch, D.J. Colin, O. Dormond, P. Nowak-Sliwinska, Short-term 3D culture systems of various complexity for treatment optimization of colorectal carcinoma, Sci Rep 9 (2019) 7103. https://doi.org/10.1038/s41598-019-42836-0.
[336] T. Zietek, E. Rath, D. Haller, H. Daniel, Intestinal organoids for assessing nutrient transport, sensing and incretin secretion, Sci Rep 5 (2015) 16831. https://doi.org/10.1038/srep16831.
[337] C. Rahner, L.L. Mitic, J.M. Anderson, Heterogeneity in expression and subcellular localization of claudins 2, 3, 4, and 5 in the rat liver, pancreas, and gut, Gastroenterology 120 (2001) 411–422. https://doi.org/10.1053/gast.2001.21736.
[338] T. Kourkoumpetis, K.E. Royse, L. Chen, M. Ravishankar, M. Ittmann, H.B. El-Serag, L. Jiao, Differential Expression of Tight Junctions and Cell Polarity Genes in Human Colon Cancer, Exploratory Research and Hypothesis in Medicine 3 (2018) 14–19. https://doi.org/10.14218/ERHM.2017.00036.
[339] S. Drayton, G. Peters, Immortalisation and transformation revisited, Current Opinion in Genetics & Development 12 (2002) 98–104. https://doi.org/10.1016/S0959-437X(01)00271-4.
[340] R.C. Mustata, G. Vasile, V. Fernandez-Vallone, S. Strollo, A. Lefort, F. Libert, D. Monteyne, D. Pérez-Morga, G. Vassart, M.-I. Garcia, Identification of Lgr5-independent spheroid-generating progenitors of the mouse fetal intestinal epithelium, Cell reports 5 (2013) 421–432. https://doi.org/10.1016/j.celrep.2013.09.005.
[341] B. Srinivasan, A.R. Kolli, M.B. Esch, H.E. Abaci, M.L. Shuler, J.J. Hickman, TEER measurement techniques for in vitro barrier model systems, Journal of laboratory automation 20 (2015) 107–126. https://doi.org/10.1177/2211068214561025.

[342] K.L. VanDussen, J.M. Marinshaw, N. Shaikh, H. Miyoshi, C. Moon, P.I. Tarr, M.A. Ciorba, T.S. Stappenbeck, Development of an enhanced human gastrointestinal epithelial culture system to facilitate patient-based assays, Gut 64 (2015) 911–920. https://doi.org/10.1136/gutjnl-2013-306651.

Appendix

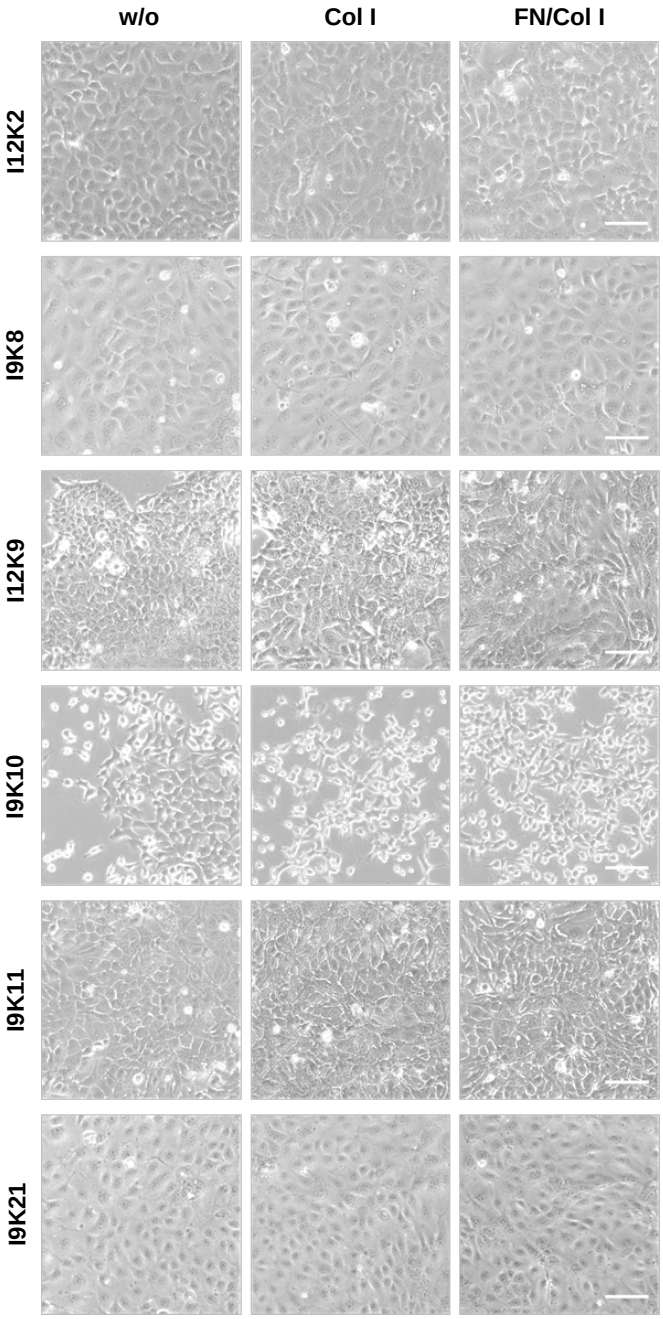

Figure A1: Murine cell clones cultured on different cell culture coatings. Cell clones were cultured on uncoated (w/o) as well as Col I or FN/Col I pre-coated plastic for 4-5 days. Microscopic images (n =3) show the cell morphology of clone I9K8 and I12K9 on d4 and of I12K2, I9K10, I9K11 and I9K21 on d5. d: day; w/o: uncoated; Col I: collagen-I; FN/Col I: fibronectin/collagen-I.

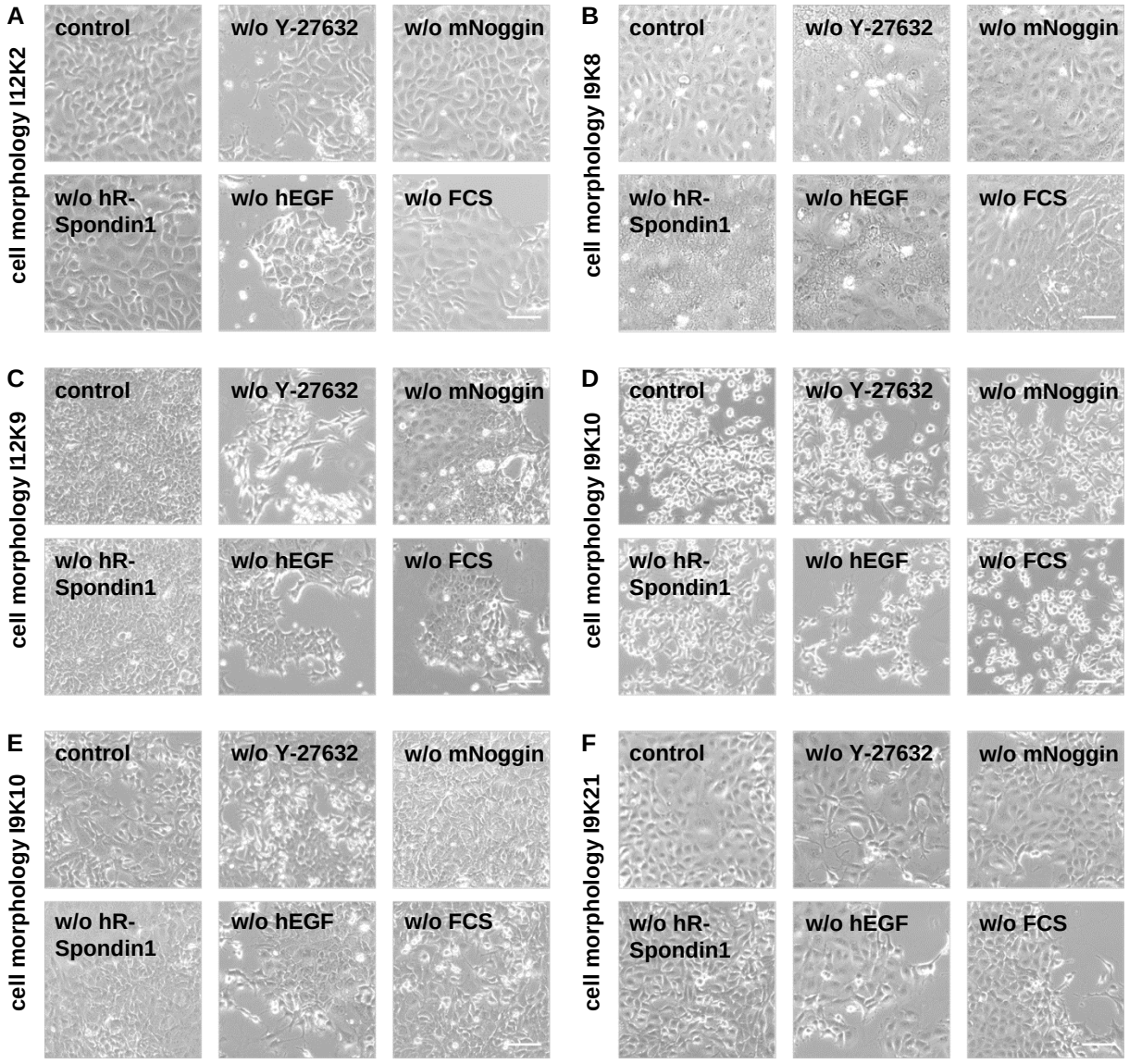

Figure A2: Testing appropriate culture conditions for murine cell clones cultured on uncoated plastic. Cell clones were cultured under control conditions and without the essential growth factors for primary murine spheroid/organoid cultures such as Y-27632, mNoggin, hR-Spondin, hEGF and FCS (10%). FCS is commonly used for cell line cultures [1,2]. Cell morphology was monitored on d4 for I9K8 **(B)** and I12K9 **(C)** or on d5 for I12K2 **(A)**, I9K10 **(D)**, I9K11 **(E)** and I9K21 **(F)** cells. Representative microscope images (n = 3) of all clones show a reduced cell density or altered morphology without Y-27632, hEGF and FCS supplementation to the medium. Scale bar = 100 µm. d: day; FCS: fetal calf serum; hEGF: human epidermal growth factor; w/o: without.

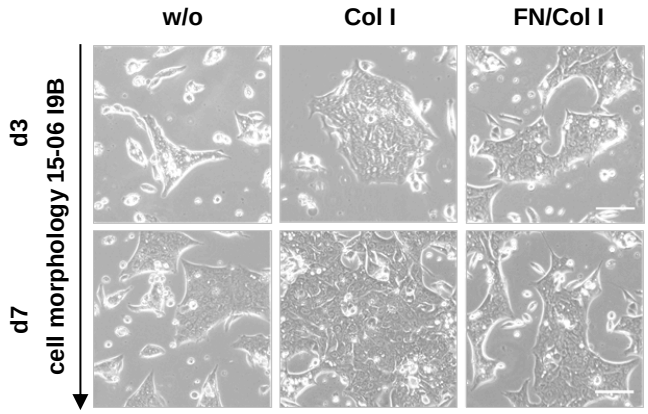

Figure A3: Human cell clone 15-06 I9B cultured on three different cell culture coatings. Cell morphology was monitored for 15-06 I9B cells cultured on uncoated (w/o), Col I and FN/Col I pre-coated plastic for 7 days and representative images (n = 3) show the cell morphology on d3 and d7. Scale bar = 100 µm. d: day; w/o: uncoated; Col I: collagen-I; FN/Col I: fibronectin/collagen-I.

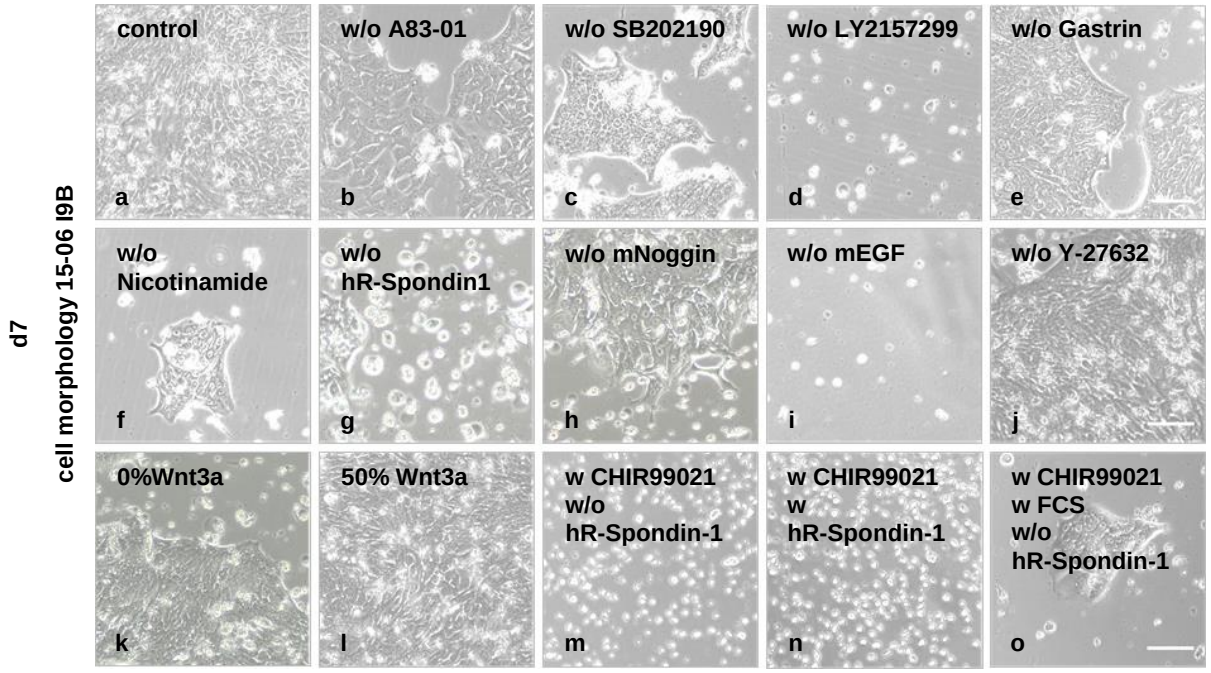

Figure A4: Testing appropriate culture conditions for the human cell clone 15-06 I9B cultured on Col I pre-coated plastic. The human cell clone was cultured under control conditions and without the essential growth factors for primary human spheroid/organoid cultures. Further, CHIR99021, a Wnt activator, was tested for standardized model setup instead of supplementation with Wnt3a conditioned medium. Next to CHIR99021, cell culture medium was supplemented with either hR-Spondin 1 or FCS for a comparative cell growth to control conditions. Representative microscope images of 15-06 I9B cells show a reduced cell density when cultured under the adapted culture conditions. Scale bar = 50 µm; n = 3. hEGF: human epidermal growth factor; FCS: fetal calf serum; Wnt: wingless related integration site; w/o: without; w: with.

Affidavit

I hereby confirm that my thesis entitled: ***„Establishment of an intestinal tissue model for pre-clinical screenings“*** is the result of my own work. I did not receive any help or support from commercial consultants. All sources and / or materials applied are listed and specified in the thesis.

Furthermore, I confirm that this thesis has not yet been submitted as part of another examination process neither in identical nor in similar form.

Place, Date Signature

Eidesstattliche Erklärung

Hiermit erkläre ich an Eides statt, die Dissertation: ***„Etablierung eines Darmgewebemodells für Präklinische Screenings“*** eigenständig, d.h. insbesondere selbstständig und ohne Hilfe einer kommerziellen Promotionsberaters, angefertigt und keine anderen als die von mir angegebenen Quellen und Hilfsmittel verwendet zu haben.

Ich erkläre außerdem, dass die Dissertation weder in gleicher noch in ähnlicher Form bereits in einem anderen Prüfungsverfahren vorgelegen hat.

Ort, Datum Unterschrift

Curriculum vitae

.....

.....

Place, Date Signature

Publications

2020: *Research article*

Meir M, Salm J, **Fey C**, Schweinlin M, Kollmann C, Kannapin F, Germer CT, Waschke J, Beck C, Burkard N, Metzger M, Schlegel N. *Enteroids generated from patients with severe inflammation in Crohn's disease maintain alterations of junctional proteins*. Journal of Crohn's and Colitis. pii: jjaa085 (2020). DOI: 10.1093/ecco-jcc/jjaa085.

Fey C, Betz J, Rosenbaum C, Kralisch D, Vielreicher M, Friedrich O, Metzger M, Zdzieblo D. *Bacterial nanocellulose as novel carrier for intestinal epithelial cells in drug delivery studies.* Materials Science and Engineering: C, 109:110613 (2020). DOI: 10.1016/j.msec.2019.110613.

Book chapter

Däullary T, **Fey C**, Berger C, Metzger M, Zdzieblo D. *Bioartificial gut - current state of small intestinal tissue engineering*. Biomaterials for Organ and Tissue Regeneration. Woodhead Publishing. ISBN 978-0-08-102906-0.

2018: *Research article*

Ungewiß H, Rötzer V, Meir M, **Fey C**, Diefenbacher M, Schlegel N, Waschke J. *Dsg2 via Src-mediated transactivation shapes EGFR signaling towards cell adhesion*. Cellular and Molecular Life Sciences, 75(22):4251-4268 (2018). DOI: 10.1007/s00018-018-2869-x.

2017: *Book chapter*

Christ B*, **Fey C***, Cubukova A, Walles H, Dembski S, Metzger M. *Screening Applications to Test Cellular Fitness in Transwell Models After Nanoparticle Treatment.* Methods in Molecular Biology, 1601:111-122 (2017). Springer Science. DOI: 10.1007/978-1-4939-6960-9_10.

Acknowledgement

First, I would like to express my gratitude to my first supervisor PD Dr. Marco Metzger and my second advisor Prof. Dr. Heike Walles. I am grateful that you provided me the opportunity to finish my doctoral thesis at the Chair of Tissue Engineering and Regenerative Medicine (TERM) in Würzburg and for the support, the scientific guidance and all the time you had for me during the last years.

My sincere thanks also go to my third and fourth supervisor Prof. Dr. Nicolas Schlegel and Prof. Dr. Andreas Friebe for their scientific suggestions and feedback during my time as PhD student. A special thanks goes to Nicolas Schlegel and his team for the great as well as fruitful cooperation during the last years, which also resulted in a joint publication.

Further, I would like to express my gratitude to Dr. Daniela Zdzieblo for her support, knowledge and guidance during the last years. Thank you for taking the time to support me, especially in the last month of my thesis.

I would like to thank all my colleagues at the TERM, especially the team around PD Dr. Marco Metzger and Dr. Daniela Zdzieblo for this unforgettable time and support during the last years. In this context, I would like to express my special thanks to Dr. Matthias Schweinlin, Sabine Wilhelm, Alevtina Cubukova, Andrea Knorz, Marion Krafft, Jana Betz, Anna Seubert, Markus Mühlemann, Constantin Berger and Thomas Däullary.

Further, I want to thank all collaboration partners. Thanks to Dr. Tobias May, Dr. Roland Schucht, Dr. Theresa Truschel and Kristina Nehlsen from InSCREENeX for the generation of the used murine and human cell clones. In addition, I want to thank Dana Kralisch from JeNaCell for the provision of the bacterial nanocellulose scaffolds and the participation in the publication to reach my first authorship. In this context I would also like to thank Dr. Martin Vielreicher und Prof. Dr. Oliver Friedrich from the Friedrich-Alexander-University (FAU) in Erlangen-Nürnberg for the support and inputs for the publication “Bacterial Nanocellulose as Novel Carrier for Intestinal Epithelial Cells in Drug Delivery Studies”. Furthermore, I would like to thank Prof. Dr. Stigloher and Claudia Gehrig for the support and the preparation of the samples analyzed by REM and TEM. My thanks also go to Prof. Dr. Roewer, Prof. Dr. Broscheit and especially Daniel Schmück for the analyses of the propranolol samples using HPLC-MS/MS.

I am grateful for the financial support from the “Bundesministerium für Bildung und Forschung BMBF - KMU innovativ”. Without this funding it would not have been possible to finish my doctoral thesis at the TERM.

A special thanks to my closest friends in Würzburg (Nina Marichikj, Johanna Kühnemundt, Phillip Fey, Marius Gensler, Sebastian Sputh), in the Allgäu (Katharina Prusko, Ramona Unruh, Tobias Unruh, Corinna Rauch, Joachim Rauch, Mirjam Sepp, Christian Pester) and to my former university colleagues (Sandra Kühne, Hans-Christian Rudloff). You helped me in the last years through your ongoing motivating mindsets, inspiring talks, the support and understanding in particularly hard times.

Last but not least, I would like to thank my family. In particular, I would like to thank my parents, Regina and Manfred Fey, for the support throughout my life in exhausting moments, for financial support all the years of studying and all the love I have got from them. I'm infinitely grateful that they always had an open ear for me. Further, I thank my brother, Alexander, for the good advice when I just couldn't find the solution to my problem.